$P2X_7$ Receptor Modulation of Visual Responses in the Retina

Thesis presented to University College London for the degree of

Doctor of Philosophy (Ph. D)

2014

Seetal Chavda

Department of Visual Neuroscience

Institute of Ophthalmology

University College London

Abstract

Adenosine 5' triphosphate (ATP)-gated $P2X_7$ receptors ($P2X_7Rs$) are known to act as conduits for photoreceptor and retinal ganglion cell (RGC) damage, consequences of various neurodegenerative conditions within the visual pathway. Growing evidence supports the notion that $P2X_7Rs$ and associated inflammatory mediators may coordinate microglia, the resident immune cells of the central nervous system (CNS), to play a genuine role in modulating neurotransmission.

This study aimed to characterise the role of $P2X_7Rs$ in modulating outer and inner retinal function within the rod-mediated pathway, and in the putative microglial-mediated modulation of signal transmission in the retina. Excitatory components of outer and inner retinal function were assessed by recording light-evoked, extracellular transretinal electroretinogram (ERG), and ON and OFF retinal ganglion cell (RGC) field excitatory postsynaptic potential (fEPSP) responses from the acutely isolated, dark-adapted, mouse retina. Alterations to microglial morphology, under similar conditions, were also explored.

Initial experiments confirmed the excitatory responses as predominantly mediated via the 'classic' rod photoreceptor – rod-ON bipolar cell – AII amacrine cell pathway. With the use of selective $P2X_7R$ antagonists, it was shown that $P2X_7R$ activation directly modulated photoreceptor, ON bipolar cell and ON RGC function, but not OFF RGC function, through partially independent mechanisms.

A novel finding of this study demonstrated that acute application of the microglia-activating bacterial component, lipopolysaccharide (LPS) modulated inner retinal function, possibly through a $P2X_7R$- and Pannexin-1-associated mechanism of microglial ATP release. These results were supported by observations of early morphometric changes to microglia caused by $P2X_7R$ activation and LPS, as revealed by immunofluorescence labelling and confocal laser scanning microscopy.

Since changes in neurotransmission and microglial function are early indicators of neuropathology, these results contribute to the understanding of early neural-immune interactions in retinal disease, and in the central nervous system as a whole.

Declaration

I, Seetal Chavda, confirm that the work presented in this thesis is my own. Where information has been derived from other sources, I confirm that this has been indicated in the thesis.

.....

Seetal Chavda

July 2014

Acknowledgements

First and foremost, I would like to thank my supervisor and mentor, Professor Tom Salt for his continuous support, patience and guidance, and his invaluable expertise, without which the completion of this project would not have been possible. I am deeply grateful for my time in the Salt Lab, which has been a fantastic learning experience, and where I have been able to progress and develop attributes that I aspire to uphold throughout my professional career. On a lighter note, I sincerely hope that my preference for stewed leaves (i.e. tea) over fresh coffee hasn't overly tainted the traditions of the Salt Lab.

Sincere thanks to Lundbeck, and University College London for providing vital funding for this project through the Impact award. Many thanks also to my secondary supervisor, Professor Phil Luthert. I am sincerely grateful for his guidance and expertise, and also for taking the time out to lead many thought-provoking discussions over the years. I would like to thank Dr Stuart Neale, whose help, patience and advice, especially during the early days, were very much appreciated. A special thanks to all at the Institute of Ophthalmology Imaging Facility, including Dr Peter Munro, Dr Hannah Armer and Dr Matt Hayes, for their extremely helpful advice and technical support with confocal microscopy. Thanks to my friends and colleagues at IoO who have made my time here an enjoyable experience, including Dr Caroline Copeland and Moussa Zouache for their friendship, humour and support over the past three years.

At this point, I would like to express my gratitude to Dr Nasrin Hameedi, Dr Sabu Abraham, Heidi Barnes, Shereen Nizari and Christine Gaughan, for providing many helpful tips and suggestions during the development of the immunostaining protocols. I would also like to take this opportunity to thank the staff members at IoO, including Nick Burt, Susan Sandford Smith, Anne Snowling, Andrew Dehaney, the graduate tutors, all the porters, and all the BRU staff, for their help, generosity and kindness throughout my time here.

Finally, thanks to my family and friends for their understanding and encouragement that have enabled me to persevere throughout this PhD. Above all, special thanks go to my parents, brother, sister and brother-in-law for their unwavering patience, belief and confidence in my aspiration to never stop learning.

Abbreviations

AC	Amacrine cell
ADO	Adenosine
ADP	Adenosine diphosphate
AII	AII amacrine cell
AMP	Adenosine monophosphate
AMPAR	α-Amino-3-hydroxy-5-methyl-4-isoxazolepropionic acid receptor
ATP	Adenosine 5'-triphosphate
BC	Bipolar cell
BSA	Bovine serum albumin
BzATP	2′(3′)-O-(4-Benzoylbenzoyl)adenosine 5′-triphosphate
cGMP	Cyclic guanosine monophosphate
CNS	Central nervous system
D-AP5	D-(-)-2-Amino-5-phosphonopentanoic acid
DAPI	4',6-diamidino-2-phenylindole
dH_2O	Distilled water
E-NTPDase	Ectonucleoside triphosphate diphosphohydrolase
EPSC	Excitatory postsynaptic current
ERG	Electroretinogram
fEPSP	Field excitatory postsynaptic potential
GABA	Gamma aminobutyric acid
GCL	Ganglion cell layer
IBA1	Ionised calcium-binding adaptor molecule 1
iGluR	Ionotropic glutamate receptor
IL-1β	Interleukin-1β
INL	Inner nuclear layer
IPL	Inner plexiform layer

IPSC	Inhibitory postsynaptic potential
IS	Photoreceptor inner segment
KAR	Kainic acid receptor
L-AP4	L-(+)-2-Amino-4-phosphonobutyric acid
LED	Light-emitting diode
LPS	Lipopolysaccharide
mGluR6	Metabotropic glutamate receptor subtype 6
NFL	Nerve fibre layer
NMDAR	N-Methyl-D-aspartic acid receptor
OFF cBC	OFF-centre cone bipolar cell
OFF RGC	OFF-centre retinal ganglion cell
ON cBC	ON-centre cone bipolar cell
ON RGC	ON-centre retinal ganglion cell
ONL	Outer nuclear layer
OP	Oscillatory potential
OPL	Outer plexiform layer
OS	Photoreceptor outer segment
$P2X_7R$	P2X receptor subtype 7
P2XR	P2X receptor
P2YR	P2Y receptor
Panx-1	Pannexin-1 hemichannel
PBS	Phosphate buffer saline
PFA	Paraformaldehyde
PIC	Picrotoxin
PMSTN	Modified Krebs' medium containing picrotoxin, low concentration of magnesium ions, strychnine, tetrodotoxin and NBQX
PNS	Peripheral nervous system
PPADS	4-[[4-Formyl-5-hydroxy-6-methyl-3-[(phosphonooxy)methyl]-2-pyridinyl]azo]-1,3-benzenedisulfonic acid tetrasodium salt

rBC	Rod ON-centre bipolar cell
RGC	Retinal ganglion cell
RPE	Retinal pigment epithelium
Sec	Seconds
STY	Strychnine
TLR4	Toll-like receptor subtype 4
TM	Transmembrane domain
TNFα	Tumour necrosis factor α
TTX	Tetrodotoxin
VNUT	Vesicular nucleotide transporter

Brief Contents

Contents

Chapter 1

Introduction

The perception of a visual scene begins when light within the visible range enters the cornea of the eye, projecting onto the surface of the retina, a highly specialised, sensory appendage of the central nervous system (CNS). Regardless of the amount of absolute light reflected by objects in a given field of view, it is the contrast difference between objects that serves as the stimulus processed by the visual system (Kandel et al., 2000; Carpenter, 1984).

The mammalian visual system, by adjusting its sensitivity accordingly, has a remarkable ability to function over a substantial range of luminances. This allows it to reliably discriminate contrast changes against varying levels of background illumination (Dowling, 2012). Visual sensitivity is inversely related to visual threshold, which is the minimum light intensity required to evoke a visual response. In turn, visual threshold is directly proportional to background illumination. Thus, low background illumination produces a lower visual threshold, which results in a higher visual sensitivity. The ability of the retinal circuitry to adapt to light and dark background luminances ensures that visual sensitivity is maintained, regardless of extreme ambient light intensities (Kandel et al., 2000; Dowling, 2012).

Some differences in the visual pathway between vertebrate species exist. However, the fundamental aspects of retinal processing remain relatively conserved between the different species due to the same basic organisation of the retinal circuitry (Dowling, 2012). Rod-dominated mammals such as the mouse are physiologically more adapted for scotopic and low mesopic vision (Huberman and Niell, 2011). The present discussion will describe the

basic circuitry and cellular organisation of the mammalian retina, with a focus on the processing of visual information mediated through the vertical rod pathways (fig. 1.1).

1.1 ON and OFF centre-surround receptive field organisation

Contrast-dependent aspects of the visual scene are processed by ON and OFF parallel channels that are formed at the level of the bipolar cells, and remain segregated throughout the visual pathway until integration in the brain. ON subclasses respond to light increments and OFF cells respond to light decrements (Schiller, 1992). Bipolar and retinal ganglion cells have concentric antagonistic centre-surround receptive fields (Kuffler, 1953; Dacheux and Miller, 1981). An ON-centre cell discharges when light is directed to the centre of its receptive field, but is inhibited when the surround is illuminated by a ring of light. Conversely, an OFF-centre cell is inhibited by a light stimulus directed to its centre, but fires when the centred illumination is removed, or when its surround is illuminated (Schiller, 1992). Thus, the opposite polarities of ON- and OFF-centre cells and their surround render them optimally responsive to differential stimulation of their receptive fields. For both ON- and OFF-centre types, collective stimulation of centre and surround regions of their receptive fields result in attenuated centre-dominant responses (Schiller, 1992). Retinal ganglion cells may also respond to both onset and termination of stimuli, and are termed ON-OFF cells. In the dark-adapted state, the surrounds of the receptive fields are significantly attenuated (Schiller, 1992, 2010).

1.2 Cellular Organisation of Retinal Circuitry

The mammalian retina is a transparent tissue with a thickness of 200 – 300 μm (Buttery et al., 1991). Its laminar structure comprises three nuclear and two plexiform (synaptic) layers, containing five major classes of neurons: photoreceptors, bipolar cells, horizontal cells,

amacrine cells and retinal ganglion cells. The retina also consists of three dominant classes of glial cells: Müller cells, astrocytes and microglia (Dowling, 2012).

1.2.1 Photoreceptors

The rod and cone photoreceptors are the light-sensitive neurons, and can be distinguished on the basis of their morphology and biochemical (visual pigment) composition. Both cell types are comprised of an outer segment which protrudes towards the retinal pigment epithelium, a nucleus-containing inner segment that resides in the outer nuclear layer (ONL), and a mitochondria-rich synaptic terminal in the outer plexiform layer (OPL) (Sjöstrand, 1953; Carter-Dawson and LaVail, 1979). The outer segment is comprised of numerous stacks of membranous discs, which contain the photosensitive opsin proteins (Sjöstrand, 1953). Rods contain the visual pigment rhodopsin, which optimally absorbs light quanta of wavelength ~500 nm, and are maximally sensitive under low light (scotopic) conditions (Wald, 1968). Cones use alternative visual pigments that optimally absorb light of different wavelengths (short, medium or long), and which form the basis of chromatic discrimination, under higher luminance (photopic) levels (Wald, 1968). The adult mouse retina is dominated by rod cells, with cones forming less than 3% of the photoreceptor mosaic (Carter-Dawson and LaVail, 1979; Jeon et al., 1998). Light traverses the full thickness of the retina, before it is mostly absorbed by the photoreceptors, which transduce the subsequent chemical changes in their visual pigment into electrical signals that are then propagated to bipolar cells in a vertical processing pathway in the outer plexiform layer.

1.2.2 Bipolar Cells

In the mammalian retina, there are at least ten subtypes of bipolar cells, one of which synapses exclusively with rod photoreceptors, whereas the others are cone-related (Kolb,

1970; Boycott and Kolb, 1973; Kolb et al., 1981). Further subdivisions of these interneurons are established on the basis of the size of their dendritic trees, the types of synaptic connections made with their respective photoreceptors, and in which sublamina of the inner plexiform layer their axons terminate. The dendrites of rod-bipolar cells form invaginating synapses with rod terminals, termed rod spherules, and their axon terminals end in the proximal part (sublamina b) of the inner plexiform layer, indicating that these cells are of the ON-type. Similarly, the dendrites of cone-BCs that form invaginating synapses with cone terminals (cone pedicles) also have terminating axons in the proximal sublamina b of the inner plexiform layer. The dendritic arbour size of rod-BCs is considerably larger than that of cone-BCs**.** Another cone-BC, which forms superficial synaptic contacts along the flattened base of the cone terminal, with its axon terminating in the distal part (sublamina a) of the inner plexiform layer, is known as the flat- or OFF-bipolar cell. In general, the cell bodies of invaginating BCs, whether rod- or cone-related, reside in the distal part of the inner nuclear layer, whereas those of the flat-BCs lie more centrally within the inner nuclear layer (Dowling, 1970; Kolb, 1970; Boycott and Kolb, 1973; Kolb et al., 1981; Ghosh et al., 2004).

1.2.3 Horizontal and Amacrine Cells

Lateral inhibitory inputs to photoreceptor and bipolar cell terminals are formed by horizontal cells in the outer plexiform layer, which contribute to the bipolar cell antagonistic centre-surround receptive fields under photopic conditions. As a generalisation of the mammalian retina, the axon terminals of HCs end exclusively in the rod terminal, where a single bipolar cell process is flanked by two lateral HC processes within the rod spherule. Conversely, the dendritic terminals of HCs connect exclusively to cone pedicles, thus forming a unidirectional signal transduction pathway. The cell bodies of horizontal cells reside in the distal part of the inner nuclear layer (Kolb, 1970, 1974; Boycott, 1988; Trümpler et al., 2008). The contribution of horizontal cells to rod ON-bipolar receptive fields remains controversial as these bipolar

cells have considerably weak or no antagonistic surround (Bloomfield and Xin, 2000; Bloomfield and Dacheux, 2001).

The lateral inhibitory pathways in the inner plexiform layer are formed by amacrine cells, the cell bodies of which are located in the proximal part of the inner nuclear layer. These interneurons are the most heterogeneous cell-type in the retina, with 20 to 30 morphological variations described in the mammal (Kolb, 1997). The most important type in the functioning of the rod pathway is the AII amacrine cell, and is amongst the most common AC type in the mammalian retina. The AII cell has a narrow dendritic field, with lobular appendages that receive input from rod-BCs, while its output occurs through gap junctions to ON cone-BCs in sublamina b of the IPL. OFF cone-BC terminals in sublamina b, and ON-centre ganglion cell dendrites in sublamina a of the IPL also receive direct synaptic input from AII cells (Kolb et al., 1981; Strettoi et al., 1992).

1.2.4 Ganglion Cells

Ganglion cells are the final output neurons of the retina, carrying the visual signal along the optic nerve to the brain. Classically, mammalian retinal ganglion cells fall into three distinct groups (alpha, beta and gamma), corresponding to their morphological and functional properties. All groups contain cells that exhibit concentric centre surround organisation. Their cell bodies reside in the ganglion cell layer and dendritic processes branch in IPL sublamina a (OFF), b (ON), or both (ON-OFF). The sizes of the dendritic trees and receptive fields are comparable (Wässle, 2004; Balasubramanian and Sterling, 2009). Alpha cells have large dendritic tree (approx. 200 µm in mouse) and axon diameters, whereas those of beta cells are relatively smaller. The circular dendritic trees of alpha and beta cells are arranged in regular arrays to cover the whole retinal surface, with minimal overlap of their peripheral

processes. The dendritic tree size and density of alpha and beta cells exhibit an inverse relation whereby the dendritic trees are large and cell density is low in the peripheral retina, whereas the opposite is apparent in the central retina (Wässle, 2004). Additionally, ON- and OFF-centre sub-types are always arranged as pairs, which cover the same visual field (Peichl and Wässle, 1979). Alpha cells exhibit brisk-transient responses that are a function of non-linear inputs originating in presynaptic bipolar and amacrine cells. The latency and conduction times of alpha cells are fast, compared to those of the beta cell, allowing alpha cell visual responses to reach the brain earlier. Beta cell responses are brisk-sustained and exhibit characteristics of linear spatial summation, which may reflect a direct and dominant input component from bipolar cells (Wässle, 2004).

The mammalian retina consists of at least 18 to 23 morphologically distinct ganglion cells. In the rod-dominant cat retina, approximately 3% of ganglion cells are of the alpha type, whereas beta cells comprise 50% of total ganglion cells (Kolb et al., 1981). The rod-dominant mouse retina, in which 22 morphological types have been characterised (Völgyi et al., 2009), most likely corresponds to the ganglion cell ratios of the cat. It is thought that more complex features of the visual image are encoded by other retinal ganglion cells that fall into the gamma cell group. These include direction-selective cells, which are bi-stratified ON-OFF cells and respond transiently to a stimulus moving in a preferred direction (Wässle, 2004). Additionally, visual pigment-containing intrinsically photosensitive ganglion cells have been identified in the mouse retina. Others include ganglion cells that are specifically responsive to approaching stimuli, particular orientations or edges. The dendritic trees of each cell type provide complete coverage of the retinal surface. Thus, a full-field light stimulus is capable of activating many ganglion cells of any given type (Wässle, 2004).

The retina exhibits a substantial convergence of neurons from the outer to the inner layers, along the vertical pathways. In the rod system alone, a single beta ganglion cell receives input from 1500 rods, 100 rod ON-BCs and 5 AII cells (Sterling et al., 1988), indicating the integration of an array of afferent inputs to encode a diverse range of complex functional features in the visual scene. Further, alpha and beta cells in rod-dominant mammals do not appear to specifically encode scotopic or photopic pathways, as the responses of these cells are generally comprised of mixed rod and cone signals (Enroth-Cugell, 1977). Importantly, regardless of the visual feature they encode, all ganglion cell types exhibit concentric ON-, OFF- or ON-OFF-centre surround organisation.

1.2.5 Glial Cells

The mammalian retina generally contains three main types of glial cells. Müller cells and astrocytes constitute the major retinal macroglial populations, which have numerous functions including providing metabolic support to neurons. Retinal astrocytes are largely restricted to the RGC axon-containing nerve fibre layer and are not thought to play a significant role in modulating neuronal function within the retina (Newman, 2004). Microglia are the resident immune cells of the retina, and are imperative for orchestrating the neuroinflammatory response to metabolic stressors and other foreign bodies in the microenvironment (Streit et al., 1999; Chen et al., 2002; Langmann, 2007).

1.2.5.1 Müller glia

Müller cells are radial glia. They typically span the entire thickness of the retina, with their nucleus residing centrally, in the INL. Each of the distal and proximal portions of the retina contains a broad Müller cell process protruding from the soma, to form membranous regions at either end of the tissue. Müller cells form junctions homogenously, and with photoreceptor

inner segments to form the outer limiting membrane. In the GCL, the processes expand into end feet, which form the inner limiting membrane, between the retinal tissue and the vitreous humour. All other retinal cell bodies and processes are typically in close proximity of the finer Müller glial processes which extend laterally from the main body. Müller cells are important in regulating potassium ion (K^+) flux in the extracellular space, as well as regulating neurotransmitter uptake, and thus may play a role in shaping visual responses in the retina (Dowling, 1970; Miller and Dowling, 1970; Dreher et al., 1992; Bringmann et al., 2006).

1.2.5.2 Microglia

Microglia in the healthy mammalian retina reside predominantly in the outer and inner plexiform layers (Hume et al., 1983; Perry et al., 1985; Ashwell et al., 1989; Santos et al., 2008) (fig. 1.3). Microglia are highly ramified in structure, with numerous processes when in their 'resting' state, but are thought to be far from quiescent. These immune cells constantly monitor neuronal synapses in their locality, as shown in other areas of the CNS (Béchade et al., 2013), although very little is known of these microglial functions in the retina. Activated microglia typically take on an amoeboid appearance, with few, short or no processes, and have the capacity to secrete a vast array of molecular signals, including cytokines, chemokines, ATP and reactive oxygen species, all of which trigger further inflammatory cascades. These activated microglia proliferate and migrate to the site of cellular stress, and provide imperative trophic support to the injured neuron, in addition to phagocytosing surrounding cellular debris (Streit et al., 1999; Chen et al., 2002; Langmann, 2007) (fig. 1.4).

1.3 Synaptic Mechanisms and Neurochemistry

All neuronal cells in the retina respond to illumination with slow, graded membrane potentials, with the exception of retinal ganglion cells, which respond by firing action

potentials. The ON and OFF vertical signalling pathways and their modulation by lateral interactions, are a result of the array of neurotransmitters and their receptors that mediate synaptic transmission between the cells of the retina (Schiller, 1992, 2010). The major excitatory neurotransmitter in the retina is glutamate, with γ-aminobutyric acid (GABA) and glycine as the major inhibitory neurotransmitters.

1.3.1 Outer Retinal Processing

The phototransduction cascade, which converts the absorption of photons into an electrical signal, is shown in fig. 1.2. The propagation of a light-evoked response from the rod photoreceptor to the rod-bipolar cell occurs within a specialised, invaginating structure, the rod spherule (Kolb, 1970; Carter-Dawson and LaVail, 1979; Singer, 2007). The dendritic process of the rod-bipolar cell is directly apposed to the rod photoreceptor glutamate release site, the ribbon synapse (Nomura et al., 1994). These synapses are elongated structures that allow the rapid and continuous release of glutamate-containing vesicles into the extracellular space, and are thus specialised for the transmission of analogue signals (Lagnado, 2000; Holt et al., 2004). Glutamate is tonically released from photoreceptors in the dark, through a tightly regulated calcium-dependent mechanism (Okawa and Sampath, 2007). Rod-bipolar cells are continuously hyperpolarised through the activation of the group III metabotropic glutamate receptor, mGluR6, which is located on the rod-bipolar dendrite (Slaughter and Miller, 1981; Massey et al., 1983; Nawy and Jahr, 1990; Masu et al., 1995). The activation of mGluR6 stimulates the hydrolysis of cGMP, a G-protein-activated mechanism that results in the closure of cation channels, believed to be of the transient receptor potential (TRP) family (Morgans et al., 2009). Thus, rod-bipolar cells are maintained in a hyperpolarised state in the dark. A light stimulus results in the cessation of glutamate release from photoreceptors and the subsequent depolarisation of rod-bipolar cells, likely due to the opening of TRPM1 channels (Nawy and Jahr, 1990; Shiells and Falk, 1990;

Nakajima et al., 1993; Morgans et al., 2009). The fast excitatory responses of OFF bipolar cells were determined to be mediated by the activation of ionotropic AMPA receptors (Sasaki and Kaneko, 1996). Therefore, the continuous glutamate release in the dark tonically depolarises OFF-bipolar cells, which become hyperpolarised during the light-evoked cessation of glutamate release.

Inhibitory horizontal cell axon processes are also located within the rod spherule, with their dendrites positioned postsynaptically to cones (Kolb, 1970, 1974). Similar to OFF-bipolar cells, horizontal cells are depolarised in the dark, and hyperpolarise in response to light, due to the expression of AMPA/KA receptors on the cell surface (Cohen and Miller, 1999). The role of horizontal cells in modulating bipolar cell centre-surround receptive fields remains unclear (Bloomfield and Dacheux, 2001). However, electrical coupling through gap junctions and inhibitory GABAergic feedback to cones are mechanisms that are thought to play a role. Interestingly, rod-bipolar cells do not display antagonistic surround properties under scotopic conditions (Bloomfield and Xin, 2000). Indeed, it is widely believed that rod-mediated signals are not largely influenced by horizontal cell feedback (Bloomfield and Dacheux, 2001).

1.3.2 Inner Retinal Processing

The presynaptic rod bipolar cell terminals convey the light-evoked signal to ON- and OFF-centre ganglion cells in the inner plexiform layer, through internuncial AII amacrine cells (Bloomfield and Dacheux, 2001). Bipolar cells make glutamatergic ribbon synapses with their postsynaptic structures, although they are not of the invaginating type as in the outer plexiform layer. Typically, two postsynaptic processes from separate amacrine cells are located directly apposed to the bipolar cell axon terminal ribbon, making an arrangement known as a dyad (Grunert and Martine, 1991; Strettoi et al., 1992; Kolb, 1997). Reciprocal inhibitory feedback onto rod bipolar cell terminals may be driven by a GABAergic AC

process, within the dyad. In the mammalian retina, ionotropic $GABA_A$ receptors have been localised to amacrine, bipolar and ganglion cells, suggesting a role in both pre- and postsynaptic modulation, whereas $GABA_c$ receptors have only been found presynaptically on bipolar cells, indicating a specific role in feedback inhibition of bipolar cell output (Wässle et al., 1998). The other half of the rod bipolar cell output is directed towards the AII amacrine cell process, which transfers the scotopic signal to the ganglion cell. The rod-mediated pathway does not consist of separate ganglion cells specifically for scotopic signal processing. Thus, ganglion cells typically receive mixed signals from both rod- and cone-mediated pathways.

In the proximal part of the inner plexiform layer, AII processes are coupled to ON-cone bipolar cell terminals via excitatory gap junctions (Kolb, 1997), mediating the transfer of scotopic signals through a feed-forward mechanism. In turn, the ON-cone bipolar cells convey the scotopic signal to ON-centre ganglion cells via conventional glutamatergic synapses. Conversely, the AII amacrine cell transfers the rod-mediated OFF signal to OFF-cone bipolar cells via an inhibitory glycinergic synapse. As with the ON pathway, the OFF signal is then propagated from the OFF-cone bipolar cell to the OFF-centre ganglion cell through an excitatory synapse (Bloomfield and Dacheux, 2001).

ON- and OFF-centre retinal ganglion cell responses are mediated by the activation of post-synaptic AMPA/KA and NMDA receptors (Brandstätter et al., 1998). Retinal ganglion cells produce depolarised responses in the presence of the agonists, AMPA, KA and NMDA, and are inhibited by their respective antagonists (Slaughter and Miller, 1983; Lukasiewicz and Mcreynolds, 1985; Coleman and Miller, 1988; Boos et al., 1990; Massey and Miller, 1990; Mittman et al., 1990; Ikeda et al., 1992; Yazejian and Fain, 1992; Zhou et al., 1994; Lukasiewicz et al., 1995, 1997). Thus, it is established that cone bipolar cells also release

glutamate, directly onto ganglion cell dendrites. The relative synaptic arrangement and properties of AMPA and NMDA receptors has been suggested to contribute to the range of processing in the inner plexiform layer. Furthermore, glutamate transporters and their function in glutamate clearance from the synapse is also thought to play an important role in shaping retinal ganglion cell responses (Higgs and Lukasiewicz, 1999; Lukasiewicz, 2005). In the dark-adapted state, the receptive field properties of ganglion cells are known to alter in parallel to a shift from cone- to rod-mediated pathways. The ganglion cell receptive field centre increases in size, with surround inhibition diminishing accordingly. This results in ganglion cell responses becoming more sustained and characteristic of their centre response (Sharpe and Stockman, 1999; Bloomfield and Dacheux, 2001).

Alternative pathways for rod-mediated scotopic signal transmission have also been characterised. Rod-cone gap junction coupling is thought to play a role under higher luminance levels, possibly in the mesopic range. Through this pathway, rods directly transfer their signal to ON and OFF cone bipolar cells and then to their corresponding ganglion cells, bypassing the requirement for the internuncial AII cells. Additionally, a direct transfer of the rod signals to the OFF cone bipolar cell has also been found, via a flat, conventional synapse (Sharpe and Stockman, 1999; Bloomfield and Dacheux, 2001; Bloomfield and Völgyi, 2009). Rod and cone circuitry for signal transmission under dark-adapted conditions is summarised in fig. 1.1.

Chapter 1 Figures

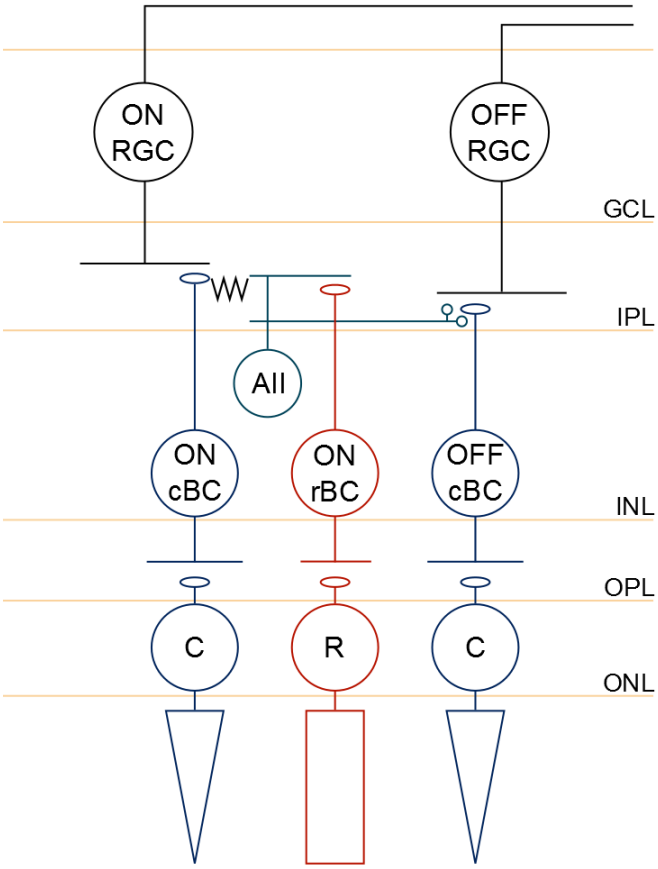

Figure 1.1 Rod and cone circuitry for signal transmission under dark adapted conditions. The pathways illustrated are highly schematic and focus on rod-mediated transmission of light-evoked signals, which is the dominant pathway under scotopic and low mesopic conditions. Rod and cone pathways are concurrent, but the rod-mediated signal is transduced to the inner retina via cone circuitry. Light increments and decrements are processed by ON and OFF sub-classes of cells, respectively. Rod and cone photoreceptors release glutamate, which induces a sustained hyperpolarisation of ON rod and cone bipolar cells (rBC and cBC, respectively) through the constitutive activation of group III metabotropic glutamate receptors (mGluR6), within ribbon synapses. Under low light conditions, OFF cBCs are concomitantly depolarised through the activation of ionotropic glutamate receptors (AMPA/KA - Rs). Light increments suppress rod and cone glutamate release, activating ON rBCs and cBCs. Rod BCs transfer their signal to ON and OFF cBCs through AII amacrine cells via electrical (Cx36) and glycinergic synapses, respectively. Retinal ganglion cells (RGCs) receive signals from cBCs, relaying them to the brain via the optic nerve. Postsynaptic ionotropic glutamate receptors (AMPA/KA- and NMDA - Rs) on both ON and OFF RGCs mediate fast excitatory neurotransmission to transduce the visual signal to the brain. Inner retinal activity and surround responses of cells are highly regulated by amacrine cell-mediated GABAergic signalling (not shown). Direct electrical coupling between rods and cones has also been found in mice, where rod-mediated signals are transduced directly through the cone circuitry, rather than through AII cells (not shown), under higher luminances. ONL, outer nuclear layer; OPL, outer plexiform layer; INL, inner nuclear layer; IPL, inner plexiform layer; GCL, ganglion cell layer.

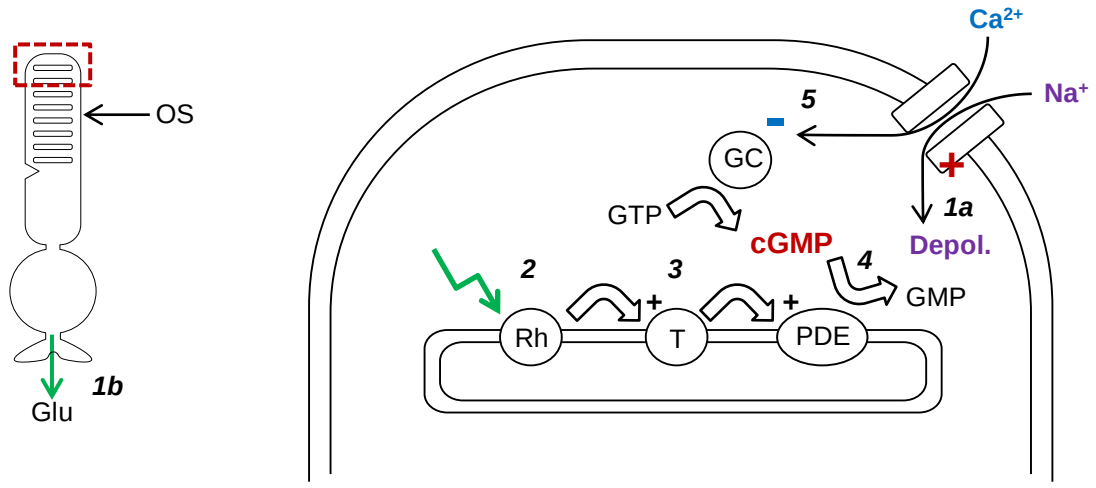

Figure 1.2 Phototransduction cascade. The outer segment (OS) of rod photoreceptors (left) contains numerous membranous discs, which provide the site for phototransduction. The cascade shown here (right) is highly schematic, and focuses on the main enzymatic steps required to transduce a light-evoked signal into an alteration in photoreceptor membrane potential. ***1a***, In the dark-adapted state, rods contain a high concentration of the second messenger molecule, cyclic guanosine 3', 5'-monophosphate (cGMP), which activates cGMP-gated cation channels in the outer segment. Thus, under such conditions, a dark current is carried by the inward flux of sodium ions (Na^+) at the outer segments, which maintains the rods in a depolarised state, constitutively releasing glutamate (***1b***). ***2***, The absorption of a photon by rhodopsin triggers a cascade of events that ultimately results in altered ion flux across the photoreceptor membrane, and thus leads to a change in membrane potential. Rhodopsin is a G-protein-associated molecule, comprised of 11-cis-retinal, a chromophore, and an opsin protein. Light-induced bleaching of the photopigment triggers a series of biochemical steps that break down rhodopsin into 11-trans-retinal and opsin. ***3***, An intermediate form of the breakdown process, metarhodopsin II, subsequently mediates the activation of phosphodiesterase (PDE), via the interaction of transducin (T). ***4***, PDE hydrolyses the second messenger molecule cGMP, leading to the closure of cGMP-gated channels and the subsequent hyperpolarisation of the rod plasma membrane. The deactivation of metarhodopsin II, transducin and PDE results in the cessation of the phototransduction cascade. During light exposure, rod sensitivity is maintained due to its capacity to regenerate the rhodopsin pigment, and its ability to partially recover from the initial light-evoked hyperpolarisation. The 11-trans-retinal product formed upon bleaching of rhodopsin is transported to the RPE, where it is then converted back to 11-cis-retinal through a series of biochemical stages. Ultimately, 11-cis-retinal is transported back into the rod outer segments to bind with opsin and regenerate rhodopsin. Visual threshold varies with the proportion of regenerated rhodopsin. ***5***, In the dark-adapted state, intracellular calcium concentration is relatively high, attenuating the action of guanylate cyclase (GC), a cGMP-generating enzyme. The light-induced closure of cGMP-gated cation channels results in a fall in intracellular calcium, which subsequently enhances guanylate cyclase-mediated cGMP generation. Thus, the increase in cGMP results in the opening of cation channels in the outer segment and the partial recovery of the rod photoreceptor towards its depolarised state. Figure partially reproduced from Dowling (2012).

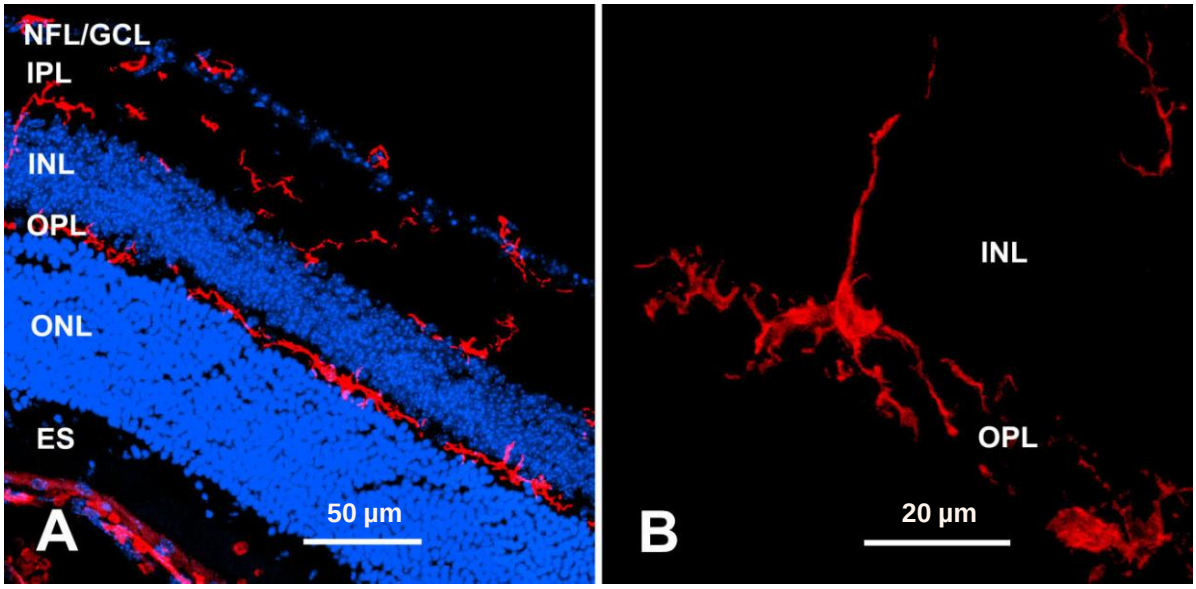

Figure 1.3 Distribution of microglia in the mouse retina. *A*, Transverse sections show the dispersion of resident monocytes of the retina, immunolabelled for the microglia-specific molecular marker IBA1 (red). In the healthy adult mouse retina, microglia are located almost exclusively in the outer and inner plexiform layers, and ganglion cell layer, but not in the nuclear layers (Hoechst-staining; blue). *B*, A ramified microglial cell, with its soma and processes residing in the outer plexiform layer. A single process extending from the microglial cell body traverses into the inner nuclear layer. Adapted from Santos et al. (2008).

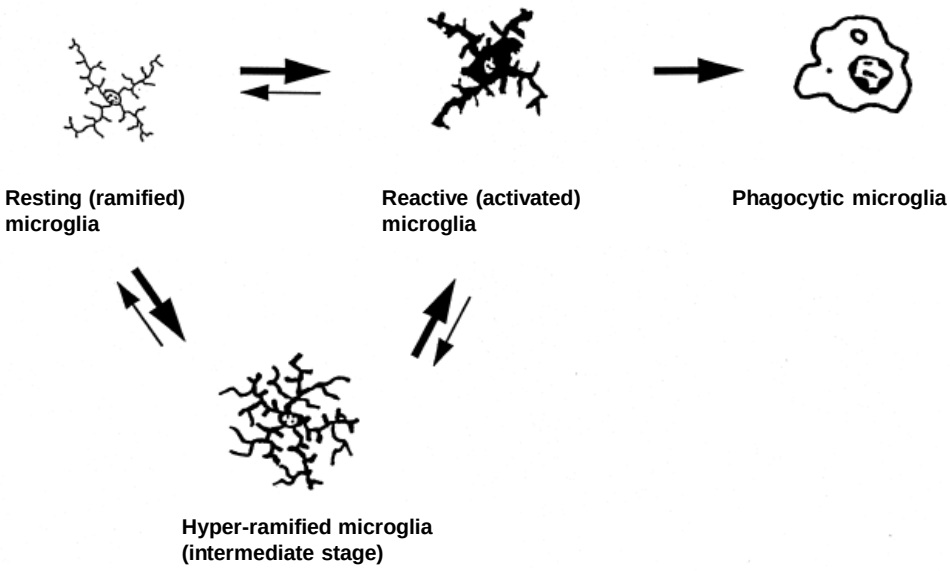

Figure 1.4 Functional states of microglia. Activation of microglia is a highly graded phenomenon, and largely dependent on specific molecular triggers present in the microenvironment. The figure illustrates the fundamental concept of three main microglial activation states, and highlights the potential occurrence of 'alerted' cells. Under physiological conditions, microglia reside in their 'resting' state. Cells of this functional phenotype exhibit typically long and thin processes that branch out and ramify. The processes are highly dynamic and constantly survey their microenvironment for any potential molecular 'danger' signals (e.g. ATP). Loss of constitutive calming signals, or the presence of mild activating triggers due to trauma or other stressors, may lead to a transition to an 'alerted' state of early activation, where microglia may appear hyper-ramified. Microglia become 'reactive' in the presence of damaged neurons and systemic influences. Such cells have characteristically shorter and thicker processes. If neuronal recovery is apparent, reactive microglia may revert back to a relatively resting state, and may also exhibit a post-activated phenotype. However, if neuronal damage persists, reactive microglia shift to a fully activated and phagocytic phenotype which appear amoeboid in shape, with very few or no processes. At this point, microglia may undergo cell death. Specific arrays of molecular markers are released by microglia, at each functional stage. Therefore, alterations in microglial morphology are important indicators of changes in microglial function. (Figure, Streit et al., 1999; Hanisch and Kettenmann, 2007).

Chapter 2

Extracellular ATP in the Retina

The purinergic nucleotide, ATP (adenosine 5' triphosphate), is abundant in all metabolically active cells. As an ubiquitous intracellular molecule, ATP acts as a biochemical currency of energy linked with various metabolic pathways. ATP is readily releasable and also acts as an extracellular signalling molecule associated with the activation of neuroinflammatory pathways and the modulation of neuronal synaptic transmission. The purinergic signalling system is widespread throughout the central and peripheral nervous systems (Burnstock, 2007), and appears to act as a bi-directional signal in neural-immune interactions. As a neuroactive molecule in the PNS, ATP mediates fast excitatory and inhibitory synaptic signalling to smooth muscle (Burnstock et al., 1970, 1972). In the CNS, ATP contributes to glutamatergic input to postsynaptic neurons (Pankratov et al., 1998), and in some areas, may itself evoke excitatory postsynaptic currents (Edwards et al., 1992). ATP is also released by non-excitable cells, including macroglial and microglial populations in the CNS (Ferrari et al., 1997; Newman, 2001), and may act as a gliotransmitter to modulate neuronal excitability. As a component of the innate immune system, ATP is considered as a danger-associated molecule, crucial for the activation of astrocytes and microglia, and the induction of early inflammatory pathways under pathological conditions (Ferrari et al., 2006). Furthermore, extracellular ATP is typically released from reactive astrocytes and acts as a chemoattractant for microglia, which in turn may release more ATP in a positive feedback mechanism. Thus, ATP is associated with neuropathic pain, trauma, ischemia and the exacerbation of various neurodegenerative diseases (Burnstock et al., 2011). The present discussion considers mechanisms of storage, release and degradation of ATP in the mammalian retina.

2.1 ATP storage and release in the retina

The bulk of intracellular ATP is generated by mitochondrial oxidative phosphorylation, within the cell (Sperlagh and Vizi, 1996), rendering all metabolically active cells potential sources of ATP secretion into the extracellular microenvironment. Under physiological conditions, the typical cytoplasmic concentration of ATP ranges between 1-10 mM (Fukuda et al., 1983; Sperlagh and Vizi, 1996)**.** Damage to the integrity of the cell membrane could result in the cytolytic release of ATP into the extracellular environment, as a result of cell necrosis. Additionally, various mechanisms of controlled ATP release have been identified. In the CNS, activity-dependent ATP release from neurons can occur through the exocytosis of ATP-containing synaptic vesicles (Abbracchio et al., 2009). Extrasynaptic and non-vesicular pathways, for example through volume-regulated anion channels (VRAC) and gap junction-related pores such as connexins and pannexins, have also been shown in neurons. Similar non-vesicular mechanisms of ATP release have been identified in glia, epithelial cells and other non-neuronal populations (Fields, 2011). These also include the cystic fibrosis transmembrane conductance regulator (CFTR), which is associated with the ATP-binding cassette (ABC) family of transporter proteins. In general, non-vesicular mechanisms of ATP release tend to occur under conditions that evoke the activation of inflammatory pathways, such as damage to the cell membrane, hypoxia, mechanical stress and cell death, although there are some notable exceptions, involving vesicular ATP release from non-neuronal cells Thus, activation of such mechanisms is dependent upon a diverse array of stimuli. In the retina, various ATP secretory pathways from both neuronal and non-neuronal cells have been identified.

2.1.2 ATP release from non-neuronal cells in the retina

ATP efflux from RPE cells into the subretinal space is suggested to occur through a variety of distinct, stimulus-dependent mechanisms, and appears important for communication

between the RPE and photoreceptor outer segments (Mitchell and Reigada, 2008). The RPE is essential for photoreceptor function, and plays a significant supporting role in the regeneration of the rhodopsin visual pigment, shedding and regeneration of photoreceptor outer segments, and the homeostatic regulation of extracellular ionic concentrations within the subretinal space (Mitchell and Reigada, 2008). ATP release from human RPE cells can be triggered by hyperosmotic stress (Eldred et al., 2003). Glutamate- and NMDA-dependent ATP release was shown to occur from cultured human ARPE-19 cells through a calcium-related mechanism. The calcium-dependence of this effect was inhibited by apyrase-hydrolysis of ATP (Reigada et al., 2006). Importantly, low micromolar concentrations of ATP triggered secondary ATP release approximately 10 min post-initial ATP application (Reigada et al., 2005)**,** supporting the notion that ATP acts as an autostimulatory signal to amplify itself within the local microenvironment. Alternative secretory pathways have also been identified by the same authors, involving CFTR-dependent ATP efflux as well as vesicular ATP secretion from human cultured RPE cells as a result of hypotonic challenge (Reigada and Mitchell, 2005). Furthermore, calcium elevation-triggered ATP release from the RPE through connexin hemichannels, during retinal development has also been characterised (Pearson et al., 2005).

Glial cells in the retina are likely to have a more direct modulatory role in synaptic transmission than other non-neuronal cell types. Müller cells have shown to act as sources of extracellular ATP. Although the precise release pathway is unclear, these glial cells release ATP upon mechanical stimulation, a mechanism mediated by the propagation of intercellular calcium waves through gap junctions (Newman, 2001). In addition, a glutamate-mediated, calcium-independent ATP release mechanism has been identified in Müller cells that have undergone hypotonic stress (Uckermann et al., 2006).

Conversely, mechanisms of ATP release from retinal microglia remain uncertain. In rat brain cultures, these resident immune cells are known to express functional nucleotide-releasing machinery associated with ABC proteins such as CFTR, which when inhibited, prevented microglial ATP efflux (Ballerini et al., 2002). Furthermore, macrophages express pannexin-1 hemichannels, which are directly involved in the ATP-mediated release of the pro-inflammatory cytokine, IL-1β (Pelegrin and Surprenant, 2006, 2009). On neurons, pannexin-1 has been shown to act as a conduit for ATP release (Xia et al., 2012), thereby suggesting that microglial ATP-release could also occur through this pore.

2.1.3 ATP release from neuronal cells in the retina

A number of release pathways associated with the exocytosis of ATP-containing vesicles at central synapses, have been identified. The concentration of ATP within a synaptic vesicle ranges between 1 – 200 mM, and has been found to be packaged together with other classical neurotransmitter molecules (Sperlagh and Vizi, 1996; Pankratov et al., 2006). Thus, ATP co-release has been shown in cholinergic (rat caudate nucleus), glutamatergic (hippocampus) and GABAergic synapses (hypothalamus and spinal cord) (Richardson and Brown, 1987; Jo and Schlichter, 1999; Mori et al., 2001; Jo and Role, 2002). ATP release also occurs from separate pools of vesicles or from separate ATPergic neurons altogether (Robertson and Edwards, 1998; Pankratov et al., 2007). ATP release was not detected in the absence of calcium, in rodent hippocampal slices and rat caudate nucleus synaptosomes, suggesting that the release of ATP-containing vesicles from presynaptic terminals is calcium-dependent (Richardson and Brown, 1987; Wieraszko et al., 1989). In the retina, the calcium-dependent endogenous ATP release was shown in cultures enriched in amacrine cell-like neurons (Santos et al., 1999).

ATP is incorporated into synaptic vesicles through the chloride-dependent vesicular nucleotide transporter (VNUT), which is highly expressed in the brain and adrenal glands (Sawada et al., 2008). In the retina, VNUT mRNA was detected in laser micro-dissected sections of the photoreceptor, inner nuclear and ganglion cell layers (Vessey and Fletcher, 2012). The presence of retinal VNUT raises the possibility of synaptic ATP release in the outer and inner retinal layers, where it may directly modulate visual processing along the vertical pathways. However, the exact localisation of the transporter at retinal synapses, as determined by immunohistochemistry, is yet to be clarified.

Non-vesicular, mechanical strain-induced ATP release from retinal ganglion cells has also been characterised. This effect was found to be mediated by pannexin-1 hemichannels, which themselves require an autostimulatory ATP signal (Xia et al., 2012). Ganglion cells in the isolated rat retina have shown to release ATP in response to light illumination, an effect which is blocked by suramin and TTX (Newman, 2005). Additionally, glutamatergic depolarisation of cultured amacrine-like neurons evoked release of ATP, which was found to be dependent on calcium influx through voltage-gated channels (Santos et al., 1999).

2.2 Degradation of extracellular ATP in the retina

Once ATP is released into the extracellular environment, it is rapidly hydrolysed into its derivatives (ADP, AMP and adenosine) by the action of ectonucleotidases enzymes, residing on the external side of the plasma membrane (Zimmermann, 2000; Burnstock, 2007). Various families of ectonucleotides have been described, including ectonucleoside triphosphate diphosphohydrolase (E-NTPDase) and ectonucleotide pyrophosphatase/phosphodiesterase (E-NPP). Both types of ecto-enzymes have been localised in human RPE cells (Mitchell and Reigada, 2008). Müller glial cells are immunoreactive for E-NTPDases, although there is some dispute over whether these are of

the E-NTPDase-1 or -2 subtype (Iandiev et al., 2007; Ricatti et al., 2009). Microglia in the neural parenchyma abundantly express an array of ectonucleotidases, suggesting that these cells are proficient in the control of extracellular ATP concentration (Dalmau et al., 1998). Prominent immunoreactivity for E-NTPDase was localised to the inner and outer plexiform layers in the mouse retina. E-NTPDase-1 was primarily expressed in the ganglion cell layer, and on horizontal cell processes, with some pre-synaptic expression in the inner plexiform layer. Conversely, E-NTPDase-2 was principally localised to ON-bipolar cell dendrites in the outer plexiform layer (Ricatti et al., 2009). Functional ectonucleotidases activity in both the inner and outer plexiform layers of the rat retina have been characterised (Puthussery et al., 2006; Puthussery and Fletcher, 2007). The authors employed an enzyme histochemical assay whereby the negatively charged phosphate generated during ATP-degradation, forms an electron-dense product when reacted with positively charged cerium ions. This reaction product was heavily localised to the plexiform layers but not to the ganglion cell layer (Puthussery et al., 2006). This is in contrast to the E-NTPDase-1-specific immunoreactivity seen in the mouse GCL, and highlights a limitation of the enzyme histochemical assay, that the specific ectoncleotidase subtype cannot be distinguished. In summary, ectonucleotidases are profusely expressed in the rodent retina, primarily in the outer and inner plexiform layers, which strongly suggests that ATP is present as a bioactive ligand in the mammalian retina, with a highly abundant system in place to eliminate excess ligand.

2.3 ATP receptors

ATP-gated neurotransmission occurs through the activation of G-protein coupled P2Y or ATP-mediated P2X-gated ion channel receptor subtypes. There are seven subtypes of P2X receptors (1-7), each of which can mediate fast neurotransmission through the opening of small cationic ion channels when activated by ATP (North, 2002). The $P2X_7$ receptor ($P2X_7R$) is the most diverse receptor subtype of the P2X family in both structure and

function. It has been associated with glial and neuronal pathology and is well-known for its association with the pannexin-1 hemichannel and neuroinflammation (Pelegrin and Surprenant, 2006). Moreover, recent evidence has come to light that $P2X_7Rs$ may play a number of significant roles in the direct or indirect regulation of neurotransmission in the CNS (Sperlágh et al., 2006). Microglia, astrocytes and retinal Müller glial cells all express $P2X_7Rs$ (see Chapter 3) and are thought to be influenced by extracellular ATP through this receptor subtype.

The role of ATP and $P2X_7R$ activation in the neuromodulation of visual responses, through a direct effect on neurons or indirectly through glial activation remains largely unexplored in the mammalian retina. It is therefore the focus of this literature review and subsequent investigation to explore and highlight the role of $P2X_7Rs$ in modulating synaptic signalling, and its association with immunological control of synaptic function in the healthy and pathological central nervous system, and primarily in the mammalian retina.

.

Chapter 3

Properties of $P2X_7Rs$

3.1 Molecular structure of $P2X_7Rs$

The $P2X_7$ receptor ($P2X_7R$) was first isolated and cloned from rat superior cervical ganglia and medial habenula (Surprenant et al., 1996). The receptor subunit is 595 amino acids in length, of which the first 395 residues share 35 to 40% homology with the other P2X receptor subunits (Surprenant et al., 1996). All receptor subunits show basic structural homology of two hydrophobic transmembrane domains (TM1 and TM2) and a large extracellular loop, with both amino and carboxyl termini located intracellularly (North, 2002) (fig. 3.2). However, the $P2X_7R$ carboxyl terminal (295 amino acids) is considerably longer than that found in other receptor subtypes (27-129 amino acids) (Surprenant et al., 1996; Sperlágh et al., 2006). Importantly, the $P2X_7R$ exhibits a biphasic agonist-evoked response, dependent upon the agonist exposure time. Similar to other P2X subtypes, a brief agonist application induces a reversible, transient inward current through a non-selective ion channel, permeable to small cations. Repeated or prolonged agonist application gives rise to a sustained current, which could ultimately lead to cell death, assumed to be associated with the opening of a large pore that is permeable to molecules of high molecular weight (< 900 Da) (Surprenant et al., 1996; Sperlágh et al., 2006). The unique intracellular C-terminus is assumed to contribute significantly, to the pore forming properties of the $P2X_7R$ (Costa-Junior et al., 2011).

The $P2X_7R$ was first functionally characterised in the J774 mouse macrophage cell line. High concentrations of ATP (2-5 mM) rapidly induced a large non-selective conductance ion channel, which was fully reversible (Buisman et al., 1988). This receptor, which was later

termed the P2Z receptor (DiVirgilio, 1995) is upregulated in monocytes and macrophages and is understood to play an important role in cytokine- and ATP-mediated inflammatory responses, often resulting in the activation of apoptotic pathways, through the opening of a cytolytic pore. The study by Surprenant and colleagues (1996), which showed that the P2Z receptor-activation also evoked small ion channel-gated currents, similar to P2X receptors, led to the use of the now generally accepted term, $P2X_7$ receptor.

The characterisation of two distinct $P2X_7R$ properties (transient inward current and pore formation) has generally been carried out in transfected cell expression systems (e.g. HEK293 cells) and macrophage cell lines in which they are known to be natively expressed. While electrophysiological recordings or fluorescent calcium uptake assays have often been used to identify $P2X_7R$-mediated inward currents, the function of the large pore can be examined through the uptake of large fluorescent dyes such as YO-PRO-1 and ethidium bromide, by $P2X_7R$-expressing cells.

3.1.1 ATP binding site

The ATP binding site is proposed to be localised within the 280-amino acid long extracellular loop, a sequence which is generally conserved among P2XR subtypes (Coddou et al., 2011). It is also predicted that the actual ligand-binding domain lies within an anti-parallel six-stranded beta-pleated sheet of the ectodomain, which also contains a cysteine-rich metal-binding domain (Freist et al., 1998).

Site-directed mutagenesis studies of the human $P2X_7R$ have identified specific residues essential for ATP-binding in the $P2X_7R$. A point mutation, which substituted arginine with glutamic acid at residue 307 (R307Q) abolished ATP-mediated barium ion influx and

ethidium dye uptake into peripheral macrophages, although protein levels and surface expression were normal. Furthermore, lysine residues located towards the ends of the extracellular loop are thought to contribute to the formation of the ATP-binding site by interacting with neighbouring P2X subunits, possibly through the formation of disulphide bonds, in the hetero- or homotrimeric receptor complexes (Wilkinson et al., 2006; Marquez-Klaka et al., 2007). Thus, it is proposed that these conserved positively charged lysine and arginine residues may be associated with binding the negatively charged phosphate of ATP (Roberts et al., 2006). Additionally, phenylalanine residues at positions 185 and 291, when mutated to alanine, have been implicated in the binding of the adenine ring of ATP (Roberts and Evans, 2004; Roberts et al., 2006).

The notion that the interface between subunits forms an ATP-binding site, also suggests that there are three possible ligand-binding domains, as P2XRs are only functional when assembled as trimeric complexes. However, the number of ATP molecules needed to activate the receptor remains elusive. Indeed, the $P2X_{2/3}R$ heterotrimer requires only two functional binding sites, although three could be available (Wilkinson et al., 2006). However, it has been suggested that the human $P2X_7R$ contains a total of four, two each of low and high affinity binding sites (Klapperstück et al., 2001). The low affinity binding site has been suggested to correspond to the linearly activating and slowly deactivating $P2X_7R$ currents, while the high affinity binding site is thought to regulate the slowly deactivating current, only. It is not clear whether it is necessary for all binding sites to be occupied for $P2X_7R$ function (Klapperstück et al., 2001). Furthermore, it has been suggested that ATP_4^-, not ATP, is the true ligand that activates the $P2X_7R$, which may explain the low affinity of ATP at the $P2X_7R$, although this notion requires further support (Cockcroft and Gomperts, 1980; Steinberg et al., 1987; Sperlágh et al., 2006).

Thus, the putative ATP binding site is proposed to be located on the interface between adjacent $P2X_7R$ subunits. Although the extracellular domain is generally conserved among the different P2XR subtypes, receptor-specific properties have been revealed in mutagenesis studies (Coddou et al., 2011). Therefore, the exact location of the ligand binding sites, and the number of occupied sites required to activate the functional $P2X_7R$ remain to be determined. Moreover, species differences in the $P2X_7R$ structure further obscure the possible location of the ATP binding site.

3.1.2 $P2X_7R$ subunit assembly and ion channel formation

It is known that all P2XR subunits form functional homo-oligomeric complexes, with the exception of $P2X_6$ (Torres et al., 1999). Furthermore, it was shown that the $P2X_{1-6}$ subunits were able to form functional hetero-oligomeric complexes, with the $P2X_7$ subunit being the exception (Torres et al., 1999). It is now established that the full repertoire of the functional P2XR family include six homomeric channels and six heteromeric channels associated with subunit pairings, which form trimeric structural arrangements (North, 2002; Dubyak, 2007). The notion that $P2X_7R$ subunits preferentially form functional homotrimeric complexes has been the generally supported view (Torres et al., 1999; Nicke, 2008; Boumechache et al., 2009). However, this has been questioned over recent years as it was found that the $P2X_7$ subunit could associate with $P2X_4$ to form functional heteromers (Guo et al., 2007). It has been suggested (Nicke, 2008; Boumechache et al., 2009) that the evidence supporting heterotrimeric $P2X_{4/7}$ complexes was elusive as the agonist-evoked responses might have been due to the formation of individual homotrimeric receptors, instead of the suggested heteromer. Indeed, it could also be possible that a heterotrimeric complex consisting of $2P2X_4/1P2X_7$ or $1P2X_4/2P2X_7$ subunits, give rise to at least one ATP-binding site on the interface between two homomeric subunits. Moreover, a further complexity subsists, as it was found that native $P2X_7Rs$ are expressed as functional hexameric complexes in

peripheral macrophages, whereas they exist as monomers in microglia of the brain (Kim et al., 2001).

The ion channel formed by the activated $P2X_7$ receptor is thought to resemble that of other P2X receptors. The ion pore is lined with both transmembrane domains (TM1 and TM2) of each subunit, giving rise to six domains in total, each contributing to cationic transport across the membrane (Rassendren et al., 1997a; Egan et al., 1998, 2006; Haines et al., 2001). The narrow pore is suggested to be between 8 and 20 Å in diameter (Virginio et al., 1999).

3.1.3 The $P2X_7R$ carboxyl terminus

In recent years, there has been much progression towards understanding the structure-function relationship of the $P2X_7R$, although the precise receptor structure and motif composition still remains to be defined. The carboxyl terminus (C-terminus) of the $P2X_7R$ is currently under intense investigation, as it is proposed to be involved in $P2X_7R$ function and expression, including ion channel gating properties, pore formation (Surprenant et al., 1996; Denlinger et al., 2001; Gu et al., 2001; Adriouch et al., 2002; Wiley et al., 2002; Pelegrin and Surprenant, 2006; Iglesias et al., 2008), cell surface expression and membrane trafficking of the receptor (Denlinger et al., 2003; Smart et al., 2003; Wiley et al., 2003; Feng et al., 2005; Gonnord et al., 2009; Jindrichova et al., 2012), and downstream signalling events associated with receptor phosphorylation and calmodulin binding (Wang et al., 2003; Roger et al., 2008, 2010). A BLAST alignment search for structural motifs in the C-terminus identified that the mouse $P2X_7R$ contained a Src homology domain (SH3; residues 441-460), which was located inside a TNFR1-like death domain (residues 436-508), and a bacterial lipopolysaccharide (LPS) binding site (residues 573-590) (Denlinger et al., 2001). These motifs are likely to bind to intracellular signalling components, and stimulate the activation of specific inflammatory cellular cascades.

In a later study, it was observed that T-lymphocytes from the BALBc mouse strain were more sensitive to ATP stimulation than T-lymphocytes of the C57BL/6 strain (Adriouch et al., 2002). A point mutation was identified at residue 451 of the C57BL/6 $P2X_7R$ C-terminus, where proline was replaced by leucine (P451L). HEK293 cells transfected with $P2X_7Rs$ expressing either P451 or L451, showed that ATP was more effective at inducing YO-PRO-1 uptake and Ca^{2+} influx in cells expressing the BALBc $P2X_7R$, when proline was present at residue 451. Therefore, it was proposed that the P451L mutation in the SH3 domain of the C57BL/6, $P2X_7R$ impairs receptor-mediated ion channel function and pore formation, corresponding to a loss of function mutation (Adriouch et al., 2002). The BALBc $P2X_7R$ shared C-terminus sequence homology with its rat and human counterparts. However, a recent species-comparison functional study observed that the apparent loss of function P451L mutation did not affect C57BL/6 $P2X_7R$ responses and showed similar properties to the BALBc $P2X_7R$ (Donnelly-Roberts et al., 2009a).

A similarly placed mutation in the human $P2X_7R$ found in some individuals with chronic lymphocytic leukaemia, where glutamine is replaced by alanine at residue 496 (E496A), also shows a loss of function in the receptor and leads to impaired activation of the $P2X_7R$-induced apoptotic pathway (Gu et al., 2001; Wiley et al., 2002). Quite recently, it has also been suggested that the $P2X_7R$-mediated large pore formation could be associated with the recruitment and activation of Pannexin-1 (Panx-1) hemichannels, which are in turn linked with the SH3 domain of the C-terminus (Pelegrin and Surprenant, 2006; Iglesias et al., 2008). The SH3 and death domains are also associated with phosphorylation sites that interact with HSP90 (heat shock protein) and protein kinase C in human macrophages and astrocytes, respectively (Adinolfi et al., 2003; Wang et al., 2003). Therefore, it is likely that the SH3 and death domains play an important role in the $P2X_7R$-mediated pore formation and apoptosis, through protein recruitment and interactions at the intracellular C-terminus of

the receptor, and that these $P2X_7R$ functions are essential in mediating immunological responses of cells of the monocytic lineage.

Mutagenesis studies in the distal portion of the C-terminus, which includes a set of highly conserved cysteine residues, have shown the importance of this amino acid sequence (residues 551-581) in membrane trafficking and cell surface expression of the $P2X_7R$ (Denlinger et al., 2003; Smart et al., 2003; Wiley et al., 2003; Feng et al., 2005; Gonnord et al., 2009; Jindrichova et al., 2012). Interactions between the $P2X_7R$ C-terminus and the calcium-binding protein, calmodulin, have been implicated in the regulation of $P2X_7R$-activated ion channel. Point mutations at residues 541 and 552 (I541T and S552C) in the rat $P2X_7R$ caused a large depression of calcium currents and blocked the co-immunoprecipitation of $P2X_7R$ and calmodulin protein, seen in cells expressing the wild-type rat $P2X_7R$. In a follow-up study, it was shown that the wild-type human $P2X_7R$, which exhibited slower ATP-induced currents than the rat $P2X_7R$, did not co-immunoprecipitate with calmodulin. This suggested that calmodulin does not normally associate with the human $P2X_7R$, although it does with the rat orthologue (Roger et al., 2008, 2010).

3.1.4 Species differences

The rat $P2X_7R$ amino acid sequence shares an 80% and 85% homology with that of the human and mouse $P2X_7R$, respectively (Surprenant et al., 1996; Rassendren et al., 1997b; Chessell et al., 1998a). Furthermore, it is unclear whether species differences in amino acid homology in the extracellular region (Young et al., 2007) or the C-terminus (Gu et al., 2001; Adriouch et al., 2002) of the $P2X_7R$ underlie the observed species differences in agonist and antagonist potencies at the receptor (Donnelly-Roberts et al., 2009a).

3.2 Pharmacological properties of $P2X_7R$

The $P2X_7R$ can be functionally distinguished from other P2XR subtypes by its unique pharmacological fingerprint and its permeability to large cations and fluorescent dyes. Much of the early studies on $P2X_7R$ function were carried out on expression systems such as human embryonic kidney 293 (HEK293) cells and *Xenopus* oocytes expressing recombinant $P2X_7Rs$. It is also known that immunological and glial cells such as macrophages, microglia and astrocytes express $P2X_7Rs$. Therefore, some studies have used macrophage cell lines to investigate the functional properties of native $P2X_7Rs$, which would indeed be more relevant to physiological conditions. To examine the effects of agonists and antagonists on the $P2X_7R$, most studies have used whole-cell patch clamp recordings to measure inward currents evoked by $P2X_7R$ activation. Furthermore, the permeation properties of the receptor were typically examined by measuring agonist-induced calcium influx or YO-PRO-1 fluorescent dye uptake in transfected cells. Fig. 3.1 summarises some pharmacological characteristics of mouse $P2X_7Rs$.

3.2.1 Agonists

3.2.1.1 Activation of membrane currents

One of the main distinguishing properties of the $P2X_7R$ is its relatively low affinity for its agonist, ATP, compared to that of other P2X receptor subtypes (Evans et al., 1996; Surprenant et al., 1996; Bianchi et al., 1999). Early studies in macrophages showed that ATP-induced currents were a result of a non-selective increase in permeability to both cations and anions (Buisman et al., 1988). However, membrane current recordings from HEK293 cells expressing recombinant rat $P2X_7Rs$ ($rP2X_7Rs$) have shown selectivity for small cations (Surprenant et al., 1996; Virginio et al., 1999). The EC_{50} value for ATP at the $P2X_7R$ was 10- to 100-fold higher than that at the other receptor subtypes expressed in 1321N1 human astrocytoma cells (Bianchi et al., 1999), and therefore less potent at

activating $P2X_7Rs$. The effect of repeated ATP applications was examined in the NTW8 mouse microglia cell line expressing native $P2X_7Rs$ and HEK293 cells expressing recombinant mouse, rat or human $P2X_7Rs$ (Chessell et al., 1998a). Repeated ATP applications (1mM) resulted in successively larger current amplitudes in NTW8 cells and at recombinant mouse $P2X_7Rs$ ($mP2X_7Rs$), so that by the eighth application, the current amplitude had increased by 303% and 74%, respectively. Additionally, rise and decay times did not significantly change over repeated agonist applications (Chessell et al., 1998a). This property may reflect the opening of a pore permeable to large molecules (North, 2002).

Although not $P2X_7R$-selective, 2', 3'-*O*-(4-benzoyl-benzoyl) adenosine 5'-triphosphate (BzATP) is the most potent agonist at the $P2X_7R$ subtype, exhibiting at least 10- to 30-fold potency than ATP, at this receptor (Surprenant et al., 1996). There are some remarkable species differences in $P2X_7R$ agonist potency. Repeated BzATP (100 µM) applications at the mouse and human $P2X_7Rs$ ($hP2X_7R$) evoked successively potentiating currents. However, this effect was only observed with $rP2X_7Rs$ when a much lower dose (1-3 µM) was applied (Chessell et al., 1998a). Higher BzATP doses (>10 µM) either had no effect or reduced the current amplitude at $rP2X_7Rs$ (Hibell et al., 2000). Furthermore, when using a supra-maximal concentration of BzATP (100uM) at $rP2X_7Rs$, the deactivation period for the evoked current response had increased by 1259%, following the eighth application (Chessell et al., 1998a). Therefore, BzATP is clearly the most potent at rat $P2X_7Rs$, compared to the human and mouse orthologues, a notion which has also been confirmed in later studies (Donnelly-Roberts et al., 2009a). This relatively high agonist potency and the increased response decay time on repeated application, both reflect higher agonist dissociation rates at rat $P2X_7Rs$, compared to its mouse and human counterparts (Hibell et al., 2001). The majority of studies investigating $P2X_7R$ function have been carried out using recombinant rat receptors. Thus, it is important that these species differences in agonist potency are noted when using alternative animal models. $P2X_1$, $P2X_2$ and $P2X_3$ receptor subtypes are also

activated by BzATP (Bianchi et al., 1999). The agonist potency order (BzATP>ATP) is also valid at $P2X_1$Rs. However, the nucleotide agonists 2-methylthioATP (2-MeSATP) and α, βmethyleneATP (α, β-meATP) are highly potent at the $P2X_1$Rs (nM to low µM range), whereas they are relatively weak agonists of $P2X_7$Rs (Bianchi et al., 1999). Thus, these differences in agonist profiles would further enable $P2X_1$ and $P2X_7$ receptor subtypes to be distinguished.

Other endogenous nucleotides, AMP and ADP, normally show no or very weak agonist activity at $P2X_7$Rs. However, recombinant mouse and rat $P2X_7$Rs expressed in *Xenopus* oocytes, when primed with an initial application of ATP, were dose-dependently activated. This was also supported by the activation of native $P2X_7$Rs in ATP-primed mouse and human microglial cells, which evoked the release of the pro-inflammatory cytokine, interleukin-1β (IL-1β) (Chakfe et al., 2002). Thus, pre-exposure to ATP sensitises $P2X_7$Rs, whether recombinant or native, such that they are susceptible to activation by weaker nucleotide agonists. This may play an important physiological role *in vivo* where extracellular ATP is rapidly hydrolysed by ectoATPases at the surface of the cell membrane (Banerjee, 1981; Ziganshin et al., 1994).

3.2.1.2 Large pore formation

It has been shown that repeated or prolonged applications of ATP or BzATP evoke successively larger currents that also display increased deactivation latencies (Chessell et al., 1998a), which may reflect the opening of a pore permeable to large molecules. Indeed, it was shown that ATP^{4-} permeabilised J774 macrophages to large fluorescent dyes such as Lucifer Yellow (457 Da) and Fura-2 (831 Da), but not larger dyes such as Evans Blue (961 Da) (Steinberg et al., 1987). Following the cloning of rat $P2X_7$Rs, it was shown that prolonged agonist application to transfected cells led to sustained currents and a subsequent

uptake of the dye YO-PRO-1 (Surprenant et al., 1996), a property also observed in mouse and human $P2X_7$Rs (Rassendren et al., 1997b; Chessell et al., 1998a). Prolonged (30 to 40 sec) BzATP application induced membrane blebbing, YO-PRO-1 uptake and cell death in HEK293 cells expressing r$P2X_7$Rs (Virginio et al., 1999), a property attributed to the activation of apoptotic pathways. The time course of dye uptake was much slower than that of the induction of ionic currents. Furthermore, it was shown with short agonist applications and YO-PRO-1 uptake, that the pore dilation was reversible (Virginio et al., 1999). Species differences have also been observed between rat, human and mouse $P2X_7$Rs in agonist-evoked YO-PRO-1 uptake in transfected cells (Donnelly-Roberts et al., 2009a). It has been shown that BzATP produced a more rapid YO-PRO-1 influx into cells expressing rat and human $P2X_7$Rs, compared to mouse $P2X_7$Rs (Hibell et al., 2000).

There are at least two possible mechanisms to explain the time-dependent increase in permeability of the $P2X_7$R-activated ion channel, to larger cationic dyes (North, 2002). One is that the agonist-evoked membrane currents and dye-uptake are both mediated through a common pathway, in which the small non-selective cation channel progressively increases in diameter to allow the entry of larger molecules, in a time and dose-dependent manner. The alternative is that the $P2X_7$R-activated ion channel and large permeable pore are separate entities, and that the large pore is activated through protein recruitment interactions with the intracellular $P2X_7$R C-terminus. Both hypotheses are supported by several lines of evidence (North, 2002; Pelegrin and Surprenant, 2009).

The common pathway model was supported by the findings that agonist-evoked $P2X_7$R membrane currents progressively increased as a result of repeated or prolonged application. A short agonist application (1 sec) led to the activation of transient membrane currents attributed to a cationic conductance. Repeated or prolonged agonist application led to a

sustained increase in the inward current, which reflected a progressive increase in permeability to large cations, such as $NMDG^+$ (Virginio et al., 1999). Due to the slower time course of dye uptake compared to the onset of agonist-evoked membrane currents, it was suggested that the small $P2X_7R$-activated cation-selective channel pore progressively dilated over a period of 10-20s to allow entry to larger cations and dyes (Virginio et al., 1999). However, the agonist dose-dependent current growth was thought to be associated with a decreased rate of agonist dissociation from the receptor, rather than a progressive increase in the pore diameter of the ion channel (Hibell et al., 2000, 2001).

The notion that the ion channel and large pore are separate, is also supported (Pelegrin and Surprenant, 2009). It was found that calmidazolium potently blocked agonist-evoked $P2X_7R$-mediated membrane currents but did not affect YO-PRO-1 uptake (Virginio et al., 1997). Additionally, initial studies in macrophage cells revealed that ATP application induced the uptake of anionic dyes such as Lucifer Yellow (Steinberg et al., 1987), which differs from the property of $P2X_7R$-activated ion channels as displaying cationic conductances. Furthermore, a C-terminus mutation of the $P2X_7R$ led to a diminished permeability to $NMDG^+$ but had no effect on dye-uptake in HEK293 cells expressing rat $P2X_7Rs$ (Jiang et al., 2005). This was also supported by the finding that $NMDG^+$ permeability did not increase with prolonged BzATP application, in the presence of a normal extracellular sodium concentration (Jiang et al., 2005). The conclusions of these studies suggest an alternative mechanism in which dye uptake may also occur through a separate large permeable pore.

3.2.2 Extracellular ions

Extracellular concentrations of divalent cations have been shown to modulate agonist-evoked $P2X_7R$ responses. BzATP-evoked currents recorded from HEK293 cells expressing recombinant $rP2X_7Rs$, were potentiated in amplitude, and prolonged on repeated

applications after the removal of magnesium (Mg^{2+}) and calcium (Ca^{2+}) ions from the external solution (Surprenant et al., 1996). However, there was only a modest increase in the agonist potency (Surprenant et al., 1996). The inhibitory effect of responses at $rP2X_7Rs$ by divalent cations was confirmed by Virginio and colleagues (1997). Currents evoked by BzATP were inhibited by the addition of extracellular Ca^{2+}, Mg^{2+}, zinc (Zn^{2+}) and copper (Cu^{2+}) ions. BzATP-evoked YO-PRO-1 uptake was also inhibited by divalent cations with similar potencies (Virginio et al., 1997).

As with the effect of agonists, there are species differences in the responses of $P2X_7Rs$ in low divalent solutions. Currents in HEK293 cells expressing recombinant rat and human $P2X_7Rs$ were evoked by BzATP (Rassendren et al., 1997b). Lowering the extracellular Ca^{2+} concentration and the removal of extracellular Mg^{2+} led to a potentiation in currents at both receptor orthologues. Furthermore, the potentiation of the $hP2X_7R$ currents was greater than that at $rP2X_7Rs$ (Rassendren et al., 1997b). This observation reflects the higher potency of BzATP at $rP2X_7Rs$, and suggests a possibility that the agonist might be competing with Mg^{2+}, at the extracellular agonist binding site, a concept that has previously been proposed (Cockcroft and Gomperts, 1980), but is widely disputed (Virginio et al., 1997; North and Surprenant, 2000). Additionally, inhibition of agonist-evoked currents by Mg^{2+} were also observed in a human macrophage cell line (Rassendren et al., 1997b). In another study, a short pre-incubation of $hP2X_7R$-transfected HEK293 cells with copper caused an inhibition of BzATP-evoked currents (Chessell et al., 1998b).

Similarly, mouse $P2X_7Rs$ expressed natively in the NTW8 microglial cell line showed a significantly larger potentiation of BzATP- and ATP-evoked currents in low divalent extracellular solution (Chessell et al., 1997). Moreover, the successively larger currents on repeated ATP exposure were further potentiated in the absence of divalent cations (Chessell

et al., 1997). Another study (Moore and Mackenzie, 2008), examined the effects of zinc and copper on mouse and rat $P2X_7$Rs. The influx of the fluorescent dye ethidium bromide (EtBr), through the $P2X_7$-activated pore, was used to measure the level of $P2X_7$ activation. Copper potently inhibited ATP- and BzATP-evoked EtBr influx in native mouse RAW264.7 macrophages and in HEK293 cells expressing recombinant mouse or rat $P2X_7$Rs. However, the effect of zinc was dependent on the expression system and the agonist used. Zinc treatment led to an inhibition of recombinant r$P2X_7$Rs when activated by ATP or BzATP. ATP-evoked recombinant m$P2X_7$R activation was potentiated by zinc but inhibited when BzATP was used as the agonist. The native receptors in mouse macrophages were not affected by zinc on ATP-mediated stimulation. However, when using BzATP as the agonist, zinc inhibited $P2X_7$R activation in mouse macrophages (Moore and Mackenzie, 2008). These findings suggest that $P2X_7$R function is modulated by zinc and copper, but also stress further the species and agonist differences in $P2X_7$R responses.

$P2X_7$R responses have also been shown to be modulated by the extracellular concentrations of monovalent ions. Rat $P2X_7$R responses were inhibited by protons when stimulated by BzATP (Virginio et al., 1997). Furthermore, the substitution of extracellular Na^+ with $NMDG^+$, led to an enhanced rate of YO-PRO-1 uptake, as well as a potentiated ionic current (Virginio et al., 1999). BzATP potency was tested at h$P2X_7$Rs in the presence of different monovalent cations while maintaining chloride as the anion in the extracellular solution (Michel et al., 1999). BzATP was more potent at h$P2X_7$Rs in the presence of choline (pEC_{50} 6.14) when compared to K^+ and Na^+ (pEC_{50} 5.87 and 5.19, respectively). It was also observed that using glutamate in place of chloride as the monovalent anion enhanced BzATP-evoked h$P2X_7$R currents, in a low divalent solution (Michel et al., 1999). These findings suggest that $P2X_7$R function is inhibited, to a certain extent, by extracellular sodium chloride (NaCl) and could explain the low agonist potency at this receptor compared to other P2XR subtypes. While under physiological conditions, it is unlikely that extracellular ion concentrations fluctuate to

such a degree, the authors (Michel et al., 1999) have suggested that $P2X_7R$ function could be enhanced under stress conditions such as ischemia, when extracellular Na^+ and Cl^- concentrations are reduced in the brain (Xie et al., 1995).

3.2.3 Antagonists

The polysulfonated dye, Coomassie Brilliant Blue G (BBG) is a potent, non-competitive antagonist at the $P2X_7R$ (Jiang et al., 2000). BBG led to an inhibition of BzATP-evoked currents at both rat and human $P2X_7Rs$ in the nanomolar range (IC_{50} 10 and 200 nM, respectively). BBG also has antagonising properties at other P2XR subtypes (IC_{50} 2-30 µM) (Jiang et al., 2000). At the $P2X_4R$, BBG inhibited currents with IC_{50} values of 10 (rat) and 3.2 (human) µM. Thus, BBG displayed a 1000-fold higher potency at $rP2X_7RS$, than at the $rP2X_4RS$. $P2X_7Rs$ and $P2X_4Rs$ are often co-expressed in the same tissues with overlapping roles in inflammation and pain (Dubyak, 2007), although their propensity to form functional heteromeric complexes is not completely understood. In another study, recombinant mouse, rat and human $P2X_7$ receptors were expressed in human astrocytoma 1321N1 cells (Donnelly-Roberts et al., 2009a). BBG only potently blocked calcium influx through rat $P2X_7Rs$, but showed effective inhibition of YO-PRO-1 uptake at mouse, human and rat $P2X_7Rs$. In this case, BBG was more potent at blocking mouse (BALB/c and C57BL/6 strains; pIC_{50} 6.71 and 6.34, respectively) YO-PRO-1 uptake, than at the rat and human receptor subtypes (pIC_{50} 6.24 and 5.71, respectively) (Donnelly-Roberts et al., 2009a).

Another antagonist of the $P2X_7R$ is the isoquinoline derivative KN-62 (1-[*N*, *O*-bis (5-isoquinolinesulfonyl)-*N*-methyl-L-tyrosyl]-4-phenylpiperazine), which displays remarkable selectivity at the human and mouse but not at rat $P2X_7Rs$ (Humphreys et al., 1998; Donnelly-Roberts et al., 2009a). KN-62 was first shown to potently inhibit ATP-stimulated barium influx and ethidium dye uptake by human lymphocytes thought to have been

mediated by $P2X_7$Rs (Gargett and Wiley, 1997). The selectivity of KN-62 to inhibit cation currents and dye uptake at the human and mouse, over rat $P2X_7$Rs has been confirmed for recombinant $P2X_7$Rs expressed in human astrocytoma 1321N1 cells (Donnelly-Roberts et al., 2009a). Although KN-62 has shown to effectively block $P2X_7$Rs function, the antagonist is also known to be a CAM-kinase-II inhibitor, which could render its use to be problematic in physiological systems, or *in vivo*. Therefore, recent developments have led to the synthesis of KN-62 derivatives that do not inhibit CAM-kinase-II but maintain $P2X_7$R-blocking properties (Baraldi et al., 2004).

Other selective $P2X_7$R antagonists include oxidised ATP (oxATP) and calmidazolium. The calmodulin antagonist, calmidazolium, was shown to effectively block currents at the rat $P2X_7$R at low concentrations, but had no effect on YO-PRO-1 dye uptake (Virginio et al., 1997). Interestingly, this finding implies that agonist-evoked $P2X_7$R-mediated currents and large dye uptake might essentially be attributed to differential pathways, instead of one common pore (see below). Other, non-selective P2XR antagonists such as suramin and PPADS (pyridoxal-phosphate-6-azophenyl-2', 4'-disulphonic acid) also inhibit $P2X_7$R-mediated currents and dye uptake, though with relatively less potency than at other P2XR subtypes. HEK293 cells expressing recombinant rat $P2X_7$R currents, stimulated with BzATP, were relatively insensitive to suramin and PPADS (IC_{50} 300 and 45 μM, respectively) (Surprenant et al., 1996). Similarly, high concentrations of the antagonists were needed to inhibit BzATP–evoked currents at $h2X_7$Rs (Rassendren et al., 1997b). In contrast, PPADS was shown to potently antagonise recombinant rat and human $P2X_7$R-mediated YO-PRO-1 uptake evoked by BzATP, in HEK293 and human astrocytoma 1321N1 cells (Chessell et al., 1998a; Donnelly-Roberts et al., 2009a). Native (NTW8) and recombinant (HEK293 cells) mouse $P2X_7$Rs were also inhibited by PPADS, but less effectively than at the rat or human counterparts (Chessell et al., 1998a). A mouse strain-specific response to PPADS inhibition was also seen with BzATP-evoked YO-PRO-1 uptake in human astrocytoma 1321N1 cells

expressing recombinant BALB/c and C57BL/6 $P2X_7Rs$ (pIC_{50} 5.31 and 4.40, respectively) (Donnelly-Roberts et al., 2009a). Suramin and PPADS display higher potencies, in the low micromolar range, at other P2XR subtypes ($P2X_{1-3}$ and $P2X_5$), although they are relatively insensitive at $P2X_4Rs$ (North and Surprenant, 2000; North, 2002).

Intensive research into $P2X_7R$ pharmacology has led to the development of novel antagonists directed at this receptor. Donnelly-Roberts and colleagues have developed two novel series of antagonists, disubstituted tetrazoles (A438079) and cyanguanidines (A-740003), both of which displayed reversible and competitive antagonism with high potencies and selectivity at rat and human $P2X_7Rs$ (Honore et al., 2006; Nelson et al., 2006; Donnelly-Roberts and Jarvis, 2007). A438079 (3-((5-(2, 3-dichlorophenyl)-1-H-tetrazole-1-yl) methyl pyridine) potently blocked BzATP-evoked calcium influx in human astrocytoma 1321N1 cells expressing rat or human $P2X_7$. The antagonist did not have any effect on cells expressing other P2XR subtypes. Furthermore, A-438079 inhibited IL-1β release from, and YO-PRO-1 uptake by human THP-1 macrophages (Nelson et al., 2006). A-740003 ((N-(1-{[(cyanoimino)(5-quinolinylamino)methyl]amino}-2,2-dimethylpropyl)-2-(3,4-dimethoxyphenyl) acetamide) was shown to be a more potent blocker at the rat and human $P2X_7Rs$ (Honore et al., 2006). Both antagonists were also tested at recombinant mouse $P2X_7Rs$, inhibiting BzATP-evoked changes in intracellular calcium concentrations and YO-PRO-1 dye uptake, at low micromolar concentrations (Donnelly-Roberts et al., 2009a).

3.3 $P2X_7R$-mediated molecular mechanisms

$P2X_7R$-associated functions in neurons and microglia are closely associated with alterations in potassium and calcium flow through the activated receptor. Such functions include the release of neurotransmitters and cytokines, shown in fig. 3.2.

3.3.1 Neurotransmitter release

The activation of $P2X_7$ receptors with BzATP has been shown to induce calcium influx into rat cerebellar granule neurons (Hervás et al., 2005) and in cerebrocortical and midbrain synaptosomal preparations (Lundy et al., 2002; Alloisio et al., 2008; Marín-García et al., 2008). BzATP-evoked increases in intracellular calcium concentrations, were blocked by the application of the antagonists BBG, A-438079 and Zn^{2+}, and potentiated in a low divalent extracellular solution (Lundy et al., 2002; Hervás et al., 2005; Alloisio et al., 2008; Marín-García et al., 2008), all hallmarks of $P2X_7R$ activation. In cerebellar granule neurons (León et al., 2008) and motor neuron terminals at the neuromuscular junction (Deuchars et al., 2001), it was found that BzATP-mediated $P2X_7R$ activation led to synaptic vesicle release, measured by the release of the fluorescent dye FM 1-43 (León et al., 2008). Furthermore, vesicle secretion was inhibited by removing extracellular calcium and by the application of BBG (Deuchars et al., 2001; León et al., 2008), suggesting that $P2X_7R$-mediated vesicle release is dependent on calcium influx. These findings imply that $P2X_7R$ activation has a role in neurotransmitter release. Indeed, several studies have shown that $P2X_7R$-mediated glutamate and GABA release occurs in some regions of the brain (Sperlágh et al., 2002; Alloisio et al., 2008; Marín-García et al., 2008; D'Amico et al., 2010).

$P2X_7R$-mediated glutamate and subsequent GABA release was shown in rat hippocampal slices (Sperlágh et al., 2002). Slices were incubated with [^{3}H] GABA or [^{14}C] glutamate before treatment with ATP or other agonists. $P2X_7R$ agonist application caused a dose-dependent release of [^{3}H] GABA and [^{14}C] glutamate with a rank order of potency of BzATP>ATP>ADP. The agonist-evoked neurotransmitter release was inhibited by PPADS, BBG and Zn^{2+}. Furthermore, [^{3}H] GABA release by electrical field stimulation and ATP application were blocked by BBG and kainate receptor antagonists, CNQX and gadolinium, respectively. These findings were supported by $P2X_7R$ immunoreactivity in area CA1 and

CA3 nerve terminals targeting pyramidal cell dendrites and parvalbumin-immunopositive puncta (Sperlágh et al., 2002). It was suggested that $P2X_7R$-activation at pre-synaptic excitatory terminals modulated the release of glutamate and glutamate-dependent GABA release in the hippocampus (Sperlágh et al., 2002).

It was also shown that ATP- and BzATP-evoked glutamate and [^{3}H]D-aspartate release was antagonised by the application of $P2X_7R$-selective inhibitors oxATP, BBG (Marín-García et al., 2008) and A-438079 (Alloisio et al., 2008) in isolated rat cerebrocortical synaptosomes. Rat caudal brainstem synaptosomal preparations showed a similar profile of $P2X_7R$-mediated [^{3}H]D-aspartate release (D'Amico et al., 2010). BzATP application increased both the basal and K^+-evoked efflux of [^{3}H] D-aspartate, which was blocked by A-438079 and PPADS. In the same study, the contribution of AMPA receptor function to mediated [^{3}H] D-aspartate release was also investigated. Treatment with AMPA did not affect the basal, but increased the K^+-evoked efflux of [^{3}H] D-aspartate. This effect was blocked by the AMPA receptor inhibitors NBQX and GYKI52466. The findings of this study suggest that the activity of AMPA and $P2X_7$ receptors may be coupled in some way, at the pre-synaptic terminal, to modulate the release of glutamate during synaptic transmission.

3.3.2 Cytokine release, the inflammasome complex and TLR4

Cytokine release from microglia is initiated in the presence of pathogens or cellular stressors in the extracellular microenvironment. The processing and release of the cytokine, interleukin-1β (IL-1β), is particularly prominent in the early stages of inflammation under such conditions, and are believed to require a dual stimulus. Firstly, activation of Toll-like receptor 4 (TLR4) by its bacterial ligand lipopolysaccharide (LPS), a pathogen-associated molecular pattern (PAMP), induces an intracellular accumulation of pro-IL-1β (31 kDa) and

components of the inflammasome enzyme complex, through NFκB signalling (Ferrari et al., 1997b, 2006; Sanz and Di Virgilio, 2000). Secondly, the activation of $P2X_7Rs$ by ATP, a damage-associated molecular pattern (DAMP), triggers a large efflux in K^+, inflammasome assembly and activation of the enzyme caspase-1. It is unclear how the change in K^+ flux stimulates these processes, although they are suppressed on inhibition of K+ efflux (Perregaux and Gabels, 1994; Ferrari et al., 1997b, 2006; Sanz and Di Virgilio, 2000). The $P2X_7R$-mediated influx of calcium is suggested to play a key role in triggering the actual release of the mature 17 kDa cytokine into the extracellular environment. Release of IL-1β may occur through multiple pathways, including microvesicle shedding or through a large pore such as the pannexin-1 (panx-1) hemichannel (Mackenzie et al., 2001; Bianco et al., 2005; Pelegrin et al., 2008; Ferrari et al., 2006).

LPS stimulation has also shown to induce panx-1 upregulation in human and mouse macrophages, in which the protein was highly expressed and which co-immunoprecipitated with the $P2X_7R$ subunit (Pelegrin and Surprenant, 2006). Inhibition of panx1 led to a subsequent inhibition of $P2X_7R$-mediated dye uptake, but did not affect the agonist-evoked membrane current or calcium influx. Inhibiting panx1 also blocked caspase-1 activation and subsequent IL-1β release from the activated macrophages. Furthermore, panx1 over-expression led to an increased rate of dye uptake (Pelegrin and Surprenant, 2006). The findings of this study suggest that $P2X_7R$ activation may be coupled to the activation of panx-1, stimulating the activation of apoptotic pathways and cytokine release (Pelegrin and Surprenant, 2006, 2009).

Considering that the upregulation and assembly of the inflammasome complex requires gene transcription (Di Virgilio, 2007), it is likely that this process may occur over a period of hours to days following the initial stimulus. It is debated whether preconditioning of microglia

with a PAMP such as LPS, is required, although a larger ATP-mediated release of IL-1β is seen upon preconditioning (i.e. with LPS), most probably due to the upregulation and assembly of the inflammasome complex (Ferrari et al., 1997b, 2006; Sanz and Di Virgilio, 2000). ATP stimulation of $P2X_7Rs$ has shown to trigger the processing and release of TNFα without the need for preconditioning, through a calcium-dependent mechanism (Suzuki et al., 2004), which may suggest a possible mechanism for non-inflammasome associated IL-1β release. Interestingly, cytokines have shown remarkable potency in modulating NMDA receptor function and synaptic plasticity in the brain (Di Filippo et al., 2008, 2013; Fogal and Hewett, 2008), and therefore could also be associated with $P2X_7R$-mediated mechanisms of neuromodulation.

Chapter 3 Figures

A

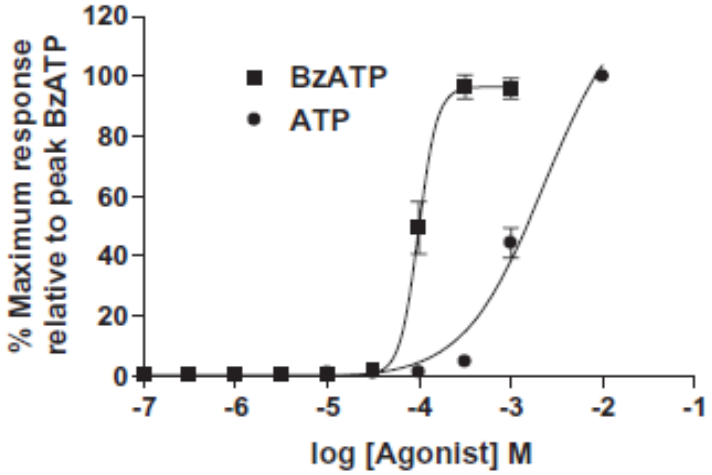

B

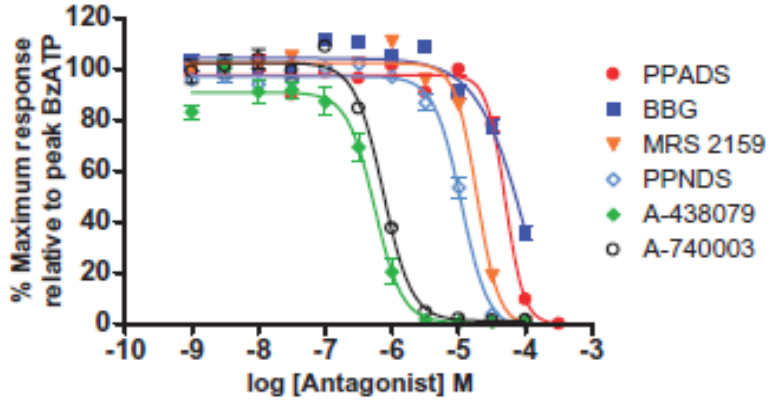

Figure 3.1 Pharmacological characteristics of mouse $P2X_7Rs$. Data shown are concentration-effect curves for agonist-induced $P2X_7R$-mediated increases in intracellular calcium (A), and for blockade of BzATP-induced effects, by various P2 receptor antagonists (B). Data represent mean ± SEM percentage of maximum BzATP-mediated response, in human astrocytoma cells transfected with recombinant C57BL/6 mouse $P2X_7Rs$. ***A***, The curves illustrate the higher potency of BzATP in stimulating $P2X_7Rs$, compared to ATP. A similar relationship was observed for agonist-induced YO-PRO-1 dye uptake (not shown). ***B***, The competitive antagonists A438079 and A740003 both exhibited the highest affinity and selectivity for blocking $P2X_7R$-mediated calcium influx, in this particular mouse line. The usually potent $P2X_7R$ blocker BBG showed similar potency to the broad-spectrum P2XR antagonist, in blocking BZATP-induced calcium influx. However, BBG exhibited comparable potency to A438079 in attenuating agonist-induced YO-PRO-1 dye uptake (not shown), suggesting that BBG may be more selective for $P2X_7R$ large pore activity. $P2X_7R$ activation was also blocked by the reported P2X1R antagonists, MRS2159 and PPNDS. Figures extracted from Donnelly-Roberts et al. (2009a).

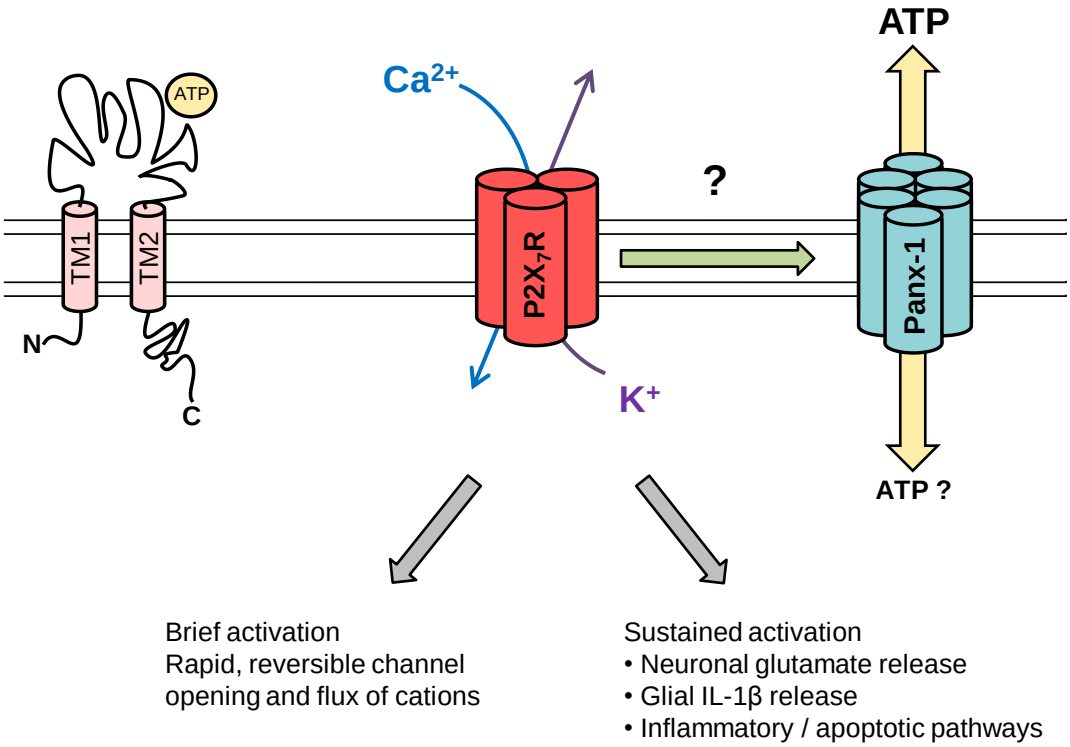

Figure 3.2 Schematic of structural and functional properties of $P2X_7Rs$. Functional $P2X_7Rs$ are comprised of three subunits, forming a homotrimer. ***Left***, Membrane topology shows each subunit consists of two hydrophobic transmembrane (TM) domains, a large extracellular loop, and both amino (N) and carboxyl (C) termini located intracellularly. The ATP binding site is located extracellularly, within a cysteine-rich metal binding domain, where it is thought to interact with positively charged lysine residues to induce receptor activation. The carboxyl terminus is relatively longer than that of other P2XRs, and contains various intracellular protein docking sites such as the TNFR1-like death domain and an LPS binding domain, which mediate further downstream signalling cascades. ***Middle***, $P2X_7Rs$ form large non-selective cation channels. Large influx of calcium (Ca^{2+}) and efflux of potassium (K^+) ions are characteristic of $P2X_7R$ activation. Brief stimulation induces a rapid and reversible increase in permeability to these cations. Sustained or repeated activation of the receptor induces larger fluxes of the ions, stimulating further downstream mechanisms such as neurotransmitter release from neurons or cytokine release from microglial cells. ***Right***, $P2X_7Rs$ are also closely associated with Pannexin-1 (Panx-1) hemichannels, which have shown to mediate ATP release. It is uncertain whether the large pore formed by sustained receptor activation is caused by the wider opening of $P2X_7Rs$ themselves, or through the activation of another pore, such as Panx-1. It has been widely reported that $P2X_7Rs$ and Panx-1 are required for the activation various glial-mediated inflammatory cascades such as interleukin-1β release (IL-1β), and the induction of various apoptotic pathways. Overall, $P2X_7R$ activation has pleiotropic effects and is important for mediating various neuronal and glial cell functions.

Chapter 4

$P2X_7R$-Mediated Neuromodulation in the Retina

4.1 $P2X_7R$ immunoreactivity in the retina

$P2X_7$ mRNA and protein expression has been detected in the rodent, primate and human retina on neuronal and glial cells, in both synapse-rich and nuclear layers (Brändle et al., 1998; Wheeler-Schilling et al., 2001; Innocenti et al., 2004; Ishii et al., 2003; Puthussery and Fletcher, 2004; Puthussery et al., 2006; Vessey and Fletcher, 2012) (fig. 4.1).

In the outer retinal layers of the rodent, specific $P2X_7R$ immunoreactivity was localised near ribbon synapses in rod spherules, as well as on postsynaptic GABAergic puncta identified as horizontal cell dendrites (Puthussery and Fletcher, 2004; Puthussery et al., 2006; Vessey and Fletcher, 2012). In the human retina, most immunoreactivity was observed in the OPL, although $P2X_7R$ mRNA did not co-localise with photoreceptor molecular markers (Niyadurupola et al., 2013). These studies put into question the specific cellular expression of $P2X_7Rs$ in photoreceptors, and highlight an important species difference in the $P2X_7R$ expression profile, between the mouse and human retina under physiological conditions. In the inner retina, $P2X_7R$ localisation was detected on processes presynaptic to rod-bipolar cell terminals, specifically at conventional synapses immunopositive for glycinergic and GABAergic molecular markers (Puthussery and Fletcher, 2004). Receptor expression on bipolar cell dendrites and axon terminals remains elusive. $P2X_7R$ immunopositive puncta appeared to co-localise with rod-bipolar cell processes in both outer and inner retinal layers. However, it has been proposed that due to the discrete nature of the staining, these puncta are most likely those of horizontal or amacrine cells (Vessey and Fletcher, 2012). Indeed, mRNA expression for $P2X_3R$, $P2X_4R$ and $P2X_5R$, but not $P2X_7R$ was detected in isolated rat bipolar cells (Wheeler-Schilling et al., 2000), suggesting that direct purinergic modulation of

bipolar cell activity may occur through alternative P2XRs, whereas $P2X_7R$-mediated modulation of bipolar cell signalling most likely occurs through presynaptic mechanisms. Taken together, these findings suggest that $P2X_7Rs$ modulate synaptic signalling in the rod-mediated visual pathway.

$P2X_7R$ localisation in the ganglion cell layer has also been determined (Brändle et al., 1998; Wheeler-Schilling et al., 2001). $P2X_7R$ immunoreactivity was observed at early postnatal stages, in the ganglion cell and neuroblastic layers (Innocenti et al., 2004), also suggesting that $P2X_7R$ activity could be important in early retinal function during development. Positive staining was detected in ganglion cell somata of the mouse (Kaneda et al., 2004; Franke et al., 2005; Vessey and Fletcher, 2012) and monkey retinae (Ishii et al., 2003), although it was not clear if the receptors were also localised at ganglion cell dendrites. Intracellular $P2X_7R$ localisation has also been observed in the cytoplasm and nuclear membrane of monkey retinal ganglion cells (Ishii et al., 2003). In the rabbit, $P2X_7R$ immunoreactivity was predominantly observed in the inner retinal layers, particularly in the ganglion cell layer, whereas most staining was observed in the OPL of the human retina (Sugiyama et al., 2006; Niyadurupola et al., 2013). Furthermore, in the human retina, high $P2X_7R$ mRNA expression detected in the inner retinal layers (Niyadurupola et al., 2013).$P2X_7R$ expression in Müller cells is disputed, as receptor immunoreactivity was not detected in some studies (Jabs et al., 2000; Innocenti et al., 2004; Vessey and Fletcher, 2012), but others have provided both immunohistochemical and functional evidence of Müller cell $P2X_7Rs$ (Pannicke et al., 2000; Bringmann et al., 2001). These differences could reflect the upregulation of $P2X_7Rs$ in Müller cell dysfunction, for example in proliferative vitreoretinopathy (Bringmann et al., 2001). Similarly, $P2X_7R$ expression in astrocytes remains uncertain. In the mouse retina, $P2X_7R$ immunoreactivity co-localised with astrocytes in the C57BL/6 strain, although no astrocytic expression of the receptor was found in the BALBc strain, suggesting a strain-specific expression profile (Franke, 2005; Vessey and Fletcher, 2012). Furthermore, microglia in the

rodent retina are known to express $P2X_7$Rs (Innocenti et al., 2004; Vessey and Fletcher, 2012). Thus, microglial $P2X_7$Rs are likely to play a significant role in the orchestration of neuroinflammatory responses in the retina.

In addition to $P2X_7$Rs, other P2R subtypes have been found in the rodent, cat and monkey retinae. The $P2X_2$R, $P2X_3$R and $P2X_5$R subtypes were strongly expressed in the dendrites and somata of cholinergic amacrine cells, in the mouse (Kaneda et al., 2004; Shigematsu et al., 2007). Furthermore, $P2X_3$Rs and $P2X_4$Rs were detected in the inner nuclear and ganglion cell layers of the rat (Wheeler-Schilling et al., 2001). $P2X_3$R immunoreactivity was localised to GABAergic amacrine cell bodies, and processes associated with rod and cone bipolar cell terminals in the rat inner plexiform layer (Puthussery and Fletcher, 2007). $P2X_1$Rs were also localised to neuronal processes in the inner plexiform layer, and to retinal ganglion cell bodies in the cat and monkey retinae (Yazulla and Studholme, 2004). $P2Y_1$R immunolabelling was observed in the ganglion cell layer, and on Müller cell processes and end feet (Ward and Fletcher, 2009). $P2Y_4$Rs were localised to presynaptic rod bipolar cell terminals in the inner plexiform layer, and to processes postsynaptic to cone bipolar cells (Ward et al., 2008).

4.2 $P2X_7$R neuromodulation in retina

The specific localisation of $P2X_7$Rs on neurons of the vertical rod-mediated pathway suggests that these receptors may have an important role in modulating scotopic visual responses under physiological conditions, as proposed by the extensive studies of Fletcher and colleagues (Puthussery et al., 2006; Vessey and Fletcher, 2012). A large body of evidence suggests a role for neuronal $P2X_7$Rs in the modulation of neurotransmitter release and subsequent regulation of synaptic function (Sperlágh et al., 2006). It would be interesting to clarify the neuronal role of this receptor in mediating synaptic efficacy within

the retinal circuitry. Furthermore, the expression of $P2X_7$Rs on Müller glia and microglia implicates a non-neuronal, modulatory contribution by the activation of these receptors, to visual responses in the retina. The following discussion highlights the current knowledge of the role of $P2X_7$Rs in modulating neuronal and glial function in the healthy mammalian retina.

Administration of an intravitreal injection of BzATP (4mM) led to a sustained potentiation in the photoreceptor-derived a-wave amplitude and a transient reduction in the post-photoreceptor b-wave component of the rat rod- and cone-mediated electroretinogram. This indicates the $P2X_7$R-mediated alteration of both rod and cone photoreceptors, and the concomitant modulation of a post-photoreceptor, ON-bipolar cell-mediated component (Puthussery et al., 2006).

In line with this notion, mixed rod and cone ERG responses were altered across all light intensities in a $P2X_7$R knockout mouse (Vessey and Fletcher, 2012). There was no change in the kinetics of the $P2X_7$R knockout rod PIII (a-wave), compared to the wild-type mouse. However, the dissected rod and cone PII (b-wave) components were larger in amplitude, along with a decreased latency to reach the maximum rod PII response (Vessey and Fletcher, 2012). The findings of this study provide compelling evidence that $P2X_7$ receptors contribute to overall retinal function by modulating both rod and cone pathways in the normal retina. Supported by immunohistochemical evidence of $P2X_7$R localisation on inhibitory horizontal and amacrine cells in the retina, the authors have suggested a role for $P2X_7$Rs at GABAergic synaptic terminals, in the regulation of synaptic transmission in the outer and inner plexiform layers (Vessey and Fletcher, 2012). However, horizontal cell contribution to the rod pathway remains controversial (Bloomfield and Dacheux, 2001), and $P2X_7$R activation in the goldfish retina does not evoke non-vesicular GABA release (Jones and

Palmer, 2009). Therefore, it would be of much interest and relevance to identify whether this $P2X_7R$-mediated alteration of the vertical rod pathway occurs in the absence of lateral inhibitory inputs.

The relative contribution of other P2-purinoceptors to retinal function has also been observed. $P2X_2R$-mediated currents sensitive to PPADS, were recorded from mouse OFF cholinergic amacrine cells, potentiating the frequency of IPSCs these cells, but not of ON cholinergic amacrine cells. Furthermore, PPADS application led to an increase in OFF- but a reduction in ON- ganglion cell firing rate. Thus, it was suggested that $P2X_2Rs$ are selectively expressed by cells of the OFF vertical pathway (Kaneda et al., 2008, 2010). It would be interesting to investigate whether there is a selective pathway dominance of the $P2X_7R$ in the mammalian retina. Thus, immunohistochemical and functional evidence have highlighted the presence of an array of P2 purinoceptor subtypes in the mammalian retina, adding to the complexity of dissecting a specific P2 purinoceptor component of ATP-gated synaptic modulation in the mammalian retina.

4.3 $P2X_7R$ modulation of Müller cell and astrocyte function

Müller cells express an array of P2X and P2Y receptors, and release ATP upon mGluR activation or osmotic membrane stretching. Autocrine, purinergic signalling is involved in the induction of intracellular glial calcium waves, and in the regulation of a variety of Müller cell functions, particularly in the uptake and metabolism of amino acid neurotransmitters (Wurm et al., 2011; Bringmann et al., 2013). Many studies have provided functional evidence for $P2X_7R$ modulation of Müller cell inflammatory processes in retinal disease. In mammalian species, in the absence of inflammation, functional $P2X_7Rs$ have only been found on human Müller cells (Wurm et al., 2011). ATP-induced $P2X_7R$-mediated large inward membrane

currents were potentiated in the absence of divalent cations, and were associated with the influx of calcium (Pannicke et al., 2000). However, prolonged $P2X_7R$ activation did not induce large pore formation (Pannicke et al., 2000), which is often characteristic of these receptors under conditions of inflammation. Thus, it has been proposed that under physiological conditions, $P2X_7Rs$ on Müller cells may be associated with the increase in glial intracellular calcium, which occurs during light illumination (Pannicke et al., 2000; Wurm et al., 2011; Newman, 2005)**.**

The close anatomical proximity between Müller cell and neuronal processes in the retinal plexiform layers suggests a role for bi-directional purinergic signalling between Müller cells and neurons. Indeed, it has been demonstrated that ATP released by retinal ganglion and/or amacrine cells upon light stimulation, induces a reduction in Müller cell intracellular calcium waves, through the activation of glial P2 receptors (Newman, 2005)**.** Furthermore, Müller cell-derived ATP, which is rapidly degraded to adenosine, has shown to inhibit retinal ganglion cell firing rate through the activation of A1 adenosine receptors and the opening of potassium channels (Newman, 2003; 2004). Although this latter finding does not directly involve the activation of P2 receptors, it highlights a neuronal target of Müller cell-released ATP. It would be interesting to investigate whether ATP from Müller cells can be released at a sufficiently high concentration to evoke $P2X_7R$ activation on neighbouring neurons in the retina, under physiological conditions.

Retinal astrocytes are largely restricted to the RGC axon-containing nerve fibre layer and are closely associated with retinal vasculature (see section 4.5.2.1) across the retinal surface and in the inner retinal layers (Newman, 2004). Although astrocytes are not thought to play a direct role in retinal neuromodulation, gap junctional coupling with Müller cells along with their role in controlling vascular tone in the retina may indirectly contribute to overall visual

function. Furthermore, the presence of $P2X_7Rs$ on retinal astrocytes is disputed, although modulation of Müller cell function may occur through the release of ATP or the propagation of intracellular calcium waves (Newman, 2004; 2005)**.** In other areas of the CNS, brain astrocytes have shown to release glutamate and other neurotransmitters on stimulation of $P2X_7Rs$ (Sperlágh et al., 2006), and thus further investigation may provide clues as to whether the same may occur in the retina.

4.4 $P2X_7R$ modulation of microglia in the retina

$P2X_7Rs$ have been located on microglia in the mammalian retina, although they have been most extensively associated with inflammatory conditions and retinal disease (Innocenti et al., 2004; Franke et al., 2005). In recent years, much research has been conducted on the role of microglia in the healthy CNS. Microglial processes are highly motile and the movement of their processes is tightly regulated by extracellular ATP/ADP balance (Davalos et al., 2005; Nimmerjahn et al., 2005; Gyoneva and Traynelis, 2013). Microglia express other P2Rs which are known to play an essential role in process extension / retraction. Under conditions of high neuronal activity within the visual pathway, microglial processes form close contacts with synaptic elements. In some cases, these contacts result in the modulation of neuronal activity (Wake et al., 2009; Tremblay et al., 2010; Li et al., 2012).

The mechanism by which this modulation occurs is uncertain, but it has been suggested that microglia may release various neuroactive substances such as glycine (Hayashi et al., 2006). Furthermore, $P2X_7R$-mediated microvesicle release from microglia has been characterised, and is thought to play a role in modulating synaptic efficacy under normal physiological conditions (Turola et al., 2012). Most studies have been carried out in the brain. Retinal microglia have shown to be influenced by the activation and blockade of

various neurotransmitter receptors (Fontainhas et al., 2011), and thus are capable of being themselves, modulated by neuron-released transmitters, including ATP. The evidence of microglial-induced fine-tuning and modulation of neuronal synaptic activity in the brain strongly supports the notion that this may also occur within the retina. Microglia are exclusively localised to the inner and outer plexiform layers within the normal adult mouse retina (Santos et al., 2008). Thus, microglial processes are in close proximity to retinal synaptic elements, pointing to the possibility of playing a genuine role in retinal visual processing by shaping and fine-tuning neuronal signalling.

4.5 $P2X_7R$ in retinal pathology

$P2X_7R$ expression is known to be significantly upregulated in many CNS pathologies in which microglial activation and proliferation are characteristic features (Monif et al., 2010). Although the function of $P2X_7Rs$ in pathology is heavily associated with the orchestration of the early microglial inflammatory response, these receptors are also known to directly co-ordinate neuronal dysfunction and cell death. The following section highlights the current knowledge of the role of $P2X_7R$ in neuronal degeneration, Müller cell dysfunction and microglial activation under pathological conditions in the mammalian retina. Furthermore, $P2X_7R$-associated molecular mechanisms of inflammation in the retina are also discussed.

4.5.1 Photoreceptor degeneration

The enhancement of $P2X_7R$ expression and activation by extracellular ATP is associated with the elevation of intracellular calcium and subsequent photoreceptor and retinal ganglion cell death, thus implicating a role for $P2X_7R$ in retinal degenerations such as retinitis pigmentosa, glaucoma, age-related macular degeneration (AMD) and retinopathies (Mitchell et al., 2009; Fletcher, 2010).

In the BALBC*rds* (retinal degeneration slow) mouse model of retinitis pigmentosa, $P2X_7R$ mRNA and protein expression were enhanced exclusively on neuronal populations, and absent on glial cells. Furthermore, $P2X_7R$ expression peaked during the stage at which photoreceptor degeneration was most pronounced, with $P2X_7R$ expression levels declining following neuronal loss (Franke et al., 2005). In line with this finding, intravitreal injection of high extracellular ATP into the normal adult rat eye induced extensive apoptosis of photoreceptors with severe degeneration of the outer nuclear layer (Puthussery and Fletcher, 2009). These morphological changes were accompanied by an irreversible reduction in the ERG a-wave amplitude, suggesting impairment in photoreceptor function. A follow-up study by the same group found that ATP had induced total photoreceptor loss by six months post-injection, with a subsequent remodelling of retinal circuitry through the formation of new synapses, which is characteristic of various retinal degenerations including AMD (Vessey et al., 2014).

Administration of the broad spectrum P2X antagonist, PPADS appeared to protect against the ATP-induced morphological changes in the normal rat retina, and also augmented photoreceptor survival in the *rd1* mouse model of retinitis pigmentosa, within the first week post-injection (Puthussery and Fletcher, 2009). However, it is still to be determined whether the administration of the P2XR antagonist also reverses the ATP-induced functional changes in the ERG responses. It has been proposed that ATP release from degenerating photoreceptors may exacerbate neuronal apoptosis through the activation of $P2X_7Rs$ and the subsequent elevation in intracellular calcium (Puthussery and Fletcher, 2009; Fletcher, 2010; Vessey et al., 2012). Interestingly, within 3-min of intravitreal BzATP (a more potent $P2X_7R$ agonist than ATP) injection into the rat eye, a potentiation in the ERG a-wave amplitude was observed, an effect which is contrary to the ATP-induced functional changes

in the ERG a-wave (Puthussery et al., 2006; Puthussery and Fletcher, 2009), and thus puts into question the specific involvement of $P2X_7R$ in the latter model of retinal degeneration. However, this disparity may be due to the different intervals at which the ERG recordings were tested post-injection (BzATP: 3, 15 and 45 min; ATP: 1 and 5 days). Therefore, these findings reveal the possibility of differential time-dependant effects of $P2X_7R$ activation on retinal processing. It would be of much therapeutic interest to establish whether a selective $P2X_7R$ antagonist can reverse the ATP-mediated neurodegeneration and dysfunction in such models of retinal dystrophies, as well as the early functional changes seen in the BzATP-treated retina.

Subretinal haemorrhage and choroidal neovascularisation are associated with severe photoreceptor degeneration in AMD. Extracellular ATP was found to be elevated in vitreous samples of AMD patients with subretinal haemorrhage, implicating a role for ATP-mediated retinal pathology (Notomi et al., 2013). In line with this notion, BzATP-mediated and BBG-sensitive $P2X_7R$ activation induced significant photoreceptor cell death associated with caspase-8 and -9 activation, in primary retinal cultures (Notomi et al., 2011). In an *in vivo* model of subretinal haemorrhage, extravascular blood injected into the subretinal space of the mouse eye induced photoreceptor apoptosis, which was markedly reduced in the presence of BBG (Notomi et al., 2013). Retinal pigment epithelial cells are known to release ATP into the subretinal space, and therefore may contribute to the ATP-mediated photoreceptor degeneration seen in several pathologies (Mitchell and Reigada, 2008). Additionally, dysregulation of lysosomal pH, lipid oxidation and impaired phagosome clearance were triggered by $P2X_7R$ activation in cultured human RPE cells (Guha et al., 2013). Furthermore, cell death in retinal microvascular cells mediated by ATP-induced $P2X_7R$ activation, was associated with the concomitant activation of voltage-gated calcium channels and the subsequent lethal elevation of intracellular calcium (Sugiyama et al., 2005). Therefore, the activation of $P2X_7Rs$ in RPE cells and on retinal microvasculature may

also exacerbate the pathological microenvironment in the retina and lead to neuronal cell death.

4.5.2 Retinal ganglion cell degeneration

Retinal ganglion cells are distinctly vulnerable to metabolic disruptions, often leading to selective and severe neuronal loss by apoptosis in diseases such as glaucoma and diabetic retinopathy (Križaj et al., 2013). The presence and activation of $P2X_7Rs$ on retinal ganglion cells are well established and suggested to play an important role in ganglion cell degeneration. Several $P2X_7R$-mediated mechanisms of ganglion cell dysfunction have been characterised in response to distinct primary triggers, including ATP-stimulated lethal elevation of intracellular calcium, mechanical/pressure-induced damage and hypoxia/ischemia-associated cytokine release.

ATP-induced increase in calcium permeability of retinal ganglion cell P2XRs was first shown in cultured rat RGCs (Taschenberger et al., 1999). Subsequently, it was shown that BzATP- and ATP-mediated $P2X_7R$ activation in isolated RGCs produced a large, sustained increase in calcium levels, which were blocked by BBG treatment (Zhang et al., 2005). Furthermore, treatment with either BBG or oxATP, but not suramin, inhibited the BzATP-induced, dose-dependent increase in retinal ganglion cell death *in vitro* and *in vivo* (Zhang et al., 2005; Hu et al., 2010). The RGCs were impermeable to YO-PRO-1, suggesting that these cells were not associated with large pore formation, which is often seen in $P2X_7R$-mediated apoptosis (Mitchell et al., 2009). These findings indicate that through direct ATP-mediated $P2X_7R$ activation, retinal ganglion cells are readily permeable to calcium, which can rapidly lead to neuronal death through a large and sustained elevation in intracellular calcium.

Elevated intraocular pressure, a hallmark of glaucoma-associated ganglion cell degeneration, is known to induce a pathological increase in extracellular ATP in the aqueous humour of human patients with acute and chronic glaucoma (Zhang et al., 2007; Li et al., 2011). In a rat model of experimentally induced pressure damage, degradation of extracellular ATP or selective blockade of $P2X_7$Rs with BBG, prevented pressure-induced ganglion cell membrane blebbing-associated damage (Resta et al., 2007). Furthermore, a rapid rise in IOP caused significant damage to these cells *in vitro* and *in vivo*, which was otherwise not seen in slow IOP elevation, suggesting that mechanisms of acute ganglion cell injury could differ from slow-developing chronic states of pathology (Resta et al., 2007). A pressure-dependent rise in extracellular ATP in the bovine retina was reduced by pannexin-1 inhibitors, carbenoxolone and NPPB, suggesting that ATP release may be driven through pannexin-1 channels (Reigada et al., 2008). Indeed, mechanical deformation of isolated rat RGCs led to the release of ATP, which was sensitive to probenicid, carbenoxolone and inhibitory peptide ^{10}Panx (Xia et al., 2012). Additionally, mechanical stretch and subsequent swelling of RGCs led to the activation of cationic membrane currents that were sensitive to the $P2X_7$R antagonists A-438079, AZ-10606120 and zinc, and to inhibitors of panx-1. Thus, it was suggested that ATP released via pannexin hemichannels on damaged RGCs acts cell-autonomously to activate $P2X_7$ receptor-mediated currents in an autostimulatory feedback loop (Xia et al., 2012).

$P2X_7$R activation has also been linked to the release of pro-inflammatory mediators in retinal ganglion cell degeneration (Sugiyama et al., 2013). Following experimental IOP elevation in rats, retinal ganglion cell loss was ameliorated in the presence of the $P2X_7$R antagonists OxATP and BBG. In addition, simultaneous upregulation of $P2X_7$R and the cytokines IL-1β, TNFα and IL-6 were markedly suppressed in the presence of the antagonists (Sugiyama et al., 2013). Taken together, the results of these studies suggest that under conditions of

acute mechanical injury due to elevated IOP, panx-1-induced ATP release from damaged ganglion cells themselves is sufficiently high to activate $P2X_7$Rs and drive cell damage, possibly through lethal calcium influx. Furthermore, the exceptionally close link between $P2X_7$Rs and enhanced cytokine release in glaucoma pathology supports the notion that $P2X_7$R activation likely drives the upregulation of these mediators from surrounding glia, leading to a secondary inflammatory response that may exacerbate the condition.

In addition to their involvement in acute mechanical stress, $P2X_7$Rs have also been linked to dysregulation in retinal blood flow and subsequent ischemia, mechanisms associated with the pathogenesis of glaucoma. RGC loss due to simulated ischemia has shown to involve $P2X_7$R activation in human organotypic retinal cultures (Niyadurupola et al., 2013). Selective $P2X_7$R blockade by BBG attenuated the effect of RGC degeneration in retinae that underwent BzATP treatment or oxygen-glucose deprivation. $P2X_7$Rs are expressed by glial cells and may have contributed to RGC loss in this model. However, it was determined under normal conditions that the $P2X_7$R expression pattern correlated with that of INL and GCL molecular markers (Niyadurupola et al., 2013). Therefore, although the indirect contribution of glial activation cannot be ruled out, a direct role of $P2X_7$Rs in RGC death is also probable under ischemic conditions, in line with a mechanism demonstrated in other models of RGC damage and degeneration (Zhang et al., 2005; Xia et al., 2012).

Hyperglycaemia and alterations in retinal vascular functions are major contributory factors to the development and progression of diabetic retinopathy-associated neuronal damage. High glucose conditions are known to enhance the release of extracellular ATP, which causes retinal neuronal death through P2XR-mediated lethal elevation of intracellular calcium (Costa et al., 2009; Oliveira Simões Pereira et al., 2010). Further to this, $P2X_7$R activation induced pore formation and apoptosis of retinovascular cells, which was associated with an increase

in intracellular calcium, in hyperglycaemic rat retinae (Sugiyama et al., 2004, 2005). Intravitreal injection of BzATP into the healthy rabbit eye caused a marked reduction in retinal blood velocity. This effect was significantly enhanced in diabetic rabbits, and was accompanied by a considerable attenuation in the amplitudes of the ERG a- and b-waves (Sugiyama et al., 2006). It is clear from these findings that $P2X_7R$-associated changes in retinal vascular function are key mechanisms involved in the disruption of visual processing in the retina.

The release of ATP from glial cells and the subsequent purinergic control of vascular tone in the retina through the activation of $P2X_1$ and $P2Y_4$ receptors has also been demonstrated in the rodent (Kawamura et. al, 2003; Kur and Newman, 2014). This phenomenon, and those discussed above (Sugiyama et al., 2004, 2005), highlight the intimate relationship between the retinal microvasculature and cells of the retinal parenchyma. Control of vascular tone and maintenance of the blood-retinal barrier is mediated by the 'neurovascular unit' (NVU) – a functional unit consisting of close interactions between various cell-types including neuronal, glial and vascular endothelial components (Metea and Newman, 2007; Stanimirovic and Friedman, 2012). A change in vascular tone can significantly modulate the diameter of the blood vessels, and is therefore important in influencing the velocity of blood flow through the vasculature (Metea and Newman, 2007). As described above, changes in retinal blood velocity can contribute significantly to the disruption of neuronal function within the retina (Sugiyama et al., 2006). Furthermore, under pathological conditions, the loss of structural integrity of the NVU and resultant uncoupling of the cells are major contributory factors in the disruption of the blood retinal barrier, and can lead to a large increase in the permeability to serum proteins and fluid, initiating an inflammatory response within the retina (Stanimirovic and Friedman, 2012). The upregulation and recruitment of inflammatory mediators may lead to a secondary injury and therefore contribute to retinal ganglion cell death. Thus, $P2X_7R$ may also modulate neuronal function and viability through the indirect

control of retinal blood flow, by facilitating local ATP release, and subsequent purinergic control of vascular tone.

4.5.3 Müller cell $P2X_7R$

Functional changes in Müller cells are characteristic of $P2X_7R$-associated mechanisms in glaucoma, retinal ischemia and diabetic retinopathy (Bringmann and Wiedemann, 2012). Under pathological conditions, reactive Müller cells are pivotal in the generation of neuroprotective adenosine from extracellular ATP, by upregulating the release of ectonucleotidases (Iandiev et al., 2007). Accordingly, high extracellular ATP and $P2X_7R$ activation are known to play a significant role the proliferation of Müller cells. BzATP-stimulation of isolated human Müller cells evoked a $P2X_7R$-mediated rise in intracellular calcium, which was coupled with the activation of large conductance Ca^{2+} -activated K^+ channel (BK) currents. Furthermore, Müller cells from patients with proliferative vitreoretinopathy demonstrated significantly larger BK and $P2X_7R$ cation currents (Bringmann et al., 2001). These findings support the notion that an increase in $P2X_7R$ expression in proliferative disease elevates intracellular calcium and subsequently promotes larger BK conductances, which drive Müller cell proliferation (Bringmann et al., 2001; Bringmann and Wiedemann, 2012). In line with this, an upregulation of $P2X_7R$ cation currents is correlated with the downregulation of inwardly rectifying potassium channel (Kir) currents in Müller cells from patients with proliferative diabetic retinopathy (Bringmann et al., 2002). Thus, a shift in potassium homeostasis triggered by $P2X_7Rs$ promotes Müller cell activation and proliferation under pathological conditions, and the promotion of inflammation (Pannicke et al., 2005). Furthermore, glutamate uptake currents were diminished in the presence of BzATP, an effect which was suppressed by KN-62, in human Müller cells (Pannicke et al., 2000; Bringmann et al., 2013). Therefore, $P2X_7R$ activation also disrupts Müller cell glutamate uptake, which likely contributes to excitotoxicity, cell swelling and

apoptosis under pathological conditions in the retina. In cultured rat Müller cells, elevated glucose conditions increased $P2X_7R$ mRNA, although the receptor protein or function were not detected in these cells (Trueblood et al., 2011).

4.5.4 Microglial $P2X_7R$

Microglia act as crucial sensors for pathological disturbances within the neural parenchyma (Kreutzberg, 1996). The activation and proliferation of microglia are characteristic features of almost all forms of trauma, stress and neurodegenerative conditions in the CNS (Monif et al., 2010). Furthermore, the concurrent upregulation of $P2X_7Rs$ on microglia under pathological conditions has led to the widely held notion that early immune responses generated by activated microglia are primarily driven through $P2X_7R$ activation (Ferrari et al., 2006; Monif et al., 2010). Extracellular ATP, released by surrounding stressed or injured neurons acts as a 'danger' signal to induce the activation and proliferation of these cells, which undergo rapid morphological and functional changes in graded responses (Raivich et al., 1999; Streit et al., 1999). Thus, delineating the morphological features of these cells can provide compelling insight into their functional behaviour. Microglia are highly ramified in structure, with numerous processes when in their 'resting' state, but are far from quiescent as they constantly monitor neuronal synapses in their locality. Activated microglia typically take on an amoeboid appearance, with few or no processes, and have the capacity to secrete a vast array of molecular signals, including cytokines, chemokines, ATP and reactive oxygen species, all of which trigger further inflammatory cascades. These activated microglia proliferate and migrate to the site of cellular stress, and provide imperative trophic support to the injured neuron, in addition to phagocytosing surrounding cellular debris. Activated microglia are notoriously associated with the secretion of ATP and pro-inflammatory cytokines such as interleukin-1β (IL-1β), tumour necrosis factor-α (TNFα) and colony-stimulating factors (CSF), which in turn are linked with mediating cell death through

apoptosis. Depending on the extent of cellular stress within the microenvironment, these inflammatory phenomena may eventually lead to either the recovery of neuronal integrity, or drive the progression towards the onset of secondary injury responses (Raivich et al., 1999; Streit et al., 1999).

Selective blockade of $P2X_7Rs$ and subsequent suppression of microglial activation, has proven effective in reducing the severity of neuronal dysfunction, degeneration and promoting recovery in *in vivo* models of spinal cord injury (Wang et al., 2004; Peng et al., 2009), mechanical injury in the nucleus accumbens (Franke et al., 2007), amyotrophic lateral sclerosis (D'Ambrosi et al., 2009), epilepsy (Vianna et al., 2002; Avignone et al., 2008) and Parkinson's disease (Marcellino et al., 2010). $P2X_7R$-mediated microglial release of inflammatory molecules and reactive oxygen species has also been implicated in the pathogenesis of Alzheimer's disease (Parvathenani et al., 2003; Mclarnon et al., 2006; Sanz et al., 2009), neuropathic pain and hyperalgesia (Chessell et al., 2005; Honore et al., 2006; McGaraughty et al., 2007; Clark et al., 2010; Teixeira et al., 2010).

As in other areas of the CNS, microglial activation and inflammation are concurrent phenomena in many retinal and ocular pathologies including photoreceptor dystrophy, AMD, acute retinal trauma, optic nerve transection, glaucoma, uveitis, diabetic retinopathy and proliferative vitreoretinopathy (Chen et al., 2002; Langmann, 2007). Although a significant body of evidence suggests a pathological role for $P2X_7R$ activation in microglia of the brain and spinal cord, investigations into the role of $P2X_7R$ in retinal microglia are still in their infancy, and thus it remains poorly understood.

In the rat retina, $P2X_7R$ activation induced pore formation exclusively in microglia. High extracellular ATP or BzATP concentrations led to YO-PRO-1 accumulation in these cells, but not in retinal ganglion or Müller cells in the ganglion cell and nerve fibre layers, an effect which was attenuated with selective $P2X_7R$ blockade (Innocenti et al., 2004). This finding suggests that $P2X_7R$-induced pore formation is microglia-specific, and likely plays an important role in the microglial inflammatory response. Additionally, under hypoxic conditions, BzATP enhanced the release of the pro-inflammatory cytokines IL-1β and TNFα in cultured rat retinal microglia (Morigiwa et al., 2000). Under hyperglycaemic conditions, high ATP or BzATP concentrations induced calcium influx through unspecified P2XRs in cultured microglia (Oliveira Simões Pereira et al., 2010). Selective inhibition of $P2X_7Rs$ suppressed the release of IL-1β, IL-6 and TNFα, and subsequently reduced retinal ganglion cell neurodegeneration in a rat model of elevated IOP (Sugiyama et al., 2013). It was not clear in this study whether these neuroprotective effects were exerted through the direct blockade of $P2X_7Rs$ on retinal ganglion cells, or indirectly through inhibition of microglial activation.

Chapter 4 Figures

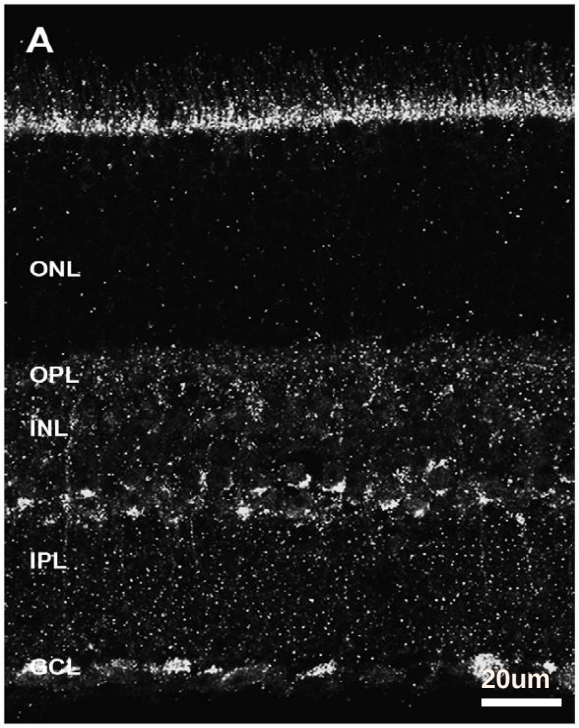

Figure 4.1 Distribution of $P2X_7Rs$ in the mouse retina. Transverse retinal section immunolabelled for the $P2X_7R$ N-terminal, in the wild type mouse. $P2X_7R$ immunoreactivity is most prominent in the outer and inner plexiform layers, inner nuclear layer and ganglion cell layer. The punctate structures indicate that $P2X_7Rs$ are present at synapses and may therefore regulate synaptic function. The ganglion cell layer and the proximal region of the inner nuclear layer show $P2X_7R$ immunolabelling in soma-like structures, suggestive of their expression on neuronal cell bodies, as well as on neurites. ONL, outer nuclear layer; OPL, outer plexiform layer; INL, inner nuclear layer; IPL, inner plexiform layer; GCL, ganglion cell layer. Figure adapted from Vessey and Fletcher (2012).

Chapter 5

Project Hypothesis

ATP-gated $P2X_7Rs$ have been specifically localised to synapses within the rod pathway of the mammalian retina. In the healthy rodent, *in vivo* electroretinogram (ERG) studies have shown alterations to both outer and inner retinal function, in response to short-term administration of the P2XR agonist, BzATP (Puthussery and Fletcher, 2004; Puthussery et al., 2006; Vessey and Fletcher, 2012). However, the specific contribution of $P2X_7Rs$ to the BzATP-mediated modulation of retinal function remains elusive. A further complexity that $P2X_7Rs$ are distributed throughout all layers of the retina, adds to the uncertainty of the specific site(s) of action for these receptors in modulating neurotransmission within the retina. In line with this notion, it is unclear from the sole use of ERG recordings, whether $P2X_7Rs$ also directly modulate retinal ganglion cell synaptic function.

Using a dark-adapted *ex vivo* mouse retinal wholemount preparation to record extracellular, light-evoked transretinal ERG responses, and ON and OFF RGC excitatory synaptic responses, and with the use of selective $P2X_7R$ antagonists, the present investigation sought to address the following questions:

- Do $P2X_7Rs$ modulate signal transmission at the photoreceptor-ON bipolar cell synapse?

- Is retinal ganglion cell function within both the ON and OFF pathways modulated by $P2X_7R$ activation?

- Are the effects of $P2X_7R$ activation in the inner retina driven by their action in the outer retina, or do these receptors have cell-specific and distinct mechanisms of action?

$P2X_7Rs$ are also expressed on retinal microglia (Innocenti et al., 2004; Franke et al., 2005), and are known to drive microglial activation and the release of inflammatory mediators associated with the early host-response to stressors in the microenvironment (Monif et al., 2010). Growing evidence supports the notion that purinergic signalling coordinates resting microglia to play a genuine role in fine-tuning synapses and modulating neuronal transmission in the healthy central nervous system (Nimmerjahn et al., 2005; Tremblay et al., 2010; Pascual et al., 2011). In the adult mouse retina, microglia are exclusively localised to the synapse-rich outer and inner plexiform layers, under physiological conditions (Santos et al., 2008). Retinal microglia have shown to undergo rapid morphological and functional alterations in response to various neurotransmitters (Fontainhas et al., 2011). However, their specific contribution to synaptic signalling in the healthy retina remains elusive. In light of this, the present investigation sought to explore the following questions:

- Does early microglial activation modulate signal transmission at the photoreceptor-ON bipolar cell synapse?

- Is retinal ganglion cell function within both the ON and OFF pathways modulated by early microglial activation?

- Does the microglial-mediated mechanism of neuromodulation specifically involve $P2X_7Rs$?

Chapter 6

Materials and Methods

To investigate effects on outer and inner retinal synaptic function, transretinal electroretinogram (ERG) or ON and OFF field excitatory postsynaptic potentials (fEPSPs) were recorded from dark-adapted *ex vivo* mouse retinae, in response to a single flash of light repeated at regular intervals. Pharmacological compounds were applied to the bathing medium, which continuously superfused the slice preparation through the course of each experiment. The effect of pharmacological compounds on microglial morphology was assessed using a combination of immunofluorescence staining, laser scanning confocal microscopy and morphometric analysis. Unless otherwise stated, all procedures during the pharmacological experiments were carried out in low-light conditions and red light was used for illumination.

The use of the acutely isolated (*ex vivo*) retinal preparation of the mouse, employed for these investigations provides many advantages over experimentation *in vivo*. The laminar structure of the retinal circuitry remains relatively intact with minimal effect to its overall structural integrity, in the isolated retina. Therefore, its full repertoire of afferent inputs from the outer to inner retinal layers remains unaltered, enabling the use of relatively natural photostimulation of neuronal responses. The isolated retina facilitates pharmacological isolation and investigation of specific retinal circuitry, and also obviates the requirement for anaesthesia of the animal, which may otherwise confound observations. Further considerations which favour this preparation include the relative ease of control over drug application and modification of the extracellular milieu, as well as the viability of the tissue, rendering stable responses to be recorded over duration of up to 6 hours.

The investigation of RGC responses *in vivo* is usually limited to the recording of signal transduction to the brain, along the optic tract. The isolated retina enables deeper exploration of mechanisms associated with the generation of RGC responses in the inner retina. The main disadvantage in using the *ex vivo* preparation is that the observations are limited to, and may reflect the artificial conditions of the experiment. In this respect, the use of *in vivo* recordings may instead provide a better understanding of physiological function in the intact animal. Additionally, the isolated retina lacks the natural optics of the intact eye, which could obscure the response properties of neurons when compared to those *in vivo*. However, there is a high degree of similarity in the response properties between transretinal *ex vivo* and corneal *in vivo* ERGs, which supports the use of the isolated retinal preparation as a valuable tool for the present investigation.

Purinergic signalling and other mediators released as a result of microglial activation are important for the recruitment of blood-borne monocytesand leukocytes, under inflammatory conditions. Thus, the isolated nature of this retinal preparation is particularly advantageous for this study, as it would enable the investigation of purinergic modulation of retinal microglia and neuronal activity, in the absence of possible systemic influences.

For both electrophysiological and microglial investigations, the protocols for preparation of the retinal wholemount and setup of the perfusion chamber were the same. The experimental procedures for all experiments are as follows.

6.1 Animals

Adult (4-12 weeks) male and female C57BL/6 mice (Harlan Laboratories) were housed on a 12-hour light/dark cycle, in the Biological Resources Unit, Institute of Ophthalmology, University College London. The animals were given unlimited access to food and water. All procedures were in accordance with the UK Animals (Scientific Procedures) Act 1986, and approved by the UK Home Office and the University College London local ethics committee.

6.2 Preparation of the *ex vivo* mouse retinal wholemount

Animals were killed by cervical dislocation and decapitation. The eyes were rapidly removed and placed into an ice-cold, oxygenated high-sucrose Krebs' medium devoid of sodium chloride, containing (mM): sucrose 202, KCl 2, KH_2PO_4 1.25, $MgSO_4$ 10, $CaCl_2$ 0.5, $NaHCO_3$ 26, glucose 10. The eyes were placed in a Petri dish containing sucrose Krebs' medium, under a dissection microscope and red light was used for illumination. In order for the wholemount to lie flat, the optic nerve and extra-ocular muscle tissue were removed from the sclera. Using forceps and a small needle, a cut was made at the ora serrata, and the cornea and iris were removed with micro-scissors. This was followed by the removal of the lens and vitreous, by gently but swiftly pulling them away from the retina, leaving the open eye-cup, consisting of the intact retina, retinal pigment epithelium and sclera. The eye-cup was cut into quadrants to allow it to lie flat, as a wholemount preparation, with the integrity of the retinal circuitry maintained.

During the isolation of the eye-cup, every effort was made to ensure minimal contact between the dissection instruments and the retina. It was extremely important to limit mechanical trauma to the retina in order to avoid any potential microglial activation or inflammation which may have otherwise arisen. Furthermore, the intact RPE layer ensured

that regeneration of the photopigment was sustained throughout the course of the experiments, which helped to maintain stability of the responses.

6.3 Perfusion / recording chamber

The retinal wholemount, ganglion cell layer side up, was transferred to a blacked-out, oxygenated (95% O_2, 5% CO_2; BOC) interface recording chamber within a Faraday cage, set on top of an air-filled anti-vibration table. The retina was held partially submerged between tissue paper and a nylon liner placed over the top, to direct the flow of fluid, with the gas flowing over the top. The slice was superfused with O_2/CO_2 Krebs' medium containing (mM): NaCl 124, KCl 2, KH_2PO_4 1.25, $MgSO_4$ 1, $CaCl_2$ 2, $NaHCO_3$ 26, glucose 10. The perfusion was carried out using a Minipuls3 Gilson pump at a flow rate of 0.4ml/min. A constant temperature of 36±0.2°C was maintained using a water bath (Grant Instruments) to heat the perfusion medium, and a heating mat contained within the recording chamber. The retina was allowed to recover for approximately 60 minutes prior to experimentation.

The particular conditions employed for these experiments were chosen and optimised to ensure the maintenance of a relatively homeostatic environment for the retinal preparation. Previous studies on isolated retinal wholemounts have shown that temperature changes, or any deviation in ionic and metabolite composition, and pH of the extracellular perfusate, induces alterations in retinal function, as assessed by transretinal ERG recordings (Winkler, 1972, 1973). Thus, the composition of the Krebs' medium ensured the proper function of the isolated retinal tissue. Furthermore, microglia in isolated retinal wholemount preparations are temperature-sensitive (Opie et al., 2012). Thus, the temperature was optimised to maintain proper function of all retinal cell-types.

6.4 Electrophysiology

The same protocols were followed for acquisition and pharmacological investigations of transretinal ERG and RGC fEPSP responses, unless otherwise stated. Differences in the recording electrodes and sensory stimulation protocols are highlighted where appropriate.

6.4.1 Recording electrode and response acquisition

Extracellular recording electrodes were pulled from borosilicate glass capillaries (1.2x0.69mm, Clark Electromedical Instruments) using a horizontal P97 Flaming/Brown micropipette puller (Sutter Instruments). The electrodes were filled with normal Krebs' medium (see above for composition), with an impedance of 2 - 8 MΩ for both ERG and RGC fEPSP recordings. An Ag - AgCl pellet submerged in a well and connected to the recording chamber was used as a reference electrode. The recording electrode was fitted into an electrode holder, filled with 1M NaCl, and attached to an HS2 headstage (Axon Instruments). Responses were amplified and low pass filtered (1 kHz) with an Axoprobe-1A multipurpose microelectrode amplifier (Axon Instruments), digitised (5 kHz) via a CED1401 interface, and stored on a computer with Spike2 software (Cambridge Electronic Design Ltd., Cambridge, UK). Mains-related noise was eliminated (50/60 Hz) with a Humbug noise reduction system (Quest Scientific).

The headstage was connected to an electronic micromanipulator (MS314, Marzhauser-Wetzier), allowing the recording electrode to be moved in the *x*-, *y*- and *z*-axis planes. To obtain transretinal ERG responses, the recording electrode was manually lowered onto the surface of the retinal wholemount, without breaking into the retinal layers. For retinal ganglion cell fEPSP acquisition, the electronic micromanipulator was used to further lower the electrode vertically (along the z-axis), from the surface of the wholemount in 5 – 10 µm

steps, at a rate of 1μm/step, every 10-15s until break-through to the ganglion cell layer, where recordings were obtained. Fig. 6.1 illustrates the positions of the recording electrodes for acquisition of ERG and fEPSP responses.

6.4.2 Visual stimulation of responses

The retinal wholemount was stimulated with a full-field, green light-emitting diode (LED; λ=562nm) set approximately 2 cm above the preparation, and co-ordinated by a Master-8 pulse generator. ERG responses were stimulated with a 10 ms - duration flash, repeated every 3 sec. RGC fEPSPs were stimulated with a 1 sec - duration flash, repeated every 3 sec.

Upon stimulation, the transretinal ERG exhibited a characteristic waveform, composed of the negative a-wave, a prominent, and large-amplitude positive b-wave, and oscillatory potentials superimposed on the leading edge of the b-wave. For the RGC fEPSP experiments, the onset and termination of the light stimulus produced negative ON- and OFF- RGC fEPSPs, respectively. Depending on the nature of the recordings (ERG or fEPSPs), the presence of the characteristic components of the waveforms was used to determine the viability of the retinal wholemount preparation. Light intensity-response functions were investigated for both ERG and fEPSP responses, and were used to establish the light intensity at which a sub-maximal response was induced. At the beginning of each experiment, the flash intensity was set to -2.32 log cd.s/m^2, and was increased with 15 sec-duration intervals, until the maximum intensity (-0.54 log cd.s/m^2) was reached. Light intensity-response functions were carried out at least twice more on one preparation, prior to the application of an investigative pharmacological compound, in order to test the viability of the retinal wholemount. The preparation was considered viable if sub-maximal responses

were observed between the typical stimulus range of -1.47 and -0.96 log cd.s/m^2 (see figs. 7.2 and 7.6).

6.4.3 Application of drugs

In all experiments, the retinal preparation was allowed to recover in Krebs' medium for approximately 60 min. Some ERG experiments were carried out in this medium. For some ERG and all RGC fEPSP experiments, consistency in recording conditions was maintained using a Krebs' medium, which was modified to isolate and enhance the NMDA-mediated component of the ON and OFF RGC fEPSPs. The solution (hereafter referred to as PMSTN) was composed of (mM): NaCl 124, KCl 2, KH_2PO_4 1.25, $CaCl_2$ 2, $NaHCO_3$ 26, glucose 10, NBQX 0.01, picrotoxin 0.1, strychnine 0.005, tetrodotoxin 0.0001. Magnesium ions were not present in the PMSTN medium to remove blockade of NMDA receptors, and thus enhance the NMDA receptor-mediated component. AMPA, $GABA_{A/C}$ and glycine receptors, and sodium channels were blocked with NBQX, picrotoxin, strychnine and tetrodotoxin, respectively.

For all experiments, the stimulus was set at a light intensity that elicited sub-maximal responses. All test compounds were prepared in dH_2O (unless otherwise stated), and added to the bathing medium at known concentrations. Table 6.1 shows all pharmacological compounds used in this study. The protocols for order and duration of drug application in specific investigations are as follow. Differences in protocols for ERG and RGC fEPSP experiments are highlighted where necessary.

6.4.3.1 L-AP4

The group III metabotropic glutamate receptor agonist, L-2-amino-4-phosphonobutyric acid (L-AP4) was tested on both ERG and RGC fEPSP responses. All L-AP4 experiments were carried out in PMSTN bathing medium. For ERG experiments, L-AP4 (50 µM) was applied for 5 min. For the RGC fEPSP dose-response investigation, L-AP4 was tested at concentrations of 10, 20, and 50 µM, applied cumulatively. In some experiments, 5 and 100 µM doses were also tested. Each application was 10 min in duration. At the beginning or end of some experiments, L-AP4 (50 µM) was applied for 5 min, to verify retinal function and assess drug access to the wholemount.

6.4.3.2 Purinergic agonists, $P2X_7R$ antagonists and LPS

The effect of BzATP on the ERG was tested in normal Krebs' perfusate, and in the absence of extracellular magnesium ions. In these experiments, BzATP was applied for 10 min. For the dose-response investigation of BzATP on ON and OFF RGC fEPSPs, no more than two applications of BzATP were used on one preparation, regardless of concentration. The same protocol was followed for the dose-response investigation of adenosine on RGC fEPSP responses.

The protocol for investigating the effect of BzATP in the presence of the $P2X_7R$ antagonist A438079 was the same for ERG and RGC fEPSP experiments. BzATP (300 µM) was applied to PMSTN medium for 10 min, followed by a 30 – 40 min washout period. A438079 was then added to the medium and allowed to superfuse the retina until a stable response was reached (~ 20 – 30 min). BzATP was then co-applied with the antagonist-containing medium. In separate experiments, the effect of the $P2X_7R$ antagonists A804598 and AF27139 (both prepared in DMSO) on the BzATP-mediated effect on RGC fEPSPs, were

tested using the same protocol as for A438079. As a control, DMSO (0.1%) was added to the PMSTN medium, in these experiments.

For both ERG and RGC fEPSP experiments, LPS (10 µg/ml) was applied for 15 min to the perfusate. To investigate the involvement of $P2X_7Rs$, A438079 was applied for ~20 – 30 min prior to a 15 min LPS application, in separate experiments.

6.4.3.3 D-AP5 and P2XR antagonists

The effect of the NMDA receptor antagonist, D-2-amino-5-phosphonopentanoic acid (D-AP5) was tested on the ON and OFF RGC fEPSPs. D-AP5 was applied for 10 min at a concentration of 100 µM, which isolated a small residual fraction of the excitatory response. In separate experiments, D-AP5 (100 µM) was applied 10 min before the addition of suramin (100 µM), PPADS (100 µM) or A438079 (10 µM). Each P2XR antagonist was superfused for approximately 10 min, in the presence of D-AP5, prior to washout.

6.4.4 Digital filtering and analysis of ERG components

The ERG traces were analysed offline using Spike2 software (Cambridge Electronic Design, UK). Waveforms were initially low-pass filtered (< 250 Hz) to reduce contamination of the signal by high frequency noise. A secondary low-pass filter (< 15 Hz) was applied to isolate a smoothed ERG and eliminate the oscillatory potentials. Fig. 6.2 shows no overall distortion in the power spectra or waveforms of the low-frequency ERG components (a-wave and b-wave), following two orders of low-pass filtering. The smoothed waveform ensured accurate measurement of the a-wave slope and b-wave amplitude without contamination from the oscillatory potentials.

The slope of the a-wave, which reflects photoreceptor activity (Hood and Birch, 1990), was measured between the onset and peak of the a-wave. The b-wave peak amplitude, was measured from the peak of the a-wave to half the recovery phase of the b-wave, and is known to reflect ON-bipolar cell function (Stockton and Slaughter, 1989) (fig. 6.3). Sweeps were analysed by averaging these parameters over 60 sec, throughout the time-course of the experiment. Drug effects on both response components were measured by calculating the mean±SEM percentage change in the measured parameters (slope / amplitude), relative to control values. The implicit time of the b-wave, in particular, can provide a measure of photoreceptor sensitivity, whereas possible contamination of the a-wave by the onset of the b-wave must also be considered during analysis of the kinetics of these ERG components (Hood and Birch, 1992). The latencies were calculated from stimulus onset to the peak amplitudes of the a-wave or b-wave, and values are shown as mean±SEM implicit time (fig. 6.3). For light intensity-response experiments, sweeps were analysed over 15 sec, and mean±SEM a-wave slope, b-wave amplitude values, or implicit times were calculated and plotted as a function of stimulus intensity.

Oscillatory potentials were analysed in the frequency domain. These high-frequency wavelets are believed to reflect inner retinal network function, particularly the activity of amacrine and ganglion cells (Wachtmeister, 1998). A secondary high pass filter (> 60 Hz) was applied to isolate the oscillatory potentials from the first filtered waveform, as shown in fig. 6.2 The oscillatory potentials exhibited a peak frequency of ~ 90 – 110 Hz, which is comparable to that of dark-adapted mouse ERGs, *in vivo* (Zhang et al., 2007). A fast Fourier transform was used to derive the power spectrum of the oscillatory potentials, from stimulus onset to the half-width of the b-wave recovery phase (~ 240 ms) (fig. 6.3). To analyse drug effects, average spectra were generated 120 sec before, during and after drug application, and the mean±SEM percentage change in peak power was compared with control values. For light intensity-response experiments, averaged (15 sec) power spectra were generated

for each flash intensity tested, and the peak power was measured. Data are plotted as mean±SEM peak power as a function of stimulus intensity.

6.4.5 Analysis of ON and OFF RGC fEPSPs

ON and OFF RGC fEPSP traces were also analysed offline using Spike2 software (Cambridge Electronic Design, UK). Responses were visualised as 3-second 'sweeps', each of which consisted of an ON and an OFF response. Sweeps were analysed by measuring the average amplitude of ON and OFF fEPSPs over 60 sec, throughout the time-course of the experiment (fig. 6.4). The effect of pharmacological agents on the ON and OFF responses was measured by calculating the mean±SEM percentage change in fEPSP amplitude, compared with control values. For light intensity-response experiments, sweeps were analysed over 15 sec, and mean±SEM ON or OFF fEPSP amplitude values were calculated and plotted as a function of stimulus intensity.

6.4.6 Statistical analysis

Data were imported from Spike2 to Excel (Microsoft, USA) for analysis and generating graphs. Statistical testing was carried out using GraphPad Prism (v.6 for Windows, CA, USA). A two-way analysis of variance (ANOVA) was used to analyse light intensity-response curves by comparing values at each flash intensity, between conditions. This particular statistical test was selected as it was considered the most appropriate to evaluate the effect of two independent variables on the given waveform parameter (dependent variable). For comparisons between baseline and drug effect on the responses, statistical significance was established using the Wilcoxon's matched-pairs test. In these comparisons, values were expressed as percentages of control and were therefore paired samples. This non-parametric test was used in this case as it does not require assumptions to be made of the

distribution of the data, and was the most appropriate to handle paired values. Comparisons between treatment groups were carried out using the non-parametric Mann-Whitney test, which was considered the most useful test to compare independent samples, in this study. For all tests, statistical significance was observed if $P < 0.05$.

6.5 Microglia investigations

Alterations in retinal microglial morphology as a result of specific pharmacological conditions were analysed. The experimental protocols are as follow.

6.5.1 Pharmacological investigation protocols

Retinal wholemounts were prepared and transferred to the perfusion chamber following the protocols as described above (section 6.4.3). Recording electrodes were not used in these investigations. For each experiment, two retinae were placed adjacently in the bath, leaving ~ 5 mm gap between them to ensure they did not come into contact with each other during the course of the experiment. The nylon liner placed over the top of the retinae was adjusted to direct fluid flow over both preparations.

6.5.2 Immunofluorescence staining protocol

At the end of each experiment, the nylon liner was removed using forceps, swiftly and carefully. To prevent movement or displacement of the retinal preparation during transfer, the top quarter of the tissue paper was cut and divided into two sections, each holding one retina. Each section (tissue paper and retina) was then placed in 4% paraformaldehyde (PFA) / 1 X phosphate buffer saline (PBS) in a 48-well plate. The tissue paper was removed from the wells, and the plate was covered in foil to ensure maintenance of dark-adapted

conditions during a 30 min fixing period, at room temperature. Under a dissecting microscope and in 1XPBS, the sclera was removed from each preparation. Any remaining RPE cells and debris were brushed off. The isolated retina was then re-fixed in the well plate for 10 min. The retina was then transferred to a vial. The following wash and incubation steps were carried out using a rotator to evoke gentle agitation, unless otherwise stated. The retina underwent 3 X 15 min washes in 1XPBS. This was followed by incubation with blocking buffer (1% bovine serum albumin, 5% goat serum, 0.3% Triton X-100, made up in 1XPBS), for 60 min at room temperature.

To stain for microglia, the retinal wholemount was incubated in anti-mouse IBA1 antibody (1/800; rabbit monoclonal, WAKO, Germany) diluted in blocking buffer for 48 hr, at 4°C. For immunofluorescence labelling of microglial cells, the retina was first rinsed in 1xPBS for 3 X 15 min, and then incubated in Alexa488-conjugated anti-rabbit IgG (1/400; goat, Vector Labs, UK) diluted in 1xPBS, at room temperature. The retina was then rinsed in 1xPBS for 3 X 15 min, incubated in DAPI (300 nM, in 1XPBS, 5 min; Life Technologies, UK), followed by a final 3 X 15 min wash in 1XPBS. After labelling, retinae were flattened and mounted ganglion cell side up, on wholemount glass microscope sides in fluorescence mounting medium (Vectashield, Vector Labs, UK), and coverslipped.

An antibody against the IBA-1 (ionised calcium binding adaptor molecule-1) molecular marker was chosen for this study, as it is specifically and constitutively expressed in microglia, independently of their activation state (Ito et al., 1998). DAPI (4', 6-diamidno-2-phenulindole) was selected to stain for cell nuclei. The concentrations of anti-IBA-1 antibody, Alexafluor488-conjugated IgG and DAPI were optimised for this protocol to ensure effective staining with minimal background noise. This was further optimised with the use of the blocking buffer constituents to minimise non-specific binding of the antibodies. The

differential excitation-emission spectra for DAPI and Alexafluor488 ensured that during visualisation with the laser scanning confocal microscope, there was negligible contamination of one fluorophore by the other.

6.5.3 Image acquisition and microglial morphometric analysis

Visualisation and image acquisition of retinae were performed with a laser scanning confocal microscope (Zeiss LSM 710, Germany) using ZEN 2011 software (Zeiss, Germany). For each retina, two confocal images were taken, each from a separate quadrant and from a mid-peripheral area. This ensured a comparable region of analysis between treatment groups. A Zeiss 10W X / 0.45 water objective was used to observe the microglia and localise the specific position for image acquisition, and then the same objective was set at 20W X magnification for acquisition. For each location, a Z-stack was taken, consisting of approximately 17-35 slices (2.65 µm) per stack. Fig. 6.5 summarises the image acquisition parameters used for these experiments

Microglial morphology was assessed using Fiji (Image J, NIH, USA) software. The protocols for analysis were adapted from previous studies of retinal microglial morphology (Fontainhas et al., 2011; Vessey et al., 2011; Opie et al., 2012), and further developed for the purposes of the present study. Each image stack was split into two separate fluorescent channels to isolate the IBA-1^{+} microglia images from the $DAPI^{+}$ images. The stack of microglia images was then flattened to produce a maximum intensity projection image for further analysis. Morphological changes in ramified microglia were quantified via measurement of the area covered by the microglial processes using the polygon tool function in the software (fig. 6.5). The criteria for identifying ramified cells were adapted from those described by Tanaka and Maeda (1996), and further refined for the purposes of the present study. A ramified microglial cell was defined as follows: The cell has a distinct soma with two or more

processes extending from the soma, and which both must be longer than half the diameter of the soma. The original image stack was used alongside the analysis, to identify and distinguish cell bodies (with DAPI), as well as the processes of a particular cell, in the case of overlap. Cells were excluded from analysis if they extended processes outside of the image (i.e. if the full cell expanse was limited by image cut-off). Amoeboid shaped-cells were rarely observed, but were excluded from analysis if encountered, as they did not fit the criteria of ramified cells.

Data were imported into Excel and analysed. Statistical testing was performed in GraphPad Prism. The effect of pharmacological compounds was compared to a vehicle control group using an unpaired, two-tailed Student's t-test. Values were expressed as mean ± SEM process area (μm^2) and were considered significantly different if $P < 0.05$.

Chapter 6 Figures and Tables

Compound	Chemical / Product name	Target receptor / function	Concentration used (µM)
A438079	3-[[5-(2,3-Dichlorophenyl)-1*H*-tetrazol-1-yl]methyl]pyridine hydrochloride	$P2X_7R$ / selective, competitive antagonist	10
A804598	N-Cyano-N″-[(1S)-1-phenylethyl]-N′-5-quinolinyl-guanidine	$P2X_7R$ / selective, competitive antagonist	30
AF27139 *****	2-Pyrimidin-2-yl-4-trifluoromethyl-thiazole-5-carboxylic acid [2-(4-chloro-phenyl)-2-morpholin-4-yl-ethyl]-amide	$P2X_7R$ / selective, competitive antagonist	30
Adenosine	9-β-D-Ribofuranosyladenine	P1-Rs / agonist	100 - 300
BzATP	2′(3′)-O-(4-Benzoylbenzoyl)adenosine 5′-triphosphate triethylammonium salt	$P2X_7R$ / agonist	10 – 300
Carbenoxolone	3β-Hydroxy-11-oxoolean-12-en-30-oic acid 3-hemisuccinate disodium salt	Pannexin-1 hemichannels / antagonist	10
D-AP5	D-(-)-2-Amino-5-phosphonopentanoic acid	NMDA-R / selective, competitive antagonist	100
L-AP4	L-(+)-2-Amino-4-phosphonobutyric acid	mGluR6 / agonist	5 - 100
LPS	Lipopolysaccharides from *Escherichia coli* 055:B5	TLR4 / agonist	10 (µg/ml)
NBQX	2,3-Dioxo-6-nitro-1,2,3,4-tetrahydrobenzo[*f*]quinoxaline-7-sulfonamide disodium salt	AMPA / KA-Rs / competitive antagonist	10
PPADS	4-[[4-Formyl-5-hydroxy-6-methyl-3-[(phosphonooxy)methyl]-2-pyridinyl]azo]-1,3-benzenedisulfonic acid tetrasodium salt	P2XRs / broad-spectrum antagonist	100
Picrotoxin	-	$GABA_{A/C}$ Rs / non-competitive antagonist	100
Suramin	8,8'-[Carbonylbis[imino-3,1-phenylenecarbonylimino(4-methyl-3,1-phenylene)carbonylimino]]bis-1,3,5-naphthalenetrisulfonic acid hexasodium salt	P2XRs / broad-spectrum antagonist	100
Strychnine	Strychnidin-10-one hydrochloride	GlyR / competitive antagonist	5
Tetrodotoxin	Octahydro-12-(hydroxymethyl)-2-imino-5,9:7,10a-dimethano-10a*H*-[1,3]dioxocino[6,5-*d*] pyrimidine-4,7,10,11,12-pentol + citrate buffer	Voltage-gated sodium ion channels / channel blocker	0.1

Table 6.1 Pharmacological compounds used in this study. A804598 and AF27139***** were provided by Lundbeck. BzATP and LPS were purchased from Sigma-Aldrich, UK. All other compounds were purchased from Abcam, UK. (***** Li H, Yuan J, Bakthavatchalam R, Hodgetts KJ, Capitosti SM, Mao J, Wustrow, DJ, Guo Q (2009). *5-membered heterocyclic amides and related compounds*. Patent: WO2009012482).

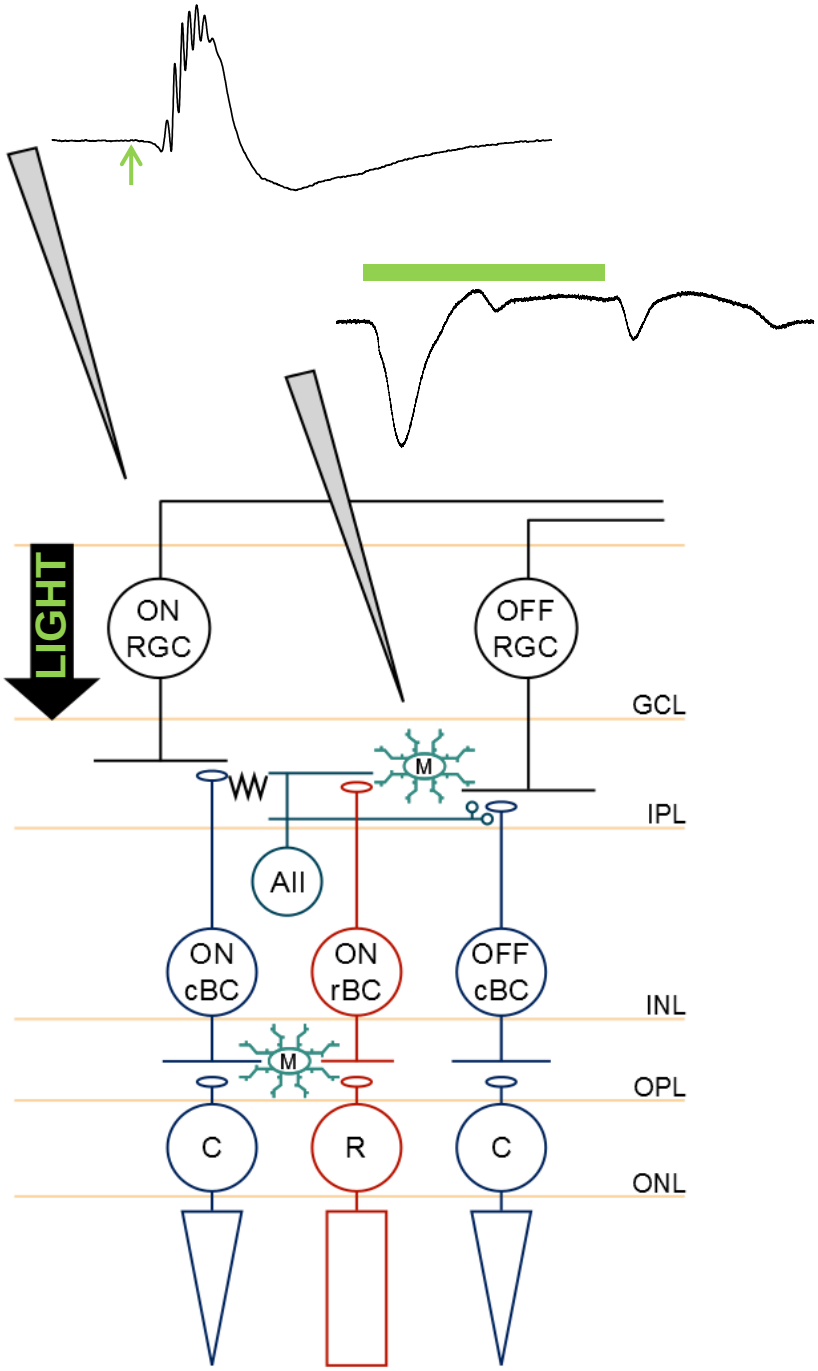

Figure 6.1 Placement of recording electrodes for acquisition of transretinal electroretinogram and retinal ganglion cell fEPSP responses. Schematic illustrates retinal circuitry and the respective positions of the recording electrode for the electrophysiological experiments. The retinal wholemount was placed in the bath, ganglion cell layer side up. The full-field light flash stimulus was placed above the slice, and the arrow shows the direction in which the light travelled. ***Top trace***, Typical transretinal electroretinogram response recorded by lowering the electrode onto the surface of the retinal wholemount, without breaking into the layers. The response was repeatedly elicited by a single 10 ms-duration flash (green arrow), with a 3-sec interval. ***Bottom trace***, Retinal ganglion cell fEPSPs were recorded by placing the electrode in the ganglion cell layer. The green bar represents the duration of the stimulus (1 sec), which was repeated at 3-sec intervals. Upon stimulus onset, an ON retinal ganglion cell fEPSP was generated. Stimulus offset produced an OFF retinal ganglion cell fEPSP. ONL, outer nuclear layer; OPL, outer plexiform layer; INL, inner nuclear layer; IPL, inner plexiform layer; GCL, ganglion cell layer.

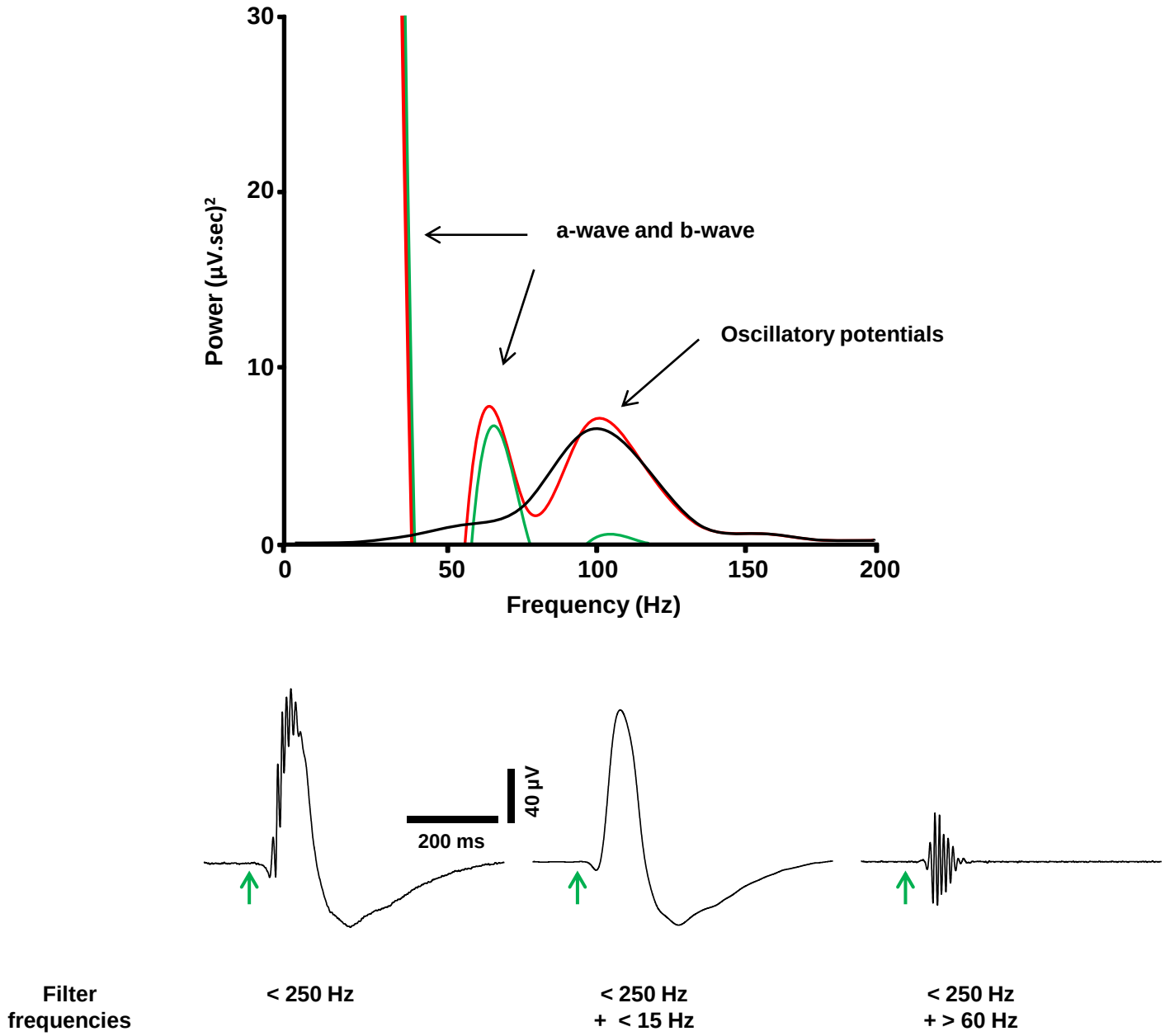

Figure 6.2 Digital filtering of transretinal electroretinogram responses. ***Top***, Dark-adapted electroretinogram (ERG) power spectra (300 sec averages) under various filter settings. The ERG was low pass-filtered (< 250 Hz; red traces), with the prominent a-wave and b-wave components within the low to mid frequency range. Further low pass filtering (< 15 Hz; green traces) eliminated the high-frequency component (oscillatory potentials). A high pass filter (> 60 Hz; black trace) was applied after the first filter, in order to isolate the high frequency oscillatory potentials, which exhibited a peak frequency of approximately 100 Hz. ***Bottom***, Waveform averages illustrate the effect of the filter settings on the shape of the ERG. Application of two orders of low pass filter did not distort the waveform, keeping the a-wave and b-wave intact. Application of the high pass filter eliminated the a-wave and b-wave, isolating the oscillatory potentials for further analysis. Green arrows represent flash stimulus (10 ms).

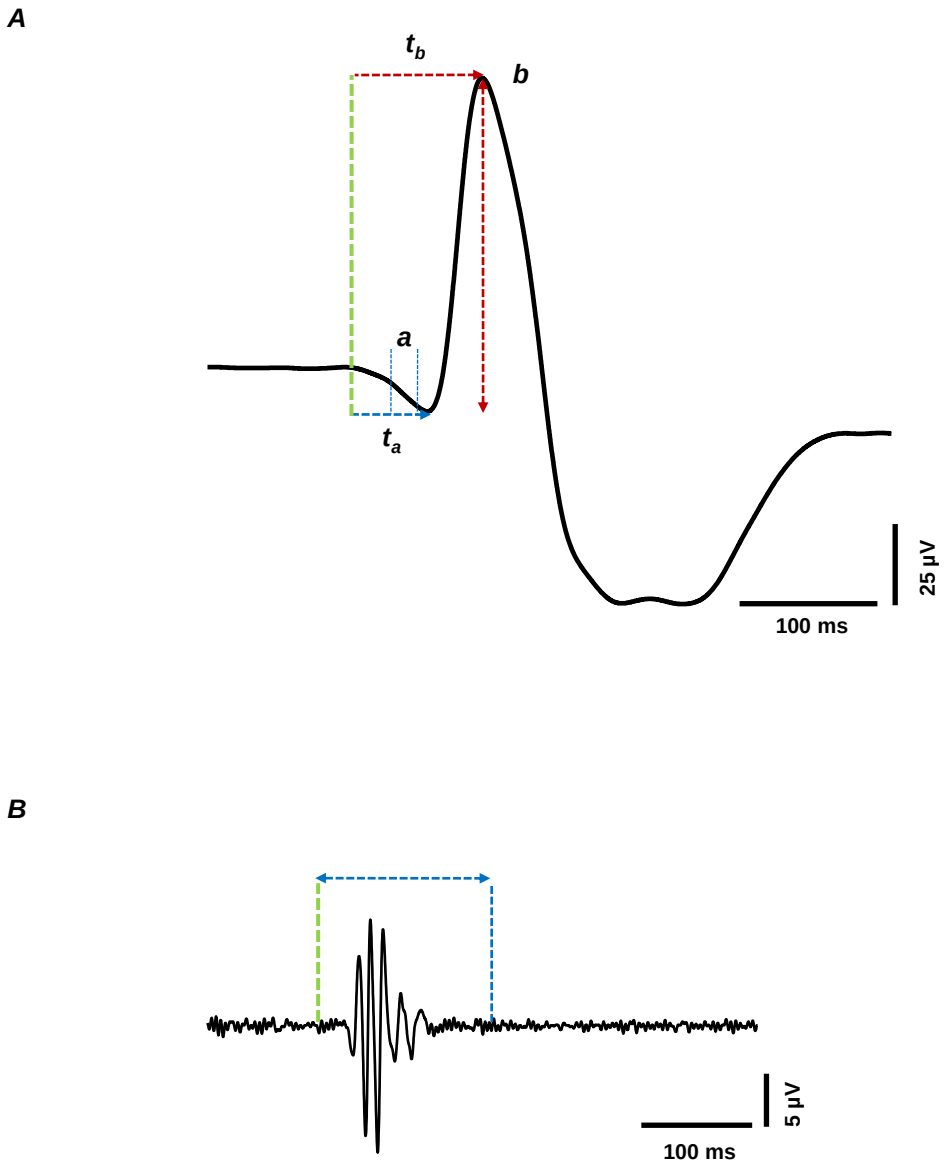

Figure 6.3 Analysis parameters for the electroretinogram components. A, The ERG a-wave was measured by calculating its slope from the onset to peak of the a-wave, shown by the vertical blue lines (a). The a-wave implicit time was measured from the onset of the stimulus (green vertical line) to the peak of the a-wave (t_a). The b-wave amplitude was measured from the peak of the a-wave to the half-width of the b-wave recovery phase. Its amplitude is depicted by the vertical red line. The implicit time of the b-wave was measured from stimulus onset to the peak of the b-wave (t_b). B, Oscillatory potentials were analysed in the frequency domain (e.g. black spectrum in figure 6.2). The power density spectrum was derived from stimulus onset to the half-width of the b-wave recovery phase. This window ensured that high-frequency noise and non-ERG components were not included in the analysis.

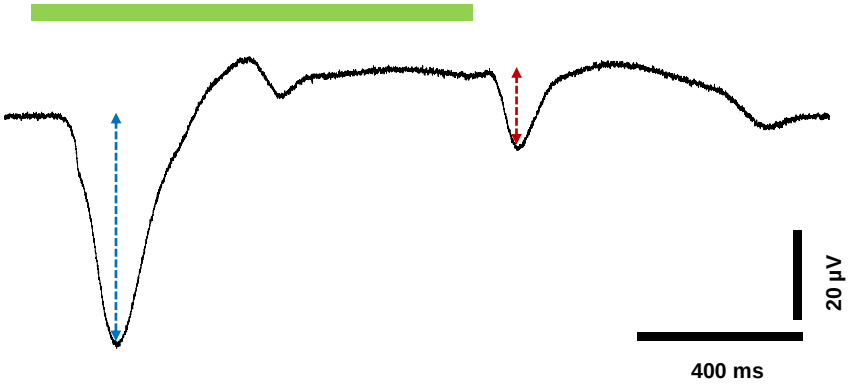

Figure 6.4 Analysis parameters for the ON and OFF retinal ganglion cell fEPSPs. Green bar represents duration of flash stimulus (1 sec). For all experiments, the ON and OFF fEPSPs were analysed by measuring their peak amplitudes. The ON fEPSP peak amplitude (vertical blue line) was measured from flash onset to the recovered phase (~ 400 ms post-stimulus onset). The OFF fEPSP peak amplitude was measured from stimulus offset to recovery (~ 300 ms post-stimulus offset).

A

Acquisition Parameters for Z-Stack Images	
Objective / Zoom factor	C-Apochromat 10w/0.45 / x 2.0
No. of slices / Slice interval	17-35 / 2.65 µm
Image size - Pixels / Scaled	1024 x 1024 px / 425.1 x 425.1 µm
Image format / Averaging	8-bit / Line-averaged x 4
Lasers	Argon 488 nm / Diode 405 nm
Pinhole size / Pixel time	16 µm / 1.27 µs

B

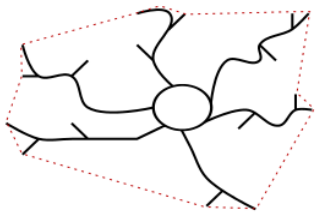

Figure 6.5 Image acquisition parameters and morphometric analysis of microglia. ***A***, Table shows the typical acquisition parameters used for all image stacks. For each retina, prior to commencing z-stack acquisition, the gain of the lasers were adjusted to reduce saturation of the images. ***B***, Highly schematic representation of a microglial cell, showing branched processes protruding from the rounded cell body. Alterations to microglial morphology were measured through analysis of the area covered by the microglial processes of ramified cells, using a polygon tool (Fiji / Image J). The red lines represent the measured microglial process area of one cell.

Chapter 7

Results: Characterisation of Visual Responses of the E*x Vivo* Mouse Retina

The effects of $P2X_7R$ activation and of microglia, in modulating visual signal transmission in the outer and inner mouse retina were investigated. All synaptic responses were obtained from acutely isolated, *ex vivo* mouse retinal wholemount preparations. Dark-adapted (scotopic to low mesopic) conditions were specifically chosen to isolate the responses of the vertical rod photoreceptor-mediated pathway. Modulation of outer retinal function was explored by recording transretinal electroretinogram (ERG) responses. Investigations of changes to retinal ganglion cell (RGC) function were carried out using recordings of ON and OFF RGC field excitatory postsynaptic potentials (fEPSPs) from the ganglion cell layer. The following results demonstrate typical response characteristics of the dark-adapted ERG, and ON and OFF RGC fEPSPs of the isolated mouse retina. Additionally, this section highlights the specific experimental conditions and pharmacological approaches employed for the primary study.

7.1 Characterisation of dark-adapted electroretinogram response components

In physiological perfusion medium (normal Krebs'), the transretinal electroretinogram (ERG) typically consisted of three major components: the a-wave, b-wave and oscillatory potentials (see methods). Fig. 7.1 shows responses evoked by a 10 ms-duration full-field, dim flash stimulus (-0.96 log cd.s/m^2), under various pharmacological conditions during the same experiment. The initial negative a-wave was followed by a larger, positive b-wave, with smaller-amplitude oscillatory potentials superimposed on the leading edge of the b-wave.

7.1.1 Properties of the ERG a-wave and b-wave

Light intensity-response properties of the a- and b-waves in normal Krebs' medium are presented in fig. 7.2A and B, respectively (blue values), with representative traces also shown (fig. 7.2C, left). The values for the a- and b-waves were measured using the digitally, low-pass filtered (< 15 Hz) waveform (section 6.4.4). For each experiment, a flash intensity that gave sub-maximal ERG responses was used. With a typically used stimulus intensity of -0.96 log cd.s/m^2, in normal Krebs' medium, the slope of the a-wave was -0.34 ± 0.07 µV/ms (mean ± SEM, n = 6) with an implicit time (time to peak from stimulus onset to a-wave maximum amplitude) of 29.4 ± 2ms (fig. 7.2Aa and Ab). The b-wave maximum amplitude was 91.8 ± 14µV, with the response peaking at 81.3 ± 2ms following stimulus onset (fig 7.2Ba and Bb). Both the a-wave slope and b-wave amplitude potentiated as a function of flash intensity, each reaching their maximum responses at -0.62 and -0.54 log cd.s/m^2, respectively. No marked changes were seen in the implicit time of the a-wave peak amplitude with increasing stimulus intensity (fig. 7.2Ab). However, the b-wave amplitude appeared to peak earlier, with increasing luminance from -1.47 to -0.54 log cd.s/m^2 (fig. 7.2Bb).

Most experiments within the primary investigation were carried out in the absence of extracellular magnesium ions (Mg^{2+}) from the Krebs' medium for two reasons. Firstly, Mg^{2+} removal is known to enhance the effects of $P2X_7R$ activation, and was therefore used as a condition to characterise $P2X_7R$ involvement in the ERG experiments. Secondly, the absence of Mg^{2+} also enhances the NMDA receptor-mediated component of excitatory synaptic responses of retinal ganglion cells (see section 7.2). The removal of extracellular Mg^{2+} appeared to enhance both a- and b-waves. Fig. 7.1 shows that the addition of tetrodotoxin (TTX; 100 nM), picrotoxin (100 µM), strychnine (5 µM) and NBQX (10 µM) to the bathing medium (hereafter referred to as PMSTN medium), further potentiated the a- and b-

waves. These pharmacological agents were used to isolate and enhance NMDA receptor-mediated retinal ganglion cell ON and OFF fEPSPs (section 7.2).

The scotopic ERG a- and b-waves are generally considered to be independent of inner retinal activity. However, with the scope of characterising specific $P2X_7R$-mediated modulation of synaptic transmission in both the outer and inner retina under the same conditions, some ERG experiments were also carried out using the PMSTN medium. In the modified bathing medium, the basic form of the ERG a- and b-waves remained essentially unaltered. Conversely, there were marked changes in the implicit times of both waves, shown in fig. 7.2Ab and Bb (red values). The time to peak of the a- and b-waves were significantly potentiated in the PMSTN perfusate, compared to responses in normal Krebs' medium. In the modified extracellular solution, the a- and b-waves showed similar stimulus-intensity response properties as in normal Krebs' (fig. 7.2A and B, respectively). The a-wave slope reached its maximum response between -0.82 and -0.71 log cd.s/m^2, a lower stimulus intensity than in normal Krebs'. The maximum response of the b-wave was achieved at the highest stimulus intensity tested (-0.54 log cd.s/m^2). There was no statistically significant difference in the a-wave slope or b-wave amplitude between ERG responses recorded in normal and modified perfusate, across all light intensities tested ($P > 0.05$). The implicit times of both a- and b-waves were reduced with increasing flash intensity ($P < 0.05$ for both). Overall, the general response properties of the ERG a- and b-waves were preserved in the presence of the pharmacologically altered perfusion medium.

7.1.2 The effect of the group III metabotropic glutamate receptor agonist, L-AP4 on the ERG b-wave

The mGluR6 glutamate receptor subtype is expressed on the tips of ON bipolar cell dendritic processes, directly postsynaptic to the photoreceptor terminals. It is established that the agonist L-AP4 selectively and reversibly eliminates the ERG b-wave, due to the hyperpolarisation of ON bipolar cells and subsequent blockade of synaptic transmission from the photoreceptors to second-order neurons. Indeed, a short (5 min) application of L-AP4 (50 µM) significantly reduced the b-wave amplitude to 6.9 ± 4% of control ($P < 0.05$, n = 6). This effect was fully reversible, as the b-wave amplitude recovered to 100.3 ± 2% of pre-treatment control ($P > 0.05$) (fig. 7.3A). The representative traces in fig. 7.3B show the selective nature of this interaction, as the negative photoreceptor-derived a-wave remained in the presence of L-AP4. These results confirmed the functionality of the photoreceptor-ON bipolar cell synapse in transmitting visual signals, under these conditions.

7.1.3 Properties of the ERG oscillatory potentials

The ERG recorded in normal Krebs' medium consisted of a series of wavelets embedded in the leading edge of the large-amplitude b-wave (fig. 7.1). These high-frequency oscillatory potentials were digitally extracted from the raw waveform (high-pass filtered, > 60 Hz), as discussed in section 6.4.4. Analysis of the frequency spectra of the scotopic oscillatory potentials revealed that their power output potentiated with increased light intensity. This effect was similar to the flash intensity-response relationship observed for the a- and b-waves. The representative traces in fig. 7.4B demonstrate that the amplitude of the oscillatory potentials became more prominent at higher flash intensities.

Shown in fig. 7.1, the oscillatory potentials were abolished in the presence of the modified PMSTN perfusion medium. This is consistent with the notion that these wavelets are generated from inner retinal network activity.

7.2 Characterisation of ON and OFF retinal ganglion cell fEPSPs

Photostimulation of the retina (1 sec-duration, full-field flash) generated a characteristic ON RGC fEPSP, followed by an OFF RGC fEPSP at termination of the stimulus (fig. 6). In some experiments in normal Krebs' medium, spiking action potentials were apparent in the ON and OFF fEPSPs. This feature is typical of inner retinal activity, particularly that of retinal ganglion cells. Application of the voltage-gated sodium channel blocker, tetrodotoxin (TTX; 100 nM) to the perfusion medium abolished the spikes (fig. 7.5), confirming that responses were recorded from the ganglion cell layer. The NMDA receptor-mediated component of the ON and OFF fEPSPs was enhanced with the removal of extracellular Mg^{2+} from the perfusate. Blockade of AMPA/KA, $GABA_{A/B}$ and glycine receptors, with NBQX (10 µM), picrotoxin (100 µM) and strychnine (5 µM), respectively, and the presence of TTX, ensured the pharmacological isolation of the NMDA-R component. The traces in fig. 7.5 illustrate the considerable potentiation of both ON and OFF fEPSPs in the PMSTN medium, indicating the enhancement of ON and OFF RGC receptive fields due to the diminished inhibitory surround input.

Fig. 7.6 shows that at any given flash intensity, the ON fEPSP was larger in amplitude than the OFF fEPSP, indicating a dominant ON pathway-mediated response. This is consistent with the suppression of transmission through the OFF pathway due to the presence of NBQX, as OFF bipolar cells are depolarised by the activation of AMPA/KA receptors. The ON fEPSP potentiated with increasing flash intensity, reaching its maximum response at -0.62 log cd.s/m^2. The OFF fEPSP displayed a similar stimulus intensity-response relationship, saturating at a lower intensity (-0.96 log cd.s/m^2). As the ON fEPSP was the dominant response in all experiments, a flash intensity that gave a sub-maximal ON fEPSP was used, typically ranging from -2.00 to -1.00 log cd.s/m^2.

7.2.1 The effect of the selective NMDA receptor antagonist, D-AP5 on ON and OFF retinal ganglion cell fEPSPs

The competitive NMDA receptor antagonist, D-AP5 was used to confirm the nature of the ON and OFF fEPSPs. D-AP5 (100 µM, 10 min application) significantly reduced the ON and OFF fEPSPs to 37 ± 6% and 50 ± 14% of control, respectively ($P < 0.05$ for both, n = 7 and 6) (fig. 7.7). On washout, both responses recovered to 91 ± 4% and 99 ± 7% of control ($P > 0.05$ for both). Fig. 7.8A illustrates that across almost all light intensities tested, the ON fEPSP was significantly suppressed in the presence of D-AP5 ($P < 0.05$, two-way ANOVA). Although the OFF fEPSP was reduced with D-AP5, its suppression across all light intensities was not statistically significant ($P > 0.05$, two-way ANOVA) (fig. 7.8B). The representative traces in fig. 7.8C illustrate that across all light intensities tested, a residual fraction of the ON fEPSP remained in the presence of D-AP5. These results suggest that the ON and OFF fEPSPs are primarily mediated by NMDA receptor activation.

7.2.2 The effect of the group III metabotropic glutamate receptor agonist, L-AP4 on the ON and OFF retinal ganglion cell fEPSPs

It is established that mGluR6 activation selectively abolishes the ON RGC response. Indeed, it was observed that application of L-AP4 resulted in a concentration-related reduction of the ON fEPSP, with no overall effect on the OFF fEPSP (fig. 7.9). Significant reduction of the ON fEPSP was achieved with L-AP4 tested at 20 µM and 50 µM, suppressing the response to 51.2 ± 8% and 17.1 ± 3% of control, respectively ($P < 0.05$, n = 6 and 26) (fig. 7.9A). Further reduction of the ON fEPSP was observed with 100 µM, but which was only tested in two experiments. Following washout, the ON fEPSP was fully recoverable to 98.4 ± 2% of control ($P > 0.05$). Across all concentrations tested, the OFF fEPSP remained essentially unaltered (99.8 ± 10% of control, $P > 0.05$, n = 26). The effect of L-AP4 on the ON fEPSP is demonstrated in fig.7.9B, which shows representative traces in the presence of L-AP4 at 10,

20 and 50 µM, applied in succession. The selective suppression of the ON fEPSP confirmed that the overall segregation of the ON and OFF visual pathways were maintained in the *ex vivo* mouse retinal wholemount preparation.

Chapter 7 Figures

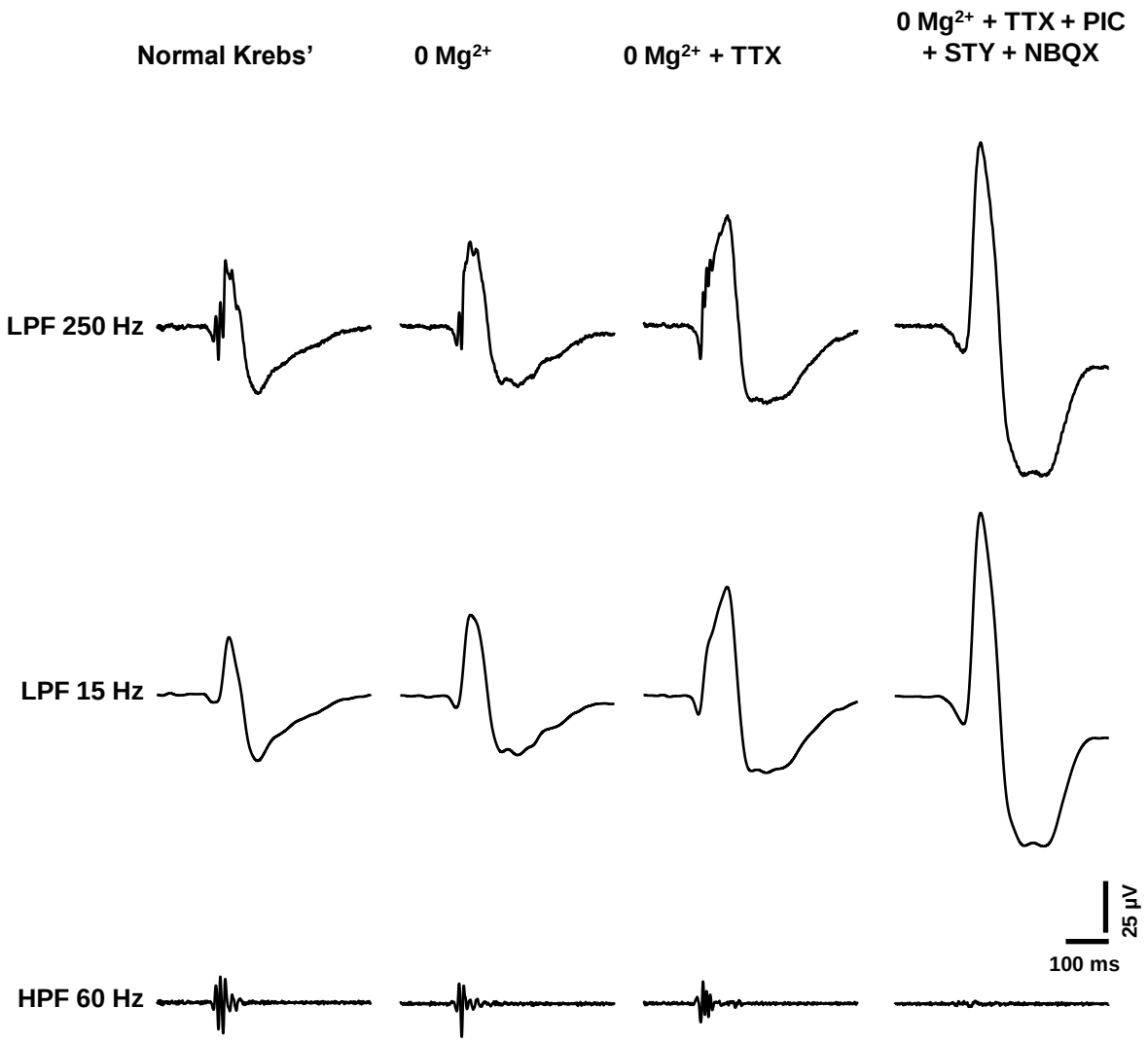

Figure 7.1 Dark-adapted ERG responses under various pharmacological conditions. Representative traces show the alterations in the ERG responses in the presence of different perfusion solutions. Each row depicts the waveform with differential filter frequencies (see Fig. 6.2). LPF, low pass filter; HPF, high pass filter. In physiological Krebs' medium, the ERG exhibited typical a-wave, b-wave and oscillatory potential components. With the addition of tetrodotoxin (100 nM; TTX), the oscillatory potentials were markedly reduced, indicating their inner retinal origin. TTX also appeared to delay the peak of the b-wave amplitude. The addition of the picrotoxin (PIC; 100 µM), strychnine (STY; 5 µM), NBQX (10 µM), and the removal of extracellular magnesium ions ($Mg2^{+}$) appeared to enhance both a-wave and b-wave components, and almost completely eliminated the oscillatory potentials. Thus, for experiments undertaken in the pharmacologically modified perfusate (PMSTN), the oscillatory potentials were not analysed. Overall, the shape of the ERG was not altered in the modified perfusate, indicating that the cellular generators of the a-wave and b-wave were on the whole, were functional under these conditions.

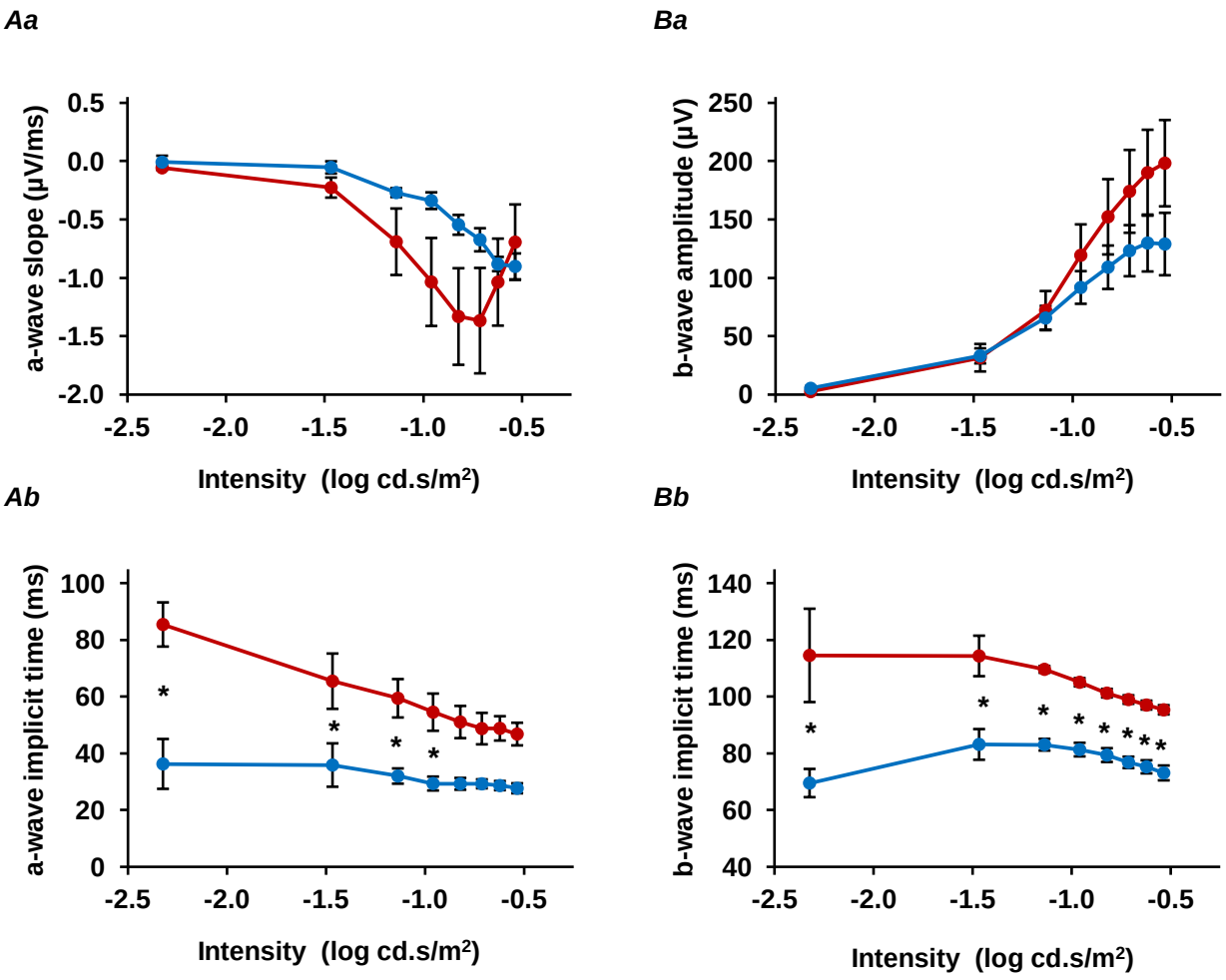
Aa
a-wave slope (µV/ms)
0.5
0.0
-0.5
-1.0
-1.5
-2.0
-2.5
-2.0
-1.5
-1.0
-0.5
Intensity (log cd.s/m²)
Ba
b-wave amplitude (µV)
250
200
150
100
50
0
-2.5
-2.0
-1.5
-1.0
-0.5
Intensity (log cd.s/m²)
Ab
a-wave implicit time (ms)
100
80
60
40
20
0
-2.5
-2.0
-1.5
-1.0
-0.5
Intensity (log cd.s/m²)
Bb
b-wave implicit time (ms)
140
120
100
80
60
40
-2.5
-2.0
-1.5
-1.0
-0.5
Intensity (log cd.s/m²)

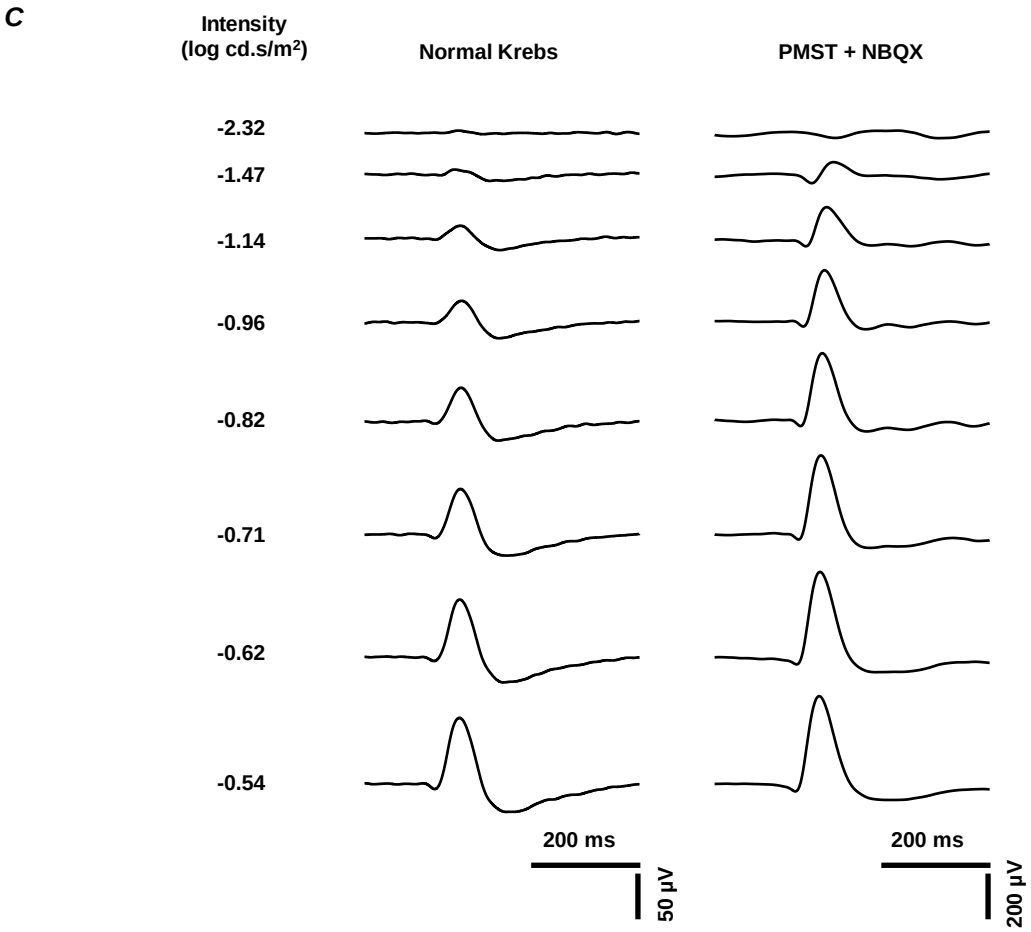
C
Intensity (log cd.s/m²)
Normal Krebs
PMST + NBQX
-2.32
-1.47
-1.14
-0.96
-0.82
-0.71
-0.62
-0.54
200 ms
50 µV
200 ms
200 µV

Figure 7.2 Stimulus-intensity response functions of the a-wave and b-wave components of the dark-adapted transretinal ERG. ***Aa*** and ***Ab***, Values are mean ± SEM a-wave slope and implicit time, respectively (n = 8). In normal physiological Krebs' medium, the a-wave slope potentiated with increasing luminance, and was not significantly different from the a-wave slope in PMSTN medium, across all intensities tested ($P > 0.05$, for all). The a-wave implicit time (defined as the time to peak of the a-wave amplitude, from stimulus onset), was significantly different between normal physiological Krebs' and PMSTN medium, at the lowest intensities tested (*, $P < 0.05$). ***Ba*** and ***Bb***, Values are mean ± SEM b-wave amplitude and implicit time, respectively. In both physiological Krebs' and PMSTN medium, the b-wave amplitude potentiated with increasing stimulus intensities. There was no significant difference between the two conditions, across all luminances tested ($P > 0.05$, for all). The peak of the b-wave amplitude was significantly more delayed in PMSTN medium, compared to that in normal physiological medium, across all intensities (*, $P < 0.05$). C, Representative traces (15 sec averages) illustrate the enhanced a-wave and b-wave at higher luminances. There was no overall alteration in the shape of the ERG waveforms in the presence of PMSTN medium, indicating that the function of the retinal circuitry was intact.

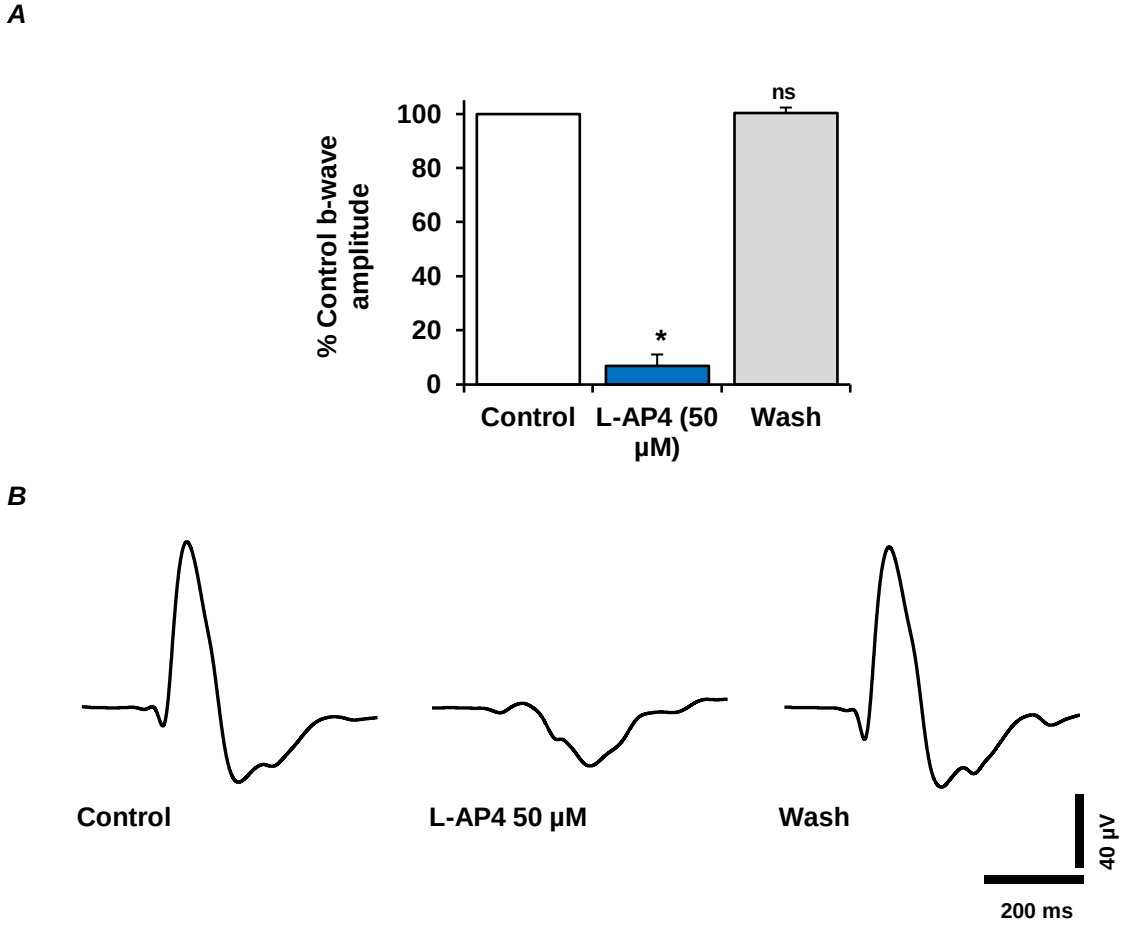

Figure 7.3 The effect of the mGluR6 agonist, L-AP4 on the ERG b-wave component. Values are mean ± SEM percentage of control b-wave amplitude. ***A***, L-AP4 (50 µM) significantly and selectively reduced the b-wave amplitude, compared to pre-treatment control ($P < 0.05$, $n = 6$). The suppression of the b-wave was readily reversible on washout ($P > 0.05$). ns, not significant; *, $P < 0.05$. ***B***, Representative traces (120 sec averages) illustrate the marked and recoverable elimination of the b-wave in the presence of L-AP4, leaving the a-wave intact. The selective effect of L-AP4 on the b-wave confirmed the function of mGluR6 activity at the photoreceptor – ON bipolar cell synapse.

A

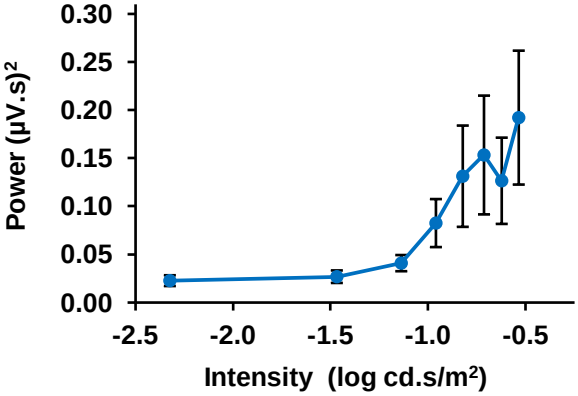

B

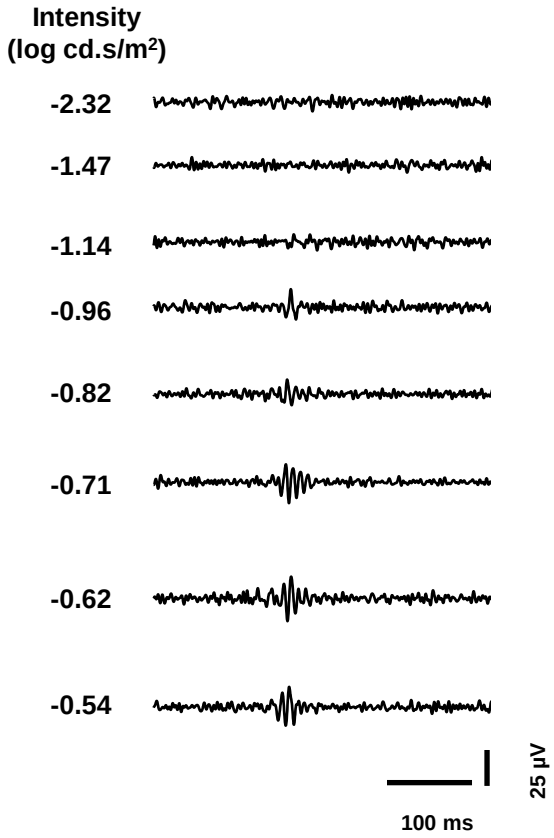

Figure 7.4 Stimulus-intensity response relationship of oscillatory potentials of the dark-adapted transretinal ERG. ***A***, Values are mean ± SEM peak power density derived from power spectra (*n* = 8) for each light intensity tested. Oscillatory potentials were extracted from the raw ERG waveform, with a high-pass filter (> 60 Hz, see section 6.4.4). The power output of the oscillatory potentials was enhanced with increased flash intensity. A steeper increase in the peak power was observed at higher light intensities, within the range tested. This is consistent with *in vivo* observations of the dark-adapted oscillatory potentials. ***B***, Characteristic traces of extracted oscillatory potentials (15 sec averages) illustrate their prominence at higher luminances.

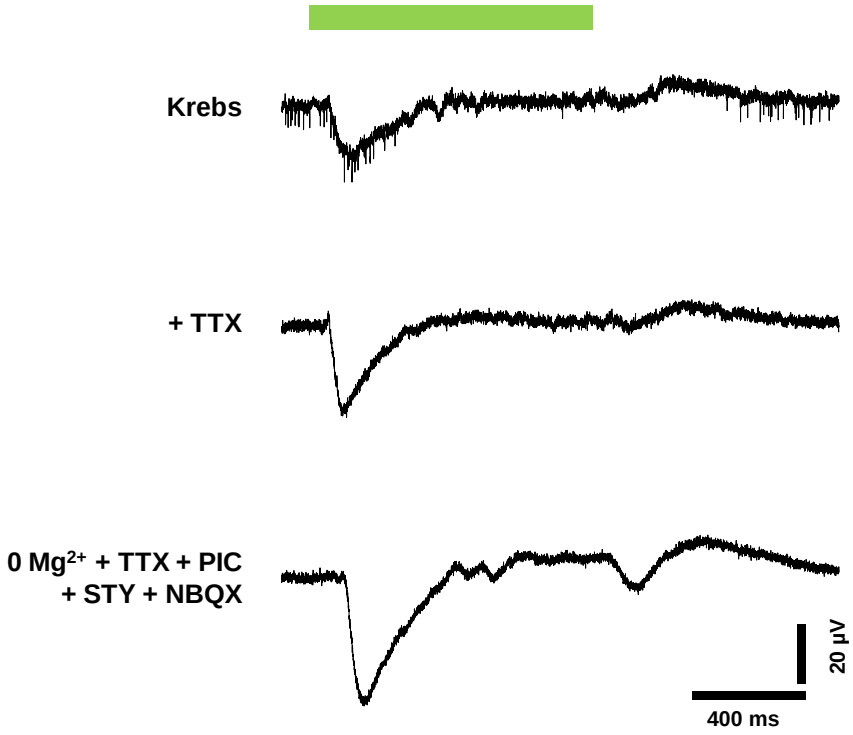

Figure 7.5 Isolation of the NMDA receptor-mediated component of dark-adapted, light-evoked ON and OFF retinal ganglion cell fEPSPs. Responses were recorded from the ganglion cell layer, in response to a 1 sec-duration light stimulus (green bar). Upon stimulus onset, an ON fEPSP was generated, and stimulus offset induced an OFF fEPSP. Representative traces are 10 sec averages. In the presence of physiological Krebs' medium (top trace), high-frequency spiking action potentials were apparent, but were diminished with the addition of the tetrodotoxin (TTX; 100 nM), a blocker of voltage-gated sodium channels (middle trace). This confirmed that responses were recorded from the inner retinal layers, as spiking activity is predominantly attributed to retinal ganglion cells. The bottom trace illustrates the changes to the ON and OFF fEPSPs with the addition of picrotoxin (PIC; 100 µM), strychnine (STY; 5 µM), NBQX (10 µM), and the removal of extracellular magnesium ions ($Mg2^{+}$). Superfusion of this pharmacologically modified Krebs' medium (referred to as PMSTN), considerably enhanced the amplitudes of both the ON and OFF fEPSPs, which exhibited characteristic waveforms of dark-adapted, isolated NMDA receptor-mediated RGC responses.

A

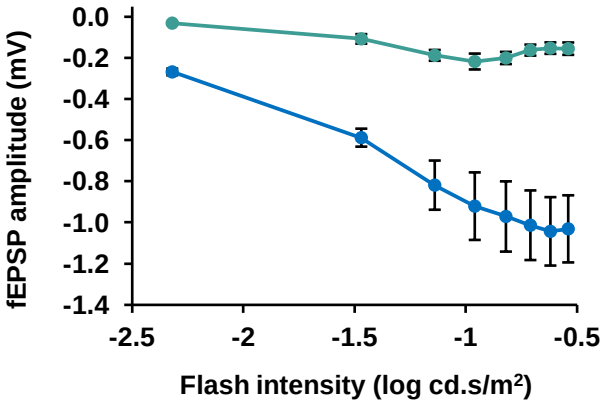
0.0
-0.2
-0.4
-0.6
-0.8
-1.0
-1.2
-1.4
fEPSP amplitude (mV)
-2.5
-2
-1.5
-1
-0.5
Flash intensity (log cd.s/m²)

B

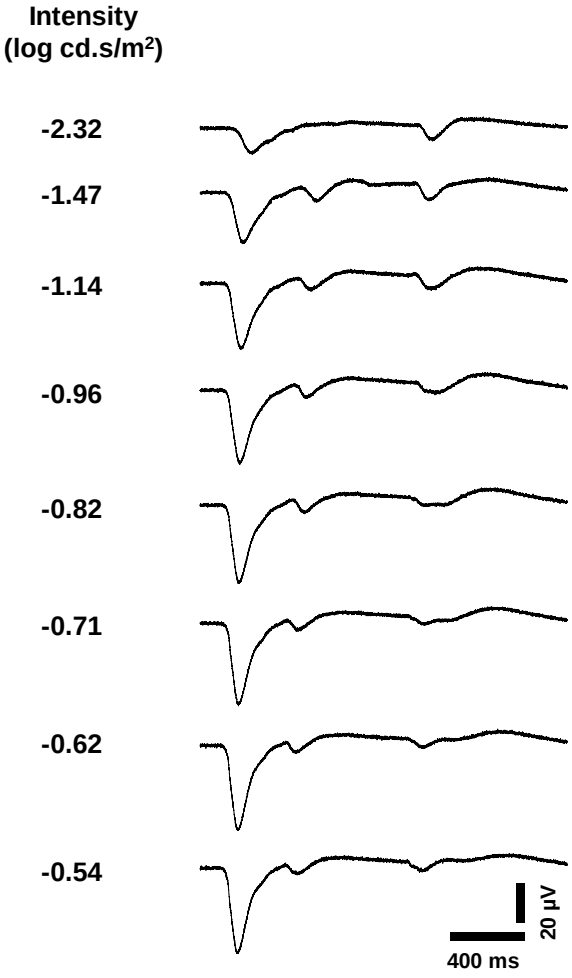
Intensity
(log cd.s/m²)
-2.32
-1.47
-1.14
-0.96
-0.82
-0.71
-0.62
-0.54
20 µV
400 ms

Figure 7.6 Stimulus intensity-response functions of light-evoked ON and OFF RGC fEPSPs. ***A***, Values are mean ± SEM fEPSP amplitudes (mV); *n* = 4. Flash intensities tested were in the scotopic to mesopic range (dim light). The ON fEPSP (blue) potentiated with increasing light intensity, typically saturating at approx. -0.62 log cd.s/m^2. The OFF fEPSP (green) also exhibited a potentiation in response to increasing flash intensity, but saturated at a much dimmer luminance (approx. -1 log cd.s/m^2). Across all stimulus intensities tested, the ON fEPSP persisted as the dominant response and thus, for all pharmacological investigations, a stimulus that induced a sub-maximal ON fEPSP was selected (typically between -2 and -1 log cd.s/m^2). ***B***, Representative traces (15 sec averages), show the dominance of the ON fEPSP, and its stimulus intensity-dependent potentiation. The OFF fEPSP seemed more apparent towards the lower end of the flash intensity range used.

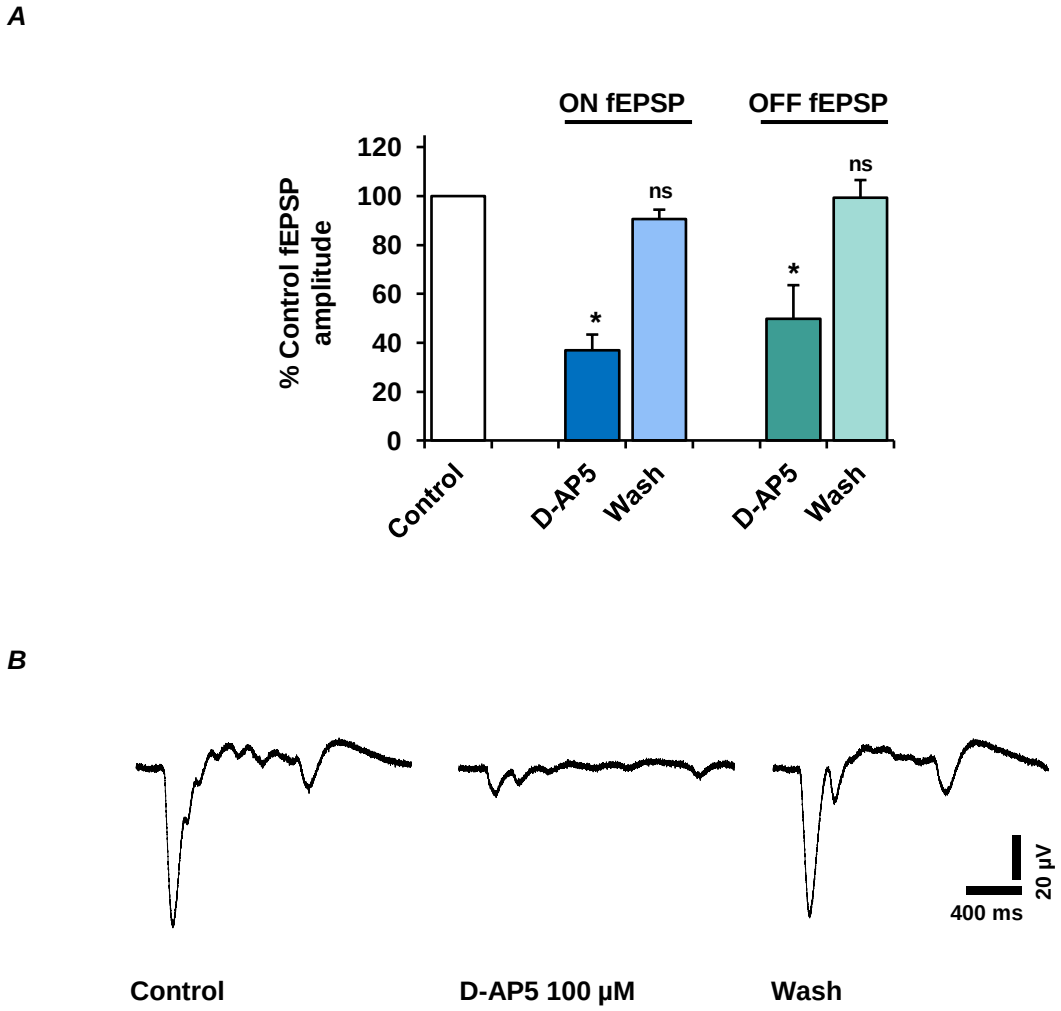

Figure 7.7 The effect of the competitive and selective NMDA receptor antagonist D-AP5 on the ON and OFF RGC fEPSPs. A, Values are mean ± SEM percentage control fEPSP amplitude. ns, not significant; *, $P < 0.05$, compared to pre-treatment control. D-AP5 (100 µM) significantly reduced both the ON ($n = 7$) and OFF ($n = 6$) fEPSPs, compared to pre-treatment control ($P < 0.05$). The D-AP5-mediated effect on both components was reversible on washout ($P > 0.05$). B, Representative traces illustrate a marked reduction in both ON and OFF responses, which then recover on washout. Note the persistence of a residual fraction of the excitatory responses in the presence of D-AP5, suggesting a non-ionotropic glutamate receptor contribution to the fast responses.

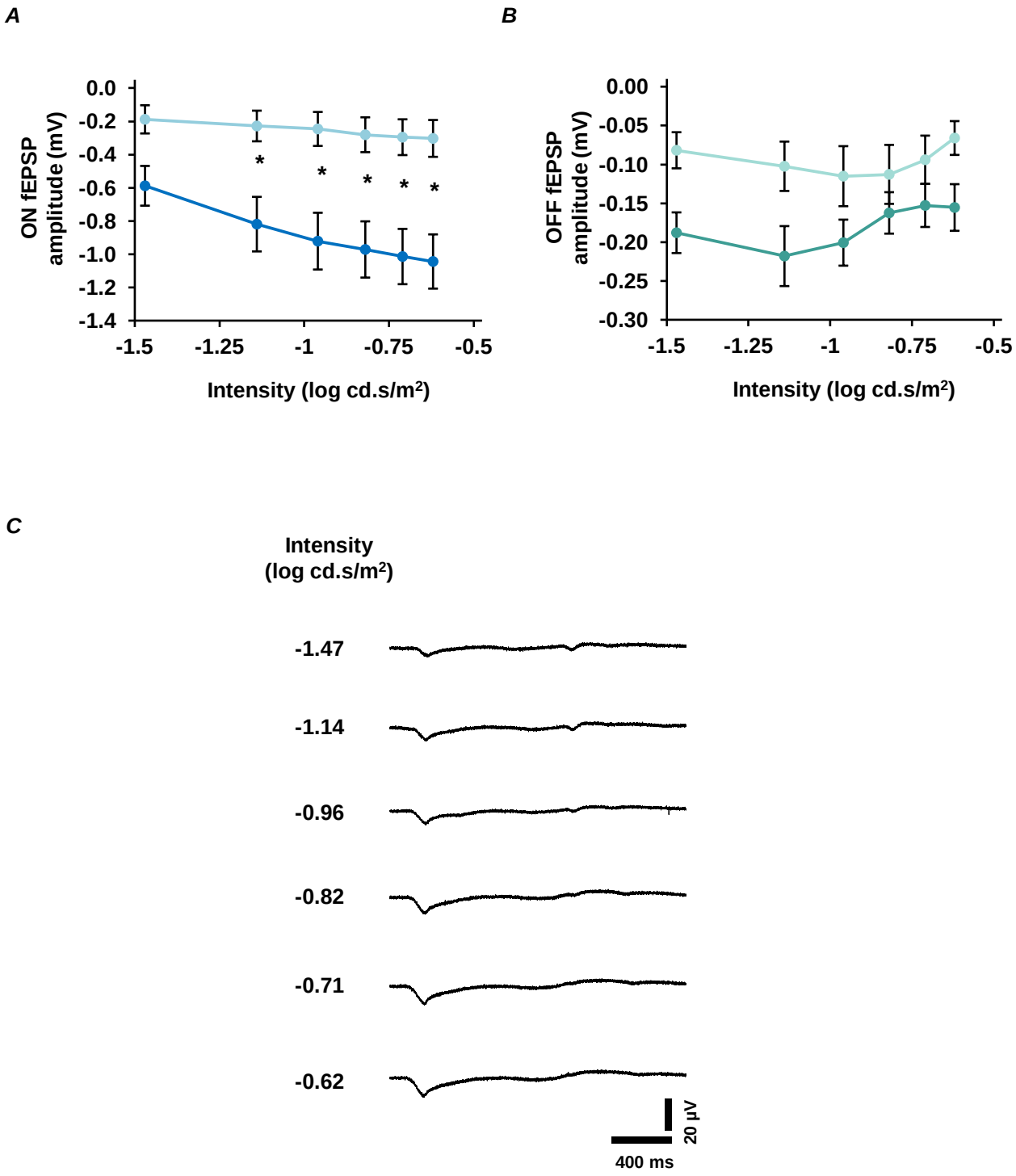

Figure 7.8 Light intensity response functions of dark-adapted, light-evoked NMDA receptor-mediated ON and OFF RGC fEPSPs, in the presence of the competitive and selective NMDA receptor antagonist D-AP5. Values are mean ± SEM fEPSP amplitude. ***A***, In the presence of D-AP5 (100 µM; pale blue), the amplitude of the ON fEPSP was significantly suppressed, across nearly all flash intensities tested, compared to control (dark blue; * $P < 0.05$, $n = 4$ each). B, There was no significant difference between the OFF fEPSP in the presence of D-AP5, compared to control, across the light intensities tested. ***C***, Representative waveform averages revealed that a residual component of the ON fEPSP remained, in the presence of D-AP5, across all stimulus intensities tested, suggesting a non-ionotropic glutamate receptor contribution to the fast responses.

A

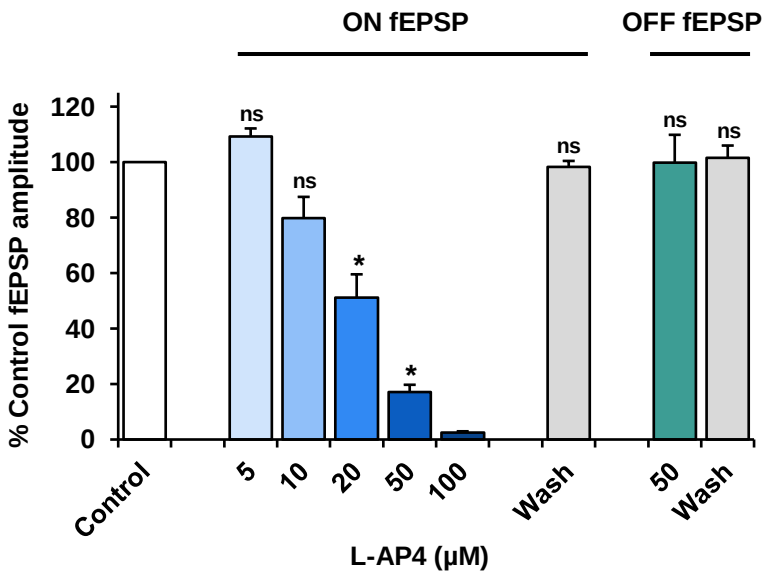

B

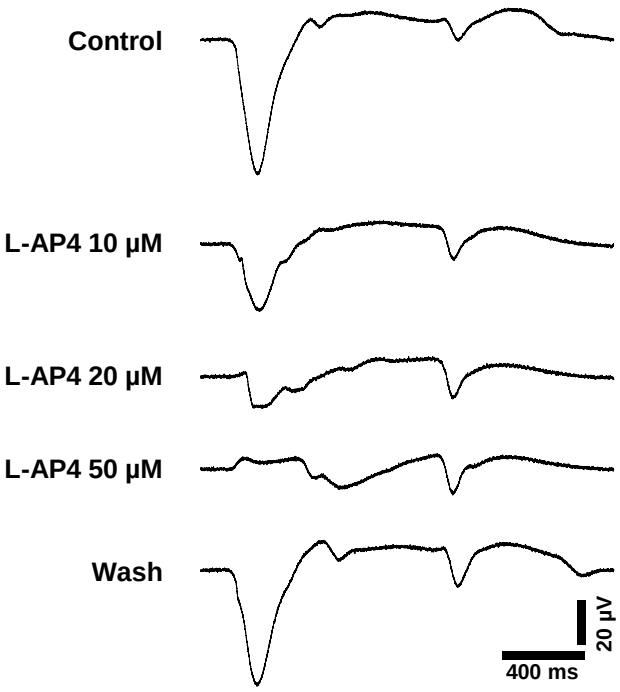

Figure 7.9 The effect of the mGluR6 agonist, L-AP4 on the ON and OFF RGC fEPSPs. Values are mean ± SEM % control fEPSP amplitude. ***A***, L-AP4 selectively reduced the NMDA receptor-mediated ON RGC fEPSP, in a concentration-related manner. ns, not significant; *, $P < 0.05$, compared to pre-treatment control. For 5, 10 and 20 µM, $n = 6$ each; 50 µM, $n = 26$; 100 µM, $n = 2$.The effect was fully reversible on washout (50 µM values). The OFF fEPSP was not affected by L-AP4, compared to control ($P > 0.05$; n = 17). ***B***, Representative waveform averages of light-evoked ON and OFF fEPSPs in response to varying doses of L-AP4.

Chapter 8

Results: The Effects of $P2X_7R$ Activation on Dark-Adapted Visual Responses

In this series of experiments, the short-term effects of $P2X_7R$ activation on the dark-adapted ERG, and ON and OFF fEPSPs were investigated and characterised, in the isolated mouse retina. BzATP was used as the $P2X_7R$ agonist, as it is currently established as the most potent activator of $P2X_7Rs$. The agonist-induced changes in the kinetics of the ERG components and RGC fEPSPs were assessed over an application period of 10 minutes, and during the recovery phase approximately 10 to 15 min post-wash. Unless otherwise stated, all effect values were taken from the final 120 sec of application, and are expressed as mean ± SEM. The selective, competitive $P2X_7R$ antagonist, A438079 was used as the primary antagonist to characterise $P2X_7R$ involvement. A438079 is well established as a potent inhibitor of $P2X_7R$ activation *in vivo* and *in vitro*. As described in the previous chapter, some ERG and all fEPSP experiments were carried out using a modified physiological perfusion medium containing NBQX (10 µM), picrotoxin (100 µM), strychnine (5 µM) and tetrodotoxin (100 nM). This ensured that consistency was maintained between investigations of outer and inner retinal function.

8.1 The effects of BzATP on dark-adapted electroretinogram a-wave and b-wave components in the presence and absence of extracellular magnesium

In physiological Krebs' medium, a 10-min application of BzATP induced a marked potentiation of the a-wave slope to 130.5 ± 12% of control ($P < 0.05$, n = 7) (fig. 8.1A). The BzATP-mediated changes in the a-wave were relatively rapid in onset, reaching a sustained maximum effect within approximately 5-6 min after the start of drug application (fig. 8.1A). Following washout of BzATP, the a-wave slope recovered to 109.1 ± 5% of control ($P >$

0.05) (fig. 8.1A). BzATP also significantly potentiated the implicit time of the a-wave maximum amplitude compared to pre-treatment control ($P < 0.05$) (fig. 8.1D and table 8.1).

A concomitant reduction of the ERG b-wave to 87.9 ± 4% of control ($P < 0.05$, n = 7) was also measured in the presence of BzATP (fig. 8.1B). The changes in the b-wave within 1-2 min of application appeared to reach maximum reduction in amplitude immediately prior to washout (Fig 8.1B). Thus, a different temporal profile of the BzATP-mediated effect was apparent between the a-wave and b-wave. Considering the direct output of the photoreceptors onto the ON-bipolar cells along the vertical pathway, it would be expected that a potentiation in the a-wave slope would lead to a subsequent increase in the b-wave amplitude. However, this does not seem to be the case here, and is consistent with the *in vivo* findings of the effect of BzATP on the rat ERG (Puthussery et al., 2006). The b-wave amplitude recovered to baseline within approximately 5 min following washout of BzATP (103.3 ± 2% of control, $P > 0.05$) (Fig. 8.1B). There was no significant effect on the implicit time of the b-wave during BzATP application, although a lasting effect on the implicit time remained following washout (Fig. 8.1D).

These results have identified that BzATP caused marked changes in the response profiles of the ERG a- and b-waves. As has been previously suggested (Puthussery et al., 2006), the differing effects on the kinetics of the a-wave and b-waves indicated that BzATP elicited independent alterations in the photoreceptor and post-photoreceptor components. Furthermore, the consistency of these results with the findings in the rodent *in vivo* confirms that the structural integrity and physiological function of the retinal preparation were maintained *in vitro*.

The effect of BzATP-mediated activation of $P2X_7Rs$ is considerably enhanced in the absence of extracellular divalent cations, particularly magnesium ions (Mg^{2+}) (Surprenant et al., 1996; Virginio et al., 1997). To further characterise the BzATP-mediated effect on the ERG response components, the $P2X_7R$ agonist was applied in normal physiological medium in the absence of magnesium. Under these conditions, BzATP induced a reduction in the a-wave slope to 90.7 ± 3% of control ($P < 0.05$, n = 6), which was typically recoverable 5 min post-wash to 97.2 ± 3% of control ($P > 0.05$) (fig 8.2A). The effect peaked approximately 8 min after the start of drug application (fig 8.2A); although the mean value was taken at the final 2 min, in order to reliably compare the effect of BzATP across the different conditions (table 8.1). Furthermore, BzATP increased the implicit time of the a-wave maximum amplitude, which did not seem to fully recover following washout. The BzATP-mediated reduction in the a-wave slope was contrary to that seen in the presence of extracellular magnesium, suggesting that the effect of $P2X_7R$ activation is reversed ($P < 0.05$; see table 8.1).

In the absence of extracellular magnesium, BzATP significantly reduced the b-wave amplitude to 89.5 ± 1% of control ($P < 0.05$, n = 6), an effect which did not recover on washout (fig 8.2B). The temporal profile of the b-wave amplitude was comparable to that of the a-wave slope during the early phase of BzATP application, where an exponential reduction in both components was apparent. However, the differing recovery periods of the a- and b-waves strongly supports the notion that BzATP elicited independent effects on photoreceptor and post-photoreceptor components. Additionally, BzATP did not elicit a significant effect on the implicit time of the b-wave maximum amplitude. The suppressive effect of BzATP on the b-wave amplitude in the presence and absence of extracellular magnesium were similar ($P > 0.05$, see table 8.1). The differences in the changes to the b-wave amplitude during the post-wash phase, under both conditions imply that magnesium was required for full recovery following BzATP application.

8.2 The effects of BzATP on dark-adapted electroretinogram a-wave and b-wave components, in the presence of the antagonists NBQX, picrotoxin, strychnine and tetrodotoxin

The following experiments were carried out in PMSTN perfusion medium. As shown in fig. 8.3A, there was a transient potentiation in the a-wave slope within the first 2-3 min of BzATP application. However, this effect reversed from 5 min, with a significant reduction in the a-wave slope to 70.1 ± 8% of pre-treatment control ($P < 0.05$, n = 7), and did not appear to recover fully following washout (76.3 ± 9% of control, $P < 0.05$). The a-wave was also significantly delayed in the presence of BzATP, recovering on washout (fig. 8.3D and table 8.1).

The effect of BzATP on the b-wave amplitude followed a similar temporal profile to that of the a-wave slope. An initial and transient potentiation in the b-wave amplitude was observed, followed by a significant reduction to 66.6 ± 10% of control ($P < 0.05$, n = 7). As with the a-wave slope, the b-wave amplitude did not appear to recover following washout of BzATP. The b-wave implicit time was also significantly increased with BzATP. Under these conditions, BzATP induced effects on the a-wave slope and b-wave amplitude which were comparable to those seen in the absence of magnesium alone, as shown in table 8.1.

8.3 The effect of the selective $P2X_7$ receptor antagonist A438079 on the BzATP-mediated changes in the dark-adapted electroretinogram a-wave and b-wave components

In order to further delineate $P2X_7R$ involvement, the effect of BzATP on the ERG components was assessed in the presence of the selective, competitive $P2X_7R$ antagonist, A438079 (10 µM). Experiments were carried out in PMSTN medium. The effect of A438079

on the BzATP-induced changes in the a- and b-waves was directly compared to the preceding application of BzATP in the same experiment.

As shown in fig. 8.4, A438079 abolished the BzATP-mediated reduction of the a-wave slope to 4 ± 16% of the effect of BzATP when applied alone ($P < 0.05$, n = 7). In the presence of A438079, the BzATP-induced increase in the implicit time of the a-wave maximum amplitude remained. The $P2X_7R$ antagonist reduced the effect of BzATP on the b-wave amplitude to 58.3 ± 16% of control (maximum BzATP effect*;* $P < 0.05$). Contrary to BzATP alone, the agonist did not significantly affect the implicit time of the b-wave amplitude in the presence of A438079. Thus, the A438079-mediated attenuation in the effect of BzATP on these components of the ERG confirms the involvement of $P2X_7R$ activation.

As illustrated in fig. 8.5, the a-wave slope was significantly potentiated in the presence of A438079 (10 μM) alone, to 125.7 ± 12% of pre-treatment control ($P < 0.05$, n = 10). A438079 also markedly reduced the b-wave amplitude to 79.1 ± 15% of control ($P < 0.05$, n = 10). The implicit times for both a- and b-waves were increased in the presence of the antagonist. These results suggest that $P2X_7R$ activation may modulate retinal function under baseline conditions.

8.4 The effect of BzATP on the oscillatory potentials of the dark-adapted electroretinogram

The effect of BzATP on the oscillatory potentials was also explored. As shown in the Methods section 6.4.4, the high-frequency oscillatory potentials were digitally extracted from the raw ERG waveform. Changes in the peak power output of the oscillatory potentials were assessed with their frequency spectra before, during and after agonist application. BzATP

significantly reduced the peak power to 63.9 ± 11% of control ($P < 0.05$) (fig. 8.6). Following washout of BzATP, the oscillatory potentials recovered to 99.9 ± 9% of control ($P > 0.05$). These results suggest that BzATP considerably suppressed the activity of inner retinal networks, and further imply that $P2X_7R$ modulation in the inner retina is at least partially independent of that in the outer retina.

8.5 The effect of BzATP on NMDA receptor-mediated ON and OFF retinal ganglion cell fEPSPs

The effect of $P2X_7R$ activation on synaptic transmission at bipolar-retinal ganglion cell (RGC) synapses was investigated. All experiments were carried out in PMSTN medium. As shown in fig. 8.7, BzATP was applied to the perfusate for ten minutes, and the agonist-induced modulation of the ON and OFF fEPSPs was compared across concentrations ranging from 10 to 300 µM. There was no significant effect on the ON fEPSP with low micromolar concentrations of BzATP. However, a dose-related reduction in the ON fEPSP peak amplitude was measured at higher micromolar concentrations. BzATP at 300 µM, the highest concentration tested, elicited a significant reduction in the ON fEPSP to 78.1 ± 3% of control ($P < 0.05$, n = 21) (Fig. 8.7Aa). BzATP elicited its effect within approximately 2-3 min of reaching the retina, and was sustained throughout the duration of application (Fig. 8.7Ab). This effect was partially recoverable on washout to 92.4 ± 2% of control ($P < 0.05$).

BzATP, at all concentrations tested, did not elicit any overall and statistically significant effect on the OFF fEPSP (fig. 8.7B). This selective effect of BzATP on the ON fEPSP, but not on the OFF fEPSP may suggest a pathway-specific modulation by $P2X_7Rs$.

8.6 The effect of the selective and competitive $P2X_7$ receptor antagonists A438079, A804598 and AF27139 on the BzATP-mediated modulation of the ON RGC fEPSP

The effect of BzATP on the ON fEPSP was assessed in the presence of the selective, competitive $P2X_7R$ antagonists A438079, A804598 or AF27139. Experiments were separate for each antagonist, and were carried out in PMSTN medium. The effect of each antagonist on the BzATP-induced changes in the ON fEPSP was directly compared to the preceding application of BzATP in the absence of the antagonist. A438079 (10 µM), A804598 (30 µM) and AF27139 (30 µM), all partially attenuated the BzATP-mediated reduction of the ON fEPSP to 68.7 ± 2%, 55.1 ± 11% and 75.2 ± 7% of control, when compared to the maximum effect of BzATP ($P < 0.05$ for all) (fig. 8.8).

These antagonists have previously shown to be potent in blocking $P2X_7R$ activation. The potency of A438079 in this respect was further supported by its inhibitory effect on the BzATP-mediated reduction in the ERG a-wave, shown earlier in this study. Therefore, these results implicate the involvement of a BzATP-activated release of endogenous agonist (ATP) that may enhance $P2X_7R$ activation and subsequently reduce the potency of the antagonists.

Fig. 8.9 illustrates the effect of these antagonists on baseline ON fEPSP responses. The ON fEPSP was reduced in the presence of A804598 to 85.0 ± 15% of control ($P < 0.05$, n = 7), but was not significantly affected by A438079 or AF27139 at the concentrations tested. The OFF fEPSP was not significantly affected by any of the antagonists.

8.7 The effect of adenosine on ON and OFF RGC fEPSPs

Extracellular ATP is rapidly degraded into its constituent adenosine, by ectonucleotidases. It has previously been suggested that the actions of BzATP in the hippocampus are due the effect of its breakdown product Bz-adenosine through the subsequent activation of A1 receptors (Kukley et al., 2004). Adenosine receptors are known to be expressed in the retina. Therefore, it was investigated whether the effect of BzATP on the RGC fEPSPs was mediated by the activation of adenosine receptors through Bz-adenosine.

The ON fEPSP was significantly potentiated by adenosine, exhibiting a dose-related effect (fig. 8.10Aa). For the highest concentration tested (300 µM), maximum potentiation was achieved within 3 – 5 min of adenosine exposure, to 109.5 ± 2% of control ($P < 0.05$, n = 8) (fig. 8.10Ab). The effect on the ON fEPSP peak amplitude was not sustained, but decayed prior to washout. A transient reduction in the ON fEPSP was also observed before recovering fully, to 99.8 ± 2% of control approximately 10 min later ($P > 0.05$), which is illustrated by the representative traces (fig. 8.10Ab and 8.10C). The OFF fEPSP was also significantly potentiated with adenosine, with a dose-related profile, similar to that of the ON fEPSP. Fig. 8.10Bb shows that the temporal profile of the effect of adenosine on the OFF fEPSP was different to that of the ON fEPSP (fig 8.10Ab). At the 5 min time point, ADO (300 µM) significantly potentiated the OFF fEPSP to 118.8 ± 8% of control ($P < 0.05$, n = 7), an effect that was sustained throughout the duration of application. Following washout, the OFF fEPSP showed a transient reduction prior to returning to 95.7 ± 5% of control ($P > 0.05$). Vehicle application had no significant effect on either the ON or OFF fEPSPs (fig 8.10).

These results suggest that the differential effects of BzATP and adenosine on the ON and OFF fEPSPs are due to the activation of different purinergic receptors. Furthermore, the

OFF fEPSP is markedly modulated by adenosine, but not by BzATP, further implicating ON-pathway dominance for $P2X_7Rs$.

8.8 The effect of BzATP and of the P2XR antagonists suramin, PPADS and A438079 on the ON fEPSP, in the presence of D-AP5

The addition of the competitive NMDA receptor antagonist, D-AP5 (100 µM) to the PMSTN perfusate revealed that a considerable residual fraction of the fEPSPs remained (figs. 7.7 and 7.8, Chapter 7). The possible contribution of P2XRs and in particular, that of $P2X_7Rs$ to the residual fraction of the ON fEPSP was investigated. All experiments were carried out in PMSTN medium in the presence of D-AP5 (100 µM). Fig. 8.11B shows the marked reduction in the ON fEPSP induced by D-AP5, as previously demonstrated in the preceding chapter. Co-application of BzATP (300 µM) induced a further reduction of the ON fEPSP to 78.8 ± 3% of the D-AP5-mediated effect ($P < 0.05$, n = 7). Following washout of BzATP, the ON fEPSP recovered to 94.8 ± 4% of its amplitude pre-BzATP ($P > 0.05$) (fig. 8.11A and B). These results suggest that the effect $P2X_7R$ activation on the ON RGCs occurs independently of NMDA-R activity.

In separate experiments, A438079 (10 µM) or the broad-spectrum P2XR antagonists suramin (100 µM) and PPADS (100 µM) were also co-applied with D-AP5 (fig. 8.12A – C). All three compounds elicited further reductions in the ON fEPSP. The residual fraction of the ON fEPSP was significantly suppressed to 44.9 ± 9%, 74.0 ± 7% and 91.1 ± 3% of control, by suramin, PPADS and A438079, respectively ($P < 0.05$, n = 6, for all) (fig. 8.12D). Together, these results suggest that $P2X_7Rs$ and other P2XR subtypes contribute to the residual component of baseline ON retinal ganglion cell activity, in the absence of NMDA-R function.

Chapter 8 Figures and Tables

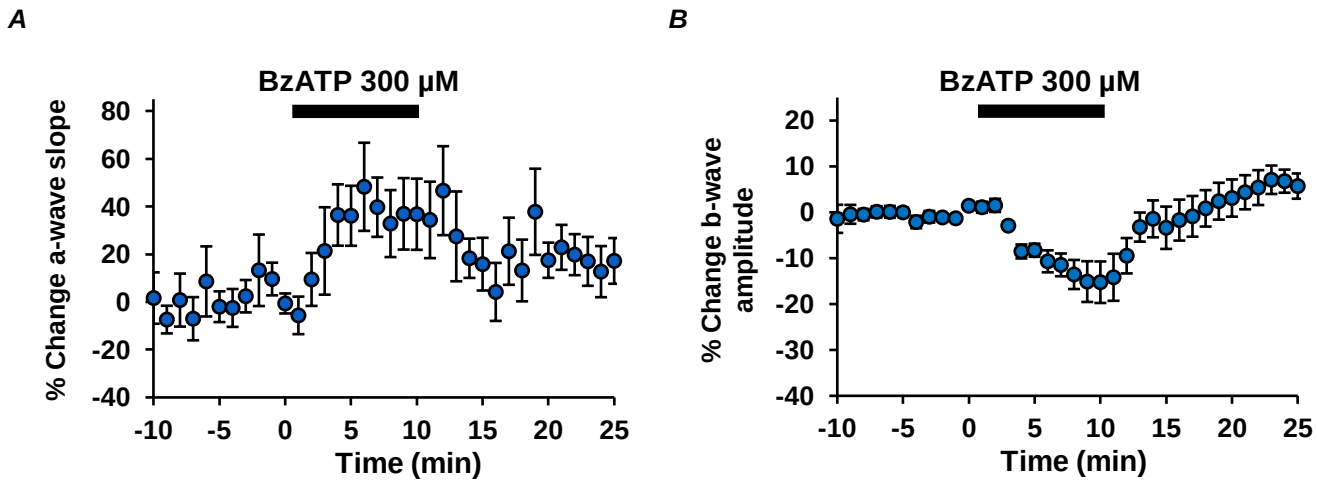

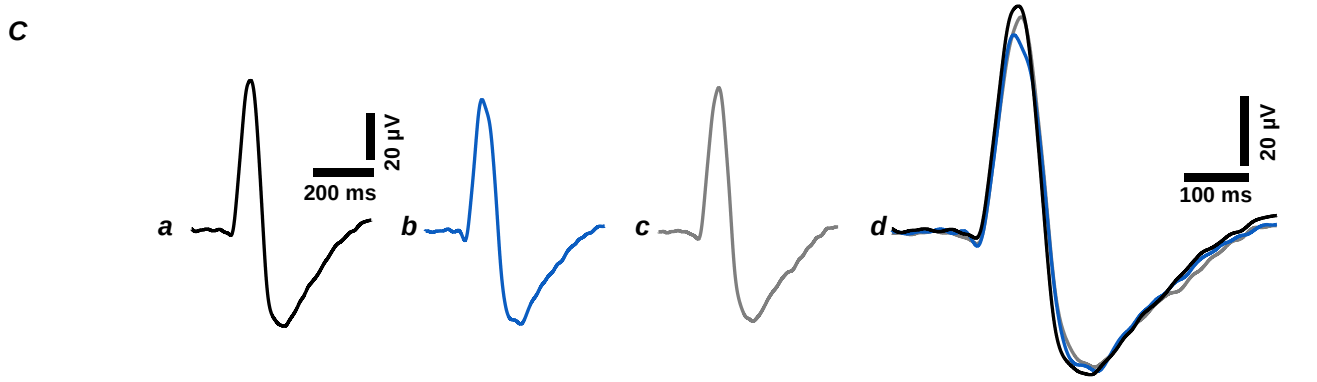

D

	Control	BzATP	Wash
a-wave			
Slope (% of control)	-	130.5 ± 12 *	109.1 ± 5 *ns*
Implicit time (ms)	40.1 ± 3	42.9 ± 3 *	41.0 ± 3 *
b-wave			
Amplitude (% of control)	-	87.9 ± 4 *	103.0 ± 2 *ns*
Implicit time (ms)	98.7 ± 4	103.0 ± 4 *ns*	104.6 ± 3 *

Figure 8.1 The effect of BzATP on the dark-adapted ERG in physiological Krebs' medium. Time course plots show the effect of BzATP (300 µM; 10 min) on the a-wave slope and b-wave amplitude. ***A***, BzATP induced a sustained potentiation of the a-wave slope, which reached maximal effect within approximately 5 min of application, and was reversible on washout. ***B***, BzATP concomitantly reduced the b-wave amplitude over the course of application, an effect which was recoverable following washout. Note the differential temporal profiles of the effect of BzATP on the ERG components. Values are mean ± SEM percentage change (n = 7). ***C***, Representative traces illustrate the effect of BzATP on the ERG. ***a***, control; ***b***, BzATP; ***c***, wash; ***d***, merge. ***D***, Summary of the actions of BzATP on the a-wave and b-wave (mean ± SEM). ns, not significant; *, $P < 0.05$, compared to control.

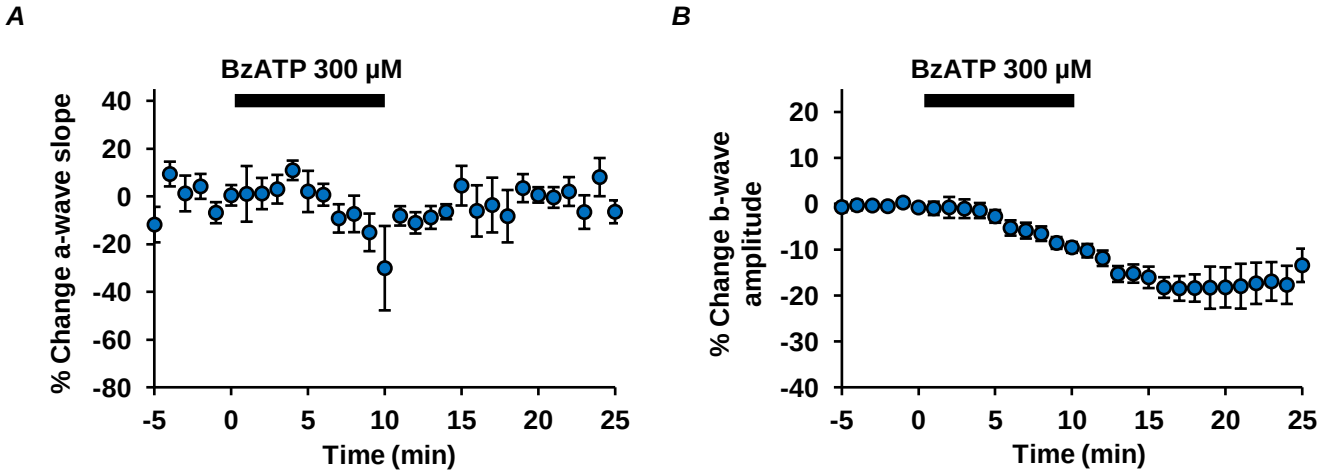

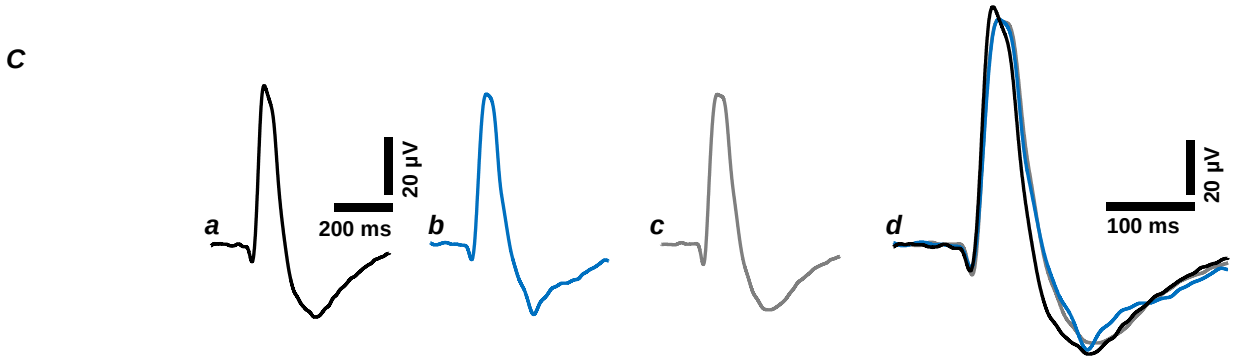

D

	Control	BzATP	Wash
a-wave			
Slope (% of control)	-	90.7 ± 3 *	97.2 ± 3 *ns*
Implicit time (ms)	29.7 ± 2	32.5 ± 2 *	31.0 ± 2 *
b-wave			
Amplitude (% of control)	-	89.5 ± 1 *	81.2 ± 4 *ns*
Implicit time (ms)	74.4 ± 2	80.6 ± 3 *ns*	77.6 ± 3 *ns*

Figure 8.2 The effect of BzATP on the dark-adapted ERG in the absence of extracellular magnesium ions. Time course plots show the effect of BzATP (300 µM; 10 min) on the a-wave slope and b-wave amplitude. ***A***, BzATP reduced the a-wave slope, an effect which was reversible on washout. ***B***, BzATP also caused a reduction in the b-wave amplitude over the course of application, which was not fully recoverable following washout. Note the differential temporal profiles of the effect of BzATP on the ERG components, particularly during the wash phase. Values are mean ± SEM percentage change (n = 6). ***C***, Representative traces illustrate the effect of BzATP on the ERG in the absence of extracellular magnesium ions. ***a***, control; ***b***, BzATP; ***c***, wash; ***d***, merge. ***D***, Summary of the actions of BzATP on the a-wave and b-wave (mean ± SEM). ns, not significant; *, P < 0.05, compared to control.

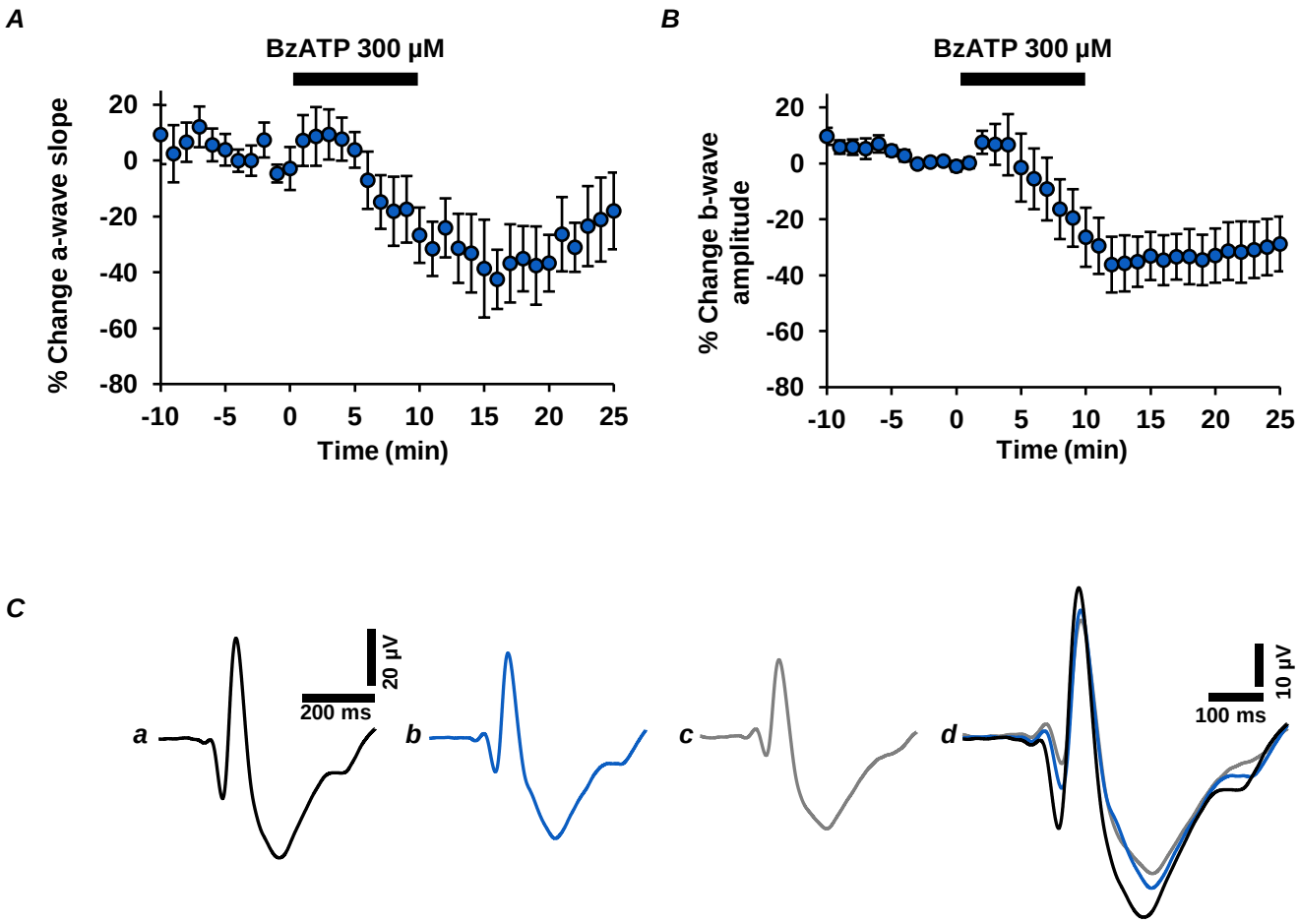

D

	Control	BzATP	Wash
a-wave			
Slope (% of control)	-	70.1 ± 8 *	78.9 ± 8 *
Implicit time (ms)	61.1 ± 7	68.5 ± 7 *	60.8 ± 7 *ns*
b-wave			
Amplitude (% of control)	-	66.6 ± 10 *	69.8 ±10 *
Implicit time (ms)	104.9 ± 3	109.8 ± 3 *	108.3 ± 3 *

Figure 8.3 The effect of BzATP on the dark-adapted ERG in the absence of extracellular magnesium ions, and in the presence of NBQX, picrotoxin, strychnine and TTX. Time course plots show the effect of BzATP (300 µM; 10 min) on the a-wave slope and b-wave amplitude. ***A***, BzATP reduced the a-wave slope, an effect which was partially reversible on washout. ***B***, The b-wave amplitude was markedly suppressed, and was not fully recoverable following washout. Note the relatively similar effect of BzATP on the b-wave, compared to that shown in fig. 8.2B. Values are mean ± SEM percentage change (n = 7). ***C***, Representative traces illustrate the effect of BzATP on the ERG under these conditions. ***a***, control; ***b***, BzATP; ***c***, wash; ***d***, merge. ***D***, Summary of the actions of BzATP on the a-wave and b-wave (mean ± SEM). ns, not significant; *, $P < 0.05$, compared to control.

	Physiological Krebs' (*n* = 7)	0 mM Mg^{2+} (*n* = 6)	Modified Krebs' (PMSTN) (*n* = 7)
a-wave			
Slope (% of control) ***A***	130.5 ± 12	90.7 ± 3	70.1 ± 8
Change in implicit time (ms)	+ 2.9 ± 1	+ 2.8 ± 0	+ 7.4 ± 2
b-wave			
Amplitude (% of control) ***B***	87.9 ± 4	89.5 ± 1	66.6 ± 10
Change in implicit time (ms)	+ 4.3 ± 2	+ 6.2 ± 3	+ 5.0 ± 1

Table 8.1 Summary of the actions of BzATP on the ERG a-wave and b-wave components, under all three conditions tested. All values are mean ± SEM. ***A***, Comparisons of the BzATP-mediated effects between conditions, on the a-wave slope: Krebs' vs. 0 mM Mg+ or PMSTN, $P < 0.05$ for both; 0 mM Mg+ vs. PMSTN, $P < 0.05$. For the change in a-wave implicit time values, there were no significant differences in the effect of BzATP between conditions tested ($P > 0.05$, for all). ***B***, Comparisons between conditions, of the BzATP-induced effect on the b-wave amplitude and implicit time. There were no significant differences between conditions tested, for changes to the amplitude ($P > 0.05$, for all comparisons) or implicit time ($P > 0.05$, for all comparisons).

A

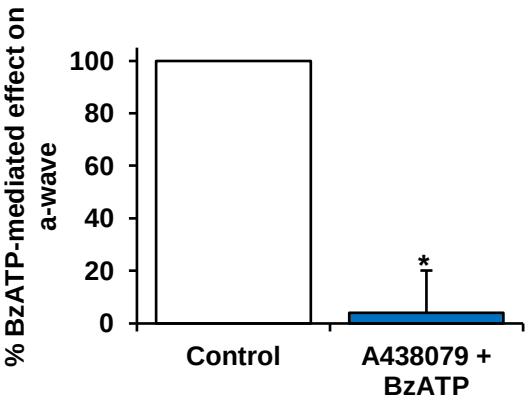

B

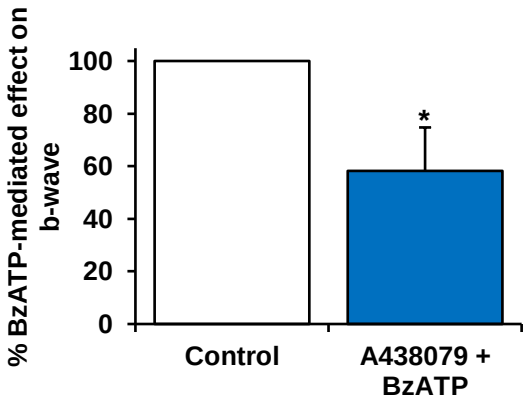

C

	Control (BzATP)	A438079 + BzATP
Implicit time (change from baseline; ms) **a-wave** **b-wave**	 + 7.4 ± 2 + 5.0 ±1	 + 3.2 ± 1 + 2.0 ± 3

Figure 8.4 Actions of the selective $P2X_7R$ antagonist A438079 on the BzATP-mediated effects on the ERG components. Values are mean ± SEM percentage of control (max. BzATP effect i.e. 100%; *n* = 7). ***A***, The BzATP-mediated potentiation of the ERG a-wave was almost completely suppressed in the presence of A438079 (10 μM), compared to control ($P < 0.05$). ***B***, A438079-induced attenuation of the BzATP-mediated reduction in the b-wave was observed ($P < 0.05$ vs. control). Note the persistent effect of BzATP on the b-wave. ***C***, BzATP-mediated changes from baseline implicit time values in the absence and presence of A438079 ($P > 0.05$ for both ERG components).

A

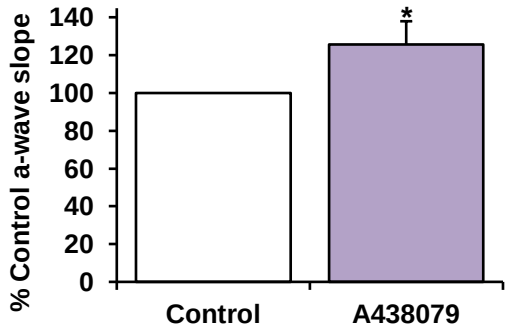

B

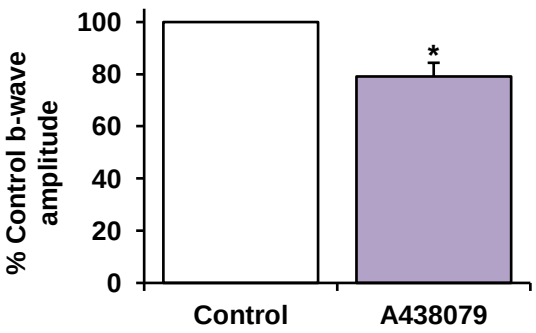

C

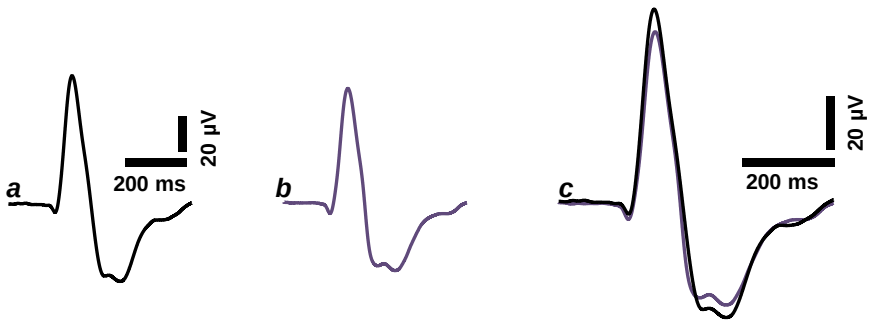

D

	Control	A438079
a-wave (ms)	56.9 ± 7	65.8 ± 7
b-wave (ms)	111.8 ± 2	114.8 ± 2

Figure 8.5 The effect of the selective $P2X_7R$ antagonist A438079 on ERG components, in normal physiological function. All experiments were carried out in PMSTN perfusion medium. Values are mean ± SEM percentage of pre-treatment control; *n* = 10. A438079 (10 µM) was superfused for 20 – 30 min, until the response was stable. ***A***, Application of A438079 alone induced a marked potentiation in the a-wave, compared to control ($P < 0.05$). **B**, The b-wave was significantly reduced in the presence of A438079 ($P < 0.05$). ***C***, Representative traces reflect the A438079-mediated alterations to ERG components. ***a***, control; ***b***, A438079; ***c***, merge. ***D***, Implicit time values (mean ± SEM) before (control) and during application of A438079 ($P < 0.05$ vs. control, for both components).

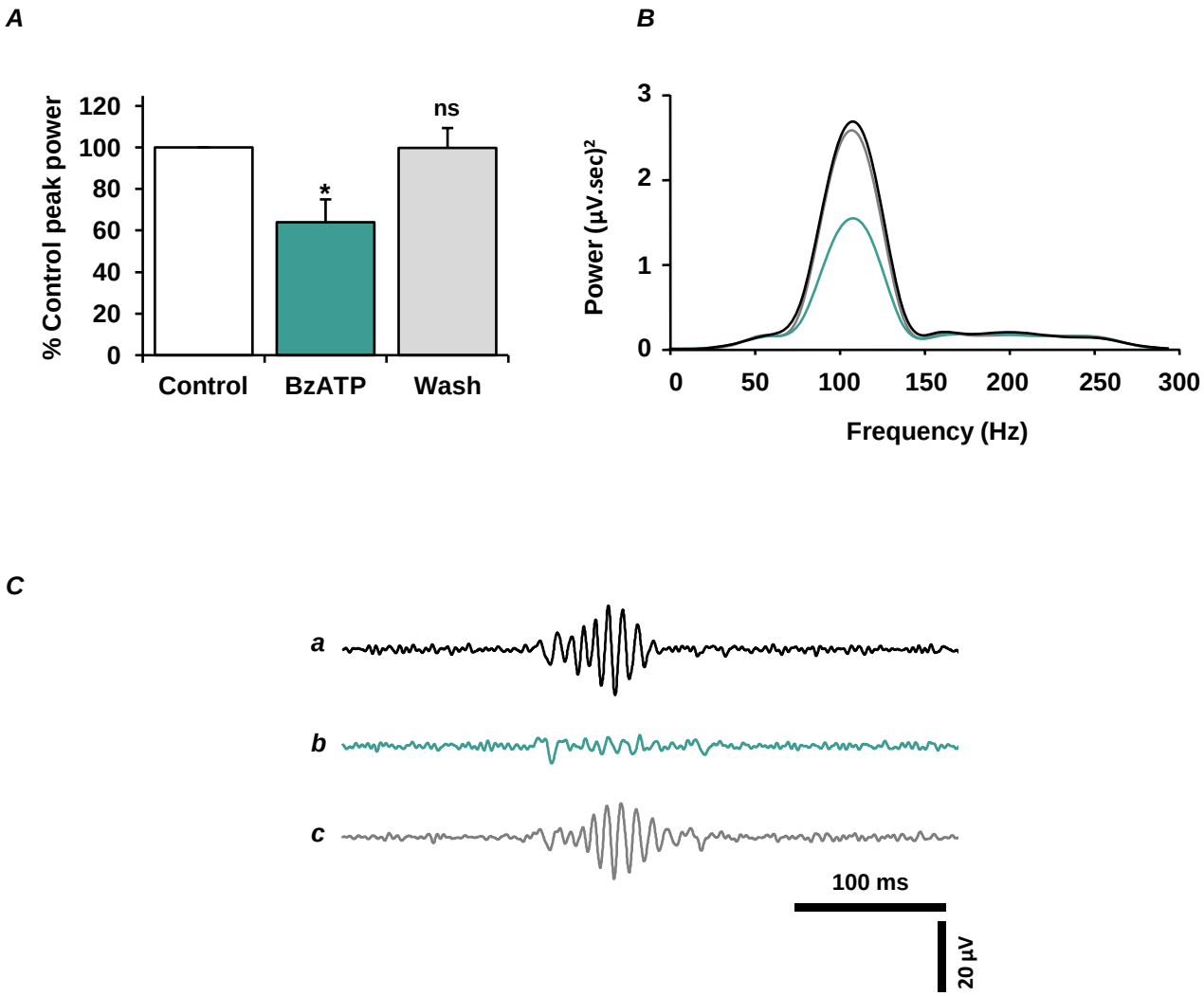

Figure 8.6 The effect of BzATP on ERG oscillatory potentials. Experiments were done in physiological Krebs' medium and were digitally extracted from the same ERG experiments shown in fig. 8.1. ***A***, Mean ± SEM percentage of control peak power; *n* = 7. BzATP (300 µM; 10 min) caused a reversible and significant reduction in the peak power output of the oscillatory potentials, compared to control ($P < 0.05$), indicating modulation of inner retinal function. ***B***, Representative power spectra of oscillatory potentials, before, during and post-BzATP application. Black, control; green, BzATP; grey, wash. Under control conditions, the oscillatory potentials exhibited a peak frequency ~ 107 Hz, typical of dark-adapted ERG responses. In the presence of BzATP, no overall shift in frequency was detected. ***C***, Waveform averages (120 sec) illustrate the BzATP-mediated suppression of the oscillatory potentials, and recovery on washout. ***a***, control; ***b***, BzATP; ***c***, wash.

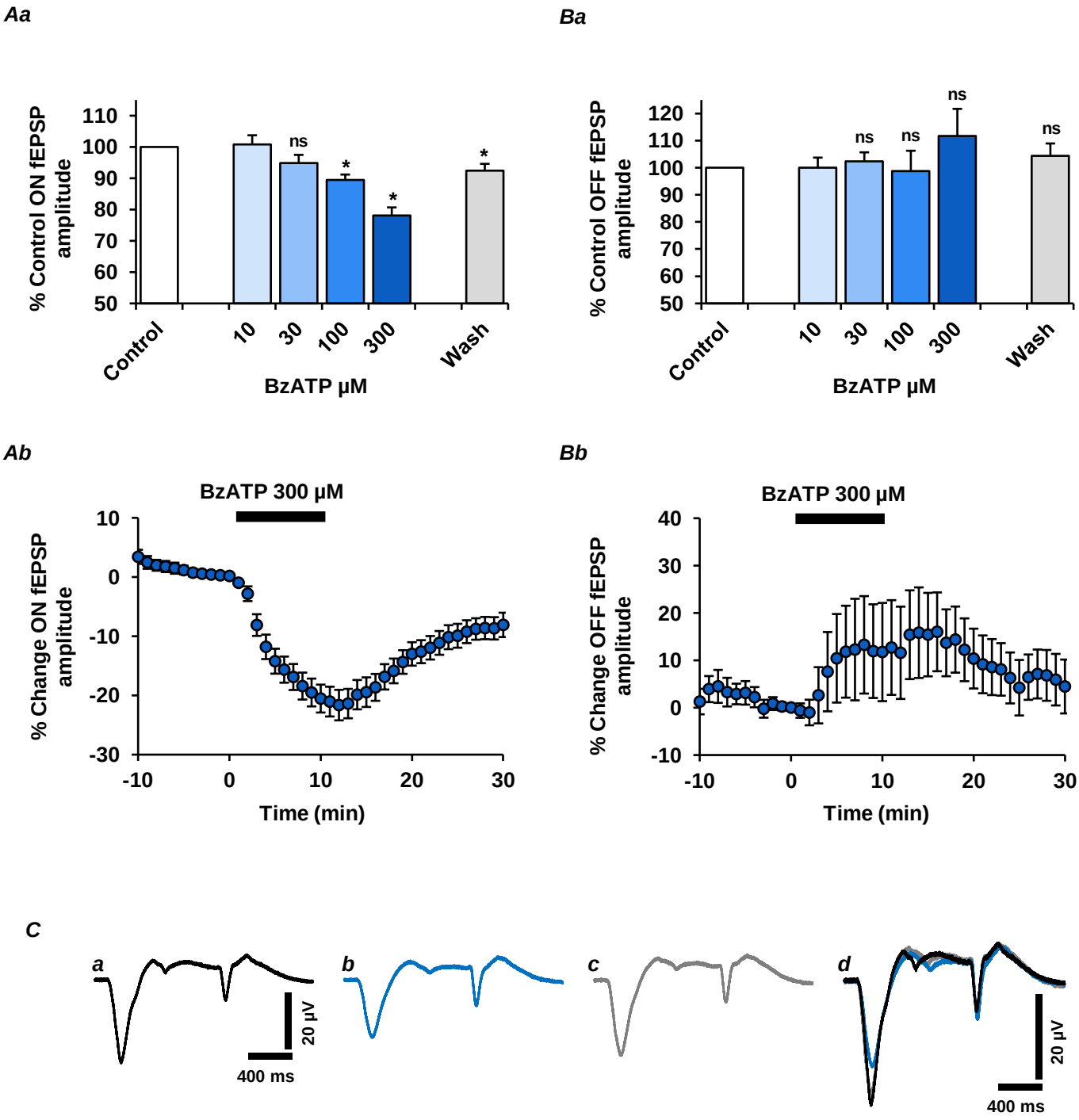

Figure 8.7 The effect of BzATP on light-evoked ON and OFF RGC fEPSPs. Responses are pharmacologically isolated, NMDAR-mediated. BzATP was applied (10 min) at concentrations of 10 (*n* = 2), 30 (*n* = 6), 100 (*n* = 6) and 300 µM (ON, *n* = 21; OFF, *n* = 17). Values are mean ± SEM percentage of pre-treatment control fEPSP peak amplitude. ***Aa***, BzATP elicited a concentration-related reduction of the ON fEPSP. Washout of BzATP (300 µM) induced recovery of the ON fEPSP. ***Ba***, No overall effect on the OFF fEPSP was measured, in the presence of BzATP across all concentrations tested. ns, not significant; *, $P < 0.05$, compared to control. ***Ab*** and ***Bb***, Time course plots show the effect of BzATP (300 µM) on the ON and OFF fEPSPs, respectively. Plotted values are mean ± SEM percentage change in fEPSP peak amplitude, relative to pre-treatment control. ***C***, Representative traces (120 sec averages) illustrate the effect of BzATP (300 µM) on the ON and OFF fEPSPs. ***a***, control; ***b***, BzATP; ***c***, wash; ***d***, merge.

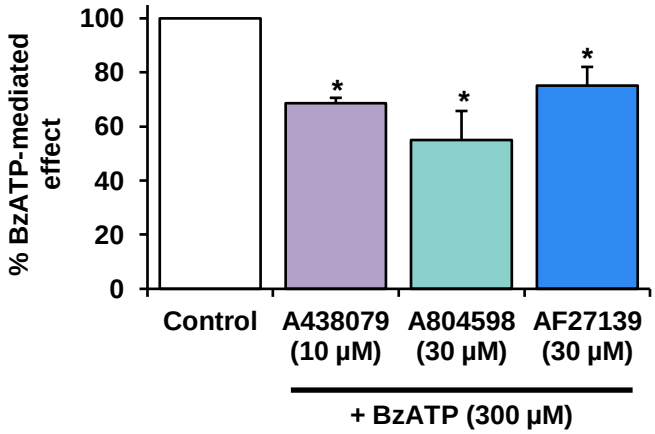

Figure 8.8 Actions of selective $P2X_7R$ antagonists on the BzATP-induced suppression of the ON fEPSP. Values are mean ± SEM percentage of control relative to the BzATP effect. The selective $P2X_7R$ antagonists, A438079 (*n* = 6), A804598 (*n* = 7) or AF27139 (*n* = 6) significantly attenuated the BzATP (300 µM)-mediated reduction of the ON fEPSP. All three compounds exhibited similar potency in blocking $P2X_7R$ function, at the concentrations tested. Note that in the presence of all antagonists, a large residual effect on the ON fEPSP persisted with BzATP application. ns, not significant; *, $P < 0.05$, compared to control.

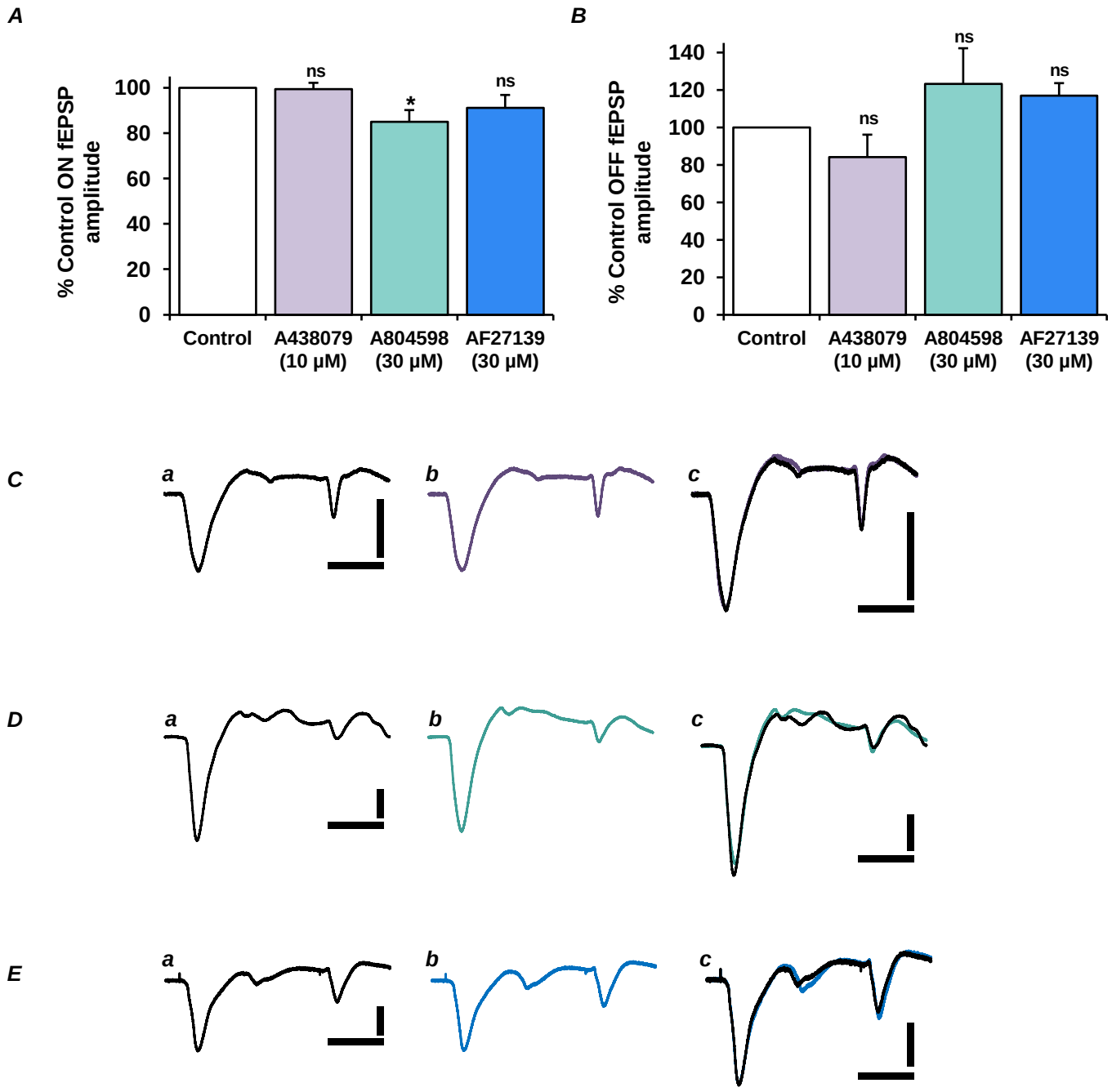

Figure 8.9 Direct actions of selective $P2X_7R$ antagonists on NMDAR-mediated ON and OFF fEPSPs. Values are mean ± SEM percentage of pre-treatment control fEPSP peak amplitude. ***A***, The ON fEPSP was significantly reduced in the presence of A804598 (n = 7), but not by A438079 (n = 6) or AF27139 (n = 6), at the concentrations tested. ***B***, There was no overall effect on the OFF fEPSP in the presence of the $P2X_7R$ antagonists. ns, not significant; *, $P < 0.05$, compared to control. Representative traces show the effect of A438079 (***C***), A804598 (***D***) and AF27139 (***E***) on the ON and OFF fEPSPs. For all: ***a***, control; ***b***, respective antagonist, ***c***, merge. All scale bars: vertical, 20 µV; horizontal, 400 ms.

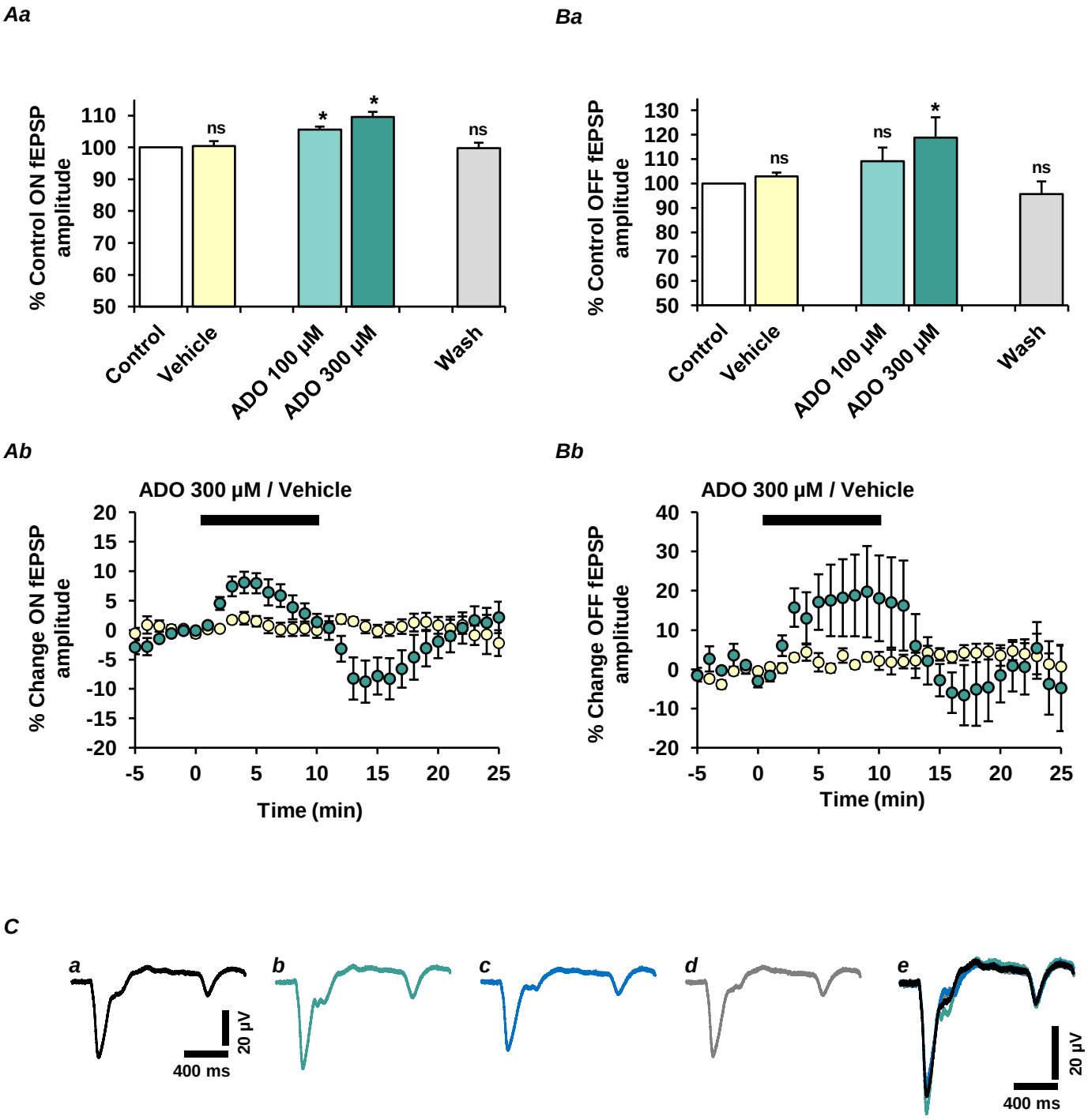

Figure 8.10 The effect of adenosine on the NMDAR-mediated ON and OFF RGC fEPSPs. Adenosine (ADO) was applied (10 min) at concentrations of 100 and 300 µM. ON, *n* = 8; OFF *n* = 7, for both concentrations tested. ***Aa*** and ***Ab***, Values are mean ± SEM percentage of pre-treatment control fEPSP peak amplitude, taken ~5 – 7 min after the start of adenosine application. Both the ON and OFF fEPSPs were reversibly and significantly potentiated by adenosine, in a concentration-related manner. Vehicle application elicited no effect on either ON or OFF fEPSPs. ns, not significant; *, $P < 0.05$, compared to control. ***Ab*** and ***Bb***, Time course plots show the effect of adenosine (300 µM; green) and vehicle (yellow) on the ON and OFF fEPSPs, respectively. Plotted values are mean ± SEM percentage change in fEPSP peak amplitude, relative to pre-treatment control. ns, not significant; *, $P < 0.05$, compared to control. ***C***, Representative traces (120 sec averages) illustrate the effect of adenosine (300 µM) on the ON and OFF fEPSPs. ***a***, control; ***b***, 5 min; ***c***, 12 min ; ***d***, wash; ***e***, merge.

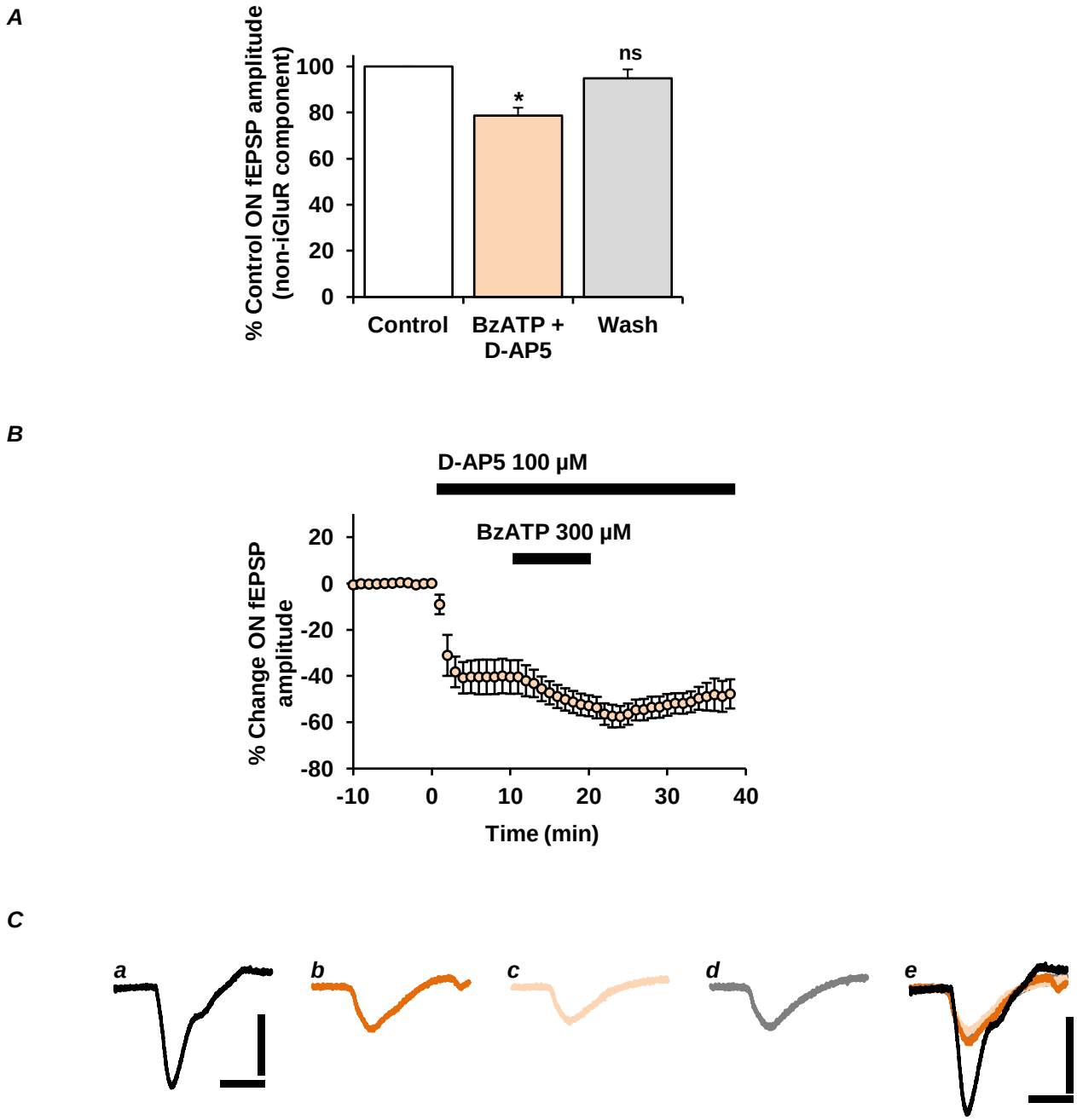

Figure 8.11 Actions of BzATP on the ON fEPSP in the presence of the NMDA receptor antagonist D-AP5. Application of D-AP5 (100 µM) significantly reduced the ON fEPSP amplitude, although a residual component of the fEPSP remained. ***A***, Co-application of BzATP (300 µM) further suppressed the ON fEPSP, an effect which was reversible on washout. Values are mean ± SEM percentage of control in the presence of D-AP5. ns, not significant; *, $P < 0.05$, compared to control; $n = 7$. ***B***, Time course plot shows mean ± SEM percentage change in fEPSP peak amplitude, relative to pre-D-AP5 application. The time course of the BzATP-mediated effect is comparable to that in the absence of D-AP5, as shown in fig. 8.7. ***C***, Waveform averages demonstrate the effect of D-AP5 and BzATP co-application on the ON fEPSP. ***a***, control; ***b***, D-AP5; ***c***, + BzATP; ***d***, wash; ***e***, merge. All scale bars: vertical, 20 µV; horizontal, 200 ms. iGluR, ionotropic glutamate receptor.

Aa

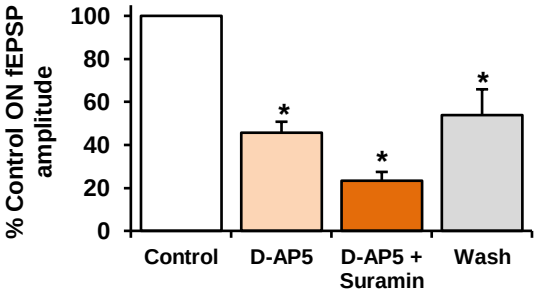
% Control ON fEPSP amplitude
100
80
60
40
20
0
Control
D-AP5
D-AP5 + Suramin
Wash

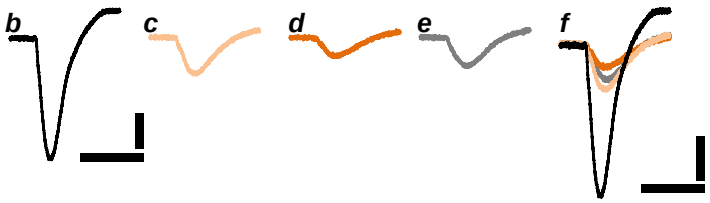
b
c
d
e
f

Ba

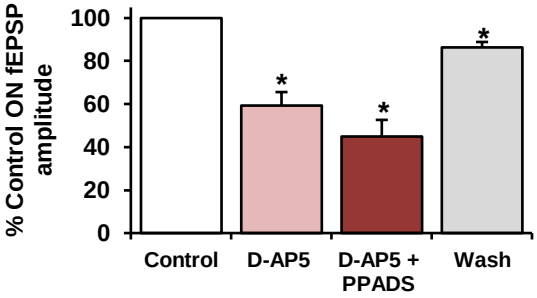
% Control ON fEPSP amplitude
100
80
60
40
20
0
Control
D-AP5
D-AP5 + PPADS
Wash

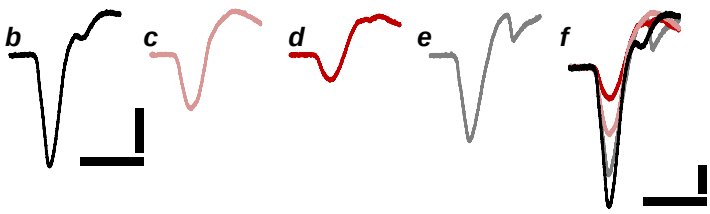
b
c
d
e
f

Ca

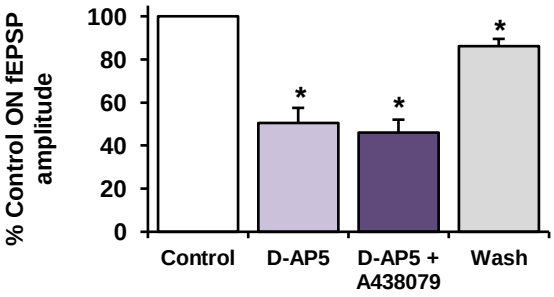
% Control ON fEPSP amplitude
100
80
60
40
20
0
Control
D-AP5
D-AP5 + A438079
Wash

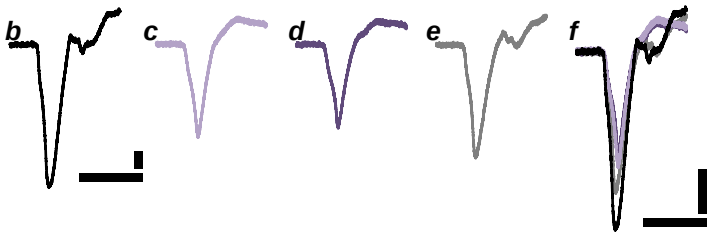
b
c
d
e
f

D

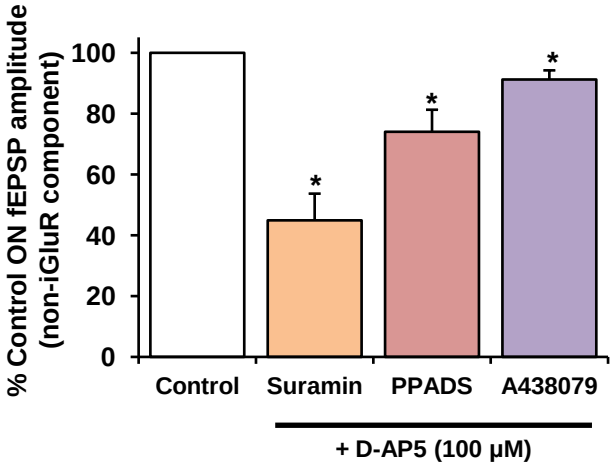
% Control ON fEPSP amplitude (non-iGluR component)
100
80
60
40
20
0
Control
Suramin
PPADS
A438079
+ D-AP5 (100 µM)

Figure 8.12 Actions of broad-spectrum P2XR antagonists suramin and PPADS, and the selective $P2X_7R$ antagonist A438079 on the ON fEPSP, in the presence of the NMDA receptor antagonist D-AP5. Compounds were applied in the presence of D-AP5 (100 μM). The residual component of the ON fEPSP was significantly reduced by suramin (***Aa***, 100 μM; *n* = 6), PPADS (***Ba***, 100 μM; *n* = 6) or A438079 (***Ca***, 10 μM; *n* = 6). Values are mean ± SEM percentage of pre-treatment control fEPSP peak amplitude. Representative traces show the effects of D-AP5 and P2XR antagonist co-application. For all, ***b***, control; ***c***, D-AP5; ***d***, respective P2XR antagonist; ***e***, wash; ***f***, merge. All scale bars: vertical, 10 μV; horizontal, 400 ms. ***D***, Summary histogram shows the effect of each compound on the residual fraction of the ON fEPSP, compared to pre-treatment control in the presence of D-AP5. The effects of suramin and PPADS suggest the involvement of other P2XRs in mediating the residual component. The A438079-induced reduction in the ON fEPSP indicates that $P2X_7Rs$ facilitate the ON fEPSP in the absence of ionotropic glutamate receptor (iGluR) activity. ns, not significant; *, $P < 0.05$, compared to control.

Chapter 9

Results: LPS and $P2X_7R$ Modulation of Microglia, and Dark-Adapted Visual Responses

In this series of experiments, the short-term effects of microglial activation on dark-adapted ERG and ON and OFF RGC fEPSP responses were explored and characterised. The bacterial endotoxin lipopolysaccharide (LPS) was used as the activator for microglia. LPS is a glycolipid, and a characteristic constituent of Gram negative bacterial cell walls (Park et al., 2009). The ability of LPS to potently stimulate the microglial innate immune response is well-established (Ferrari et al., 1997a, 2006; Sanz and Di Virgilio, 2000). The length and composition of the polysaccharide chains of LPS can vary with bacterial strain, although the hydrophobic lipid A component, the cytotoxic portion of LPS, is generally conserved (product information, LPS *E. coli* 055:B5, product no. L4524, Sigma-Aldrich, UK). The binding of LPS to its receptor TLR4 and associated proteins (Park et al., 2009), induces microglial activation, and the initiation of downstream intracellular signalling cascades, ultimately resulting in the upregulation and release of pro-inflammatory mediators and cytokines (see section 3.3.2). LPS is also known to stimulate ATP release from microglia within minutes of exposure (Sperlágh et al., 1998; Pascual et al., 2011).

Microglial morphology is closely related to its functional state. Thus, the effect of endogenous signals on retinal microglial morphology was first investigated, in order to determine whether microglial functional changes are plausible within the experimental time course. The LPS-induced changes in the kinetics of the ERG components and RGC fEPSPs were assessed over an application period of 15 min, and during the recovery phase approximately 10 to 15 min post-wash. Unless otherwise stated, all effect values were taken

from the final 120 sec of application, and are expressed as mean ± SEM. In order to delineate the involvement of $P2X_7Rs$ or pannexin-1 hemichannels in the LPS-mediated effect on visual responses, the antagonists A438079 and carbenoxolone were also used. Unless otherwise stated, all experiments were carried out in PMSTN perfusion medium to maintain consistent recording conditions between ERG and fEPSP experiments.

9.1 The effect of lipopolysaccharide and BzATP on retinal microglial morphology

Under control conditions, in PMSTN bathing medium, IBA-1^+ microglia were dispersed across the retinal wholemount, from the central optic nerve head to peripheral regions. The cells typically displayed a non-overlapping distribution, indicative of a relatively non-activated state, as shown in fig. 9.1. Cells within the mid-peripheral regions of the retina exhibited characteristic morphology of 'resting' microglia. Overall, cells with amoeboid morphology, which is suggestive of a typically activated microglial cell (Streit, 1999), were not observed. They had typically long, thin processes protruding from a relatively smaller and rounded soma, and had an average microglial process area of 2656.6 ± 106 µm (n = 110 cells, 6 retinae) (fig. 9.2A and 9.3).

Application of BzATP (300 µM; 10 min) induced an observable increase in branching of microglial processes, compared to control, as shown in fig. 9.2. The overall morphology of the microglia treated with BzATP remained unchanged, with cells maintaining a typically ramified state. In the presence of BzATP, microglial process area was on average 3152.8 ± 98 µm (n = 170 cells, 6 retinae), which was significantly increased, compared to control ($P < 0.05$) (fig. 9.3). In the presence of LPS (10 µg/ml; 15 min), microglial processes appeared less branched, compared to control, suggesting retraction of processes may have occurred (fig. 9.2C). Morphometric analysis of the cells treated with LPS revealed an average process

area of 2112.9 ± 111 µm (n = 108 cells, 6 retinae), which was markedly reduced in comparison to control conditions ($P < 0.05$) (fig. 9.3). These results demonstrated that microglia in the retina have the capability to undergo rapid morphological alterations in response to $P2X_7R$ or TLR4 activation. However, BzATP and LPS elicited opposite effects on microglia, suggesting transitions to early, but differential states of microglial activation.

9.2 The effect of lipopolysaccharide on the dark-adapted ERG a-wave

LPS (10 µg/ml) did not seem to modulate the a-wave slope, following a 15 min application of the bacterial component (91.2 ± 10% of control; $P > 0.05$, n = 7), as shown in fig. 9.4. Furthermore, there was no overall effect on the a-wave with vehicle application, compared to control (107.4 ± 6% of control, $P > 0.05$, n = 6), and no significant difference in the a-wave slope between LPS and vehicle treatment ($P > 0.05$) (fig. 9.4A). Neither LPS nor vehicle application affected the implicit time of the a-wave maximum amplitude, compared to values prior to treatment ($P > 0.05$ for both). These results suggest that LPS had no overall effect on the photoreceptor-derived a-wave, at the given concentration.

9.3 The effect of lipopolysaccharide alone, and in the presence of A438079, on the scotopic ERG b-wave

LPS (10 µg/ml) induced a significant reduction in the b-wave amplitude to 82.2 ± 4% of control ($P < 0.05$, n = 7), as illustrated in fig. 9.5. The suppressive effect of LPS on the b-wave amplitude developed relatively slowly and progressed throughout the duration of application (fig. 9.5B). Following washout of the bacterial component, the reduction in the b-wave amplitude was not reversible (87.9 2 ± 4% of control, $P > 0.05$), although a transient period of recovery within 2 to 5 min following washout was observed in some experiments. LPS significantly delayed the implicit time of the b-wave amplitude, an effect which remained

after washout (fig. 9.5C). Application of vehicle had no effect on the b-wave amplitude or implicit time (fig. 9.5A and C).

The effect of LPS on the ERG b-wave in the presence of the $P2X_7R$ antagonist A438079 (10 µM), was also investigated. Co-application of A438079 did not reduce the effect of LPS on the b-wave amplitude. In the presence of the antagonist, changes to the b-wave amplitude mediated by LPS appeared to follow a similar temporal profile to those observed with LPS alone (fig. 9.5B). Furthermore, there was no significant difference between the LPS-mediated suppression of the b-wave in the absence and presence of A438079 ($P > 0.05$). The LPS-induced delay in the b-wave amplitude was not apparent in the presence of A438079 during the application of the bacterial component (fig. 9.5C). Overall, these results suggest that post-photoreceptor activity is modulated by LPS-activated glial cells. At this stage, the involvement of $P2X_7Rs$ is uncertain, and could implicate a role for third-order neurons in modulating b-wave kinetics in the presence of LPS.

9.4 The effect of lipopolysaccharide alone, and in the presence of A438079 or carbenoxolone, on the ON and OFF retinal ganglion cell fEPSPs

The ON and OFF RGC fEPSPs were significantly reduced with a 15 min application of LPS (10 µg/ml), to 85.5 ± 3% of control ($P < 0.05$, n = 10) and 65.1 ± 6% of control ($P < 0.05$, n = 8), respectively (figs. 9.6A and 9.7A). The time courses for both ON and OFF fEPSPs (fig. 9.6B and 9.7B) show that LPS took effect within 6-8 min, on both responses. Furthermore, no effect was elicited by vehicle application, on the ON or OFF fEPSPs ($P > 0.05$ vs. pre-treatment control, n = 7; $P < 0.05$ vs. LPS for both) (fig. 9.6A and 9.7A). In the presence of the $P2X_7R$ antagonist, A438079 (10 µM), small reductions in both the ON and OFF fEPSPs to 96.0 ± 2% and 95.2 ± 2% of control, respectively were observed, although these were not

statistically significant, compared to control values, pre-LPS ($P > 0.05$, n = 7 and 6, respectively). The effects of LPS on both the ON and OFF fEPSPs were markedly attenuated with A438079 ($P < 0.05$ vs. LPS alone for both). These results suggested the LPS-mediated release of endogenous ATP either through $P2X_7Rs$ themselves, or through an alternative pathway.

To investigate whether endogenous agonist was released through pannexin-1 hemichannels, the panx-1 inhibitor, carbenoxolone (10 µM) was applied. CBX alone caused no significant effect on baseline ON and OFF fEPSPs ($P > 0.05$, n = 6 for both). This confirmed that CBX had no overall effect on retinal network activity. The suppressive effect of LPS on the ON fEPSP in the presence of CBX was comparable to its effect when applied alone as shown in fig. 9.6. Conversely, CBX apparently reduced the effect of LPS on the OFF fEPSP (fig. 9.7), indicating that pannexin-1 hemichannel release of ATP may have occurred from a sub-population of neurons within the OFF pathway.

Chapter 9 Figures

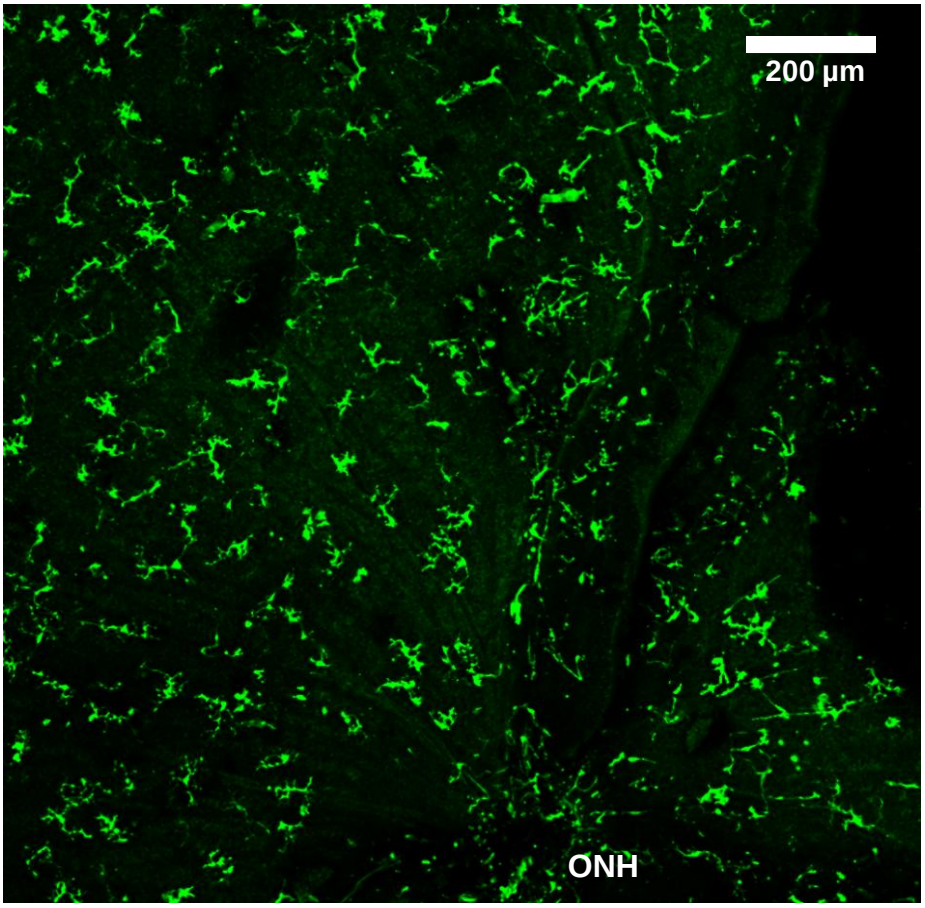

Figure 9.1 Distribution of microglia across the mid-peripheral region of the mouse retinal wholemount, under control conditions. The maximum intensity projection image (mag. x5w) illustrates that IBA-1^{+} microglia were widely dispersed throughout the retinal quadrants. Retinae were in the presence of a modified Krebs' medium containing picrotoxin, strychnine, tetrodotoxin, and with extracellular magnesium ions removed from the perfusate. Under these control conditions, microglia within the mid-peripheral region typically exhibited a non-overlapping distribution, characteristic of a 'resting' state. For consistency between treatment groups, cells around the optic nerve head (ONH) and far-peripheral regions (~ 500 µm from the edges) were excluded from further analysis.

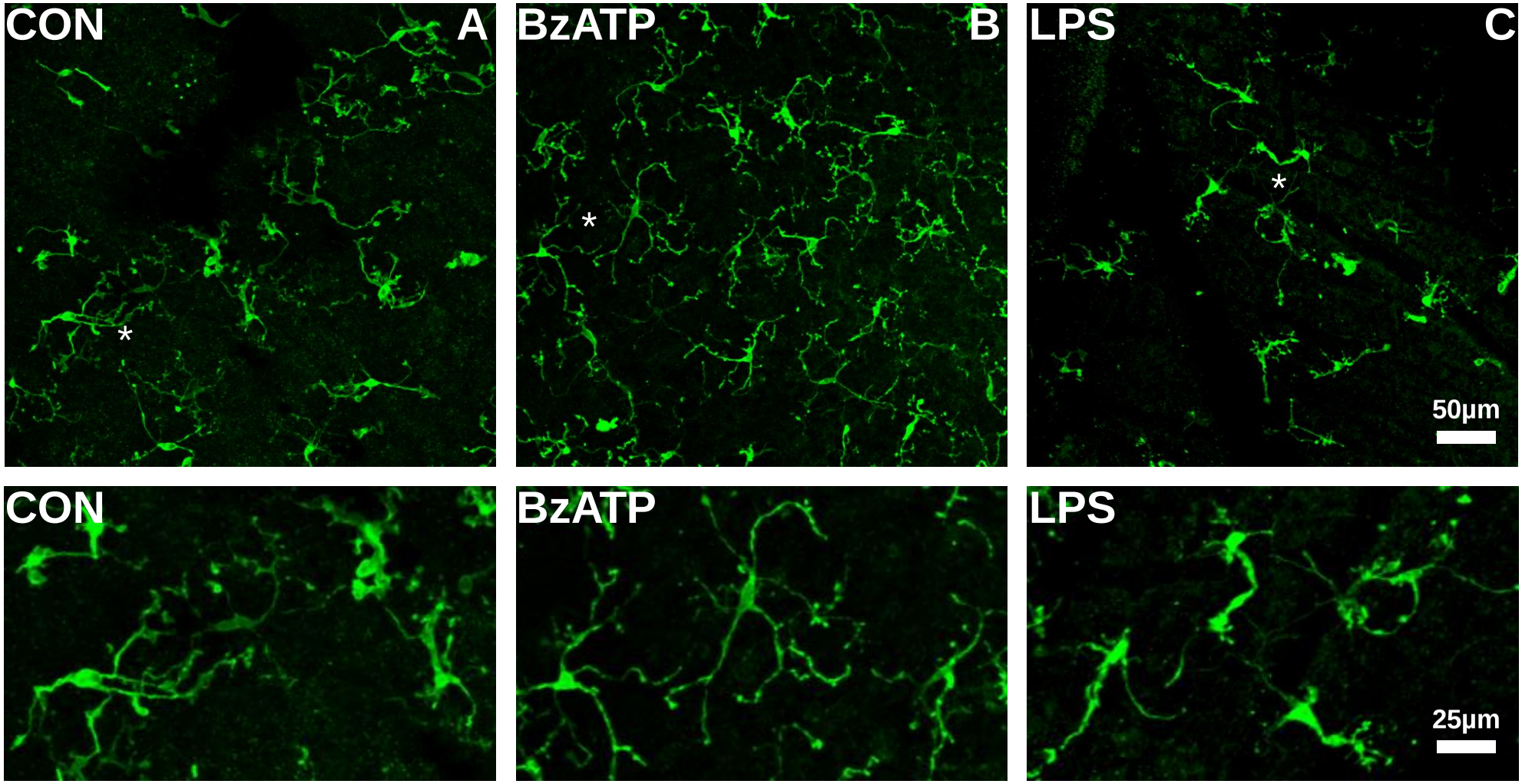

Figure 9.2 Effects of BzATP or LPS on retinal microglial morphology. Images are maximum intensity projections of z-stacks (mag. x20W, top row) acquired from the mid-peripheral regions of retinal wholemounts. Bottom row, magnified (x2) regions from top image (*). ***A***, Under control conditions (in PMSTN medium), microglia (IBA-1^{+}) displayed distinct cell bodies with ramified morphology and long, thin processes, typical of a 'resting' state. Some branching at the ends of processes was also apparent, but overlapping of processes was minimal. ***B***, Top image, in the presence of BzATP (300 µM; 10 min), an observable increase in branching of microglia was apparent, compared to control. However, microglia maintained their characteristic ramified morphology (bottom) and were not generally found to be overlapping. ***C***, In the presence of LPS (10 µg/ml; 15 min), microglial processes appeared considerably shorter, compared to control, seeming to cover a smaller area. Overall, the cell bodies of microglia appeared consistent across all conditions tested.

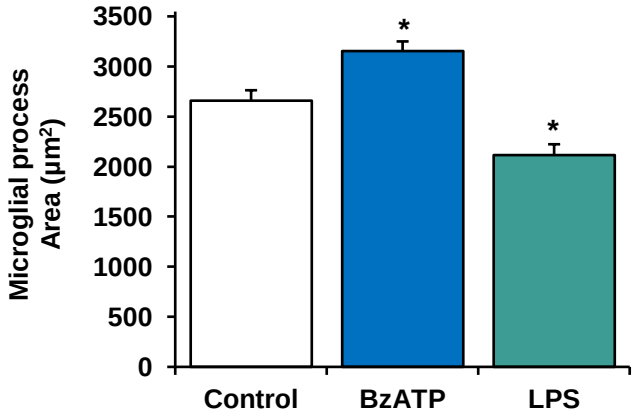

Figure 9.3 Actions of BzATP or LPS on retinal microglial process area. Values are mean ± SEM process area. IBA-1$^+$ microglial process area was measured from maximum intensity projection images of z-stacks. Control, *n* = 110 cells, 6 retinae; BzATP, *n* = 170, 6 retinae; LPS, *n* = 108, 6 retinae). With a short-term (10 min) application of BzATP (300 µM), microglial process area was significantly increased, compared to control ($P < 0.05$). Conversely, in the presence of LPS (10 µg/ml; 15 min), microglial process area was markedly reduced, compared to control ($P < 0.05$). Thus, BzATP and LPS induce rapid alterations to microglial morphology, suggesting that they stimulate a transition to differential states of 'alertness' or early stages of activation.

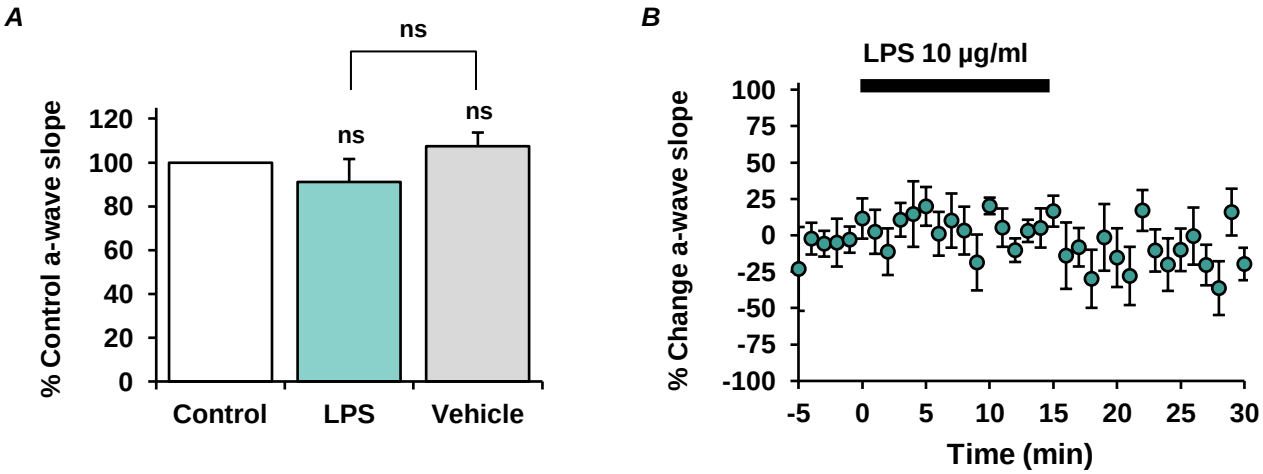

C

	LPS	Vehicle
Implicit time (change from baseline; ms)	+ 2.1 ± 1	+ 1.3 ± 1

Figure 9.4 The effect of lipopolysaccharide on the ERG a-wave. All values are mean ± SEM; *n* = 7, LPS; *n* = 6, vehicle. ***A***, The a-wave slope was not significantly affected with vehicle application or a 15 min bath-application of LPS (10 µg/ml) (*P* > 0.05, for both, compared to pre-treatment control). Comparison between LPS and vehicle indicates no overall difference in their effect on the a-wave, between LPS and vehicle application (*P* > 0.05). ***B***, Time course plot shows mean ± SEM percentage change in the a-wave slope. No overall effect on the a-wave was observed in the presence of LPS. ***C***, Change from baseline implicit time values. Comparison between LPS and vehicle show no significant difference (*P* > 0.05).

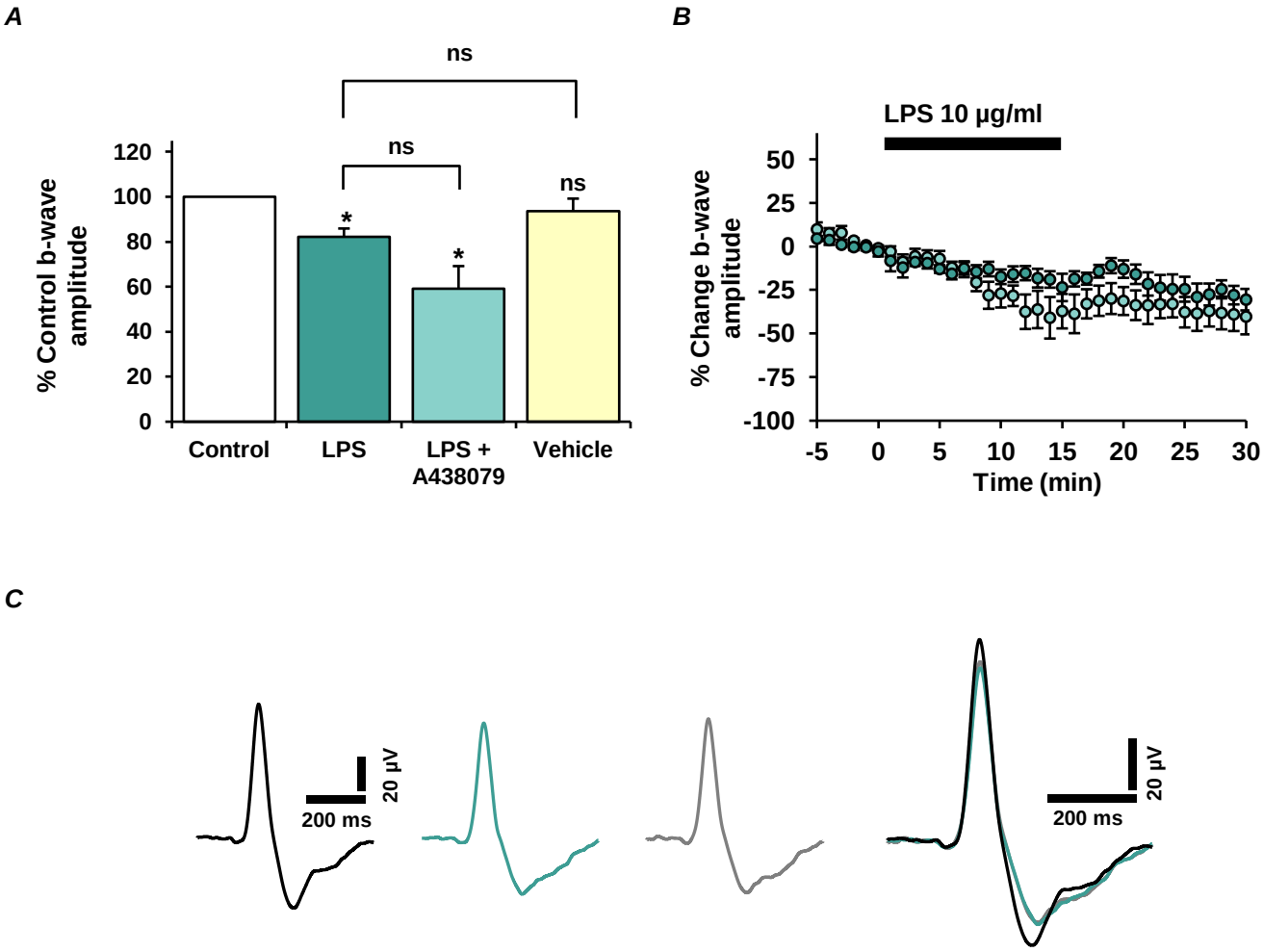

	LPS	A438079 + LPS	Vehicle
Implicit time (change from baseline; ms)	+ 3.2 ± 2	+ 2.7 ± 0	+ 1.9 ± 1

Figure 9.5 The effect of lipopolysaccharide alone, and in the presence of the $P2X_7R$ antagonist A438079, on the ERG b-wave. All values are mean ± SEM; *n* = 7, LPS; *n* = 6, vehicle, *n* = 6, LPS + A438079. ***A***, The b-wave amplitude was significantly reduced with direct application (15 min) of LPS (10 µg/ml) alone, and in the presence of A438079 (*P* < 0.05, for both, compared to pre-treatment control). Furthermore, there was no overall difference in the effect of LPS on the b-wave amplitude in the absence and presence of A438079 (*P* > 0.05). Application of vehicle had no significant effect on the b-wave amplitude (P > 0.05, compared to pre-treatment control), but was not considered statistically significant from the effect of LPS (*P* > 0.05). ***B***, Time course plot shows the percentage change in b-wave amplitude with LPS alone, and co-applied with A438079. The $P2X_7R$ antagonist did not affect the LPS-mediated suppression of the b-wave. ***C***, Representative traces illustrate the LPS-induced reduction in the b-wave amplitude, and no overall effect on the a-wave slope (see Fig. 9.4). ***a***, control; ***b***, LPS; ***c***, wash; ***d***, merge. ***D***, Change from baseline implicit time values. Comparison between LPS and LPS + A438079 or vehicle (*P* > 0.05) suggested no significant differences in implicit time alterations across groups.

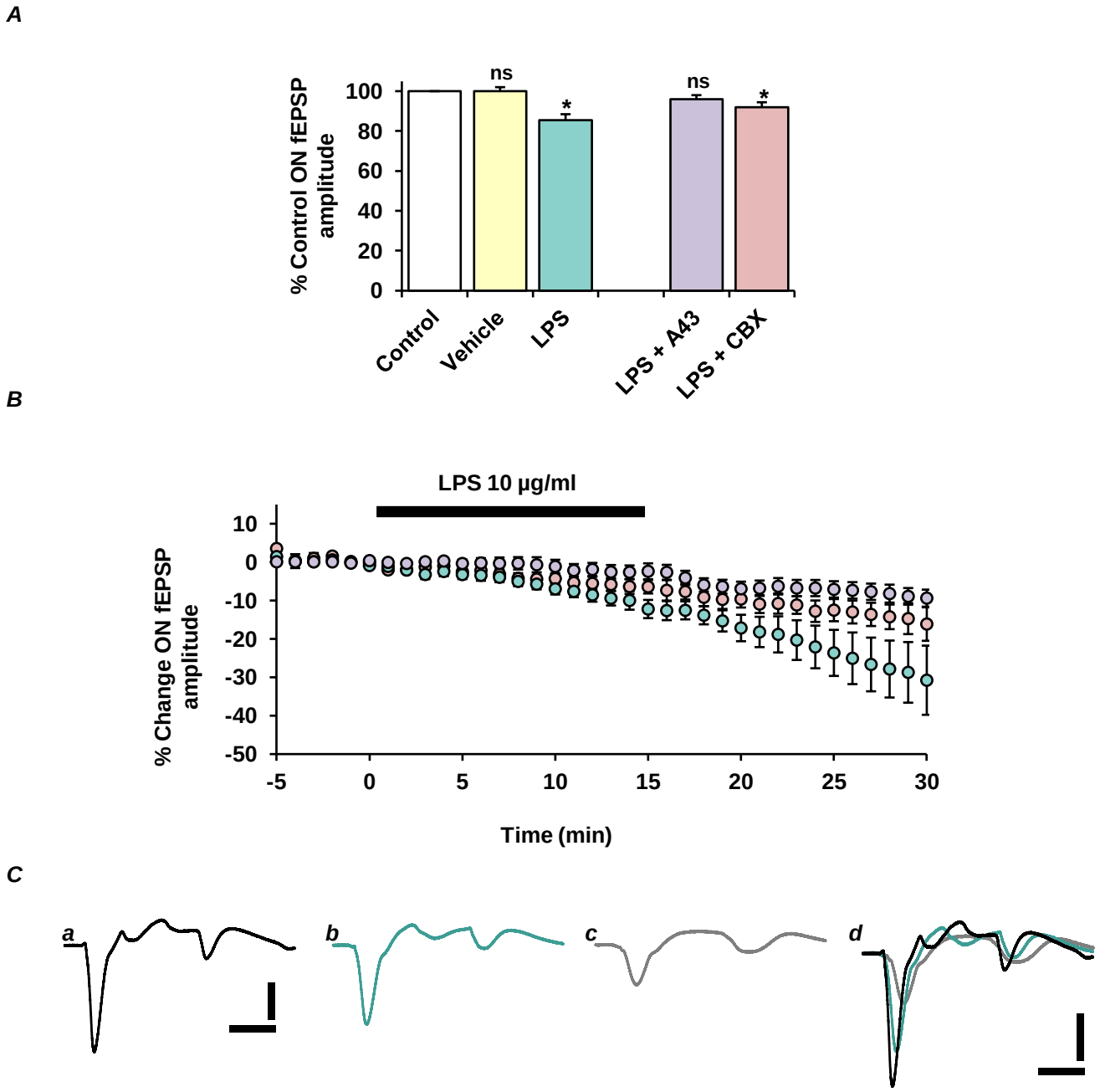

Figure 9.6 Actions of lipopolysaccharide alone, and in the presence of the $P2X_7R$ antagonist A438079 or the pannexin-1 hemichannel blocker carbenoxolone, on the ON RGC fEPSP. All values are mean ± SEM; vehicle, *n* = 7; LPS, *n* = 10; LPS + A438079, *n* = 7; LPS + CBX, *n* = 6. ***A***, ns, not significant; *, $P < 0.05$, compared to pre-treatment control. LPS (10 µg/ml; 15 min) induced a significant reduction in the ON fEPSP amplitude, compared to pre-treatment control. Comparisons between groups suggest that the LPS-mediated effect was attenuated in the presence of A438079 (10 µM; $P < 0.05$), but not with carbenoxolone (CBX; 10 µM; $P > 0.05$). Vehicle application had no overall effect on the ON fEPSP amplitude. ***B***, Time course plot shows percentage change in the ON fEPSP amplitude with LPS alone and in the presence of the antagonists. Although there is no overall difference during LPS application, CBX appears to show a slight reduction in the effect of LPS during the washout phase. Inhibition of the LPS-mediated suppression of the ON fEPSP with A438079 is more apparent following washout. ***C***, Representative traces (120 sec averages) illustrate the effect of LPS on the ON and OFF (see Fig. 9.7) RGC fEPSPs. ***a***, control; ***b***, LPS; ***c***, wash; ***d***, merge. All scale bars: vertical, 20 µV; Horizontal, 400 ms.

A

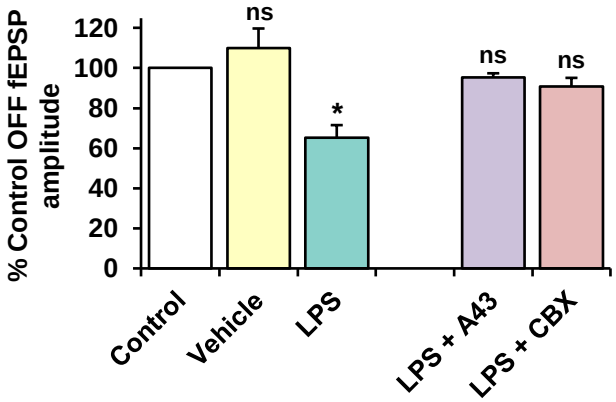

B

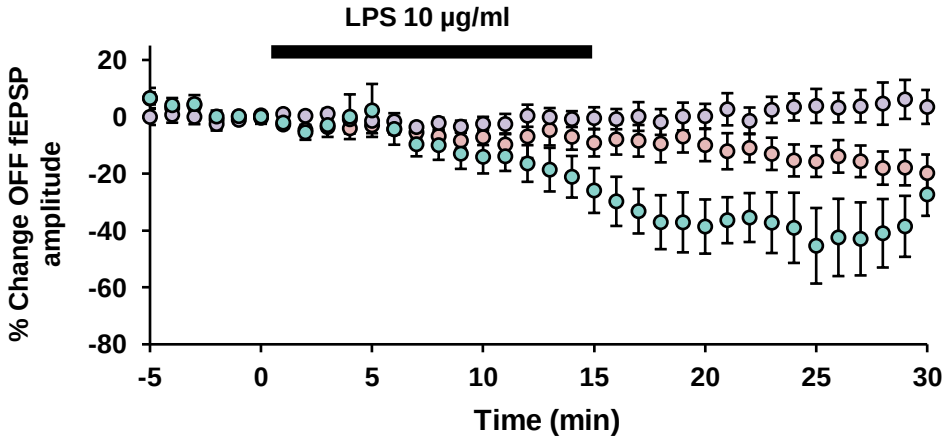

Figure 9.7 Actions of lipopolysaccharide alone, and in the presence of the $P2X_7R$ antagonist A438079 or the pannexin-1 hemichannel blocker carbenoxolone, on the OFF RGC fEPSP. All values are mean ± SEM; vehicle, n = 7; LPS, n = 7; LPS + A438079, n = 6; LPS + CBX, n = 6. ***A***, ns, not significant; *, $P < 0.05$, compared to pre-treatment control. LPS (10 µg/ml; 15 min) significantly reduced the OFF fEPSP amplitude, compared to pre-treatment control. Comparisons between groups suggest that the LPS-mediated effect was attenuated in the presence of A438079 (10 µM; $P < 0.05$), or carbenoxolone (CBX; 10 µM; $P < 0.05$). Vehicle application had no overall effect on the OFF fEPSP amplitude. ***B***, Time course plot shows the percentage change in the OFF fEPSP amplitude with LPS alone and in the presence of the antagonists. A progressive and marked suppression of the OFF fEPSP induced by LPS was considerably attenuated in the presence of either antagonist, with comparable potency.

Chapter 10

Discussion

The investigations presented in this thesis sought to verify and characterise a role for $P2X_7Rs$ in modulating rod photoreceptor-mediated outer and inner retinal function, using an *ex vivo* mouse retinal wholemount preparation. Furthermore, the involvement of $P2X_7Rs$ in the putative microglial-mediated modulation of signal transmission in the retina was also explored.

The dark-adapted, light-evoked electroretinogram (ERG), and excitatory ON retinal ganglion cell (RGC) fEPSP responses were identified as predominantly glutamatergic, mediated via the 'classic' rod photoreceptor – rod-ON bipolar cell pathway. It was shown that $P2X_7R$ activation directly modulates photoreceptor, ON bipolar cell and ON RGC function, but not OFF RGC function. The differential spatiotemporal effects mediated by this receptor indicate that $P2X_7R$ activation modulates inner retinal function independently of its effects in the outer retina. In addition, it was demonstrated that acute application of the microglial-activating bacterial component, lipopolysaccharide (LPS), modulates inner retinal function, possibly through a $P2X_7R$-associated mechanism of endogenous ATP release. Furthermore, $P2X_7Rs$ and other P2XR subtypes were found to contribute to an excitatory residual component of the ON RGC fEPSP, which was not mediated through ionotropic glutamate receptors.

10.1 Dark-adapted, extracellular electroretinogram and retinal ganglion cell responses are predominantly mediated by the rod photoreceptor – ON bipolar cell pathway

The mouse retina largely consists of rods, with cones comprising ~3% of the photoreceptor mosaic (Jeon et al., 1998). Thus, depending on the state of dark or light adaptation, retinal synaptic responses can essentially be driven by 'mixed' rod- and cone-mediated inputs (Rosolen et al., 2008). Dark-adapted recording conditions and the use of a dim light stimulus ensured that rod-driven pathways were dominant in these experiments (Peachey and Ball, 2003).

10.1.1 Electroretinogram characterisation

Changes to photoreceptor function were determined through analysis of the negative ERG a-wave, which under dark-adapted conditions, is recognised to be predominantly driven by rod photoreceptors (Lamb and Pugh, 2006). The light intensity-response relationship of the a-wave (fig. 7.2Aa) shows that in physiological medium, the a-wave saturated at -0.62 log cd.s/m^2, an intensity well within the scotopic to mesopic range. The a-wave appeared to be enhanced when recorded in the pharmacologically modified perfusion medium, possibly reflecting release of inhibition of rods by horizontal cells, due to the addition of the $GABA_{A/C}$ receptor antagonist picrotoxin. However, the specific role of horizontal cells in providing inhibitory inputs to rods is disputed, as receptive field surround properties in the retina are diminished under dark-adapted conditions. In support of this notion, mammalian rod-ON bipolar cells have not shown to express surround responses (Bloomfield and Xin, 2000). Alternatively, the observed enhancement of the a-wave could also be due to an increase in the Na^+-driven rod dark current, promoted by a reduction in extracellular magnesium in the perfusate. Essentially, normal photoreceptor function was not disrupted across the range of light intensities, when comparing responses between the different bathing solutions, as supported by the comparable stimulus intensity-response data.

The relatively large-amplitude, positive ERG b-wave is classically known to reflect ON bipolar cell activity (Massey et al., 1983; Stockton and Slaughter, 1989). Connected directly in series with its photoreceptor input (Boycott and Kolb, 1973), this relationship is supported by its stimulus intensity-response function, where the b-wave amplitude exhibits potentiation with increasing light intensity. Considering that in the outer retina, the rod photoreceptor signal is exclusively transduced to rod-ON bipolar cells, it is reasonable to conclude that this is the dominant pathway driving the ERG responses. Although the b-wave appears delayed with the change in perfusion medium, overall function of the rod-ON bipolar cells is not affected, as supported by the stimulus intensity-response data and the preservation of the waveform. The increase in the implicit time of the b-wave is probably due to the addition of TTX, picrotoxin and strychnine, which are likely to block regulation of presynaptic bipolar cell terminals in the inner retina, by third order neurons (Dong and Hare, 2000, 2002). The ON pathway dominance of the b-wave is further ensured with the addition of NBQX in the modified perfusion medium, which blocks any possible contribution to the b-wave from OFF bipolar cells, as they are normally depolarised by AMPA/KA receptors (Euler et al., 1996). This is confirmed by the substantial sensitivity of the b-wave to the mGluR6 agonist L-AP4, which selectively and potently abolished post-photoreceptor responses of the ON pathway, previously demonstrated in classic studies (Massey et al., 1983; Slaughter and Miller, 1983; Stockton and Slaughter, 1989).

Although a selective agonist for group III mGluRs ($mGluR_{4/6/7/8}$), L-AP4 does not show selectivity at any particular subtype within the group, all of which have been localised within the retina (Brandstätter et al., 1998). Therefore, it is possible that the agonist may bind to an alternative group III subtype. In particular, mGluR8 has been shown to act as an autoreceptor at photoreceptor terminals. Its activation leads to the closure of L-type calcium channels, decreasing intracellular calcium within photoreceptors and subsequently reducing glutamate release (Koulen, 1999). This would result in a sign-conserving effect on the ON-

bipolar cell, rather than the hyperpolarisation seen with mGluR6 activation (a sign-inverting effect). The mGluR4 and mGluR7 subtypes, which are primarily expressed in the inner retinal layers, are unlikely to have a direct and such a pronounced effect on the outer retinal, ON-bipolar cell response (Brandstätter et al., 1998). Therefore, in the present study, it is most probable that L-AP4 exerts its effects through the activation of postsynaptic mGluR6 in ON-bipolar cells.All experiments were carried out using stimulus intensities that elicited sub-maximal responses, typically within the range of -2 to -1 log cd.s/m^2. Additional evidence for rod pathway dominance of the ERG responses recorded within this luminance range comes from the characterisation of the oscillatory potentials. Digital filtering of the ERG and corresponding analysis of the frequency spectrum identified that the dominant frequency of the oscillatory potentials peaked at approximately 100 Hz (fig. 6.2) when evoked by a stimulus intensity within the given range. This frequency is characteristic of rod-driven inputs under dark-adapted conditions, which is higher than that of cone-derived oscillatory potentials in the mouse ERG (~ 75 Hz) (Asi and Perlman, 1992; Lei et al., 2006; Zhang et al., 2007). Thus, several lines of evidence support the notion that the ERG responses recorded during the course of this study were predominantly driven by the rod photoreceptor – ON-bipolar cell pathway.

10.1.2 Retinal ganglion cell fEPSP characterisation

The ON and OFF retinal ganglion cell fEPSPs recorded in this study displayed characteristic properties of dark-adapted retinal ganglion cells. Dark-adapted RGC fEPSP responses are typically enhanced with the isolation of the NMDA-R component of the excitatory responses (fig. 7.5). Across all light intensities tested, the ON fEPSP was consistently larger, indicating ON pathway dominance of the responses. Furthermore, the ON fEPSP amplitude potentiated with increasing luminance, exhibiting similar properties to the ERG a- and b-waves, whereas the OFF fEPSP was more prominent at lower luminances.

The removal of extracellular magnesium ions from the perfusion medium as well as the addition of a combination of compounds enhanced NMDA-R activity (Yu and Miller, 1996). Voltage-gated sodium channel-mediated spiking activity of RGCs was blocked with TTX, whilst AMPA/KA, $GABA_{A/C}$ and glycine receptor functions were abolished with NBQX, picrotoxin and strychnine, respectively. The resultant suppression of amacrine cell-mediated GABAergic inhibitory surround ensured the subsequent enlargement of RGC receptive field centres. The dominance of the rod – rod-bipolar cell – AII cell pathway in eliciting the ON RGC fEPSP was further confirmed with its sensitivity to L-AP4, which suppressed rod-ON BC signal transmission. Furthermore, suppression of the ON and OFF RGC fEPSPs with D-AP5 revealed a predominant NMDA-R component of both responses.

The presence of NBQX and strychnine to the medium did not abolish the OFF pathway, and a residual OFF fEPSP persisted. This response was not sensitive to L-AP4 either, altogether confirming that it was not mediated via the rod – rod-ON BC – AII pathway. Thus, it is unlikely that the OFF fEPSP is generated directly from outer retinal input. Furthermore, a rod pathway involving connexin-mediated coupling to cones and subsequent transmission to OFF cone BCs is also ruled out due to the blockade of cone – OFF cone BC transmission with NBQX. Thus, it is suggested that the OFF fEPSP originates from the inner retina, rather than generated from a direct outer retinal drive.

Indeed, recent evidence suggests that connexin-mediated electrical coupling between ganglion cells coordinate concerted activity between homologous cell types (Bloomfield and Völgyi, 2009). However, it is unclear whether ON and OFF cells are directly coupled, although connexin-mediated modulation of ON and OFF pathways has shown to occur

through glycinergic AII amacrine cells (Manookin et al., 2008; Liang and Freed, 2010). Light intensity-response data indicate that the OFF fEPSP generated under these conditions is maximally responsive with lower intensity stimuli, as the responses appear to saturate when approaching the higher end of the tested intensity scale. Thus, it could be suggested that if direct coupling between ON and OFF ganglion cells is indeed the case, it may serve to extend the operating range of the OFF pathway at lower light intensities.

10.2 $P2X_7Rs$ selectively modulate the ON pathway in the outer and inner retina

The present study has demonstrated that neuronal function in both the outer and inner mouse retina is considerably altered by $P2X_7R$ activation, under dark-adapted conditions. Furthermore, the actions of $P2X_7Rs$ are apparently selective for the rod-mediated ON pathway, as supported by several lines of evidence. It is also suggested that $P2X_7R$-modulation of visual responses occurs through independent mechanisms, at different levels of the rod pathway. These findings are not unexpected, as $P2X_7Rs$ are expressed on photoreceptors, horizontal, amacrine and retinal ganglion cells, and on non-neuronal cells including microglia and vascular endothelial cells within the retina. As of yet, $P2X_7Rs$ have not been localised to bipolar cells.

10.2.1 Modulation of outer retinal function

$P2X_7R$-mediated alterations to synaptic transmission from rod photoreceptors to rod-ON bipolar cells were assessed using the dark-adapted ERG. Under physiological conditions, $P2X_7R$ activation by its agonist, BzATP potentiated the a-wave, with a concomitant reduction in the b-wave. This finding is consistent with previous work in the rat, *in vivo* (Puthussery et al., 2006). BzATP also delayed the time to peak of the a-wave, which could indicate a reduction in photosensitivity of the rods (Hood and Birch, 1997). However, in the study by

Puthussery et al. (2006), computational extraction of the sensitivity parameter of the a-wave leading edge, indicated no change in photoreceptor sensitivity as a result of $P2X_7R$ activation. Thus, the change in implicit time of the a-wave in this investigation could instead be attributed to a possible contamination of the BzATP-induced effect on the b-wave.

The contradictory effects of BzATP on the photoreceptor and bipolar cell response components could be explained by a mechanism associated with a change in the dark current of the photoreceptors. Depolarisation of the photoreceptor terminal, induced by $P2X_7R$ activation would subsequently potentiate the a-wave during photostimulation, due to a greater change in the photoreceptor dark current, as has been suggested previously (Puthussery et al., 2006). Concurrently, facilitation of the photoreceptor dark current would increase the rate of glutamate release in the dark, thus eliciting a smaller light-induced depolarisation of the ON-BCs. Stable calcium influx through L-type channels is imperative for the sustained release of glutamate from rod terminals, in darkness (Okawa and Sampath, 2007). A $P2X_7R$-dependent rise in intracellular calcium has previously shown to directly stimulate vesicular glutamate release from hippocampal and cortical presynaptic terminals (Sperlágh et al., 2002; Alloisio et al., 2008; Marín-García et al., 2008). The present findings suggest that $P2X_7R$ activation may modulate ERG responses through a similar calcium-dependent mechanism, although direct $P2X_7R$ modulation of ribbon synapses has not yet been shown.

$P2X_7R$ activity is enhanced in the absence of extracellular magnesium (Surprenant et al., 1996; Virginio et al., 1997). In the present study, removal of magnesium ions from the perfusate reversed the effect of $P2X_7R$ activation on the a-wave, instead inducing a marked reduction in the photoreceptor response. This could suggest a dual function for $P2X_7R$ modulation of photoreceptor activity, whereby an ionic imbalance in the extracellular

environment could promote the switch to a detrimental function for $P2X_7Rs$. Without extracellular magnesium, the b-wave was suppressed by BzATP, to a similar magnitude, when compared to the effect in the presence of the divalent cation. Contrary to the observed effect in physiological perfusate, the BzATP-mediated suppression of the b-wave was not reversible in the absence of magnesium. The differential temporal profiles of the effect of BzATP on the a- and b-waves highlight independent sites of modulation by $P2X_7Rs$ in both the inner and outer retina.

In the present study, the suppressive effect of $P2X_7R$ activation on the photoreceptor response was enhanced in the presence of blockers of $GABA_{A/C}$, glycine and AMPA/KA receptors, and of voltage-gated sodium channels. It has previously been suggested that $P2X_7R$-associated modulation of the mouse ERG may be due to alterations in horizontal and amacrine cell feedback (Vessey and Fletcher, 2012). However, the underlying mechanism of modulation of the photoreceptor response may not be associated with the release of inhibitory inputs to the rod terminals under dark-adapted conditions (Bloomfield and Xin, 2000). Indeed, the study by Vessey and Fletcher (2012) found that the ERG a-wave was unaltered, whereas the b-wave was markedly potentiated in a $P2X_7R$-knockout mouse model. In the present investigation, there was no overall difference in the BzATP-induced reduction in the b-wave, between responses recorded in the absence of magnesium alone, and with the addition of pharmacological blockers of inhibitory neurotransmission. This indicates that $P2X_7R$-mediated modulation of the ON BCs is not due to an effect on inhibitory feedback at the ON BC terminal in the inner retina. Since BCs do not themselves express $P2X_7Rs$, these results could reflect a possible modulation of both ERG components by non-neuronal cells during $P2X_7R$ stimulation.

The involvement of $P2X_7R$-mediated modulation of the a-wave was confirmed with the selective antagonist A438079, which abolished the effect of $P2X_7R$ on the photoreceptor response. However, a residual effect of $P2X_7R$ modulation remained on the bipolar cell response in the presence of the antagonist. This supports the notion of an additional mechanism, whereby a localised release of endogenous ATP in the inner retinal layers could act to enhance the $P2X_7R$-mediated effect on the ON BCs, and not at the photoreceptor terminals. $P2X_7Rs$ are known to drive ATP release which then acts cell-autonomously. Indeed, $P2X_7R$-mediated, non-vesicular release of ATP has been shown in retinal ganglion cells (Xia et al., 2012).

These results strongly suggest a direct role for $P2X_7Rs$ in photoreceptors in modulating outer retinal processing, and is supported by studies that have shown $P2X_7R$ immunoreactivity at ribbon synapses within the rod spherule, in the rodent retina (Puthussery and Fletcher, 2004; Puthussery et al., 2006; Vessey and Fletcher, 2012). However, $P2X_7R$ modulation of photoreceptor function through alternative mechanisms cannot be ruled out. The $P2X_7R$ expression profile in the human retina has shown no evidence of immunoreactivity in photoreceptors (Niyadurupola et al., 2013), and may instead support the notion that $P2X_7Rs$ may modulate photoreceptor function through its expression in retinal pigment epithelial cells. Indeed, RPE cells are sources of ATP, which can be released in response to hyperosmotic stress (Eldred et al., 2003), through various mechanisms including ATP-triggered secondary ATP release, CFTR-dependent ATP efflux as well as vesicular ATP secretion (Reigada and Mitchell, 2005; Reigada et al., 2005). This autostimulatory ATP release, may be driven through $P2X_7R$-associated panx-1 hemichannels (Reigada et al., 2008). Furthermore, RPE cells have demonstrated the presence of ectonucleotidases (Eldred et al., 2003; Reigada et al., 2005), which may rapidly degrade ATP into its constituents, in order to activate other P2 and adenosine receptors in cells of the outer retina.

10.2.2 Modulation of inner retinal function

A selective effect of $P2X_7R$ activation on the ON pathway was apparent, as BzATP suppressed the ON fEPSP in a concentration-related manner, but had no overall effect on the OFF fEPSP. The involvement of $P2X_7Rs$ in modulating the ON fEPSP was supported by the partially attenuated effect of BzATP in the presence of the selective $P2X_7R$ antagonists A438079, A804598 or AF27139. With each antagonist, a residual effect of BzATP on the ON fEPSP remained, which could be explained by a lack of potency of these compounds for blocking $P2X_7R$-mediated effects in the inner retinal layers. This is supported by an almost complete attenuation of the BzATP-mediated reduction in the ERG a-wave, but only a partial reduction in the agonist-induced effect on the b-wave, in the presence of A438079.

Compared to the more classically used $P2X_7R$ antagonists, A438079 and A804598 are generally considered amongst the most potent suppressors of mouse $P2X_7R$ function, of those commercially available (Donnelly-Roberts et al., 2009a, 2009b). AF27139 is not yet commercially available, and A804598 has not been widely tested, but both have shown to potently block $P2X_7R$-mediated cytokine release in cell culture preparations, across species (Donnelly-Roberts et al., 2009b; Lundbeck, DK). The less novel A438079 was chosen for this study as it has demonstrated potent suppression of $P2X_7R$ function in models of chronic pain, microglial neuroinflammation and neurodegenerative disorders in the spinal cord and brain (Donnelly-Roberts and Jarvis, 2007; McGaraughty et al., 2007; Clark et al., 2010; Marcellino et al., 2010; Teixeira et al., 2010). The use of A438079 in *ex vivo* retinal preparations has not previously been reported, although the compound has proved potent in suppressing swelling-induced damage to isolated retinal ganglion cells (Xia et al., 2012).

Agonist-induced $P2X_7R$ activation is known to elicit further release of ATP, through $P2X_7Rs$ themselves. Thus, the lack of potency of these compounds in suppressing the BzATP-mediated reduction in ON RGC responses could be due to the stimulated release of endogenous ATP within the inner retinal layers. $P2X_7Rs$ are expressed on amacrine, ganglion and microglial cells in the inner mouse retina, and are all therefore potential sources of ATP-mediated ATP release. In mammalian species, in the absence of pathology or inflammation, functional $P2X_7Rs$ have only been found on human Müller cells (Wurm et al., 2011). However, it has been shown in the rat retina that light-evoked ATP release from ganglion cells increases Müller cell Ca^{2+} transients through activation of glial P2YRs. This in turn mediates release of glial ATP, which is rapidly hydrolysed into adenosine; in turn hyperpolarising ganglion cells through the activation of A1 receptors (Newman, 2005).

It has been proposed that the BzATP-mediated suppression of excitatory responses in the rodent hippocampus and brainstem was attributed to its breakdown product Bz-adenosine and subsequent activation of adenosine receptors (Kukley et al., 2004; Tautenhahn et al., 2012). However, in the present study, the possible contribution of A1 receptors to the BzATP-mediated reduction of the ON fEPSP was ruled out. Adenosine produced a dose-related potentiation in the ON fEPSP, an effect which followed a differential temporal profile to that seen for the effect of BzATP. Furthermore, adenosine also elicited a dose-related and sustained effect on the OFF fEPSP. This suggests that adenosine facilitates, possibly through A3 receptors, both the ON and OFF pathways whereas $P2X_7Rs$ appear to selectively reduce neuronal activity within the ON pathway.

Although BzATP is a potent agonist of $P2X_7Rs$, it is not selective for the receptor and can bind to $P2X_1$, $P2X_2$ and $P2X_3$ receptors with similar potency (Sperlágh et al., 2006), and therefore the possibility remains that these receptor subtypes may also be activated in the

presence of the agonist. $P2X_1R$ immunoreactivity has been localised to the inner retinal layers of the cat and monkey retina (Yazulla and Studholme, 2004), although its expression in the mouse is uncertain. In the rodent, $P2X_3Rs$ have been detected in the inner plexiform layer (Puthussery and Fletcher, 2007). On activation, both $P2X_1Rs$ and $P2X_3Rs$ rapidly desensitise (North, 2002), and thus their kinetic profiles do not correlate with the BzATP-mediated effects observed in the present study. Selective expression of $P2X_2Rs$ in starburst amacrine cells within the OFF vertical pathway has been demonstrated in the mouse retina (Kaneda et al., 2008, 2010). Although $P2X_2Rs$ display slowly desensitising properties similar to $P2X_7Rs$, it is uncertain whether they would directly affect neuronal responses within the ON pathway. Therefore, the major component of the BzATP-mediated effects observed in the present investigations is most likely attributed to the activation of $P2X_7Rs$.

10.3 Functional significance of short-term $P2X_7R$- and lipopolysaccharide-induced alterations to retinal microglial morphology

Microglia are highly dynamic and motile, constantly surveying their microenvironment, even in the absence of pathological stressors (Nimmerjahn et al., 2005). Growing evidence suggests that microglia are genuine partners of neurotransmission, fine-tuning neuronal responses while also regulating physical synaptic structure (Tremblay et al., 2010; Li et al., 2012). In the adult mouse retina, resting microglia reside exclusively in the outer and inner plexiform layers (Santos et al., 2008), although their role in modulating visual function remains unexplored.

Retinal microglia are known to express both $P2X_7Rs$ and TLR4, which are stimulated by BzATP and LPS, respectively. The present study demonstrated that microglial morphology was altered relatively rapidly with short-term application of BzATP or LPS. Under baseline

conditions, the microglial cells exhibited typically ramified morphology, suggestive of a 'resting' state. The presence of NBQX in the bathing medium may have reduced the size and complexity of the microglial processes, as shown previously in the isolated mouse retina (Fontainhas et al., 2011). BzATP induced an increase in microglial process area, whereas the same was decreased in the presence of LPS. These findings support the notion that microglia are highly dynamic and responsive to rapid changes in the microenvironment.

The varied effects of BzATP and LPS on retinal microglia suggest the transition to differential stages of early microglial activation. Indeed, microglial activation is a graded response, and the stage of activation is highly dependent upon the levels of potential stressors in their external surroundings. The increase in microglial expanse with BzATP treatment indicates an 'alerted' state whereby cells become hyper-ramified, with an increased capacity for process extension and retraction. ATP is a strong chemoattractant of microglia and is known to regulate rapid changes in microglial motility through $P2Y_{12}Rs$ (Haynes et al., 2006). ATP in the extracellular space is readily hydrolysed into adenosine, which is also known to regulate microglial process retraction and extension at later stages of the microglial response (hours to days) (Gyoneva et al., 2009). BzATP is unlikely to activate these P2Rs at the concentration tested. However, release of endogenous ATP, through BzATP-activated $P2X_7Rs$ themselves, is highly plausible. Although, it is unclear whether BzATP acts directly on microglia, nearby neurons or both cell types, to elicit ATP release.

LPS is a highly potent activator of microglia, and is typically used to simulate inflammation and cytokine-rich conditions. The present findings demonstrate that short-term LPS application elicits a rapid transition to a more classically 'activated' microglial phenotype, which is not surprising. An important observation in this study is that the change in microglial morphology occurs within minutes *in situ*. This could suggest that microglial mediators such

as IL-1β and ATP, which have classically been associated with longer periods (hours to days) of LPS treatment, could in effect be released at detectable concentrations, much earlier.

10.4 Lipopolysaccharide-induced microglial activation modulates retinal ganglion cell function through $P2X_7R$- and Pannexin-1- mediated release of ATP

$P2X_7Rs$ have classically been associated with ATP and cytokine release from microglia, when these cells are primed with lipopolysaccharide (LPS) for a few hours. A recent study has demonstrated that direct bath-application of LPS modulates excitatory neurotransmission through an initial release of endogenous ATP from microglia, in mouse hippocampal slices (Pascual et al., 2011). Furthermore, LPS has previously shown to inhibit long-term potentiation in the rat hippocampus, when applied directly to the slice preparation (Cunningham et al., 1996).

The data reported in this investigation indicate that an acute inflammatory response induced by bath-application of lipopolysaccharide (LPS), induces a rapid modulation of excitatory responses in the retina. LPS acts through binding its toll-like receptor TLR4, which is predominantly expressed by microglia and RPE cells in the retina (Ko et al., 2011; Kohno et al., 2013). TLR4 has also been localised to photoreceptors and Müller cells (Tu et al., 2011; Lin et al., 2013). The results of the present study showed that LPS had no overall effect on the a-wave, but induced a marked reduction in the b-wave. Furthermore, LPS suppressed both the ON and OFF RGC fEPSPs. This suggests that, at least in this investigation, the site of action of LPS was primarily within the inner layers of the retina, and rules out any modulation of the photoreceptors. In the mouse retina, TLR4 was co-localised almost

exclusively to microglia within the inner retinal layers, in the absence of inflammation (Halder et al., 2013), further supporting an inner retinal site of action for LPS.

The LPS-induced suppression of both ON and OFF fEPSPs was attenuated in the presence of the $P2X_7R$ antagonist, A438079. This strongly suggests the involvement of $P2X_7Rs$ in mediating the effect of LPS. Contrary to the action of BzATP, the effect of LPS was extended to modulate the OFF pathway, which indicates the involvement of non-neuronal, presynaptic $P2X_7Rs$. Indeed, cultured microglia treated with LPS have shown to elicit a rapid release of ATP at nanomolar concentrations after only 15 min of endotoxin exposure (Sperlágh et al., 1998). Furthermore, bath-applied LPS has shown to trigger microglial ATP, which in turn mediates further release from astrocytes, subsequently modulating excitatory synaptic responses in the mouse hippocampus (Pascual et al., 2011). After the initial release of ATP from microglia, possibly through $P2X_7R$-mediated vesicular exocytosis (Imura et al., 2013; Kato et al., 2013), the amplification of the ATP signal via a secondary source could be attributed to Müller glia through P2YR activation (as considered above). However, the present investigation implicates a mechanism by which further ATP release occurs via pannexin-1 (panx-1) hemichannels, which are predominantly expressed on retinal ganglion cells in the adult mouse retina (Dvoriantchikova et al., 2006), and are found abundantly co-localised with $P2X_7Rs$ in rat ganglion cells (Xia et al., 2012).

It was found that the panx-1 inhibitor, carbenoxolone, markedly attenuated the LPS-mediated effect on the OFF fEPSP. A small reduction in the LPS-mediated effect on the ON fEPSP was observed in the presence of carbenoxolone although this was not statistically significant, possibly suggesting the persistence of a panx-1-independent mechanism of ATP release. Indeed, $P2X_7Rs$ can act as conduits for ATP release either through their own transmembrane channel, as well as via associated panx-1 hemichannels (Praetorius and

Leipziger, 2009; Fields, 2011; Xia et al., 2012). The present investigation has demonstrated that OFF RGC fEPSPs are not modulated by $P2X_7Rs$, thus an OFF-pathway specific mechanism of action of panx-1 is considered unlikely as ATP release via panx-1 normally requires $P2X_7R$ activation. A438079 is also known to inhibit panx-1 activity. It is proposed that the attenuated LPS-mediated effect of both ON and OFF RGC fEPSPs in the presence of A438079 may be due to the inhibition of microglial $P2X_7Rs$, as well as the combined blockade of $P2X_7Rs$ and panx-1 on the ON RGCs. In the absence of panx-1 activity, $P2X_7Rs$ may still mediate localised ATP release (through microglia or RGCs) and subsequent cell-autonomous $P2X_7R$ activation in ON RGCs, resulting in a persistent reduction of the ON fEPSP with LPS. It is possible that panx-1 blockade prevents a large spillover of ATP, which could otherwise suppress OFF RGC responses through the activation of alternative purinergic receptors.

Following washout of LPS, its effect on the ON fEPSP was not reversible, whereas the OFF fEPSP showed partial recovery. This further supports the notion of a localised and sustained release of ATP near synapses within the ON pathway, which is likely to initiate further inflammatory responses. At this point, it would not be unreasonable to consider the role of multiple ATP-mediated mechanisms as the signal is rapidly and effectively amplified in response to acute stressors.

As well as ATP release, LPS and $P2X_7R$ stimulation of microglia induces the release of cytokines, such as Il-1β and TNFα, which have shown to specifically modulate NMDA receptor-mediated neuronal function and hippocampal long-term potentiation *in vitro* and *in vivo* (Katsuki et al., 1990; Plata-Salamán and Ffrench-Mullen, 1992; Zeise et al., 1992; Bellinger et al., 1993; Cunningham et al., 1996; Schneider et al., 1998; Coogan and O'Connor, 1999; Vereker et al., 2001). Under pathological conditions, cytokine release

stimulated through this pathway is believed to involve the inflammasome complex (see section 3.3.2). However, upregulation and assembly of the associated proteins would be on a time scale of hours upon LPS stimulation, due to the requirement for gene transcription, therefore ruling out inflammasome involvement in the present investigation. $P2X_7R$ activation has been shown to induce IL-1β release via alternative mechanisms such as microvesicle shedding, from microglia (Dubyak, 2012).

10.5 $P2X_7Rs$ contribute an excitatory non-iGluR residual component of the ON RGC fEPSP

When applied alone, A438079 induced a marked potentiation in the ERG a-wave while suppressing the b-wave, suggesting that in the absence of a high extracellular concentration of ATP, $P2X_7Rs$ modulate normal neuronal function in the retina. A438079 or AF27139 had no effect on the ON fEPSP, whereas the response was reduced by A804598. Overall, the OFF fEPSP was not affected by A438079, A804598 or AF27139, further suggesting ON pathway dominance for $P2X_7R$ modulation in the retina.

Exclusion of the fast responses to glutamate and GABA with their respective antagonists identified a small residual component of the ON and OFF RGC fEPSPs persisted. A438079, as well as the broad-spectrum P2XR antagonists suramin and PPADS were used to further characterise the ON RGC fEPSP residual fraction, and to investigate whether this was mediated via a purinergic receptor. In the presence of D-AP5, suramin and PPADS induced relatively large suppressive effects on the ON fEPSP. This strongly suggests a contribution of P2XRs in mediating this residual component. Furthermore, A438079 induced a small reduction in the ON fEPSP in the presence of D-AP5, contrary to its effect in the absence of

the NMDA-R antagonist. This could suggest that $P2X_7Rs$ could compensate for a loss of ionotropic glutamate receptor activity by facilitating the excitatory drive.

The co-application of BzATP in the presence of D-AP5 induced a reversible reduction in the ON fEPSP, comparable to the BzATP-mediated effect in the absence of the antagonist. This demonstrates that a high extracellular concentration of agonist switches the $P2X_7R$ function from facilitatory to inhibitory, and thus supports the notion that $P2X_7Rs$ may exemplify a dual function depending on the conditions of the extracellular environment.

10.6 Conclusions

The findings of the present study verify the previously reported notion that acute activation of $P2X_7Rs$ with the agonist, BzATP markedly alters outer and inner retinal function (Puthussery et al., 2006). $P2X_7Rs$ have been specifically localised to synapses within the rod pathway of the mammalian retina (Puthussery and Fletcher, 2004; Puthussery et al., 2006; Vessey and Fletcher, 2012). With the use of a dark-adapted, *ex vivo* mouse retinal wholemount preparation, it was possible to investigate and dissect $P2X_7R$ involvement in the purinergic modulation of predominantly rod-mediated responses, in the outer and inner retina.

Photoreceptor and rod ON bipolar cell responses were investigated using transretinal ERG recordings. In physiological perfusion medium, the photoreceptor response was facilitated with BzATP, whereas the same was suppressed on removal of magnesium. This suggests that a detrimental $P2X_7R$ function could be activated under unfavourable or stressed conditions within the extracellular environment. Such an effect was not seen on the ON bipolar cell-mediated ERG b-wave response, which was markedly reduced with BzATP in all

perfusates tested. The presence of the $P2X_7R$ antagonist, A438079 almost completely suppressed the effect of BzATP on the photoreceptor response, whereas the agonist-induced effect on the ON bipolar cell-derived b-wave was only partially reduced with A438079. Thus, it is proposed that $P2X_7R$ activation occurs at differential sites in the outer and inner retina.

ON and OFF retinal ganglion cell function were explored by recording light-evoked NMDA receptor-mediated extracellular fEPSPs from the ganglion cell layer of the retinal wholemount. $P2X_7R$ activation significantly attenuated ON RGC fEPSPs, with no overall effect on the OFF RGC fEPSPs, indicating a selective modulation of the ON pathway, by $P2X_7Rs$. In the presence of selective $P2X_7R$ antagonists, a residual BzATP-mediated effect on the ON fEPSP remained, suggesting that potential endogenous ATP release in the inner retinal layers may reduce the potency of these antagonists.

$P2X_7Rs$ are also present on microglia, which reside in the outer and inner plexiform layers in the adult retina. Investigation of retinal microglia revealed that BzATP and LPS rapidly modulate microglial morphology, under similar conditions, and within the same time course as for the electrophysiological experiments. Such morphological changes indicate that microglial function is also altered, and may effectively modulate neuronal responses. Indeed, LPS-mediated acute microglial activation revealed a novel mechanism by which an initial $P2X_7R$-mediated ATP release from LPS-activated microglia resulted in suppression of neuronal responses in the inner retina, through rapid amplification of the extracellular ATP signal. Such amplification is suggested to involve $P2X_7R$-associated pannexin-1 hemichannels, which are known to localise predominantly on retinal ganglion cells and mediate neuronal ATP release (Xia et al., 2012), which subsequently activates neuronal $P2X_7Rs$, suppressing retinal ganglion cell function. Fig. 10.1 illustrates a possible

mechanism by which LPS and subsequent $P2X_7R$ activation may modulate inner retinal synapses within the rod-mediate ON pathway.

Release of extracellular ATP and the activation of $P2X_7Rs$, along with the initiation of various inflammatory cascades are phenomena common to many retinal diseases that lead to reduced, or loss of vision, such as neuronal degeneration in retinitis pigmentosa and glaucoma. Furthermore, $P2X_7Rs$ are heavily associated with diabetic retinopathy and retinal ischemia. Thus, $P2X_7Rs$ are highly plausible therapeutic targets for alleviation of various retinal degenerative conditions. The role of microglia as genuine partners in retinal neurotransmission has also been highlighted. This study provides evidence that through purinergic signalling, early changes in the immunological state of the central nervous system can have detrimental effects on neuronal function, and offers a wider understanding of local neural-immune interactions, which may precede more prominent, symptomatic changes in disease.

10.7 Future Directions

A novel finding of this thesis, that an early stage of microglial activation can modulate visual responses in the retina through purinergic signalling, offers an exciting avenue for extending this work. Under physiological conditions, microglia are highly dynamic and motile in their resting state (Davalos et al., 2005; Nimmerjahn et al., 2005). In the mouse visual cortex, resting microglia have shown to contact dendritic spines with their processes, modifying or eliminating synapses *in vivo* (Wake et al., 2009; Tremblay et al., 2010). Further, in the zebrafish optic tectum, high neuronal activity has been demonstrated to attract microglial processes through purinergic signalling, which then reduce spontaneous and visually evoked responses, thereby regulating normal neuronal function (Li et al., 2012). It would be possible

to explore such putative, dynamic microglial-neuronal contacts in the *ex vivo* retinal wholemount preparation, through the use of time-lapse confocal imaging and green fluorescent protein-labelled microglia. Employing the wholemount preparation for further study would also enable the recording of neuronal responses, simultaneously with visualising microglia, under physiological conditions.

Other mediators of inflammation released through $P2X_7R$ activation, such as the cytokine IL-1β, have previously shown to modulate neuronal activity in the hippocampus. Microglial activation, ATP release, $P2X_7R$ activation and IL-1β release are phenomena which occur in the presence of various acute stressors in the microenvironment. Extending the current work, to explore the possible neuromodulatory function of IL-1β and other cytokines in retinal visual processing, would provide a better understanding of neural-immune interactions at the very early stages of inflammation and disease, not only in the retina, but across the central nervous system.

Chapter 10 Figures

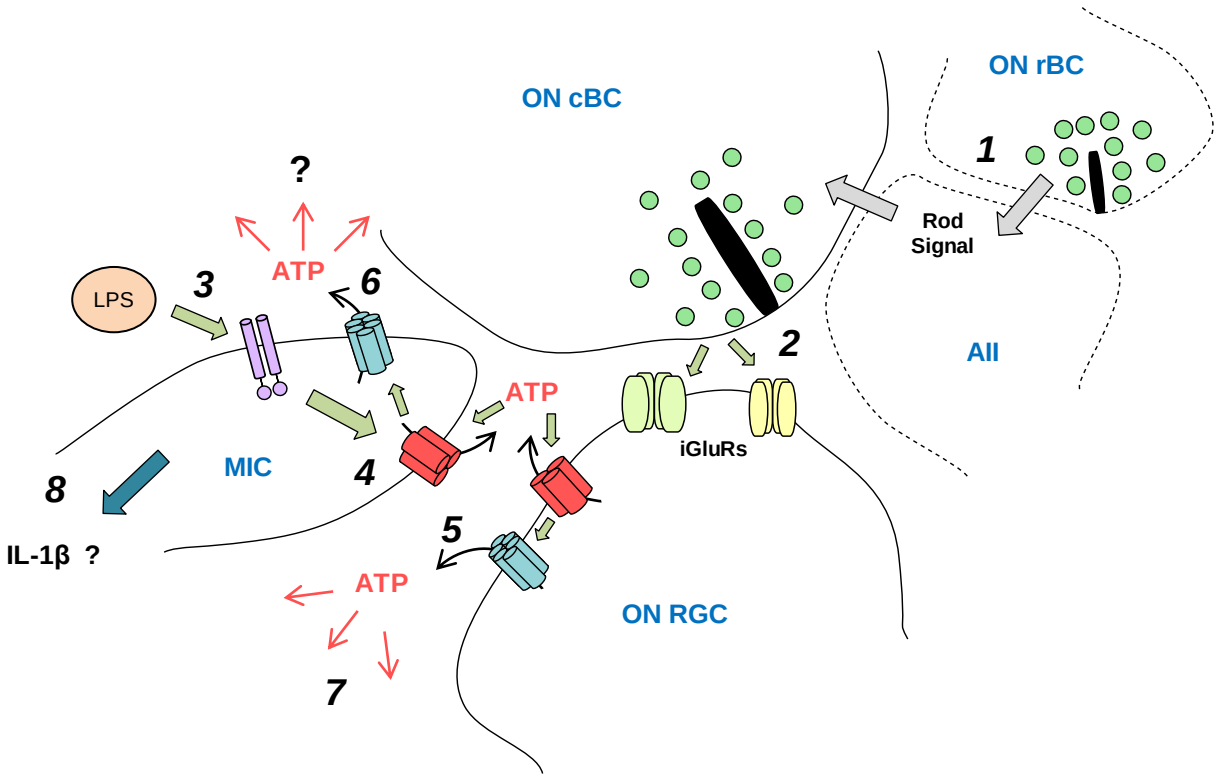

Figure 10.1 Schematic of the possible mechanism by which early lipopolysaccharide-induced microglial activation and $P2X_7Rs$ could modulate the rod ON pathway through extracellular ATP release in the inner retina. ***1***, In the inner plexiform layer, the ON rod bipolar cell (ON rBC) signal is transduced to the ON retinal ganglion cell (ON RGC) via the AII amacrine cell (AII) pathway. Glutamate is released from ON rBC ribbon synapses, activating postsynaptic ionotropic glutamate receptors (iGluRs) on the AII cell. In turn, the AII cell transmits the rod signal to the ON cone bipolar cell (ON cBC) terminal, through gap junctions. ***2***, Activation of postsynaptic iGluRs on the ON RGC results in depolarisation. ***3***, Lipopolysaccharide (LPS) binds to toll-like receptor-4 (TLR4; purple) on the microglial cell (MIC), inducing the release of ATP, possibly through $P2X_7Rs$ themselves (***4***). TLR4 activation is known to enhance $P2X_7R$ activity, although the exact mechanism by which this occurs is uncertain. The C-terminus of the $P2X_7R$ contains an LPS binding domain, which could be modulated by an internalised LPS-TLR4 complex. ***5***, The presence of high levels of extracellular ATP in the local microcircuit may stimulate postsynaptic $P2X_7Rs$ on the ON RGC, resulting in an overall attenuation of ON RGC function. In turn, further ATP release occurs through $P2X_7R$-associated Pannexin-1 hemichannels, ultimately amplifying extracellular ATP release, and activating further downstream mechanisms. ***6***, It is uncertain whether Pannexin-1 hemichannels are functional on resting microglia in the retina. However, these channels are known to be important in mediating cytokine release from microglia under inflammatory conditions, in other areas of the central nervous system. ATP release may also occur through microglial Pannexin-1 channels. ***7***, Potentially, the large, amplified release of ATP may spillover to cellular targets within the OFF pathway, to modulate OFF RGC function. ATP is rapidly hydrolysed in the extracellular space, and could therefore alter neuronal and Müller glial activity through the activation of alternative purinergic receptors. ***8***, TLR4 and $P2X_7R$ activation are also associated with the release of other inflammatory mediators from microglia, such as the cytokine interleukin-1β (IL-1β). In the brain, IL-1β has shown to potently modulate NMDA-R-mediated neuronal function, and therefore, may also play a role in regulating synaptic function in the inner retina.

References

Abbracchio MP, Burnstock G, Verkhratsky A, Zimmermann H (2009) Purinergic signalling in the nervous system: an overview. Trends Neurosci 32:19–29.

Adinolfi E, Kim M, Young MT, Di Virgilio F, Surprenant A (2003) Tyrosine phosphorylation of HSP90 within the P2X7 receptor complex negatively regulates P2X7 receptors. J Biol Chem 278:37344–37351.

Adriouch S, Dox C, Welge V, Seman M, Koch-Nolte F, Haag F (2002) Cutting edge: a natural P451L mutation in the cytoplasmic domain impairs the function of the mouse P2X7 receptor. J Immunol 169:4108–4112.

Alloisio S, Cervetto C, Passalacqua M, Barbieri R, Maura G, Nobile M, Marcoli M (2008) Functional evidence for presynaptic P2X7 receptors in adult rat cerebrocortical nerve terminals. FEBS Lett 582:3948–3953.

Ashwell KW, Holländer H, Streit W, Stone J (1989) The appearance and distribution of microglia in the developing retina of the rat. Vis Neurosci 2:437–448.

Asi H, Perlman I (1992) Relationships between the electroretinogram a-wave , b-wave and oscillatory potentials and their application to clinical diagnosis. Doc Ophthalmol 79:125–139.

Avignone E, Ulmann L, Levavasseur F, Rassendren F, Audinat E (2008) Status epilepticus induces a particular microglial activation state characterized by enhanced purinergic signaling. J Neurosci 28:9133–9144.

Balasubramanian V, Sterling P (2009) Receptive fields and functional architecture in the retina. J Physiol 587:2753–2767.

Ballerini P, Di Iorio P, Ciccarelli R, Nargi E, D'Alimonte I, Traversa U, Rathbone MP, Caciagli F (2002) Glial cells express multiple ATP binding cassette proteins which are involved in ATP release. Neuroreport 13:1789–1792.

Banerjee RK (1981) Ecto-ATPase. Mol Cell Biochem 37:91–99.

Baraldi PG, Di Virgilio F, Romagnoli R (2004) Agonists and antagonists acting at P2X7 receptor. Curr Top Med Chem 4:1707–1717.

Béchade C, Cantaut-Belarif Y, Bessis A (2013) Microglial control of neuronal activity. Front Cell Neurosci 7:32.

Bellinger FP, Madamba S, Siggins R (1993) Interleukin 1-beta inhibits synaptic strength and long-term potentiation in the rat CA1 hippocampus. Brain Res 628:227–234.

Bianchi BR, Lynch KJ, Touma E, Niforatos W, Burgard EC, Alexander KM, Park HS, Yu H, Metzger R, Kowaluk E, Jarvis MF, van Biesen T (1999) Pharmacological characterization of recombinant human and rat P2X receptor subtypes. Eur J Pharmacol 376:127–138.

Bianco F, Pravettoni E, Colombo A, Schenk U, Moller T, Matteoli M, Verderio C (2005) Astrocyte-Derived ATP Induces Vesicle Shedding and IL-1 Release from Microglia. J Immunol 174:7268–7277.

Bloomfield S, Dacheux R (2001) Rod vision: pathways and processing in the mammalian retina. Prog Retin Eye Res 20:351–384.

Bloomfield S, Xin D (2000) Surround inhibition of mammalian AII amacrine cells is generated in the proximal retina. J Physiol 523 Pt 3:771–783.

Bloomfield SA, Völgyi B (2009) The diverse functional roles and regulation of neuronal gap junctions in the retina. Nat Rev Neurosci 10:495–506.

Boos R, Muller F, Wassle H (1990) Actions of excitatory amino acids on brisk ganglion cells in the cat retina. J Neurophysiol 65:1368–1379.

Boumechache M, Masin M, Edwardson JM, Górecki DC, Murrell-Lagnado R (2009) Analysis of assembly and trafficking of native P2X4 and P2X7 receptor complexes in rodent immune cells. J Biol Chem 284:13446–13454.

Boycott BB (1988) Horizontal cells of mammalian retinae. Neurosci Res 8:S97–S111.

Boycott BB, Kolb H (1973) The connections between bipolar cells and photoreceptors in the retina of the domestic cat. J Comp Neurol 148:91–114.

Brändle U, Kohler K, Wheeler-Schilling TH (1998) Expression of the P2X7-receptor subunit in neurons of the rat retina. Mol brain Res 62:106–109.

Brandstätter JH, Koulen P, Wässle H (1998) Diversity of glutamate receptors in the mammalian retina. Vision Res 38:1385–1397.

Bringmann A, Grosche A, Pannicke T, Reichenbach A (2013) GABA and glutamate uptake and metabolism in retinal glial (Müller) cells. Front Endocrinol (Lausanne) 4:48.

Bringmann A, Pannicke T, Grosche J, Francke M, Wiedemann P, Skatchkov SN, Osborne NN, Reichenbach A (2006) Müller cells in the healthy and diseased retina. Prog Retin Eye Res 25:397–424.

Bringmann A, Pannicke T, Moll V, Milenkovic I, Faude F, Enzmann V, Wolf S, Reichenbach A (2001) Upregulation of P2X(7) receptor currents in Müller glial cells during proliferative vitreoretinopathy. Invest Ophthalmol Vis Sci 42:860–867.

Bringmann A, Pannicke T, Uhlmann S, Kohen L, Wiedemann P, Reichenbach A (2002) Membrane conductance of Müller glial cells in proliferative diabetic retinopathy. Can J Ophthalmol 37:221–227.

Bringmann A, Wiedemann P (2012) Müller glial cells in retinal disease. Ophthalmologica 227:1–19.

Buisman HP, Steinberg TH, Fischbarg J, Silverstein SC, Vogelzang S, Ince C, Ypey DL, Leijh PC (1988) Extracellular ATP induces a large nonselective conductance in macrophage plasma membranes. Proc Natl Acad Sci U S A 85:7988–7992.

Burnstock G (2007) Physiology and Pathophysiology of Purinergic Neurotransmission. Auton Neurosci:659 –797.

Burnstock G, Campbell G, Satchell D, Smythe A (1970) Evidence that adenosine triphosphate or a related nucleotide is the transmitter substance released by non-adrenergic inhibitory nerves in the gut. Br J Pharmacol 40:668–688.

Burnstock G, Krügel U, Abbracchio MP, Illes P (2011) Purinergic signalling: From normal behaviour to pathological brain function. Prog Neurobiol 95:229–274.

Burnstock G, Satchell DG, Smythe A (1972) A comparison of the excitatory and inhibitory effects of non-adrenergic , non-cholinergic nerve stimulation and exogenously applied ATP on a variety of smooth muscle preparations from different vertebrate species. Br J Pharmacol 46:234–242.

Buttery RG, Hinrichsen CF, Weller WL, Haight JR (1991) How thick should a retina be? A comparative study of mammalian species with and without intraretinal vasculature. Vision Res 31:169–187.

Carter-Dawson LD, LaVail MM (1979) Rods and cones in the mouse retina. I. Structural analysis using light and electron microscopy. J Comp Neurol 188:245–262.

Chakfe Y, Seguin R, Antel JP, Malo D, Henderson D, Philippe S (2002) ADP and AMP induce interleukin-1-beta release from microglial cells through activation of ATP-primed P2X7 receptor channels. J Neurosci 22:3061–3069.

Chen L, Yang P, Kijlstra A (2002) Distribution, markers, and functions of retinal microglia. Ocul Immunol Inflamm 10:27–39.

Chessell I, Simon J, Hibell A., Michel A., Barnard E., Humphrey PP. (1998a) Cloning and functional characterisation of the mouse P2X7 receptor. FEBS Lett 439:26–30.

Chessell IP, Hatcher JP, Bountra C, Michel AD, Hughes JP, Green P, Egerton J, Murfin M, Richardson J, Peck WL, Grahames CB a, Casula MA, Yiangou Y, Birch R, Anand P, Buell GN (2005) Disruption of the P2X7 purinoceptor gene abolishes chronic inflammatory and neuropathic pain. Pain 114:386–396.

Chessell IP, Michel AD, Humphrey PP (1997) Properties of the pore-forming P2X7 purinoceptor in mouse NTW8 microglial cells. Br J Pharmacol 121:1429–1437.

Chessell IP, Michel AD, Humphrey PPA (1998b) Effects of antagonists at the human recombinant P2X7 receptor. Br J Pharmacol:1314–1320.

Clark AK, Staniland AA, Marchand F, Kaan TKY, McMahon SB, Malcangio M (2010) P2X7-dependent release of interleukin-1beta and nociception in the spinal cord following lipopolysaccharide. J Neurosci 30:573–582.

Cockcroft S, Gomperts BD (1980) The ATP4- receptor of rat mast cells. Biochem J 188:789–798.

Coddou C, Yan Z, Obsil T, Huidobro-toro JP, Stojilkovic SS (2011) Activation and regulation of purinergic P2X receptor channels. Pharmacol Rev 63:641–683.

Cohen ED, Miller RF (1999) The network-selective actions of quinoxalines on the neurocircuitry operations of the rabbit retina. Brain Res 831:206–228.

Coleman PA, Miller F (1988) Do N-methyl-D-aspartate receptors mediate synaptic responses in the mudpuppy retina? J Neurosci 8:4728–4733.

Coogan AN, O'Connor JJ (1999) Interleukin-1beta inhibits a tetraethylammonium-induced synaptic potentiation in the rat dentate gyrus in vitro. Eur J Pharmacol 374:197–206.

Costa G, Pereira T, Neto a M, Cristóvão a J, Ambrósio AF, Santos PF (2009) High glucose changes extracellular adenosine triphosphate levels in rat retinal cultures. J Neurosci Res 87:1375–1380.

Costa-Junior HM, Sarmento Vieira F, Coutinho-Silva R (2011) C terminus of the P2X7 receptor: treasure hunting. Purinergic Signal 7:7–19.

Cunningham AJ, Murray CA, O'Neill LAJ, Lynch MA, O'Connor JJ (1996) Interleukin-1β (IL-1β) and tumour necrosis factor (TNF) inhibit long-term potentiation in the rat dentate gyrus in vitro. Neurosci Lett 203:17–20.

D'Ambrosi N, Finocchi P, Apolloni S, Cozzolino M, Ferri A, Padovano V, Pietrini G, Carrì MT, Volonté C (2009) The proinflammatory action of microglial P2 receptors is enhanced in SOD1 models for amyotrophic lateral sclerosis. J Immunol 183:4648–4656.

D'Amico M, Samengo I, Navarra P, Taglialatela M, Martire M (2010) AMPA- and P2X7-receptor-mediated facilitation of [3H]D-aspartate release from nerve terminals isolated from the rat caudal brainstem. Neurochem Int 57:623–628.

Dacheux RF, Miller RF (1981) An intracellular electrophysiological study of the ontogeny of functional synapses in the rabbit retina. I. Receptors, horizontal, and bipolar cells. J Comp Neurol 198:307–326.

Dalmau I, Vela JM, González B, Castellano B (1998) Expression of purine metabolism-related enzymes by microglial cells in the developing rat brain. J Comp Neurol 398:333–346.

Davalos D, Grutzendler J, Yang G, Kim JV, Zuo Y, Jung S, Littman DR, Dustin ML, Gan WB (2005) ATP mediates rapid microglial response to local brain injury in vivo. Nat Neurosci 8:752–758.

Denlinger LC, Fisette PL, Sommer J a, Watters JJ, Prabhu U, Dubyak GR, Proctor RA, Bertics PJ (2001) Cutting edge: the nucleotide receptor P2X7 contains multiple protein- and lipid-interaction motifs including a potential binding site for bacterial lipopolysaccharide. J Immunol 167:1871–1876.

Denlinger LC, Sommer JA, Parker K, Fisette PL, Watters JW, Richard A, Dubyak GR, Bertics PJ, Gudipaty L, Proctor RA (2003) Mutation of a dibasic amino acid motif within the C terminus of the P2X7 nucleotide receptor results in trafficking defects and impaired function. J Immunol 171:1304–1311.

Deuchars S, Atkinson L, Brooke RE, Musa H, Milligan CJ, Batten TF, Buckley NJ, Parson SH, Deuchars J (2001) Neuronal P2X7 receptors are targeted to presynaptic terminals in the central and peripheral nervous systems. J Neurosci 21:7143–7152.

DiVirgilio F (1995) The P2Z purinoceptor: an intriguing role in immunity, inflammation and cell death. Immunol Today 16:524–528.

Dong CJ, Hare WA (2000) Contribution to the kinetics and amplitude of the electroretinogram b-wave by third-order retinal neurons in the rabbit retina. Vision Res 40:579–589.

Dong CJ, Hare WA (2002) GABAc feedback pathway modulates the amplitude and kinetics of ERG b-wave in a mammalian retina in vivo. Vision Res 42:1081–1087.

Donnelly-Roberts DL, Jarvis MF (2007) Discovery of P2X7 receptor-selective antagonists offers new insights into P2X7 receptor function and indicates a role in chronic pain states. Br J Pharmacol 151:571–579.

Donnelly-Roberts DL, Namovic MT, Han P, Jarvis MF (2009a) Mammalian P2X7 receptor pharmacology: comparison of recombinant mouse, rat and human P2X7 receptors. Br J Pharmacol 157:1203–1214.

Donnelly-Roberts DL, Namovic MT, Surber B, Vaidyanathan SX, Perez-Medrano A, Wang Y, Carroll W, Jarvis MF (2009b) [3H]A-804598 ([3H]2-cyano-1-[(1S)-1-phenylethyl]-3-quinolin-5-ylguanidine) is a novel, potent, and selective antagonist radioligand for P2X7 receptors. Neuropharmacology 56:223–229.

Dowling JE (1970) Organization of vertebrate retinas. Invest Ophthalmol 9:655–680.

Dreher Z, Robinson SR, Distler C (1992) Müller cells in vascular and avascular retinae: a survey of seven mammals. J Comp Neurol 323:59–80.

Dubyak GR (2007) Go it alone no more — P2X7 joins the society of heteromeric ATP-gated receptor channels. Mol Pharmacol 72:1402–1405.

Dubyak GR (2012) P2X7 receptor regulation of non-classical secretion from immune effector cells. Cell Microbiol 14:1697–1706.

Dvoriantchikova G, Ivanov D, Panchin Y, Shestopalov VI (2006) Expression of pannexin family of proteins in the retina. FEBS Lett 580:2178–2182.

Edwards F, Gibb A, Colquhoun D (1992) ATP receptor-mediated synaptic currents in the central nervous system. Nature 359:144–147.

Egan TM, Haines WR, Voigt MM (1998) A domain contributing to the ion channel of ATP-gated P2X2 receptors identified by the substituted cysteine accessibility method. J Neurosci 18:2350–2359.

Egan TM, Samways DSK, Li Z (2006) Biophysics of P2X receptors. Eur J Physiol 452:501–512.

Eldred J, Sanderson J, Wormstone M, Reddan JR, Duncan G (2003) Stress-induced ATP release from and growth modulation of human lens and retinal pigment epithelial cells. Biochem Soc Trans 31:1213–1215.

Engel T, Gomez-Villafuertes R, Tanaka K, Mesuret G, Sanz-Rodriguez A, Garcia-Huerta P, Miras-Portugal MT, Henshall DC, Diaz-Hernandez M (2011) Seizure suppression and

neuroprotection by targeting the purinergic P2X7 receptor during status epilepticus in mice. FASEB J 26:1–13.

Enroth-Cugell C (1977) Convergence of rod and cone signals in the cat's retina. J Physiol 269:297–318.

Euler T, Schneider H, Wassle H (1996) Glutamate responses of bipolar cells in a slice preparation of the rat retina. J neurosc 16:2934–2944.

Evans RJ, Lewis C, Virginio C, Lundstrom K, Buell G, Surprenant A, North R (1996) Ionic permeability of, and divalent cation effects on, two ATP-gated cation channels (P2X receptors) expressed in mammalian cells. J Physiol 497.2:413–422.

Feng Y-H, Wang L, Wang Q, Li X, Zeng R, Gorodeski GI (2005) ATP stimulates GRK-3 phosphorylation and beta-arrestin-2-dependent internalization of P2X7 receptor. Am J Physiol Cell Physiol 288:C1342–56.

Ferrari D, Chiozzi P, Falzoni S, Hanau S, Di Virgilio F (1997a) Purinergic modulation of interleukin-1b release from micrgolial cells stimulated with bacterial endotoxin. J Exp Med 185:579–582.

Ferrari D, Chiozzi P, Falzoni S, Susino MD, Melchiorri L, Baricordi OR, Di Virgilio F (1997b) Extracellular ATP triggers IL-1beta release by activating the putinergic P2Z receptor of human macrophages. J Immunol 159:1451–1458.

Ferrari D, Pizzirani C, Adinolfi E, Lemoli RM, Curti A, Idzko M, Panther E, Di Virgilio F (2006) The P2X7 receptor: a key player in IL-1 processing and release. J Immunol 176:3877–3883.

Fields RD (2011) Nonsynaptic and nonvesicular ATP release from neurons and relevance to neuron-glia signaling. Semin Cell Dev Biol 22:214–219.

Di Filippo M, Chiasserini D, Gardoni F, Viviani B, Tozzi A, Giampà C, Costa C, Tantucci M, Zianni E, Boraso M, Siliquini S, De Iure A, Ghiglieri V, Colcelli E, Baker D, Sarchielli P, Fusco FR, Di Luca M, Calabresi P (2013) Effects of central and peripheral inflammation on hippocampal synaptic plasticity. Neurobiol Dis 52:229–236.

Di Filippo M, Sarchielli P, Picconi B, Calabresi P (2008) Neuroinflammation and synaptic plasticity: theoretical basis for a novel, immune-centred, therapeutic approach to neurological disorders. Trends Pharmacol Sci 29:402–412.

Fletcher EL (2010) Mechanisms of photoreceptor death during retinal degeneration. Optom Vis Sci 87:269–275.

Fogal B, Hewett S (2008) Interleukin-1b: a bridge between inflammation and excitotoxicity? J Neurochem 106:1–23.

Fontainhas AM, Wang M, Liang KJ, Chen S, Mettu P, Damani M, Fariss RN, Li W, Wong WT (2011) Microglial morphology and dynamic behavior is regulated by ionotropic glutamatergic and GABAergic neurotransmission. PLoS One 6:e15973.

Franke H, Klimke K, Brinckmann U, Grosche J, Francke M, Sperlagh B, Reichenbach A, Liebert UG, Illes P (2005) P2X(7) receptor-mRNA and -protein in the mouse retina; changes during retinal degeneration in BALBCrds mice. Neurochem Int 47:235–242.

Franke H, Schepper C, Illes P, Krügel U (2007) Involvement of P2X and P2Y receptors in microglial activation in vivo. Purinergic Signal 3:435–445.

Freist W, Verhey JF, Stühmer W, Gauss DH (1998) ATP binding site of P2X channel proteins: structural similarities with class II aminoacyl-tRNA synthetases. FEBS Lett 434:61–65.

Fukuda J, Fujita Y, Ohsawa K (1983) ATP content in isolated mammalian nerve cells assayed by a modified luciferin-luciferase method. J Neurosci Methods 8:295–302.

Gargett CE, Wiley JS (1997) The isoquinoline derivative KN-62 a potent antagonist of the P2Z-receptor of human lymphocytes. Br J Pharmacol 120:1483–1490.

Ghosh KK, Bujan S, Haverkamp S, Feigenspan A, Wässle H (2004) Types of bipolar cells in the mouse retina. J Comp Neurol 469:70–82.

Gonnord P, Delarasse C, Auger R, Benihoud K, Prigent M, Cuif MH, Lamaze C, Kanellopoulos JM (2009) Palmitoylation of the P2X7 receptor, an ATP-gated channel, controls its expression and association with lipid rafts. FASEB J 23:795–805.

Grunert U, Martine PR (1991) Rod bipolar cells in the macaque monkey retina: Immunoreactivty and connectivity. J Neurosci 11:2742–2758.

Gu BJ, Zhang W, Worthington R, Sluyter R, Dao-Ung P, Petrou S, Barden J, Wiley JS (2001) A Glu-496 to Ala polymorphism leads to loss of function of the human P2X7 receptor. J Biol Chem 276:11135–11142.

Guha S, Baltazar GC, Coffey EE, Tu L-A, Lim JC, Beckel JM, Patel S, Eysteinsson T, Lu W, O'Brien-Jenkins A, Laties AM, Mitchell CH (2013) Lysosomal alkalinization, lipid oxidation, and reduced phagosome clearance triggered by activation of the P2X7 receptor. FASEB J 27:4500–4509.

Guo C, Masin M, Qureshi OS, Murrell-lagnado RD (2007) Evidence for functional P2X4/P2X7 heteromeric receptors. Mol Pharmacol 72:1447–1456.

Gyoneva S, Orr AG, Traynelis SF (2009) Differential regulation of microglial motility by ATP/ADP and adenosine. Parkinsonism Relat Disord 15 Suppl 3:S195–9.

Gyoneva S, Traynelis SF (2013) Norepinephrine modulates the motility of resting and activated microglia via different adrenergic receptors. J Biol Chem 288:15291–15302.

Haines WR, Voigt MM, Migita K, Torres GE, Egan TM (2001) On the contribution of the first transmembrane domain to whole-cell current through an ATP-gated ionotropic P2X receptor. J Neurosci 21:5885–5892.

Halder SK, Matsunaga H, Ishii KJ, Akira S, Miyake K, Ueda H (2013) Retinal cell type-specific prevention of ischemia-induced damages by LPS-TLR4 signaling through microglia. J Neurochem 126:243–260.

Hayashi Y, Ishibashi H, Hashimoto K, Nakanishi H (2006) Potentiation of the NMDA receptor-mediated responses through the activation of the glycine site by microglia secreting soluble factors. Glia 53:660–668.

Haynes SE, Hollopeter G, Yang G, Kurpius D, Dailey ME, Gan W-B, Julius D (2006) The P2Y12 receptor regulates microglial activation by extracellular nucleotides. Nat Neurosci 9:1512–1519.

Hervás C, Pérez-Sen R, Miras-Portugal MT (2005) Presence of diverse functional P2X receptors in rat cerebellar synaptic terminals. Biochem Pharmacol 70:770–785.

Hibell A, Kidd EJ, Chessell IP, Humphrey PP, Michel A (2000) Apparent species differences in the kinetic properties of P2X(7) receptors. Br J Pharmacol 130:167–173.

Hibell AD, Thompson KM, Simon J, Xing M, Humphrey PP, Michel AD (2001) Species- and agonist-dependent differences in the deactivation-kinetics of P2X7 receptors. Naunyn Schmiedebergs Arch Pharmacol 363:639–648.

Higgs MH, Lukasiewicz PD (1999) Glutamate uptake limits synaptic excitation of retinal ganglion cells. J Neurosci 19:3691–3700.

Holt M, Cooke A, Neef A, Lagnado L (2004) High mobility of vesicles supports continuous exocytosis at a ribbon synapse. Curr Biol 14:173–183.

Honore P, Donnelly-Roberts D, Namovic MT, Hsieh G, Zhu CZ, Mikusa JP, Hernandez G, Zhong C, Gauvin DM, Chandran P, Harris R, Medrano AP, Carroll W, Marsh K, Sullivan JP, Faltynek CR, Jarvis MF (2006) A-740003 [N-(1-{[(Cyanoimino)(5-quinolinylamino)dimethoxyphenyl)acetamide], a novel and selective P2X7 receptor antagonist, dose-dependently reduces neuropathic pain in the rat. J Pharmacol Exp Ther 319:1376–1385.

Hood DC, Birch DG (1990) A quantitative measure of the electrical activity of human rod photoreceptors using electroretinography. Vis Neurosci 5:379–387.

Hood DC, Birch DG (1992) A computational model of the amplitude and implicit time of the b-wave of the human ERG. Vis Neurosci 8:107–126.

Hood DC, Birch DG (1997) Assessing abnormal rod photoreceptor activity with the a-wave of the electroretinogram: applications and methods. Doc Ophthalmol 92:253–267.

Hu H, Lu W, Zhang M, Zhang X, Argall AJ, Patel S, Lee GE, Kim Y-C, Jacobson KA, Laties AM, Mitchell CH (2010) Stimulation of the P2X7 receptor kills rat retinal ganglion cells in vivo. Exp Eye Res 91:425–432.

Huberman AD, Niell CM (2011) What can mice tell us about how vision works? Trends Neurosci 34:464–473.

Hume D, Perry VH, Gordon S (1983) Immunohistochemical localization of a macrophage-specific antigen in developing mouse retina: phagocytosis of dying neurons and differentiation of microglial cells to form a regular array in the plexiform layers. J Cell Biol 97:253–257.

Humphreys BD, Virginio C, Surprenant A, Rice J, Dubyak GR (1998) Isoquinolines as antagonists of the P2X7 nucleotide receptor: high selectivity for the human versus rat receptor homologues. Mol Pharmacol 54:22–32.

Iandiev I, Wurm A, Pannicke T, Wiedemann P, Reichenbach A, Robson SC, Zimmermann H, Bringmann A (2007) Ectonucleotidases in Müller glial cells of the rodent retina: Involvement in inhibition of osmotic cell swelling. Purinergic Signal 3:423–433.

Iglesias R, Locovei S, Roque A, Alberto AP, Dahl G, Spray DC, Scemes E (2008) P2X7 receptor-Pannexin1 complex: pharmacology and signaling. Am J Physiol Cell Physiol 295:C752–60.

Ikeda H, Dawes E, Hankins M (1992) Spontaneous firing level distinguishes the effects of NMDA and non-NMDA receptor antagonists on the ganglion cells in the cat retina. Eur J Pharmacol 210:53–59.

Imura Y, Morizawa Y, Komatsu R, Shibata K, Shinozaki Y, Kasai H, Moriishi K, Moriyama Y, Koizumi S (2013) Microglia release ATP by exocytosis. Glia 61:1320–1330.

Innocenti B, Pfeiffer S, Zrenner E, Kohler K, Guenther E (2004) ATP-induced non-neuronal cell permeabilization in the rat inner retina. J Neurosci 24:8577–8583.

Ishii K, Kaneda M, Li H, Rockland KS, Hashikawa T (2003) Neuron-specific distribution of P2X7 purinergic receptors in the monkey retina. J Comp Neurol 459:267–277.

Ito D, Imai Y, Ohsawa K, Nakajima K, Fukuuchi Y, Kohsaka S (1998) Microglia-specific localisation of a novel calcium binding protein, Iba1. Brain Res Mol Brain Res 57:1–9.

Jabs R, Guenther E, Marquordt K, Wheeler-Schilling TH (2000) Evidence for P2X3, P2X4, P2X5 but not for P2X7 containing purinergic receptors in Müller cells of the rat retina. Mol Brain Res 76:205–210.

Jeon CJ, Strettoi E, Masland RH (1998) The major cell populations of the mouse retina. J Neurosci 18:8936–8946.

Jiang L, Rassendren F, Mackenzie A, Zhang Y, Surprenant A, North RA (2005) N-methyl-D-glucamine and propidium dyes utilize different permeation pathways at rat P2X7 receptors. Am J Physiol Cell Physiol 289:C1295–1302.

Jiang LH, Mackenzie AB, North RA, Surprenant A (2000) Brilliant blue G selectively blocks ATP-gated rat P2X(7) receptors. Mol Pharmacol 58:82–88.

Jindrichova M, Kuzyk P, Li S, Stojilkovic SS, Zemkova H (2012) Conserved ectodomain cysteines are essential for rat P2X7 receptor trafficking. Purinergic Signal 8:317–325.

Jo Y-H, Role LW (2002) Coordinate release of ATP and GABA at in vitro synapses of lateral hypothalamic neurons. J Neurosci 22:4794–4804.

Jo YH, Schlichter R (1999) Synaptic corelease of ATP and GABA in cultured spinal neurons. Nat Neurosci 2:241–245.

Jones SM, Palmer MJ (2009) Activation of the tonic GABAC receptor current in retinal bipolar cell terminals by nonvesicular GABA release. J Neurophysiol 102:691–699.

Kaneda M, Ishii K, Morishima Y, Akagi T, Yamazaki Y, Nakanishi S, Hashikawa T (2004) OFF-cholinergic-pathway-selective localization of P2X2 purinoceptors in the mouse retina. J Comp Neurol 476:103–111.

Kaneda M, Ishii T, Hosoya T (2008) Pathway-dependent modulation by P2-purinoceptors in the mouse retina. Eur J Neurosci 28:128–136.

Kaneda M, Ito K, Shigematsu Y, Shimoda Y (2010) The OFF-pathway dominance of P2X(2)-purinoceptors is formed without visual experience. Neurosci Res 66:86–91.

Kato Y, Omote H, Miyaji T (2013) Inhibitors of ATP release inhibit vesicular nucleotide transporter. Biol Pharm Bull 36:1688–1691.

Katsuki H, Nakai S, Hirai Y, Akaji K, Kiso Y, Satoh M (1990) Interleukin-1 beta inhibits long-term potentiation in the CA3 region of mouse hippocampal slices. Eur J Pharmacol 181:323–326.

Kawamura H, Sugiyama T, Wu DM, Kobayashi M, Yamanishi S, Katsumura K, Puro DG (2003) ATP: a vasoactive signal in the pericyte-containing microvasculature of the rat retina. J Physiol 551:787-99

Kim M, Spelta V, Sim J, North RA, Surprenant A (2001) Differential assembly of rat purinergic P2X7 receptor in immune cells of the brain and periphery. J Biol Chem 276:23262–23267.

Klapperstück M, Schmalzing G, Markwardt F (2001) Characteristics of bindings sites for ATP4- at the Human P2X7 Receptor. Drug Dev Res 82:77–82.

Ko MK, Saraswathy S, Parikh JG, Rao N (2011) The role of TLR4 activation in photoreceptor mitochondrial oxidative stress. Invest Ophthalmol Vis Sci 52:5824–5835.

Kohno H, Chen Y, Kevany BM, Pearlman E, Miyagi M, Maeda T, Palczewski K, Maeda A (2013) Photoreceptor proteins initiate microglial activation via Toll-like receptor 4 in retinal degeneration mediated by all-trans-retinal. J Biol Chem 288:15326–15341.

Kolb H (1970) Organization of the outer plexiform layer of the primate retina: electron microscopy of Golgi-impregnated cells. Philos Trans R Soc Lond B Biol Sci 258:261–283.

Kolb H (1974) The connections between horizontal cells and photoreceptors in the retina of the cat: electron microscopy of Golgi preparations. J Comp Neurol 155:1–14.

Kolb H (1997) Amacrine cells of the mammalian retina: neurocircuitry and functional roles. Eye (Lond) 11 (Pt 6):904–923.

Kolb H, Nelson R, Mariani a (1981) Amacrine cells, bipolar cells and ganglion cells of the cat retina: a Golgi study. Vision Res 21:1081–1114.

Koulen P, Kuhn R, Wassle H, Brandstatter JH (1999) Modulation of the intracellular calcium concentration in photoreceptor terminals by a presynaptic metabotropic glutamate receptor

Kreutzberg GW (1996) Microglia: a sensor for pathological events in the CNS. Trends Neurosci 19:312–318.

Križaj D, Ryskamp D, Tian N, Tezel G, Mitchell CH, Slepak VZ, Shestopalov VI (2013) From mechanosensitivity to inflammatory responses: New players in the pathology of glaucoma. Curr Eye Res:1–15.

Kuffler SW (1953) Discharge patterns of functional organisation of mammalian retina. J Neurophysiol 16:37–68.

Kukley M, Stausberg P, Adelmann G, Chessell IP, Dietrich D (2004) Ecto-nucleotidases and nucleoside transporters mediate activation of adenosine receptors on hippocampal mossy fibers by P2X7 receptor agonist 2'-3'-O-(4-benzoylbenzoyl)-ATP. J Neurosci 24:7128–7139.

Kur J, Newman EA (2014) Purinergic control of vascular tone in the retina. J Physiol 592:491-504.

Lagnado L (2000) Ribbon Synapses. Curr Biol:R631.

Lamb TD, Pugh EN (2006) Phototransduction, dark adaptation, and rhodopsin regeneration the proctor lecture. Invest Ophthalmol Vis Sci 47:5137–5152.

Langmann T (2007) Microglia activation in retinal degeneration. J Leukoc Biol 81:1345–1351.

Lei B, Yao G, Zhang K, Hofeldt KJ, Chang B (2006) Study of rod- and cone-driven oscillatory potentials in mice. Invest Ophthalmol Vis Sci 47:2732–2738.

León D, Sánchez-Nogueiro J, Marín-García P, Miras-Portugal M (2008) Glutamate release and synapsin-I phosphorylation induced by P2X7 receptors activation in cerebellar granule neurons. Neurochem Int 52:1148–1159.

Li A, Zhang X, Zheng D, Ge J, Laties AM, Mitchell CH (2011) Sustained elevation of extracellular ATP in aqueous humor from humans with primary chronic angle-closure glaucoma. Exp Eye Res 93:528–533.

Li Y, Du X-F, Liu C-S, Wen Z-L, Du J-L (2012) Reciprocal regulation between resting microglial dynamics and neuronal activity in vivo. Dev Cell 23:1189–1202.

Liang Z, Freed M a (2010) The ON pathway rectifies the OFF pathway of the mammalian retina. J Neurosci 30:5533–5543.

Lin X, Fang D, Zhou H, Su SB (2013) The expression of Toll-like receptors in murine Müller cells, the glial cells in retina. Neurol Sci 34:1339–1346.

Lukasiewicz P, Lawrence E, Valentino L (1995) Desensitizing glutamate receptors inputs to tiger salamander retinal shape excitatory ganglion cells synaptic. J Neurosci 15:6189–6199.

Lukasiewicz PD (2005) Synaptic mechanisms that shape visual signaling at the inner retina. Prog Brain Res 147:205–218.

Lukasiewicz PD, Mcreynolds JS (1985) Synaptic transmission at the N-methyl-D-aspartate receptors in the proximal retinal of the mudpuppy. J Physiol 367:99–115.

Lukasiewicz PD, Wilson JA, Lawrence JE (1997) AMPA-preferring receptors mediate excitatory synaptic inputs to retinal ganglion cells. Jounral Neurophysiol 77:57–64.

Lundy PM, Hamilton MG, Mi L, Gong W, Vair C, Sawyer TW, Frew R (2002) Stimulation of Ca2+ influx through ATP receptors on rat brain synaptosomes : identification of functional P2X7 receptor subtypes. Br J Pharmacol 135:1616–1626.

Mackenzie A, Wilson HL, Kiss-toth E, Dower SK, North RA, Surprenant A, Sheffield S (2001) Rapid secretion of interleukin-1beta by microvesicle shedding. Immunity 8:825–835.

Manookin MB, Beaudoin DL, Ernst ZR, Flagel LJ, Demb JB (2008) Disinhibition combines with excitation to extend the operating range of the OFF visual pathway in daylight. J Neurosci 28:4136–4150.

Marcellino D, Suárez-Boomgaard D, Sánchez-Reina MD, Aguirre J, Yoshitake T, Yoshitake S, Hagman B, Kehr J, Agnati LF, Fuxe K, Rivera A (2010) On the role of P2X(7) receptors in dopamine nerve cell degeneration in a rat model of Parkinson's disease: studies with the P2X(7) receptor antagonist A-438079. J Neural Transm 117:681–687.

Marín-García P, Sánchez-Nogueiro J, Gómez-Villafuertes R, León D, Miras-Portugal MT (2008) Synaptic terminals from mice midbrain exhibit functional P2X7 receptor. Neuroscience 151:361–373.

Marquez-Klaka B, Rettinger J, Bhargava Y, Eisele T, Nicke A (2007) Identification of an intersubunit cross-link between substituted cysteine residues located in the putative ATP binding site of the P2X1 receptor. J Neurosci 27:1456–1466.

Massey C, Miller RF (1990) Receptors of Ganglion Cells in Rabbit Retina. J Neurophysiol 63:16–30.

Massey S, Redburn DA, Crawford MLJ (1983) The effects of 2-amino-4-phosphonobutyric acid (APB) on the ERG and ganglion cell discharge of rabbit retina. Vision Res 23:1607–1613.

Masu M, Iwakabe H, Tagawa Y, Miyoshi T, Yamashita M, Fukuda Y, Sasaki H, Hiroi K, Nakamura Y, Shigemoto R (1995) Specific deficit of the ON response in visual transmission by targeted disruption of the mGluR6 gene. Cell 80:757–765.

McGaraughty S, Chu KL, Namovic MT, Donnelly-Roberts DL, Harris RR, Zhang X-F, Shieh C-C, Wismer CT, Zhu CZ, Gauvin DM, Fabiyi AC, Honore P, Gregg RJ, Kort ME, Nelson DW, Carroll W, Marsh K, Faltynek CR, Jarvis MF (2007) P2X7-related modulation of pathological nociception in rats. Neuroscience 146:1817–1828.

Mclarnon JG, Ryu JK, Walker DG, Choi HB (2006) Upregulated ecxpression of purinergic P2X7 receptor in Alzheimer disease and amyloid-beta peptide-treated microglia and in peptide-injected rat hippocampus. J Neuropathol Exp Neurol 65:1090–1097.

Metea M, Newman EA (2007) Signalling within the neurovascular unit in the mammalian retina. Exp Physiol 92:635-40

Michel A, Chessell IP, Humphrey PP (1999) Ionic effects on human recombinant P2X7 receptor function. Naunyn Schmiedebergs Arch Pharmacol 359:102–109.

Miller R, Dowling J (1970) Intracellular responses of the Muller (glial) cells of mudpuppy retina: Their relation to b-wave of the electroretinogram. J Neurophysiol 33:323–341.

Mitchell CH, Lu W, Hu H, Zhang X, Reigada D, Zhang M (2009) The P2X(7) receptor in retinal ganglion cells: A neuronal model of pressure-induced damage and protection by a shifting purinergic balance. Purinergic Signal 5:241–249.

Mitchell CH, Reigada D (2008) Purinergic signalling in the subretinal space: a role in the communication between the retina and the RPE. Purinergic Signal 4:101–107.

Mittman S, Taylor WR, Copenhagen DR (1990) Concomitant activation of two types of glutamate receptor mediates excitation of salamander retinal ganglion cells. J Physiol 428:175–197.

Monif M, Burnstock G, Williams DA (2010) Microglia: proliferation and activation driven by the P2X7 receptor. Int J Biochem Cell Biol 42:1753–1756.

Moore SF, Mackenzie AB (2008) Species and agonist dependent zinc modulation of endogenous and recombinant ATP-gated P2X7 receptors. Biochem Pharmacol 76:1740–1747.

Morgans CW, Zhang J, Jeffrey BG, Nelson SM, Burke NS, Duvoisin RM, Brown RL (2009) TRPM1 is required for the depolarizing light response in retinal ON-bipolar cells. Proc Natl Acad Sci U S A 106:19174–19178.

Mori M, Heuss C, Gähwiler BH, Gerber U (2001) Fast synaptic transmission mediated by P2X receptors in CA3 pyramidal cells of rat hippocampal slice cultures. J Physiol 535:115–123.

Morigiwa K, Quan M, Murakami M, Yamashita M, Fukuda Y (2000) P2 Purinoceptor expression and functional changes of hypoxia-activated cultured rat retinal microglia. Neurosci Lett 282:153–156.

Nakajima Y, Iwakabe H, Akazawa C, Nawa H, Shigemoto R, Mizuno N, Nakanishi S (1993) Molecular characterization of a novel retinal metabotropic glutamate receptor mGluR6 with a high agonist selectivity for L-2-amino-4-phosphonobutyrate. J Biol Chem 268:11868–11873.

Nawy S, Jahr C (1990) Suppression by glutamate of cGMP-activated conductance in retinal bipolar cells. Nature 346:269–271.

Nelson DW, Gregg RJ, Kort ME, Perez-Medrano A, Voight EA, Wang Y, Grayson G, Namovic MT, Donnelly-Roberts DL, Niforatos W, Honore P, Jarvis MF, Faltynek CR, Carroll WA (2006) Structure-activity relationship studies on a series of novel, substituted 1-benzyl-5-phenyltetrazole P2X7 antagonists. J Med Chem 49:3659–3666.

Newman EA (2001) Propagation of intercellular calcium waves in retinal astrocytes and Müller cells. J Neurosci 21:2215–2223.

Newman EA (2004) Glial modulation of synaptic transmission in the retina. Glia 47:268–274.

Newman EA (2005) Calcium increases in retinal glial cells evoked by light-induced neuronal activity. J Neurosci 25:5502–5510.

Newman EA (2003) Glial cell inhibition of neurons by release of ATP. J Neurosci 23:1659–1666.

Nicke A (2008) Homotrimeric complexes are the dominant assembly state of native P2X7 subunits. Biochem Biophys Res Commun 377:803–808.

Nimmerjahn A, Kirchhoff F, Helmchen F (2005) Resting microglial cells are highly dynamic surveillants of brain parenchyma in vivo. Science (80-) 308:1314–1318.

Niyadurupola N, Sidaway P, Ma N, Rhodes JD, Broadway DC, Sanderson J (2013) P2X7 receptor activation mediates retinal ganglion cell death in a human retina model of ischemic neurodegeneration. Invest Ophthalmol Vis Sci 54:2163–2170.

Nomura A, Shigemoto R, Nakamura Y, Okamoto N, Mizuno N, Nakanishi S (1994) Developmentally regulated postsynaptic localization of a metabotropic glutamate receptor in rat rod bipolar cells. Cell 77:361–369.

North RA (2002) Molecular physiology of P2X receptors. Physiol Rev 82:1013–1067.

North RA, Surprenant A (2000) Pharmacology of cloned P2X Receptors. Annu Rev Pharmacol Toxicol 40:563–580.

Notomi S, Hisatomi T, Kanemaru T, Takeda A, Ikeda Y, Enaida H, Kroemer G, Ishibashi T (2011) Critical involvement of extracellular ATP acting on P2RX7 purinergic receptors in photoreceptor cell death. Am J Pathol 179:2798–2809.

Notomi S, Hisatomi T, Murakami Y, Terasaki H, Sonoda S, Asato R, Takeda A, Ikeda Y, Enaida H, Sakamoto T, Ishibashi T (2013) Dynamic increase in extracellular ATP accelerates photoreceptor cell apoptosis via ligation of P2RX7 in subretinal hemorrhage. PLoS One 8:e53338.

Okawa H, Sampath AP (2007) Optimization of single-photon response transmission at the rod-to-rod bipolar synapse. Physiology (Bethesda) 22:279–286.

Oliveira Simões Pereira T de, da Costa GNF, Santiago ARS, Ambrósio AF, dos Santos PFM (2010) High glucose enhances intracellular Ca2+ responses triggered by purinergic stimulation in retinal neurons and microglia. Brain Res 1316:129–138.

Opie NL, Greferath U, Vessey K, Burkitt AN, Meffin H, Grayden DB, Fletcher EL (2012) Retinal prosthesis safety: Alterations in microglia morphology due to thermal damage and retinal implant contact. Invest Ophthalmol Vis Sci 53:7802–7812.

Pankratov Y, Castro E, Miras-portugal MT, Krishtal O (1998) A purinergic component of the excitatory postsynaptic current mediated by P2X receptors in the CA1 neurons of the rat hippocampus. Eur J Neurosci 10:3898–3902.

Pankratov Y, Lalo U, Verkhratsky A, North RA (2006) Vesicular release of ATP at central synapses. Eur J Physiol:589–597.

Pankratov Y, Lalo U, Verkhratsky A, North RA (2007) Quantal release of ATP in mouse cortex. J Gen Physiol 129:257–265.

Pannicke T, Fischer W, Biedermann B, Schädlich H, Grosche J, Faude F, Wiedemann P, Allgaier C, Illes P, Burnstock G, Reichenbach A (2000) P2X7 receptors in Müller glial cells from the human retina. J Neurosci 20:5965–5972.

Pannicke T, Uckermann O, Iandiev I, Wiedemann P, Reichenbach A, Bringmann A (2005) Ocular inflammation alters swelling and membrane characteristics of rat Müller glial cells. J Neuroimmunol 161:145–154.

Park BS, Song DH, Kim HM, Choi B-S, Lee H, Lee J-O (2009) The structural basis of lipopolysaccharide recognition by the TLR4-MD-2 complex. Nature 458:1191–1195.

Parvathenani LK, Tertyshnikova S, Greco CR, Roberts SB, Robertson B, Posmantur R (2003) P2X7 mediates superoxide production in primary microglia and is up-regulated in a transgenic mouse model of Alzheimer's disease. J Biol Chem 278:13309–13317.

Pascual O, Ben Achour S, Rostaing P, Triller A, Bessis A (2011) Microglia activation triggers astrocyte-mediated modulation of excitatory neurotransmission. Proc Natl Acad Sci U S A 109:E197–205.

Peachey NS, Ball SL (2003) Electrophysiological analysis of visual function in mutant mice. Doc Ophthalmol 107:13–36.

Pearson RA, Dale N, Llaudet E, Mobbs P (2005) ATP released via gap junction hemichannels from the pigment epithelium regulates neural retinal progenitor proliferation. Neuron 46:731–744.

Peichl L, Wässle H (1979) Size, scatter and coverage of ganglion cell receptive field centres in the cat retina. J Physiol 291:117–141.

Pelegrin P, Barroso-gutierrez C, Surprenant A (2008) P2X7 receptor differentially couples to distinct release pathways for IL-1beta in mouse macrophage. J Immunol 180:7147–7157.

Pelegrin P, Surprenant A (2006) Pannexin-1 mediates large pore formation and interleukin-1beta release by the ATP-gated P2X7 receptor. EMBO J 25:5071–5082.

Pelegrin P, Surprenant A (2009) The P2X(7) receptor-pannexin connection to dye uptake and IL-1beta release. Purinergic Signal 5:129–137.

Peng W, Cotrina ML, Han X, Yu H, Bekar L, Blum L, Takano T, Tian G-F, Goldman S, Nedergaard M (2009) Systemic administration of an antagonist of the ATP-sensitive receptor P2X7 improves recovery after spinal cord injury. PNAS 106:12489–12493.

Perregaux D, Gabels A (1994) Interleukin-lP Maturation and Release in Response to ATP and Nigericin.

Perry VH, Hume DA, Gordon S (1985) Immunohistochemical localization of macrophages and microglia in the adult and developing mouse brain. Neuroscience 15:313–326.

Plata-Salamán CR, Ffrench-Mullen JM (1992) Interleukin-1 beta depresses calcium currents in CA1 hippocampal neurons at pathophysiological concentrations. Brain Res Bull 29:221–223.

Praetorius HA, Leipziger J (2009) ATP release from non-excitable cells. Purinergic Signal 5:433–446.

Puthussery T, Fletcher E (2009) Extracellular ATP induces retinal photoreceptor apoptosis through activation of purinoceptors in rodents. J Comp Neurol 513:430–440.

Puthussery T, Fletcher EL (2004) Synaptic localization of P2X7 receptors in the rat retina. J Comp Neurol 472:13–23.

Puthussery T, Fletcher EL (2007) Neuronal expression of P2X3 purinoceptors in the rat retina. Neuroscience 146:403–414.

Puthussery T, Yee P, Vingrys AJ, Fletcher EL (2006) Evidence for the involvement of purinergic P2X receptors in outer retinal processing. Eur J Neurosci 24:7–19.

Raivich G (2005) Like cops on the beat: the active role of resting microglia. Trends Neurosci 28:571–573.

Raivich G, Bohatschek M, Kloss CU, Werner A, Jones LL, Kreutzberg GW (1999) Neuroglial activation repertoire in the injured brain: graded response, molecular mechanisms and cues to physiological function. Brain Res Rev 30:77–105.

Rassendren F, Buell G, Newbolt A, North RA (1997a) Identification of amino acid residues contributing to the pore of a P2X receptor Franc. EMBO J 16:3446–3454.

Rassendren F, Buell GN, Virginio C, Collo G, North RA, Surprenant A (1997b) The permeabilizing ATP receptor, P2X7. J Biol Chem 272:5482–5486.

Reigada D, Lu W, Mitchell CH (2006) Glutamate acts at NMDA receptors on fresh bovine and on cultured human retinal pigment epithelial cells to trigger release of ATP. J Physiol 575:707–720.

Reigada D, Lu W, Zhang M, Mitchell CH (2008) Elevated pressure triggers a physiological release of ATP from the retina: Possible role for pannexin hemichannels. Neuroscience 157:396–404.

Reigada D, Lu W, Zhang X, Friedman C, Pendrak K, Mcglinn A, Stone RA, Laties AM, Mitchell CH (2005) Degradation of extracellular ATP by the retinal pigment epithelium. Am J Physiol Cell Physiol 289:617–624.

Reigada D, Mitchell CH (2005) Release of ATP from retinal pigment epithelial cells involves both CFTR and vesicular transport. 6085:132–140.

Resta V, Novelli E, Vozzi G, Scarpa C, Caleo M, Ahluwalia A, Solini A, Santini E, Parisi V, Di Virgilio F, Galli-Resta L (2007) Acute retinal ganglion cell injury caused by intraocular pressure spikes is mediated by endogenous extracellular ATP. Eur J Neurosci 25:2741–2754.

Ricatti MJ, Alfie LD, Lavoie EG, Sévigny J, Schwarzbaum PJ, Faillace MP (2009) Immunocytochemical localization of NTPDases1 and 2 in the neural retina of mouse and zebrafish. Synapse 63:291–307.

Richardson PJ, Brown SJ (1987) ATP release from affinity-purified rat cholinergic nerve terminals. J Neurochem 48:622–630.

Roberts J, Evans RJ (2004) ATP binding at human P2X1 receptors. Contribution of aromatic and basic amino acids revealed using mutagenesis and partial agonists. J Biol Chem 279:9043–9055.

Roberts J, Vial C, Digby HR, Agboh KC, Wen H, Atterbury-Thomas A, Evans RJ (2006) Molecular properties of P2X receptors. Eur J Physiol 452:486–500.

Robertson SJ, Edwards FA (1998) ATP and glutamate are released from separate neurones in the rat medial habenula nucleus : frequency dependence and adenosine-mediated inhibition of release. J Physiol 508:691–701.

Roger S, Gillet L, Baroja-Mazo A, Surprenant A, Pelegrin P (2010) C-terminal calmodulin-binding motif differentially controls human and rat P2X7 receptor current facilitation. J Biol Chem 285:17514–17524.

Roger S, Pelegrin P, Surprenant A (2008) Facilitation of P2X7 receptor currents and membrane blebbing via constitutive and dynamic calmodulin binding. J Neurosci 28:6393–6401.

Rosolen SG, Kolomiets B, Varela O, Picaud S (2008) Retinal electrophysiology for toxicology studies: applications and limits of ERG in animals and ex vivo recordings. Exp Toxicol Pathol 60:17–32.

Santos AM, Calvente R, Tassi M, Mari L, Carrasco M, Marti D (2008) Embryonic and postnatal development of microglial cells in the mouse retina. Comp Gen Pharmacol 239:224 –239.

Santos PF, Caramelo OL, Carvalho AP, Duarte CB (1999) Characterization of ATP release from cultures enriched in cholinergic amacrine-like neurons. J Neurobiol 41:340–348.

Sanz JM, Chiozzi P, Ferrari D, Colaianna M, Idzko M, Falzoni S, Fellin R, Trabace L, Di Virgilio F (2009) Activation of microglia by amyloid {beta} requires P2X7 receptor expression. J Immunol 182:4378–4385.

Sanz JM, Di Virgilio F (2000) Kinetics and mechanism of ATP-dependent IL-1 beta release from microglial cells. J Immunol 164:4893–4898.

Sasaki T, Kaneko A (1996) L-Glutamate-induced responses in OFF-type bipolar cells of the cat retina. Vision Res 36:787–795.

Sawada K, Echigo N, Juge N, Miyaji T, Otsuka M, Omote H, Yamamoto A, Moriyama Y (2008) Identification of a vesicular nucleotide transporter. PNAS 105:5683–5686.

Schiller PH (1992) The ON and OFF channels of the visual system. Trends Neurosci 15:86–92.

Schiller PH (2010) Parallel information processing channels created in the retina. PNAS 107:17087–17094.

Schneider H, Pitossi F, Balschun D, Wagner A, Del Rey A, Besedovsky H (1998) A neuromodulatory role of interleukin-1β in the hippocampus. Proc Natl Acad Sci U S A 95:7778–7783.

Sharpe LT, Stockman A (1999) Rod pathways: the importance of seeing nothing. Trends Neurosci 22:497–504.

Shiells RA, Falk G (1990) Glutamate receptors of rod bipolar cells are linked to a cyclic GMP cascade via a G-protein. Proceedings Biol Sci 242:91–94.

Shigematsu Y, Shimoda Y, Kaneda M (2007) Distribution of immunoreactivity for P2X3, P2X5, and P2X6-purinoceptors in mouse retina. J Mol Histol 38:369–371.

Singer JH (2007) Multivesicular release and saturation of glutamatergic signalling at retinal ribbon synapses. J Physiol 580:23–29.

Sjöstrand FS (1953) The ultrastructure of the outer segments of rods and cones of the eye as revealed by the electron microscope. J Cell Comp Physiol 42:15–44.

Slaughter MM, Miller RF (1981) 2-amino-4-phosphonobutyric acid: A new pharmacological tool for retina research. Science (80-) 211:182–185.

Slaughter MM, Miller RF (1983) The role of excitatory amino acid transmitters in the mudpuppy retina: an analysis with kainic acid and N-methyl aspartate. J Neurosci 3:1701–1711.

Smart ML, Gu B, Panchal RG, Wiley J, Cromer B, Williams D, Petrou S (2003) P2X7 receptor cell surface expression and cytolytic pore formation are regulated by a distal C-terminal region. J Biol Chem 278:8853–8860.

Sperlágh B, Haskó G, Németh Z, Vizi ES (1998) ATP released by LPS increases nitric oxide production in raw 264.7 macrophage cell line via P2Z/P2X7 receptors. Neurochem Int 33:209–215.

Sperlágh B, Köfalvi A, Deuchars J, Atkinson L, Milligan CJ, Buckley NJ, Vizi ES (2002) Involvement of P2X7 receptors in the regulation of neurotransmitter release in the rat hippocampus. J Neurochem 81:1196–1211.

Sperlagh B, Vizi ES (1996) Neuronal synthesis , storage and release of ATP Be ata. Semin Neurosci 8:175–186.

Sperlágh B, Vizi ES, Wirkner K, Illes P (2006) P2X7 receptors in the nervous system. Prog Neurobiol 78:327–346.

Stanimirovic D, Friedman A (2012) Pathophysiology of the neurovascular unit: disease cause or consequence? J Cereb Blood Flow Metab 32:1207-21.

Steinberg TH, Newman a S, Swanson J, Silverstein SC (1987) ATP4- permeabilizes the plasma membrane of mouse macrophages to fluorescent dyes. J Biol Chem 262:8884–8888.

Sterling P, Freed M, Smith R (1988) Architecture of rod and cone circuits to the On-beta ganglion cell. J Neurosci 8:623–642.

Stockton R a, Slaughter MM (1989) B-wave of the electroretinogram. A reflection of ON bipolar cell activity. J Gen Physiol 93:101–122.

Streit WJ, Walter S a, Pennell N a (1999) Reactive microgliosis. Prog Neurobiol 57:563–581.

Strettoi E, Raviola E, Dacheux RF (1992) Synaptic connections of the narrow-field, bistratified rod amacrine cell (AII) in the rabbit retina. J Comp Neurol 325:152–168.

Sugiyama T, Kawamura H, Yamanishi S, Kobayashi M, Katsumura K, Puro DG (2005) Regulation of P2X7-induced pore formation and cell death in pericyte-containing retinal microvessels. Am J Physiol Cell Physiol 288:C568–76.

Sugiyama T, Kobayashi M, Kawamura H, Li Q, Puro DG (2004) Enhancement of P2X7-induced pore formation and apoptosis: An early effect of diabetes on the retinal microvasculature. Invest Ophthalmol Vis Sci 45:1026–1032.

Sugiyama T, Lee SY, Horie T, Oku H, Takai S, Tanioka H, Kuriki Y, Kojima S, Ikeda T (2013) $P2X_7$ receptor activation may be involved in neuronal loss in the retinal ganglion cell layer after acute elevation of intraocular pressure in rats. Mol Vis 19:2080–2091.

Sugiyama T, Oku H, Komori A, Ikeda T (2006) Effect of P2X7 receptor activation on the retinal blood velocity of diabetic rabbits. Arch Ophthalmol 124:1143–1149.

Surprenant A, Rassendren F, Kawashima E, North R, Buell G (1996) The cytolytic P2Z receptor for extracellular ATP identified as a P2X receptor (P2X7). Science (80-) 272:735–738.

Suzuki T, Hide I, Ido K, Kohsaka S, Inoue K, Nakata Y (2004) Production and release of neuroprotective tumor necrosis factor by P2X7 receptor-activated microglia. J Neurosci 24:1–7.

Taschenberger H, Jüttner R, Grantyn R (1999) Ca2+-permeable P2X receptor channels in cultured rat retinal ganglion cells. J Neurosci 19:3353–3366.

Tautenhahn M, Leichsenring A, Servettini I, Pesic M, Sperlagh B, Nörenberg W, Illes P (2012) Purinergic modulation of the excitatory synaptic input onto rat striatal neurons. Neuropharmacology 62:1756–1766.

Teixeira JM, Oliveira MCG, Parada CA, Tambeli CH (2010) Peripheral mechanisms underlying the essential role of P2X7 receptors in the development of inflammatory hyperalgesia. Eur J Pharmacol 644:55–60.

Torres GE, Egan TM, Voigt MM (1999) Hetero-oligomeric assembly of P2X receptor subunits. J Biol Chem 274:6653–6659.

Tremblay M-È, Lowery RL, Majewska AK (2010) Microglial interactions with synapses are modulated by visual experience. PLoS Biol 8:e1000527.

Trueblood KE, Mohr S, Dubyak GR (2011) Purinergic regulation of high-glucose-induced caspase-1 activation in the rat retinal Müller cell line rMC-1. :1213–1223.

Trümpler J, Dedek K, Schubert T, de Sevilla Müller LP, Seeliger M, Humphries P, Biel M, Weiler R (2008) Rod and cone contributions to horizontal cell light responses in the mouse retina. J Neurosci 28:6818–6825.

Tu Z, Portillo J-AC, Howell S, Bu H, Subauste CS, Al-Ubaidi MR, Pearlman E, Lin F (2011) Photoreceptor cells constitutively express functional TLR4. J Neuroimmunol 230:183–187.

Turola E, Furlan R, Bianco F, Matteoli M, Verderio C (2012) Microglial microvesicle secretion and intercellular signaling. Front Physiol 3:149.

Uckermann O, Wolf A, Kutzera F, Kalisch F, Beck-sickinger AG, Wiedemann P, Reichenbach A, Bringmann A (2006) Glutamate release by neurons evoked a purinergic inhibitory mechanism of osmotic glial swelling in the rat retina: activation by neuropeptide Y. J Neurosci Res 83:538–550.

Vereker E, O'Donnell E, Lynch A, Kelly A, Nolan Y, Lynch M a (2001) Evidence that interleukin-1beta and reactive oxygen species production play a pivotal role in stress-induced impairment of LTP in the rat dentate gyrus. Eur J Neurosci 14:1809–1819.

Vessey K, Wilkinson-Berka JL, Fletcher EL (2011) Characterization of retinal function and glial cell response in a mouse model of oxygen-induced retinopathy. J Comp Neurol 519:506–527.

Vessey KA, Fletcher EL (2012) Rode and cone pathway signalling is altered in the P2X7 receptor knock out mouse. PLoS One 7:e29990.

Vessey KA, Greferath U, Aplin FP, Jobling AI, Phipps JA, Ho T, de Iongh RU, Fletcher EL (2014) Adenosine triphosphate-induced photoreceptor death and retinal remodelling in rats. J Comp Neurol 522:2928–2950.

Vessey KA, Jobling AI, Greferath U, Fletcher EL (2012) The role of the P2X7 receptor in the retina: cell signalling and dysfunction. Adv Exp Med Biol 723:813–819.

Vianna E, Ferreira A, Naffah-Mazzacoratti M, Sanabria E, Funke M, Cavalheiro EA, Fernandes MJS (2002) Evidence that ATP participates in the pathophysiology of pilocarpine-induced temporal lobe epilepsy: Fluorometric, immunohistochemical, and western blot studies. Epilepsia 43:227–229.

Di Virgilio F (2007) Liaisons dangereuses: P2X(7) and the inflammasome. Trends Pharmacol Sci 28:465–472.

Virginio C, Church D, North R, Surprenant A (1997) Effects of divalent cations, protons and calmidazolium at the rat P2X7 receptor. Neuropharmacology 36:1285–1294.

Virginio C, MacKenzie A, North RA, Surprenant A (1999) Kinetics of cell lysis, dye uptake and permeability changes in cells expressing the rat P2X7 receptor. J Physiol 519:335–346.

Völgyi B, Chheda S, Bloomfield S a (2009) Tracer coupling patterns of the ganglion cell subtypes in the mouse retina. J Comp Neurol 512:664–687.

Wachtmeister L (1998) Oscillatory potentials in the retina: what do they reveal. Prog Retin Eye Res 17:485–521.

Wake H, Moorhouse AJ, Jinno S, Kohsaka S, Nabekura J (2009) Resting microglia directly monitor the functional state of synapses in vivo and determine the fate of ischemic terminals. J Neurosci 29:3974–3980.

Wald G (1968) The molecular basis of visual excitation. Nature 219:800–807.

Wang C-M, Chang Y-Y, Sun SH (2003) Activation of P2X7 purinoceptor-stimulated TGF-β1 mRNA expression involves PKC/MAPK signalling pathway in a rat brain-derived type-2 astrocyte cell line, RBA-2. Cell Signal 15:1129–1137.

Wang X, Arcuino G, Takano T, Lin J, Peng WG, Wan P, Li P, Xu Q, Liu QS, Goldman SA, Nedergaard M (2004) P2X7 receptor inhibition improves recovery after spinal cord injury. Nat Med 10:821–827.

Ward MM, Fletcher EL (2009) Subsets of retinal neurons and glia express P2Y1 receptors. Neuroscience 160:555–566.

Ward MM, Puthussery T, Fletcher EL (2008) Localization and possible function of P2Y(4) receptors in the rodent retina. Neuroscience 155:1262–1274.

Wässle H (2004) Parallel processing in the mammalian retina. Nat Rev Neurosci 5:747–757.

Wässle H, Koulen P, Brandstätter JH, Fletcher EL, Becker CM (1998) Glycine and GABA receptors in the mammalian retina. Vision Res 38:1411–1430.

Wheeler-Schilling TH, Marquordt K, Kohler K, Guenther E, Jabs R (2001) Identification of purinergic receptors in retinal ganglion cells. Brain Res Mol Brain Res 92:177–180.

Wheeler-Schilling TH, Marquordt K, Kohler K, Jabs R, Guenther E (2000) Expression of purinergic receptors in bipolar cells of the rat retina. Brain Res Mol Brain Res 76:415–418.

Wieraszko a, Goldsmith G, Seyfried TN (1989) Stimulation-dependent release of adenosine triphosphate from hippocampal slices. Brain Res 485:244–250.

Wiley JS, Dao-ung LP, Gu BJ, Sluyter R, Shemon AN, Li C, Taper J, Gallo J (2002) A loss-of-function polymorphic mutation in the cytolytic P2X7 receptor gene and chronic lymphocytic leukaemia : a molecular study. Lancet 359:1114–1119.

Wiley JS, Dao-Ung L-P, Li C, Shemon AN, Gu BJ, Smart ML, Fuller SJ, Barden J, Petrou S, Sluyter R (2003) An Ile-568 to Asn polymorphism prevents normal trafficking and function of the human P2X7 receptor. J Biol Chem 278:17108–17113.

Wilkinson WJ, Jiang L, Surprenant A, North RA (2006) Role of Ectodomain Lysines in the Subunits of the Heteromeric P2X2/3 Receptor. Mol Pharmacol 70:1159–1163.

Winkler BS (1972) The electroretinogram of the isolated rat retina. Vision Res 12:1183–1198.

Winkler BS (1973) Dependence of fast components of the electroretinogram of the isolated rat retina on the ionic environment. Vision Res 13:457–463.

Wurm A, Pannicke T, Iandiev I, Francke M, Hollborn M, Wiedemann P, Reichenbach A, Osborne NN, Bringmann A (2011) Purinergic signaling involved in Müller cell function in the mammalian retina. Prog Retin Eye Res 30:324–342.

Xia J, Lim JC, Lu W, Beckel JM, Macarak EJ, Laties AM, Mitchell CH (2012) Neurons respond directly to mechanical deformation with pannexin-mediated ATP release and autostimulation of P2X7 receptors. J Physiol 10:2285–2304.

Xie Y, Zacharias E, Hoff P, Tegtmeier F (1995) Ion channel involvement in anoxic depolarization induced by cardiac arrest in rat brain. J Cereb Blood Flow Metab 15:587–594.

Yazejian B, Fain GL (1992) Excitatory amino acid receptors on isolated retinal ganglion cells from the goldfish. J Neurophysiol 67:94–107.

Yazulla S, Studholme KM (2004) Vanilloid receptor like 1 (VRL1) immunoreactivity in mammalian retina: colocalization with somatostatin and purinergic P2X1 receptors. J Comp Neurol 474:407–418.

Young MT, Pelegrin P, Surprenant A (2007) Amino acid residues in the P2X7 receptor that mediate differential sensitivity to ATP and BzATP. Mol Pharmacol 71:92–100.

Yu W, Miller RF (1996) The mechanism by which NBQX enhances NMDA currents in retinal ganglion cells. Brain Res 709:184–196.

Zeise ML, Madamba S, Siggins GR (1992) Interleukin-1 beta increases synaptic inhibition in rat hippocampal pyramidal neurons in vitro. Regul Pept 39:1–7.

Zhang K, Yao G, Gao Y, Hofeldt KJ, Lei B (2007) Frequency spectrum and amplitude analysis of dark- and light-adapted oscillatory potentials in albino mouse, rat and rabbit. Doc Ophthalmol 115:85–93.

Zhang X, Li A, Ge J, Reigada D, Laties AM, Mitchell CH (2007) Acute increase of intraocular pressure releases ATP into the anterior chamber. Exp Eye Res 85:637–643.

Zhang X, Zhang M, Laties AM, Mitchell CH (2005) Stimulation of P2X7 receptors elevates Ca2+ and kills retinal ganglion cells. Invest Ophthalmol Vis Sci 46:2183–2191.

Zhou ZJ, Marshak DW, Fain GL (1994) Amino acid receptors of midget and parasol ganglion cells in primate retina. Proc Natl Acad Sci U S A 91:4907–4911.

Ziganshin AU, Hoyle CH V., Burnstock G (1994) Ecto-enzymes and metabolism of extracellular ATP. Drug Dev Res 32:134–146.

Zimmermann H (2000) Extracellular metabolism of ATP and other nucleotides. Naunyn Schmiedebergs Arch Pharmacol 362:299–309.